


The Thermodynamic Temperature in Statistical Mechanics

Owen George Jepps
B.A. B.Sc., ANU, Australia

March, 2001

A thesis submitted for the degree of Doctor of
Philosophy of The Australian National University.

I hereby declare that this submission is my own work and that, to the best of my knowledge and belief, it contains no material previously published or written by another person, except where due acknowledgement is made in the text of the thesis.



Acknowledgements

I would like, first and foremost, to thank Niki, my wife, for her continuing love, encouragement, support and understanding over the last four years. Without you, I would not be who I am. I dedicate this thesis to you.

I must also thank my supervisors — particularly Prof. Denis Evans, and Dr. Gary Ayton — for their ongoing support, encouragement and helpful advice. Thank you, Denis, for giving me the freedom to pursue my own path with only the gentlest of reining. I have grown greatly as a researcher under your tutelage. Thank you, Gary, for showing me that there is more to statistical mechanics than mind-bending maths, but also frisbees and potatoes on wires.

Thanks also to my Honours supervisor, Prof. Stjepan Marcelja, for his enthusiasm, support, and wisdom in suggesting that I take up a PhD project with Prof. Evans.

Thank you to those who have helped me get through these post-graduate years, either at work or at play — the members of the Evans research group, present and past; other members of the RSC community; my PARSA friends, students and staff; and finally, my closest friends who continually amaze me by their interest in my work. You have all inspired, encouraged, consoled, and kept me sane.

Finally, I thank my family — particularly my parents — for their love and support. From all these miles away, it does not go unnoticed.

Le savant doit ordonner; on fait la science avec des faits comme une maison avec des pierres; mais une accumulation de faits n'est pas plus une science qu'un tas de pierres n'est une maison.

Henri Poincaré

The woods are lovely, dark, and deep,
But I have promises to keep,
And miles to go before I sleep,
And miles to go before I sleep.

Robert Frost

Abstract

Statistical mechanics provides a means of deriving the empirical results of thermodynamics. This is achieved, *inter alia*, by the association of thermodynamic quantities with the ensemble averages of phase functions. In this thesis, we examine phase functions whose ensemble averages equal the thermodynamic temperature of a system. We derive a general expression which can be used to generate such phase functions.

We consider the application of this result to the simulation of molecular systems. We determine the necessary conditions for this result to be applied in periodic systems, and in systems described by sets of non-canonical variables. We also consider the generation and application of temperature expressions which are functions of position only — the so-called configurational temperatures.

We extend the existing theory of kinetic thermostat control, to develop a more general thermostating method. In particular, we develop equations of motion for a molecular system that control the temperature by altering the coordinate equations of motion, rather than the momenta equations of motion — coordinate thermostats. We demonstrate the effectiveness of these thermostats in the simulation of constant-temperature molecular systems.

Contents

Introductory Remarks	vii
1 Theoretical Background	1
1.1 Temperature and Thermodynamics	2
1.1.1 The Zeroth Law - What is Temperature? . . .	3
1.1.2 The First Law - Energy Conservation	3
1.2 Equilibrium Statistical Mechanics	4
1.2.1 Hamiltonian Dynamics	5
1.2.2 From Mechanics to Statistical Mechanics . . .	8
1.2.3 The Microcanonical Ensemble	9
1.2.4 The Canonical Ensemble	13
1.2.5 The Thermodynamic Limit and Equivalence of Ensembles	14
1.3 Non-Equilibrium Systems	16
1.3.1 Navier-Stokes Hydrodynamics	16
1.3.2 Couette Flow	17
1.4 Computer Simulation Techniques	18
1.4.1 SLLOD Dynamics	19
1.4.2 Force Calculations	21
1.4.3 Integration Methods	24
1.4.4 The Theory of Periodic Boundary Systems . .	25
1.4.5 Collecting Averages	28
1.5 Quaternions and Rigid-Body Dynamics	29
1.5.1 Representing Rotation - Euler Angles	30
1.5.2 Hamilton's Quaternion	31
1.5.3 Quaternion Mathematics	33
1.5.4 Quaternion Dynamics	34
1.5.5 The Hamiltonian Formalism with Quaternions	35
2 Generalised Temperature Expressions	39
2.1 Existing Temperature Expressions	39
2.2 Rugh's Temperature Expressions	43
2.2.1 Derivation	44
2.2.2 Extension I — the Heat Capacity	48
2.2.3 Extension II — the Thermodynamic Pressure	50

2.3	A More Generalised Temperature Expression	51
2.3.1	Canonical Ensembles	52
2.3.2	Microcanonical Ensembles	54
2.3.3	Conditions for \mathcal{H} and \mathbf{B}	55
2.3.4	Consistency with Earlier Expressions	55
2.4	Extensions to Eqn.(2.16)	56
2.4.1	Non-Canonical Variables	56
2.4.2	Over-Parametrised Descriptions	59
2.4.3	Periodic Boundary Conditions	63
2.5	Microscopic Temperature Expressions	66
2.5.1	Microscopic Heat Capacity Expressions	72
2.6	Appendix: Useful Quaternion Results	73
3	Thermostats	76
3.1	The First Thermostats	77
3.2	The Nose-Hoover Thermostat	78
3.3	The Liouville Theorem	79
3.4	Gauss' Principle of Least Constraint	81
3.4.1	Application of Gauss' Principle	81
3.4.2	Holonomic Constraints	82
3.5	The Isokinetic Thermostat	83
3.6	New Approaches to Thermostatting Systems	85
3.6.1	Generalised Nose-Hoover	87
3.6.2	The Iso- \mathcal{T} Thermostats	89
4	Simulation Applications	91
4.1	Measurement of Equilibrium Properties	92
4.1.1	Instantaneous Temperatures	92
4.1.2	Temperature Variation with System Parameters	98
4.1.3	Heat Capacity Calculations	103
4.1.4	Other Equilibrium Results	106
4.2	Measurement of Non-Equilibrium Temperatures	109
4.2.1	Atomic Non-Equilibrium Systems	109
4.2.2	Rigid-Body Non-Equilibrium Systems	112
4.2.3	Other Non-Equilibrium Results	117
4.3	Constant Temperature Simulations	118
4.3.1	The Coordinate Thermostats	120
4.3.2	Thermostatting Equilibrium Systems	122
4.3.3	Thermostatting Non-Equilibrium Systems	128
5	Conclusion	135

Introductory Remarks

Thermodynamics is a science of the macroscopic. Its objects are whole systems, like gases, which are studied in terms of their properties as a whole. These properties are macroscopic observables with which we are generally familiar at the experiential level — volume, temperature, pressure, and so on. Thermodynamics, as a science, provides us with a set of empirical laws that relate these various macroscopic properties.

Mechanics, on the other hand, is a science of the microscopic. Its objects are the constituents of a system, like atoms in the gas, which are studied in terms of their mechanical interaction. While certain thermodynamic properties, such as energy and pressure, find a natural place within the framework of mechanics, two of the thermodynamic quantities — temperature and entropy — do not.

Statistical mechanics is the bridge over this divide between thermodynamics and mechanics. In his treatise of 1938, Tolman writes that “[t]he explanation of the complete science of thermodynamics in terms of the more abstract science of statistical mechanics is one of the greatest achievements of physics.” (Tolman 1979, p9). Where mechanics deals with a single starting point, and its evolution in time, statistical mechanics deals with a set of possible starting points, and their collective evolution. This is where the quantities that find no place in traditional mechanics arise in the theory. The development of the statistical mechanics of Boltzmann, Maxwell and Gibbs has allowed us to understand thermodynamic phenomena in terms of the behaviour of the constituent elements of the system. While the theoretical developments of statistical mechanics can be applied to more abstract fields such as the chaos theory and information theory, our main interest in this thesis will be in the application to real fluids, where the interacting elements are real molecules.

Furthermore, the development of statistical mechanics has enabled us to study the thermodynamic properties of systems through the study of the mechanical interaction of the elements. The advent and development of molecular simulation techniques such as the Monte Carlo (Metropolis et al. 1953) and Molecular Dynamics (Alder and Wainwright 1957) methods have permitted the examination of real systems in computationally-simulated environments.

Our ability to interpret the results of such simulations relies on the identification, within our microscopic theory, of the macroscopic, thermodynamic properties of a system.

This cornerstone of statistical mechanics will be the main focus of this thesis, as we examine the identification of the thermodynamic temperature within the framework of statistical mechanics. In the first chapters of this thesis, we will examine how one forges the links between these two different approaches, in order to develop consistent physical theories. Specifically, after building up much of the necessary ground work in the first chapter, we will examine the various expressions that can be used in statistical mechanics to determine the thermodynamic temperature of a system. In particular, we will consider the following question — can we use information about the positions of particles in order to determine the temperature of a system?

Consider Fig. 1, which shows two ‘snapshots’, taken from two molecular dynamics simulations of a molecular fluid. Thermodynamically, the simulations from which these snapshots were taken differ in only one respect — the temperatures of the systems are different. At first glance, it may appear that there is not really much difference between the two pictures. On closer inspection, however, some differences become apparent. The separation of atoms in the bottom system appears more even — there are not as many atoms that are very close together. Furthermore, the atoms in the bottom system are arranged in a (somewhat) more collinear fashion.

These structural qualities are typically associated with the phase of a system — whether it is solid or fluid. We identify in the bottom system, where particles are more evenly distributed, a structure that is closer to crystalline than in the top system. Consequently, from our understanding of the way in which systems crystallise as they cool, we identify the bottom system as being cooler than the top.

These simple differences demonstrate an important point that is often overlooked in modern computer simulations of atomic and molecular systems — temperature is not simply a measure of how fast particles are travelling. The Equipartition theorem, which tells us the relation between the kinetic energy and the temperature of a system, has become almost enshrined as a definition of temperature among practitioners of molecular simulation techniques, and statistical mechanics in general. This is hardly surprising — it is an elementary result whose derivation can be made accessible to high-school students of physics, and is therefore familiar to students who proceed to study fluid dynamics at higher levels. Furthermore, the simple nature of the Equipartition temperature — the expression for the temperature deduced from the Equipartition theorem — lends itself perfectly to calculation during computer simulations.

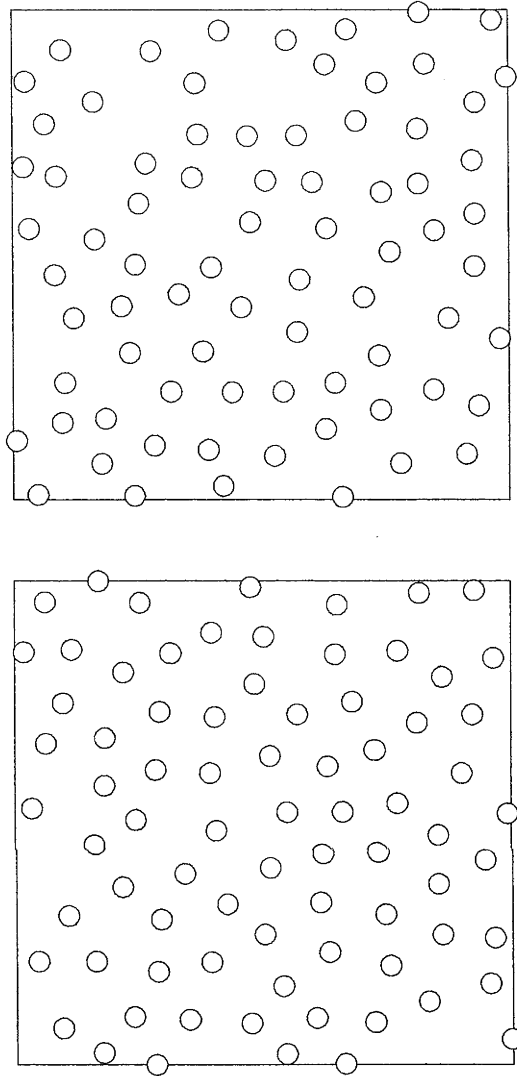


Figure 1: Two 'snapshots' of the same system of particles at two different temperatures. The system on the bottom, with its more even distribution of particles, is indeed the system at the lower temperature.

The association of temperature and position is not new — the Clausius virial theorem, a simple relation between positions, forces, and temperature, has been known for 150 years. However, for technical reasons, this expression cannot be used in many molecular simulations. A brief survey of the literature of statistical physics and molecular simulations reveals that the notions of temperature and kinetic energy are used with what verges on synonymity. It is a combination of the ease with which the Equipartition result can be used, and the absence of any viable alternative, that has led us to this point.

As with all traditions, there is value in questioning their role from time to time. The aim of this thesis, then, apart from deriving microscopic expressions for the thermodynamic temperature, is to (re)consider this somewhat unconscious choice of the Equipartition expression. But by which criteria should we judge one expression preferable to another?

The primary criterion, for the purposes of this thesis, will be the usefulness of temperature expressions in the simulation of molecular systems. To this end, we will need to calculate and compare these expressions in various simulations. In particular, we shall demonstrate that there *are* expressions that are functions of position only, and which can be used in computer simulations to determine the temperature of the system. What will become evident, though, is that the Equipartition temperature is an excellent means of measuring the temperature of an equilibrium system. Its behaviour is reliable, and the errors involved in its use are small compared with the alternatives that we present.

However, measurement is only one aspect of how we can use such temperature expressions. Apart from measuring the thermodynamic temperature of a simulated system, we can also *control* its temperature, by the introduction of thermostats. In the third chapter of this thesis, we examine some of the existing methods of thermostating a system, which all have one feature in common — they all work by controlling the Equipartition temperature of a system, either by holding it constant, or by holding its average constant. We consider — and realise — the possibility of thermostating a system by controlling the *coordinates* of particles, rather than their momenta.

For equilibrium systems, our results demonstrate that these ‘coordinate thermostats’ function as well as their traditional ‘momentum’ counterparts. However, our interest in developing such thermostats goes beyond the equilibrium case. An important part of performing close-to-equilibrium simulations (and, indeed, far-from-equilibrium) is the maintenance of a steady state. Such a steady state is often generated for non-equilibrium molecular dynamics simulations by the introduction of thermostats. The motivation for this

method is based on the premise that real systems, with which such simulations may be compared, are in thermal contact with their surroundings. Thus, it is useful, for the purposes of comparing real and simulated experiments, to be able to use temperature as an input variable for the simulation.

There are practical difficulties in applying ‘kinetic’ thermostats to non-equilibrium systems, which we shall discuss later in this thesis. They are based on the need to define local temperatures in terms of velocities *relative to the local flow*. In non-equilibrium systems, this local motion can be extremely difficult to characterise. The advantage, then, of having a ‘configurational’ temperature, and a ‘configurational’ thermostat, is that they can elegantly circumvent this problem faced by practitioners of ‘kinetic’ thermostats. The final element of this thesis, therefore, will be to examine these configurational thermostats, in both equilibrium and non-equilibrium simulations. At this stage, we will be ready to draw conclusions from the work we have performed about future directions of research in this area.

About this thesis

Text which appears in bold is used to denote the first reference to a concept important to this thesis. Definitions of these terms follow in the immediate text, and these definitions will carry through the entire text of the thesis. Scalar quantities appear as italic text (eg p_i), vector quantities appear as bold text (eg \mathbf{p}). Roman indices (such as i and j) are used to range over the number of particles, or number of degrees of freedom, in a system. Greek indices (such as α and β) are used to range over the coordinates by which we describe a single particle in the system.

Chapter 1

Theoretical Background

In a thesis dedicated to the concept of temperature in statistical mechanics, it is important to provide the reader with a firm foundation by which to understand what temperature is, and what it is not. Most students of physics are familiar with the Equipartition theorem, and the association of temperature with kinetic energy. As will become apparent over the course of this thesis, it is by no means the only quantity that can be associated with the temperature of a system. Furthermore, to treat the Equipartition relation as definitive, or in some way fundamental, is to relegate the role of temperature in statistical mechanics to the status of a mere ‘molecular speedometer’.

In order to re-assess our view of the thermodynamic temperature in statistical mechanics, we will need to understand how the two fields are inter-related. This will take us back to some of the more fundamental theory of statistical mechanics. Much of the content of this chapter can be found in the various standard textbooks available on the subjects of thermodynamics and statistical mechanics*. However, the focus of our presentation will often be different to that of the authors of these texts. It will also provide an opportunity to introduce and develop the concepts, definitions and notation that will be used in this thesis.

We will begin by a brief tour of relevant elements of thermodynamics, in particular the first and second laws of thermodynamics (§1.1). We shall then take an in-depth look at the main model by which we will study thermodynamic systems — statistical mechanics (§1.2). After reviewing the principles of Hamiltonian mechanics (§1.2.1), we will consider why one adopts a statistical approach to the study of thermodynamic systems (§1.2.2), before taking up the matter of how one goes about this statistical approach (§1.2.3-§1.2.5). At this stage of our examination, we will consider how one links the fields of thermodynamics and statistical mechanics, by

*for example, (Tolman 1979; Münster 1969; MacQuarrie 1976; Balescu 1975).

identifying thermodynamic quantities within the theoretical framework provided by statistical mechanics. We shall then be prepared to consider the various expressions that are available for the thermodynamic temperature of a system in Chapter 2.

Up to this point, we will have considered the theory of equilibrium systems only. In §1.3, we will turn our attention to a non-equilibrium process — Couette flow — to which we will apply some of our work in later chapters. In this section we will define Couette flow by briefly introducing the necessary concepts of Navier-Stokes hydrodynamics.

The last sections of this chapter will consider matters related to the computer simulation of molecular fluids, as we will use such simulations to test our theories. We will look at the various techniques used to perform these simulations, by solving the equations of motion for a system of particles and calculating average properties of the system (§1.4). Finally, we will look at the mathematics of the quaternion (§1.5), a mathematical object that proves useful in solving the equations of motion for systems of rigid bodies.

1.1 Temperature and Thermodynamics

The very first models of the behaviour of gases began with the development of thermodynamics. These were empirical theories, founded on the observations of early scientists (Sklar 1995; Torretti 1999). Consequently, they were based on quantities that are measurable at the macroscopic level. We shall refer to such quantities as **macroscopic observables**. Such quantities can be divided into two types. **Mechanical** observables are the familiar quantities that are encountered in a study of the motion of a system — quantities such as **pressure** P , **volume** V , **internal energy** E . **Thermodynamic** observables are those other observables more specific to the study of thermodynamics, the key quantities being **temperature** T and **entropy** S . The macroscopic observables are **state functions**, in that once a state is defined by setting the values of a subset of these variables, the values of the others follow through the **equations of state**. These values are therefore independent of how the system arrived at this state.

Other useful definitions from thermodynamics include the concepts of **extensivity** (a property being extensive if it is proportional to the **number of particles** N) and **intensity** (a property being intensive if it is independent of N), and the notions of a **closed** system (where N is constant) and an **isolated** system (where E is constant). We will also borrow the concept of **equilibrium**, defined to be when the macroscopic observables of a system do not change in time, and its complement, **non-equilibrium**. Another important

notion of thermodynamic theory is the **ideal gas** — a gas of point particles with no energy of interaction between particles.

Out of the empirical relations at its origins developed the four laws that form the heart of thermodynamics. While most of the mystery of thermodynamics is encapsulated in the last two laws, it is the first two that are more immediately relevant to us as we explore the thermodynamic definition of temperature.

1.1.1 The Zeroth Law - What is Temperature?

Suppose that system A and system B are in thermodynamic equilibrium with one another, and that system B and system C are in thermodynamic equilibrium with one another. Then systems A and C will also be in thermodynamic equilibrium with one another.

Computer science was not the first science to number objects by starting with zero. So called because it was identified as a law after the first and second laws, but felt to be more fundamental, the zeroth law of thermodynamics is a comment on the nature of temperature, or perhaps more accurately, thermodynamic equilibrium. The quantity that we use to determine whether or not two systems are in equilibrium is the temperature. Thus the zeroth law reduces to an equivalence theorem about temperature — heat will not be exchanged between systems at the same temperature[†].

1.1.2 The First Law - Energy Conservation

The change in internal energy of a system is given by the sum of the work done on the system and the heat flowing into the system:

$$dE = dQ + dW.$$

The first law of thermodynamics is in essence a conservation law for the energy of a thermodynamic system. Here, dE represents the change in internal energy of the system, dQ represents the heat flowing *into* the system, and dW represents the work done *on* the system.

It is worth noting a fundamental difference in nature between E and Q or W . E is a state function — a macroscopic property of a system, independent of how we arrived at this state. Q and W , on the other hand, are not state functions — this is why we

[†]To this extent, the zeroth law is as much a law about heat as it is a law about temperature.

write their differential as an imperfect differential δ . They depend on the history of the system. While the *changes* in energy due to the heat flow or work are essential ingredients in understanding the behaviour of the system, the values of Q and W (if indeed such values can be ascribed) are of no importance in the general theory.

Consequently, the first law as it stands does not lend itself to immediate service, because it is not written in terms of the macroscopic properties of the system. But while the heat flowing into, and the work done on the system may not be readily quantified in terms of their *source*, they can be quantified in terms of their *effect* on the system, with explicit reference to the system's macroscopic properties.

Specific examples of the work include terms such as $-p dV$ or $\mu_i dN_i$ for multi-species systems of (chemically) interacting particles, where μ_i represents the chemical potential for the i -th species of gas, and N_i represents the number of particles of that species. We can summarise these contributions with a generic representation $f_i dX_i$, where the f_i and dX_i represent so-called thermodynamic forces and fields respectively. Consequently, the first law becomes

$$dE = \delta Q + f_i dX_i.$$

Having transformed the work contribution from source terms into effect terms, we now do the same for the heat contribution. This can be done through Clausius' definition of the entropy, $T dS = \delta Q$, resulting in the **Gibbs fundamental equation** (Beck and Schlögl 1995)

$$dE = T dS - p dV + \sum_i \mu_i dN_i (+ f_i dX_i). \quad (1.1)$$

Now we have an equation linking the various state functions of the system with one another, from which we determine the temperature as

$$T = \left. \frac{dE}{dS} \right|_{V, N_i, X_i}. \quad (1.2)$$

Eqn.(1.2) is the fundamental definition of temperature that we will use throughout this thesis. Together with the zeroth law, it will prove an essential element as we develop our statistical model in the next few sections, and reconcile it with thermodynamics.

1.2 Equilibrium Statistical Mechanics

If the keyword for thermodynamics was 'macroscopic', then this was to contrast it with the microscopic considerations of statistical mechanics. While thermodynamics describes the observed behaviour

of a system as a whole, the aim of statistical mechanics is to consider this problem in terms of the mechanical interactions of the constituent molecules.

Our mechanical model will therefore be a collection of particles that evolves in time according to a set of equations of motion. Although the principles of statistical mechanics can be applied to systems other than fluids, we will retain the terminology of thermodynamics in describing our system. Thus our system will be made up of particles (either atoms or molecules), each of which requiring a set of coordinates to describe mechanically. Unless otherwise indicated, however, all of the theory that we develop through this thesis can be applied to other types of classical mechanical systems.

We will adopt the formalism of Hamiltonian mechanics, largely because of the more general (not to mention more geometrically appealing) framework it provides. Consequently, we begin this section by describing the mechanical theory we will use throughout our work (§1.2.1). We will then examine the statistical element of statistical mechanics (§1.2.2), to understand why we take a probabilistic approach to a problem that is fundamentally deterministic in nature. In §1.2.3–§1.2.4 we will construct the objects that we will use to model thermodynamic systems — ensembles — and link the thermodynamic observables to their statistical mechanical equivalents. Finally, we comment on the connection between the various ensembles of statistical mechanics (§1.2.5).

1.2.1 Hamiltonian Dynamics

The mechanics considered in this thesis is pseudo-classical — that is, it is classical in nature, except for the inclusion of combinatorial terms that are fundamentally quantal. Although these terms (factors of Planck’s constant h or $N!$) can only be derived theoretically through the theory of quantum mechanics, they initially appeared as a solution to Gibbs’ first paradox (Huang 1963).

The mechanical world that we will be exploring will therefore be the world of Newtonian mechanics. In this world, the motion of an object is determined by the **force** that is exerted on it. This force is proportional to the second derivative of the position, and we assert through empirical evidence that the force is a function of the positions and velocities only (and possibly time). Consequently the equations of motion are second order, of the form $m\ddot{\mathbf{r}}_i(t) = \mathbf{f}(\dot{\mathbf{r}}_i(t), \mathbf{r}_i(t), t)$. Here, $\mathbf{r}_i(t)$ represents the position of particle i in Cartesian (ie x , y , and z) coordinates, and $\dot{\mathbf{r}}_i$ denotes the time derivative of \mathbf{r}_i (so that $\ddot{\mathbf{r}}_i$ denotes the second time-derivative of \mathbf{r}_i , etc.).

For a broad class of systems, it is possible to take a different

mathematical approach, using the theory of Hamiltonian dynamics. As was mentioned earlier, the advantage of this approach is that it allows us to characterise our system more freely. Newton's equations of motion as they stand are only valid for rectilinear coordinate systems (such as Cartesian coordinates). The Hamiltonian approach gives us the freedom to choose any coordinate system that describes each different physical arrangement (or **configuration**) of the system uniquely, and has the same number of coordinates as the system has **degrees of freedom**[‡]. In some instances (such as with rigid body mechanics), this freedom allows us to choose coordinates such that the resulting equations of motion can be solved more easily, or offer greater insight into the problem.

Therefore, the theory that we develop will not be specific to a particular coordinate system, but generally applicable to any such system. For this reason, we use **generalised coordinates** in our theoretical development. We use the symbol M to denote the number of generalised coordinates for our system, corresponding to the number of degrees of freedom in the system. We denote by \mathbf{q} the vector (q_1, \dots, q_M) of all the generalised coordinates. A specific set of coordinates can later be substituted, and we call such a specific choice a **description** of our system[§].

Among the class of systems that can be studied using the Hamiltonian formalism are the **conservative** systems. Conservative systems are those in which the work done in taking a system from one configuration to another is independent of the path taken. It follows from this that the **generalised forces** $\mathbf{F} = \ddot{\mathbf{q}}$ can be written as the negative gradient field of a scalar quantity that we call the **potential energy** $\Phi(\mathbf{q})$ — that is, $\mathbf{F} = -\nabla_{\mathbf{q}}\Phi(\mathbf{q})$, where $\nabla_{\mathbf{q}} = [\frac{\partial}{\partial q_1}, \dots, \frac{\partial}{\partial q_M}]$. Consequently, the energy of a conservative system is made up of a potential term Φ that depends only upon the coordinates \mathbf{q} , and a kinetic term K that depends upon the $\dot{\mathbf{q}}$ (and possibly on the \mathbf{q} as well). It can be shown that the kinetic energy is a quadratic form of the $\dot{\mathbf{q}}$ (Goldstein 1980). In this thesis, we shall only consider systems where the energy can be written in the form $E = K(\mathbf{p}, \mathbf{q}) + \Phi(\mathbf{q})$.

In developing the Hamiltonian formalism, we start with the generalisation of Newtonian mechanics due to Lagrange. We introduce the **Lagrangian** $\mathcal{L}(\mathbf{q}, \dot{\mathbf{q}}) = K(\dot{\mathbf{q}}, \mathbf{q}) - \Phi(\mathbf{q})$: the difference between the kinetic energy and the potential energy of the system. The laws of Newtonian mechanics then transform to the following relations

[‡]The number of degrees of freedom of a system is the minimum number of coordinates required to uniquely describe each possible configuration of that system. If a system is parametrised using this number of coordinates, then each coordinate represents a possible independent path of motion of the system, and is itself a degree of freedom of the system.

[§]Hereafter, we will use \mathbf{r} to refer to Cartesian coordinates only.

(Goldstein 1980):

$$\frac{d}{dt} \left(\frac{\partial \mathcal{L}}{\partial \dot{q}_i} \right) - \frac{\partial \mathcal{L}}{\partial q_i} = 0.$$

Thus we have a second-order differential equation to solve for each coordinate, as with Newton's equations of motion. That Lagrange's equations of motion reduce to Newton's is straightforward, considering the Lagrangian $\mathcal{L} = \dot{\mathbf{q}}^T \mathbf{M} \dot{\mathbf{q}} / 2 - \Phi(\mathbf{q})$, where $[\mathbf{M}]_{ij} = m_i \delta_{ij}$ [¶] and $\dot{\mathbf{q}}^T$ is the transpose of $\dot{\mathbf{q}}$.

The Hamiltonian formalism transforms the representation $(\mathbf{q}, \dot{\mathbf{q}}, t)$ to the representation $(\mathbf{q}, \mathbf{p}, t)$, where the new variables

$$p_i = \frac{\partial \mathcal{L}(\mathbf{q}, \dot{\mathbf{q}})}{\partial \dot{q}_i}$$

are the **generalised or conjugate momenta** of the coordinates \mathbf{q} (with $\mathbf{p} = (p_1, \dots, p_M)$). We achieve this via a Legendre transformation of the Lagrangian to our new function, the **Hamiltonian** \mathcal{H} , ie

$$\mathcal{H}(q, p) = \sum_{i=1}^M p_i \dot{q}_i - \mathcal{L}(q, \dot{q}).$$

While the Lagrangian formalism yields M second-order differential equations to solve, the Hamiltonian approach replaces this with $2M$ first-order equations, of the form

$$\dot{q}_i = \frac{\partial \mathcal{H}}{\partial p_i}, \quad \dot{p}_i = -\frac{\partial \mathcal{H}}{\partial q_i}.$$

Thus the vector $\mathbf{\Gamma}(t) = (\mathbf{q}(t), \mathbf{p}(t))$ uniquely and completely describes the system at time t , as all other properties at time t can be written as a function of these variables. We call this space (which is isomorphic to \mathbb{R}^{2M}) **phase space**, and use the term **phase variable**, or **canonical variable**^{||} to denote the set of $2M$ generalised coordinates and momenta. Any function of these variables $g(\mathbf{\Gamma})$ is called a **phase function**. Each point in phase space therefore corresponds to a different microscopic state, or **microstate**.

The time evolution of a microstate $\mathbf{\Gamma}$ is the trajectory through phase space given by the solution to Hamilton's equations. Since our system is conservative, it follows that \mathcal{H} has no explicit time dependence. Consequently

$$\dot{\mathcal{H}} = \nabla_{\mathbf{q}} \mathcal{H} \cdot \dot{\mathbf{q}} + \nabla_{\mathbf{p}} \mathcal{H} \cdot \dot{\mathbf{p}} = \nabla_{\mathbf{q}} \mathcal{H} \cdot \nabla_{\mathbf{p}} \mathcal{H} - \nabla_{\mathbf{p}} \mathcal{H} \cdot \nabla_{\mathbf{q}} \mathcal{H} = 0. \quad (1.3)$$

[¶] δ here is the Kronecker delta: $\delta_{ij} = 1$ if $i = j$, and $\delta_{ij} = 0$ otherwise.

^{||}Although potentially confusing in the context of statistical mechanics, we will prefer this term in contradistinction to sets of *non*-canonical variables.

The Hamiltonian is therefore a constant of the motion. For conservative systems, the Hamiltonian corresponds to the total energy of the system.

While the derivation of Hamilton's equations via Lagrangian mechanics may appear arduous, it is also ultimately unnecessary — the Hamiltonian will simply be the energy of the system, written as a phase function. Furthermore, Eqn.(1.3) implies that this energy will be conserved. Any property (or quality) that does not change during the time-evolution of a mechanical system is called **invariant**.

1.2.2 From Mechanics to Statistical Mechanics

Hamiltonian mechanics is entirely deterministic. Once we have an expression for the kinetic and potential energy of our system, and know the positions and momenta of its particles at a given time, we can determine the microstate of our system at any time in the past or future. Why should we then want to give up this determinism by embarking on a statistical study of a system?

One of the original reasons why the probabilistic approach was considered is that there are simply too many equations of motion to solve for a real system. For a three-dimensional system, each particle will require six parameters — three coordinates and three corresponding momenta. Consequently, there will be six equations of motion to be solved *for each particle*, in order to fully determine the internal dynamics of the gas. When a litre of gas at room temperature and pressure contains of the order of Avogadro's number of particles, then even small** quantities of gas will require the solution of a formidable number of differential equations. It is useful, therefore, to be able to take an alternative route to studying the dynamics of such a system.

The key problem, however, is that, in general, we do not have this detailed information about the systems we wish to study in thermodynamics. We are not trying to understand the behaviour of a gas whose initial microstate is already known. Instead, we are studying a gas whose macroscopic properties are known, but whose initial microstate *is not known*. There will clearly be many different possible microstates, and our mechanical model for this system will have to deal with these possibilities. Furthermore, the initial microstate should be unimportant in determining macroscopic properties from our model, as long as this microstate belongs to the set of possible microstates. This reflects the empirical nature of the results of thermodynamics, which make no reference to the microstate of the system.

**on a macroscopic scale

Our model will therefore consist of ascribing probabilities to all of our microstates. These probabilities reflect the likelihood of observing a system in a given state. In this way, our aim is to reproduce the macroscopic results of thermodynamics with a model that does not require information about an initial microstate. In the following subsections, we approach the problem of determining appropriate probability distributions for our model.

1.2.3 The Microcanonical Ensemble

Given that energy is a constant of the motion during the evolution of conservative systems, the most natural place to begin building the tools of statistical mechanics is by considering groups of phase points with the same energy. These correspond to **energy hypersurfaces**^{††} $A(N, V, E)$ in our phase space, defined as $A(E, V, N) = \{\Gamma : \mathcal{H}(\Gamma) = E\}$. For convenience, we will usually write $A(N, V, E)$ as $A(E)$, since it is the variation of $A(N, V, E)$ with E that will interest us most. We also define the set of points whose energies lie between a and b as $\Omega(a, b) = \{\Gamma : a < \mathcal{H}(\Gamma) < b\}$. Further we define $\Omega(b) = \lim_{a \rightarrow -\infty} \Omega(a, b)$ as the set of all points with energy less than b , and $\Omega = \lim_{b \rightarrow \infty} \Omega(b)$ as the set of all points with finite energy.

It is clear that these surfaces and volumes are invariant under Hamiltonian dynamics. More interestingly, if we define the **extent** $\mathfrak{v}(X)^*$ of a set $X \in \Omega$ as its Lebesgue measure in $2M$ dimensions, then we find that the measure of any set is also invariant under Hamiltonian dynamics (Petersen 1983).

Suppose, then, that we have a closed box of particles, with total energy E . We ask the question, *can we assign a probability distribution over all the possible microstates, that reflects the behaviour of this macroscopic system?* This seemingly innocent question has been the source of a long polemic running through the history of statistical mechanics. Although a subject of great interest, we will consider only the most relevant issues here.

The difficulties that this question poses are on several levels. Of fundamental importance is what we mean for a selection of phase points to ‘reflect the behaviour’ of an equilibrium macroscopic system. The standard approach is to equate the value of a macroscopic observable (such as the pressure P) with the time-average of the microscopic, mechanical equivalent (in this case the instan-

^{††}We use the prefix ‘hyper-’ to highlight the analogy between phase space and ‘real’ space, \mathbb{R}^3 . The surface in real space is a two-dimensional manifold — a hypersurface in our $2M$ -dimensional space is therefore a manifold of $2M - 1$ dimensions.

*In order to avoid confusion with the macroscopic variable V , denoting the volume of a gas, we will use the word *extent* and the symbol \mathfrak{v} to refer to the ‘phase space volume’ of a set.

taneous mechanical pressure p). In the framework of our model, this amounts to the (infinite) time average along the trajectory that passes through the (as yet unknown) initial microstate. Thus we arrive at a probability distribution over phase space that is proportional to the time the system spends in the region of a point — its local ‘speed’ through phase space. On the presumption that such an average exists and is unique[†], this choice of correspondence seems quite plausible, although it raises philosophical problems of its own[‡].

An alternative approach, attributed to Maxwell in the late 1870s[§], takes a philosophical shift away from single trajectories, and towards the concept of an **ensemble**. We choose a probability distribution $f(\mathbf{\Gamma})$ over our points in phase space, and determine the value of a macroscopic observable as the average, using this probability measure, of the corresponding equivalent phase function over phase space — $P = \int f(\mathbf{\Gamma})p(\mathbf{\Gamma}) d\mathbf{\Gamma}$. For an arbitrary probability distribution, $f(\mathbf{\Gamma})$ will change over time, and so therefore will P . If f is an invariant quantity, however, P will not change. Maxwell could not show that such an invariant probability distribution is unique, without a further stipulation — that the system pass through all phase points with the corresponding energy. This is the infamous Ergodic hypothesis. This pairing of a set of accessible points in phase space, and an invariant probability distribution over it, is called an **ensemble**, and the corresponding average is called an **ensemble average**.

The advantage of this approach is that, instead of thinking in terms of averages over time, one can think of performing an average over a set of points in phase space, with the appropriate probability distribution. Thus we do not need to know the trajectories of points through phase space, yet can still derive invariant properties that will correspond to infinite time averages (and therefore, we assert, to macroscopic properties).

The convenience of the ensemble approach is not without a price, however. The Ergodic hypothesis is not possibly true, as a single continuous trajectory cannot fill the space in which it is embedded. The pursuit of alternative theorems allowing us to equate the infinite time and phase averages has a checkered, but fascinating history, evident in many of the seminal texts on the foundations of statistical mechanics. As Sklar writes, “The difficulties encountered led to skepticism in general about the ergodic approach. Typical was R. Tolman’s text of 1938, which took the standard probability distribution, the uniform distribution over the standard measure — the microcanonical probability distribution — as a basic postulate

[†]on the basis of observations of equilibrium systems

[‡]not least of which are these presumptions – see (Sklar 1995).

[§]but considered in a nascent form by Boltzmann as early as 1871

of the theory of equilibrium statistical mechanics. The correctness of the postulate was to be justified epistemically by [sic] its success. Ergodic theory was dismissed as both something whose aims could not be accomplished, and that, even if successfully obtained, would fail to serve any useful foundational role in the theory." (Sklar 1995, pp.161-2)

The focus of ergodic theory, a subject in its own right, is to determine for which systems the infinite time and ensemble averages can be equated. While the ergodic *hypothesis* itself is not valid, other approaches have been adopted in the effort to vindicate our method of equating macroscopic observables with ensemble and infinite time averages of corresponding mechanical phase functions. In particular, Sinai's proof of ergodicity for hard spheres in a parallelepiped box (Sinai 1970) is a significant advancement, in as much as the mixing properties of hard spheres, fundamental to the proof, are plausibly extendible to the sharp potentials that we commonly use in molecular simulations.

On making this assumption, then, the invariant distribution required to equate infinite time and ensemble averages turns out to be the uniform distribution — each point is equally likely. Thus we can define an ensemble corresponding to a system of constant energy E , which we call the **microcanonical ensemble**. In fact, there are two different definitions of the microcanonical ensemble that we can choose. For an energy E , the **shell microcanonical ensemble** corresponds to the set of points $\Omega(E, E + \Delta)$ ($\Delta \ll E$), with the uniform probability distribution $f(\Gamma)$ over this set (which, for convenience, we denote $\mu C(E)$). Typically in statistical mechanics, we determine the function $f(\Gamma)$ via knowledge of the *relative* probabilities $w(\Gamma)$ of different states. Consequently we write

$$f(\Gamma) = \frac{w(\Gamma)}{\int_{\mu C(E)} w(\Gamma) d\Gamma} = \frac{w(\Gamma)}{\mathcal{Z}^{\text{shell}}},$$

where \mathcal{Z} is the *Zustandsumme* or **partition function**. In this case $w(\Gamma) = 1$, so we determine $f(\Gamma)$ to be

$$f(\Gamma) = \frac{1}{\int_{\mu C(E)} d\Gamma} = \frac{1}{\mathfrak{v}},$$

where \mathfrak{v} represents the extent of the shell ensemble. We can also determine the shell ensemble average of a quantity $B(\Gamma)$, denoted $\langle B \rangle$, as the integral

$$\langle B \rangle = \int_{\mu C(E)} f(\Gamma) B(\Gamma) d\Gamma = \frac{\int_{\mu C(E)} B(\Gamma) w(\Gamma) d\Gamma}{\mathcal{Z}^{\text{shell}}} \left(= \frac{\int_{\mu C(E)} B(\Gamma) d\Gamma}{\mathfrak{v}} \right).$$

However, a single trajectory of a Hamiltonian system does not span a range of energy levels, but sits on a single energy level. Thus, our main interest will be in the **surface microcanonical ensemble**. For an energy E , this ensemble consists of the set of points $A(E)$, with the partition function $\int \delta(\mathcal{H}(\mathbf{\Gamma}) - E) d\mathbf{\Gamma}$, where $\delta(x)$ is the usual **Dirac delta function** in $6N$ dimensions (Rudin 1987). This ensemble is the natural limit of the shell ensemble as $\Delta E \rightarrow 0$. It is relatively straightforward[¶] that

$$\begin{aligned} Z^E &= \frac{1}{h^{3N} N!} \int_{\Omega} \delta(\mathcal{H}(\mathbf{\Gamma}) - E) d\mathbf{\Gamma} \\ &= \frac{1}{h^{3N} N!} \int_{A(E)} \frac{1}{|\nabla \mathcal{H}(\mathbf{\Gamma})|} dA_E = \frac{1}{h^{3N} N!} \int_{A(E)} \mu_E(\mathbf{\Gamma}), \end{aligned}$$

where $\mu_E = \frac{1}{|\nabla \mathcal{H}|}$. Here, $\nabla = (\frac{\partial}{\partial \Gamma_1}, \dots, \frac{\partial}{\partial \Gamma_{2M}})$ and $|\cdot|$ represents the Euclidean norm. Strictly speaking, μ_E is a function only of points of energy E — however, writing it as a function of $\mathbf{\Gamma}$ is an unambiguous and convenient notation. We note, however, the dimensional inconsistency of the expression $|\nabla \mathcal{H}(\mathbf{\Gamma})|$. From a physical point of view, it is necessary at this point to reduce the spatial coordinates and momenta to dimensionless units p_i^* and q_i^* . However, since there is no unique choice of units for converting the phase space coordinates to a reduced form, there will be infinitely many different instantaneous expressions for the temperature which will all give equivalent values in different bases of units (see, e.g., (Morris and Rondoni 1999)). In what follows, we will assume that our p_i and q_i are dimensionless as required (as will be the factor h^{3N}).

The ensemble average of a quantity $B(\mathbf{\Gamma})$ over the surface ensemble is denoted

$$\langle B \rangle_E = \frac{\int_{\Omega} B(\mathbf{\Gamma}) \delta(\mathcal{H}(\mathbf{\Gamma}) - E) d\mathbf{\Gamma}}{\int_{\Omega} \delta(\mathcal{H}(\mathbf{\Gamma}) - E) d\mathbf{\Gamma}}.$$

We note that we should include the subscripts ‘ NV ’ as well as E , since the microcanonical ensemble is entirely defined once N , V , and E have been fixed. We can therefore think of the microcanonical ensemble as the NVE ensemble. As we will be contrasting these results with the canonical ensemble (§1.2.4), where N , V and T define the ensemble, we omit the ‘ NV ’ from our subscripts for convenience.

Under the assumption that our system is ergodic, the **infinite time average** of B , which we denote \bar{B} , is equal to the ensemble average $\langle B \rangle_E$, and therefore independent of the initial conditions^{||} of our system.

[¶]See, for example, (Münster 1969).

^{||}given, say, as the microstate of the system at a time t_0

Our statistical mechanics model is based on associating the value of thermodynamic properties with the ensemble averages of corresponding phase functions. This is certainly possible for mechanical properties such as pressure and energy, where such ‘microscopic’ equivalents exist. But how do we deal with the inherently thermodynamic quantities, such as entropy and temperature?

We must find an expression for the entropy that is extensive, and consistent with the laws of thermodynamics (Huang 1963). These requirements are met by choosing the definition

$$S = k \ln \mathcal{Z},$$

whose most famous appearance is on the grave stone of Ludwig Boltzmann. In the case of the shell ensemble, this expression equates the entropy to the logarithm of the extent of the ensemble.

Note that we have not shown the uniqueness of these expressions — indeed, we notice that, independent of our choice of ensemble, either expression for \mathcal{Z} could be used to define the entropy. We shall examine this ostensible dilemma in §1.2.5.

We leave the matter of a statistical mechanical expression for the thermodynamic temperature to Chapter 2.

1.2.4 The Canonical Ensemble

We noted earlier that the uniform probability distribution is invariant under Hamiltonian dynamics, but it is not the only such invariant probability distribution when phase points of differing energies are admitted. Since energy is invariant, any probability distribution that is a function of energy only will also be invariant. Gibbs denoted a particular such probability — $w(\Gamma) = e^{-\beta\mathcal{H}(\Gamma)}$ — as the **canonical distribution**. The **canonical ensemble** consists of the whole of phase space, under the canonical probability distribution. While the microcanonical ensemble seems most appropriately used in modelling closed, isolated systems, the canonical ensemble can be used to represent a closed system at thermal equilibrium with its surroundings — a system at constant *temperature*.

The usual way to arrive at this distribution is to consider a small closed subsystem Σ_1 of a much larger microcanonical ensemble Σ , and to consider the relative probabilities of observing the Σ_1 at different energies. The subsystem is in thermal contact with the rest of the system (denoted Σ_2), so the two have the same temperature. For a given state of the subsystem, the probability of observing that state is proportional to the number of configurations of the rest of the system, ie $w(\Gamma_1) \propto \nu_2(E - E_1(\Gamma_1))$. However

$$\nu_2(E - E_1) = e^{S_2(E - E_1)/k} = e^{S_2(E)/k - E_1 \frac{\partial S_2(E)}{\partial E}} = e^{S_2(E)/k} e^{-\frac{E_1}{kT}}.$$

Cancelling the common factor $e^{S_2(E)/k}$, we obtain the **canonical ensemble partition function**

$$\mathcal{Z}^\beta = \int e^{-\frac{\mathcal{H}(\Gamma)}{kT}} d\Gamma = \int e^{-\beta\mathcal{H}(\Gamma)} d\Gamma.$$

In analogy with the microcanonical ensemble, \mathcal{Z}^β is determined once T , V , and N are known. We can therefore think of the canonical ensemble as the NVT ensemble. The canonical ensemble average of a quantity $B(\Gamma)$ will be denoted $\langle B(\Gamma) \rangle_\beta$.

As with the microcanonical ensemble, mechanical thermodynamic variables are generated from the ensemble average of phase functions. The entropy, however, is not given by $k \ln \mathcal{Z}$. Consider $\mathcal{Z} = e^{-\beta A(V,T)}$. We know $\int e^{-\beta[\mathcal{H}(\Gamma)-A(V,T)]} d\Gamma = 1$. Taking the derivative of both sides leads to $\langle \mathcal{H} \rangle_\beta = A - T \frac{\partial A}{\partial T}$. A designation for A consistent with the laws of thermodynamics is not the entropy, but the **Helmholtz free energy** $A = U - TS$. The entropy is therefore

$$\begin{aligned} S = \frac{\partial kT \ln \mathcal{Z}^\beta}{\partial T} &= k \ln \mathcal{Z}^\beta + kT \left\langle \frac{\partial \mathcal{Z}^\beta}{\partial T} \right\rangle_\beta \\ &= k \ln \mathcal{Z}^\beta + k \left\langle \frac{\mathcal{H}}{T} \right\rangle_\beta \\ &= k \ln \mathcal{Z}^\beta - k \langle \ln w \rangle_\beta = -k \langle \ln f \rangle_\beta. \end{aligned}$$

It is worth noting that this definition is consistent with the microcanonical ensemble. As with the microcanonical ensemble, the infinite time average of B in a system at constant temperature $\bar{B} = \langle B \rangle_\beta$.

We defer our development of statistical mechanical expressions for the thermodynamic temperature until Chapter 2.

1.2.5 The Thermodynamic Limit and Equivalence of Ensembles

In developing the statistical approach outlined in this section, we have aimed to reproduce the macroscopic results of thermodynamics, which hold for systems whose degrees of freedom number in the order of Avogadro's number. The behaviour of systems with only 10s, 100s, or 1000s of degrees of freedom is outside of our experience in a thermodynamic sense, so we can only confirm the validity of our model against the laws of thermodynamics in the limit of a vast number of degrees of freedom. This is the so-called **thermodynamic limit**, the limiting behaviour as $N \rightarrow \infty, V \rightarrow \infty, N/V = \rho$ for some finite, non-zero ρ .

Tacitly assumed in much of the above is proximity to the thermodynamic limit. The extensive quality of thermodynamic properties such as energy and entropy, for example, is only reproduced by our statistical model in the thermodynamic limit. It is important to realise that we are interested in the limit, rather than the limiting case (the infinite system). This will be particularly relevant later on when we compare our theoretical endeavours with computational experiments. For finite-sized systems, we expect discrepancies between the values obtained from our statistical model, and the ‘true’ thermodynamic values of the infinite system. These discrepancies should disappear as the size of the system increases. Using the example of the thermodynamic pressure P and the mechanical equivalent $p(\Gamma)$, the statistical approach assumes that P and $\overline{p(\Gamma(t))}$ are **equal in the thermodynamic limit**, a relation that we denote $P \asymp \overline{p(\Gamma(t))}$.

As we develop different expressions for the temperature, we can only expect them to be equal in the thermodynamic limit. For finite-sized simulated systems, therefore, we will expect discrepancies between these expressions. We will be interested in observing the **order** of these discrepancies, with respect to N . The order of a function $h(N)$ is defined such that

$$h(N) = \mathcal{O}(N^a) \Rightarrow 0 < \lim_{N \rightarrow \infty} \left| \frac{h(N)}{N^a} \right| < \infty.$$

We hope that the discrepancies between our temperature expressions and the thermodynamic temperature will be at least of $\mathcal{O}(1/N)$, so that they will converge relatively quickly in the thermodynamic limit, and we will obtain accurate measures of the temperature for small systems.

For a long period the existence and uniqueness of this limit was assumed, largely on an empirical basis. In the more recent history of statistical mechanics, the existence and uniqueness of the thermodynamic limit have been proven (Ruelle 1969). Associated with this work is the theorem on the **equivalence of ensembles**, an important result which makes rigorous the observations (dating back as far as Gibbs) that the ensemble averages of a phase function, in different ensembles, converge in the thermodynamic limit to $\mathcal{O}(1/N)$. This result is often relied upon in the development of statistical mechanics. It has certainly been used in the development of expressions for the temperature (as we shall see in the next Chapter), usually in applying results from the canonical ensemble to the microcanonical ensemble, since averages in the canonical ensemble are generally more easily calculated.

1.3 Non-Equilibrium Systems

Up to now, all that we have considered has lain in the domain of systems at equilibrium. Temperature also has a role to play in the non-equilibrium domain, however. At the heart of the second law of thermodynamics is the flow of energy, or **heat**, due to a difference in temperature between two systems. One can also consider localising the macroscopic functions of thermodynamics, including temperature, and consider the behaviour of (non-equilibrium) systems where these local functions vary within a system. Outside of a few simple comments in the following chapter, we will have little to say on the application of the theory developed in this thesis to such systems: there are many questions surrounding the nature of temperature in such systems that are beyond the scope of this thesis.

Another set of non-equilibrium systems which we will consider are systems close to equilibrium. In this case, we shall not take on this issue of localised temperatures within the system. Rather, we will look at ways in which to ascribe temperatures to the system as a whole. Many experimental results for close-to-equilibrium systems are conducted, usually when the system is in thermal contact with its surroundings (rather than in isolation from them). Thus it is convenient to be able to conduct computer simulations at constant temperature, rather than at constant energy.

A more suitable framework for describing non-equilibrium systems is provided by Navier-Stokes hydrodynamics. We will look briefly at this approach, inasmuch as we can use it to describe Couette flow — one of the simplest forms of non-equilibrium behaviour, and one that we shall use to test our theoretical work later in this thesis.

1.3.1 Navier-Stokes Hydrodynamics

One of the disadvantages of the microscopic, statistical mechanical approach — even in the equilibrium case — is that the local forces that reflect the ‘push’ from equilibrium are not always known. We can circumvent these problems, however, by introducing additional forces in the equations of motion. These forces may not reproduce the effects found in nature at the microscopic level, but we hope that they will do so on the macroscopic scale — that is, we hope that the averages of microscopic quantities will still correspond with macroscopic properties.

An alternative approach is that of **hydrodynamics**, where we consider the time evolution of the densities of various extensive quantities. Hydrodynamics returns our level of theory to the macroscopic domain. The standard hydrodynamical approach is to combine three balance equations — conservation of mass, energy, and

momentum — with three **linear constitutive relations**. These latter equations, by means of Curie's Law, provide a linear relation between various thermodynamic forces and fluxes, such as the relation between heat flow \mathbf{J}_Q and the temperature gradient ∇T . The coefficients of proportionality between these forces and fluxes are known as **transport coefficients**. In the case of $\mathbf{J}_Q = \lambda \nabla T$, λ is the thermal conductivity. The equations resulting from the combination of these conservation laws and constitutive relations are known as the **Navier-Stokes** equations. While we will not be using the Navier-Stokes equations during this thesis, we can define certain non-equilibrium systems more easily with an understanding of these principles.

Another of these constitutive relations, that will be particularly relevant to our studies of shear flow, relates the pressure to the velocity field. The **pressure tensor** \mathbf{P} is a second-rank tensor whose components $P_{\alpha\beta}$ represent the unit time flow of α -component momentum through unit area in the β direction (where $\{\alpha, \beta\} \in \{x, y, z\}$), and has the form (Evans and Morriss 1990)

$$P_{\alpha\beta}V = \sum_i \frac{(\mathbf{p}_i)_\alpha (\mathbf{p}_i)_\beta}{m_i} - \frac{1}{2} \sum_{ij} (\mathbf{r}_{ij})_\alpha (\mathbf{F}_{ij})_\beta,$$

where \mathbf{p}_i represents the (three-dimensional) momentum vector of particle i , $\mathbf{r}_{ij} = \mathbf{r}_j - \mathbf{r}_i$ represents the **displacement** of particle i from particle j , and \mathbf{F}_{ij} represents the force acting on particle i due to its interaction with particle j . In an atomic fluid, where the lines of force act between centres of mass, the pressure tensor is diagonal. The pressure is given by one-third of the trace of the pressure tensor — in an isotropic fluid, these diagonal elements are equal.

We can similarly define the tensor $\nabla \mathbf{u}$ as the gradient of the velocity field \mathbf{u} , where $[\nabla \mathbf{u}]_{\alpha\beta} = \frac{\partial}{\partial x_\alpha} u_\beta$. We denote by $\overset{\circ}{\mathbf{P}}$ the (traceless) antisymmetric part of \mathbf{P} , so that $\overset{\circ}{\mathbf{P}} = (\mathbf{P} - \mathbf{P}^T)/2$. Similarly, we define $(\overset{\circ}{\nabla \mathbf{u}}) = (\nabla \mathbf{u} - \nabla \mathbf{u}^T)/2$. From the constitutive relation

$$\overset{\circ}{\mathbf{P}} = -2\eta(\overset{\circ}{\nabla \mathbf{u}}), \quad (1.4)$$

we define the (shear) **viscosity** as the transport coefficient η (de Groot and Mazur 1962). We will use this definition to determine the viscosity in our non-equilibrium simulations.

1.3.2 Couette Flow

Couette flow is one of the simplest non-equilibrium systems exhibiting non-zero shearing behaviour, and is therefore an excellent candidate for simple tests of our theory to non-equilibrium systems. Consider a system that is confined between two surfaces in the xz -plane,

separated by a small distance^{**}. At time t_0 , the top surface moves at velocity v in the positive x -direction, and the bottom surface is stationary. The viscous forces in the system cause the particles near the top wall to be dragged along with it — these particles in turn drag their neighbours with them. The Navier-Stokes equations can be used to determine the steady-state solution that these initial conditions lead to. We define the **shear rate** γ for Couette flow as the difference in velocities between the top and bottom surfaces, divided by their separation. Thus, for the plates above separated by a distance L , the shear rate would be v/L . For low enough shear rates^{††}, the steady state solution is an x -velocity profile that depends linearly on y , matching the boundary conditions $u_x(y) = \gamma y$ (Evans and Morriss 1990).

In the linear-profile regime, the only non-zero element of the tensor $\nabla \mathbf{u}$ is $[\nabla \mathbf{u}]_{xy} = \frac{\partial}{\partial y} u_x(y)$. From Eqn.(1.4) we obtain the value of the viscosity in a system undergoing Couette flow

$$\eta = \frac{-P_{xy}}{\gamma}. \quad (1.5)$$

We will consider how one can perform simulations of Couette flow in §1.4.1.

1.4 Computer Simulation Techniques

In order to test the theory that we develop over the course of this thesis, we will conduct computational experiments. Our theoretical endeavours result in various ensemble averages that we cannot evaluate in a closed form, so we shall instead determine these averages through computer simulation. We will use **molecular dynamics** (MD) techniques, meaning that we simulate the time evolution of our system. The key point of MD is not that the path taken be the actual path (or as close as is possible, within the error of our machine), but rather that the results of the simulation — the time average of quantities over these paths — be as close to the actual time averages as possible. We expect these time averages to converge to the infinite time average, and consequently the ensemble average, as the duration of the simulation increases.

We will perform simulations of conservative systems of atomic and rigid-body particles, as well as conservative systems driven away from equilibrium under Couette flow. It is therefore important to understand how one can model both conservative and Couette systems using MD. We shall outline this in §1.4.1. After having de-

^{**}See Fig. 1.2, p.28.

^{††}or, more properly, for low enough **Reynold's numbers** $\gamma \rho m L^2 / \eta$

terminated the equations of motion, we must determine how to calculate the quantities needed to solve these equations. The most problematic of these will be the inter-atomic forces, and we consider how these are determined in §1.4.2. Once we have the equations of motion and know how to determine the necessary quantities at a particular time, we need to consider a method of integrating these equations of motion, which we shall outline in §1.4.3. As we are simulating finite systems of particles, we must also consider how to deal with the boundaries of our system. In our case, we use periodic boundary conditions, as defined in §1.4.4. In this section we will discuss some of the implications of using periodic boundary conditions that we must understand. Finally, we will establish how one obtains the ‘results’ of the simulation — the average values of microscopic quantities that we hope to equate with ensemble averages, and with macroscopic variables (§1.4.5).

1.4.1 SLLOD Dynamics

Our model for Couette flow is based on the behaviour far from the walls of the system, in the linear regime (ie where the linear constitutive relations hold, and where the linear velocity profile is a good approximation). We therefore avoid any surface effects due to contact with the walls, and consider only the properties of the bulk. In order to model this flow, we will use the equations of motion of SLLOD dynamics (Morriss and Evans 1984)^{††}. As Couette flow reduces to Newtonian dynamics in the limit of zero shear, we can use the SLLOD equations of motion for both equilibrium and non-equilibrium simulations.

The equations of motion for SLLOD dynamics are as follows

$$\begin{aligned}\dot{\mathbf{r}}_i &= \frac{\mathbf{p}_i}{m} + \mathbf{r}_i \cdot \nabla \mathbf{u}, \\ \dot{\mathbf{p}}_i &= \mathbf{F}_i - \mathbf{p}_i \cdot \nabla \mathbf{u},\end{aligned}$$

which reduce to

$$\begin{aligned}\dot{\mathbf{r}}_i &= \frac{\mathbf{p}_i}{m} + \mathbf{i}\gamma y_i, \\ \dot{\mathbf{p}}_i &= \mathbf{F}_i - \mathbf{i}\gamma p_{y_i},\end{aligned}\tag{1.6}$$

in the case of Couette flow, where \mathbf{i} represents the unit vector in the x -direction*.

^{††}The name “SLLOD” is obtained from the related DOLLS-tensor equations of motion. Neither of these names are in fact acronyms, but a tongue-in-cheek reference to the form of the DOLLS-tensor Hamiltonian, which contains a term \mathbf{qp} .

*We recall that \mathbf{r}_i , \mathbf{p}_i , and \mathbf{F}_i are the (Cartesian) positions, momenta, and forces of the i -th atom in our system, and γ is the shear rate of the flow.

These equations cannot be derived from a Hamiltonian, and can be best understood from the following exposition (Evans and Morriss 1990). Let us consider the acceleration of a particle, as determined from these equations of motion. We see that

$$\begin{aligned} m\ddot{\mathbf{r}}_i &= m \frac{d}{dt} \dot{\mathbf{r}}_i \\ &= m \frac{d}{dt} \left(\frac{\mathbf{p}_i}{m} + \mathbf{i}\gamma y_i \right) \\ &= \dot{\mathbf{p}}_i + \mathbf{i}m\dot{\gamma}y_i + \mathbf{i}m\gamma\dot{y} \\ &= \mathbf{F}_i - \mathbf{i}\gamma p_{y_i} + \mathbf{i}m\dot{\gamma}y_i + \mathbf{i}m\gamma\dot{y}. \end{aligned}$$

However, from the $\dot{\mathbf{r}}$ equation we know that $m\dot{y} = p_{y_i}$, so that

$$\begin{aligned} m\ddot{\mathbf{r}}_i &= \mathbf{F}_i - \mathbf{i}\gamma p_{y_i} + \mathbf{i}m\dot{\gamma}y_i + \mathbf{i}\gamma p_{y_i} \\ &= \mathbf{F}_i + \mathbf{i}m\dot{\gamma}y_i. \end{aligned} \tag{1.7}$$

As we know, the shear rate γ is constant for Couette flow, so that during the flow the SLLOD equations reduce to Newton's equations. Suppose, though, that for times $t < 0$ our system was at equilibrium. At $t = 0$ the shear is 'switched on'. In this case, $\dot{\gamma}(t) = \gamma\delta(t)$: it is zero everywhere except when $t = 0$, where it is a delta function. From Eqn.(1.7) we find that

$$\dot{q}_i(t_2) - \dot{q}_i(t_1) = \int_{t_1}^{t_2} \frac{F_i(\xi)}{m} d\xi + \mathbf{i}y_i(0)\gamma \int_{t_1}^{t_2} \delta(\xi) d\xi.$$

Thus the SLLOD equations of motion are the same as Newton's equations, except for at time $t = 0$ when the velocities of particles are advanced in proportion to their y coordinate at that time. This has the effect of transforming the equilibrium distribution at $t = 0^-$ (ie just before $t = 0$) to the local-equilibrium distribution with a linear velocity profile at time $t = 0^+$. This is not the steady state distribution, but a useful intermediate distribution. The process of transforming from the equilibrium distribution to the local-equilibrium-with-linear-velocity-profile distribution requires relaxation on a macroscopic scale, and is therefore impossible to achieve during a computer simulation with current facilities. Relaxation from the local-equilibrium-with-linear-velocity-profile distribution to the steady state distribution, however, requires relaxation on the microscopic scale, and is what we obtain during SLLOD simulations of Couette flow.

It is clear that, if $\gamma(t) \equiv 0 \forall t$, then SLLOD reduces to Newtonian mechanics for all times.

So what do the \mathbf{p}_i represent? From the $\dot{\mathbf{r}}_i$ equation, \mathbf{p}_i represents that part of the motion that does not include the velocity term $\mathbf{i}\gamma y = \mathbf{r}_i \cdot \nabla \mathbf{u}$, which is the first term in the Taylor expansion of $\mathbf{u}(\mathbf{r})$.

This first term is referred to as the **zero wavevector profile** — it represents the velocity profile in the limiting case of low shear rates. Consequently, the \mathbf{p}_i are the velocities of the particles *relative to the zero wavevector profile*. Since this profile forms the **streaming velocity**, or average local velocity, at low shear rates, the \mathbf{p}_i are also the velocities of the particles relative to the local stream. Velocities relative to the local stream are called **peculiar velocities**.

At low shear rates, therefore, the \mathbf{p}_i are the peculiar velocities, and can consequently be used to determine the local temperature via the equipartition theorem. We shall return to this concept in Chapter 2.

The equations of motion for SLLOD, as they stand, act to change the energy of the system. These equations can be adapted to run at constant energy or at constant temperature, with extra terms that are functions of γ . We defer the discussion of this adaptation until Chapter 3.

In conclusion, we note a useful property of the SLLOD equations. While they cannot be derived from a Hamiltonian, the equations of motion for Couette flow preserve the extent of a set of points in phase space —

$$\nabla \cdot \dot{\Gamma} = \sum_{i,\alpha} \left(\frac{\partial}{\partial q_{i\alpha}} \mathbf{i}\gamma y_i - \frac{\partial}{\partial p_{i\alpha}} \mathbf{i}\gamma p_{y_i} \right) = N(\mathbf{i}\gamma - \mathbf{i}\gamma) = 0.$$

1.4.2 Force Calculations

We note that the SLLOD equations of motion require knowledge of the \mathbf{r}_i , \mathbf{p}_i , and \mathbf{F}_i as functions of time. While the \mathbf{r}_i and \mathbf{p}_i will automatically be known, since they are the subjects of the equations of motion, we will need additionally to calculate the forces \mathbf{F}_i .

The forces \mathbf{F}_i in the systems we shall examine will be derivable from a potential energy Φ . We employ **pair potentials** — that is, the potential energy of the whole system is the sum of the potential energies ϕ_{ij} associated with each pair of particles i and j . Therefore

$$\Phi = \sum_{\{i,j\}} \phi_{ij},$$

where the summation is over each *pair* $\{i, j\}$. If $\phi_{ij} = \phi_{ji}$, then we have

$$\Phi = \sum_{\{i,j\}} \phi_{ij} = \sum_{i=2}^N \sum_{j=1}^{i-1} \phi_{ij} = \frac{1}{2} \sum_{i=1}^N \sum_{\substack{j=1 \\ j \neq i}}^N \phi_{ij}.$$

In this thesis, we will simulate systems of atomic systems and systems of rigid-body molecules. One of the pair-potentials that we

shall use in this thesis will be the **Lennard-Jones** (LJ) potential, given by

$$\phi_{LJ}(\mathbf{r}_{ij}) = 4\epsilon \left[\left(\frac{\sigma}{r_{ij}} \right)^{12} - \left(\frac{\sigma}{r_{ij}} \right)^6 \right],$$

where $r_{ij} = |\mathbf{r}_{ij}|$ represents the **separation** of particles i and j . The quantities σ and ϵ determine our choice of units for the measurements of length and energy respectively. They are set to $\sigma = \epsilon = 1$ during a simulation, as is the mass of our atoms m and the Boltzmann constant k . Thus, the values we obtain from our simulation are determined in **reduced units**. The numerical values obtained at the end of our simulations can then be ‘translated’ into the real values for a given system, by substituting the appropriate values of σ , ϵ and m^* .

The LJ potential consists of an attractive term ($-r^{-6}$) that represents the dispersion interaction between neutral atoms with induced (non-permanent) electric dipoles (Watts and McGee 1976, §2.2-3, Maitland 1981, §2.2.3), and a repulsive term (r^{-12}) that acts as a barrier to keep atoms apart. The form of this barrier can be somewhat arbitrary, however the choice of r^{-12} is convenient in combination with the dispersion term. Such a potential agrees well with empirically based potentials such as the ‘BMSS’ potential for Argon (Allen and Tildesley 1987; Maitland 1981).

Clearly, the LJ potential is non-zero for almost every separation. Given that we are simulating finite systems, it is convenient to truncate the potential at a predefined separation r_{cutoff} , known as the **cutoff radius**. Given the convergence of the LJ potential to zero for large separations, the errors involved in this approximation are not large, provided $\phi(r_{\text{cutoff}}) \approx 0$. We shall therefore use the following form in our simulations:

$$\phi_{LJ}(r_{ij}) = \begin{cases} 4\epsilon \left[\left(\frac{\sigma}{r_{ij}} \right)^{12} - \left(\frac{\sigma}{r_{ij}} \right)^6 \right] & r_{ij} \leq r_{\text{cutoff}}, \\ 0 & r_{ij} > r_{\text{cutoff}}. \end{cases} \quad (1.8)$$

Usually, r_{cutoff} is set to no less than 3σ . Unless otherwise specified, we will use $r_{\text{cutoff}} = 4.5\sigma$.

When truncated in this fashion, the LJ potential clearly suffers from a discontinuity at r_{cutoff} [†]. One way to avoid this discontinuity is to set the cutoff radius to the minimum of the LJ potential, at $r = 2^{1/6}\sigma \approx 1.12\sigma$. This model, the **Weeks-Chandler-Andersen**

*For a system of argon atoms, for example, $\epsilon = 119.8\text{K}/k_B$, $\sigma = 3.405 \times 10^{-10}\text{m}$ and $m = 0.03994\text{kg/mol}$ (Frenkel and Smit 1996).

†This will lead to errors in the reported values of time averages. However, such effects are minimal at large cutoff radii. Alternatively, corrections can be determined, based on assumptions on the isotropic distribution of particles.

(WCA) potential $\phi_{\text{WCA}}(r_{ij})$, is a purely repulsive potential, and has a continuous derivative at every point. In this sense it is smoother than the truncated LJ model — however, the truncation of the LJ potential at larger separations provides a much smaller perturbation.

Weeks, Chandler and Andersen showed that, for systems with reduced densities $\rho^* \gtrsim 0.5$, the repulsive part of the LJ potential affects the structure of the system much more than the attractive part, so that WCA and LJ liquids are structurally similar (converging in the high-temperature limit) (Weeks, Chandler, and Andersen 1971). However, various differences in the properties of the WCA and LJ fluids, such as in the phase diagram, manifest themselves due to the absence of attractive forces in the WCA model. The WCA potential is therefore not a realistic model of real molecules (except in the high-temperature limit for ideal gases).

The main advantage of the WCA potential over the LJ potential is due to its much shorter range. There are far fewer interactions between particles with a WCA interaction, thus speeding up the simulation considerably relative to an identical system of LJ atoms with a typical cutoff radius. In Chapter 4 our studies will focus on WCA fluids, due to this advantage. In the following chapter we will examine why it is reasonable to anticipate that the similarities between WCA and LJ fluids will enable us to extend our conclusions from studying WCA fluids to LJ fluids as well (and hence to more realistic models).

For our rigid-body systems, we augment the LJ potential to include an anisotropic potential term dependent on the relative orientation of the two bodies. It is a simple potential that is consistent with the Maier-Saupe theory of nematic liquid crystals (Luckhurst and Romano 1980), and is therefore an excellent candidate to test our theory against. It describes a pair-wise interaction between bodies with one axis of symmetry, and therefore depends on the separation r_{ij} of particles, as well as the angle between these axes of symmetry θ_{ij} . We shall refer to this potential as the **P2** potential

$$\phi_{\text{P2}}(r_{ij}, \theta_{ij}) = 4\epsilon \left[\left(\frac{\sigma}{r_{ij}} \right)^{12} - \left(1 + \lambda \frac{3 \cos^2 \theta_{ij} - 1}{2} \right) \left(\frac{\sigma}{r_{ij}} \right)^6 \right], \quad (1.9)$$

where λ represents the anisotropic interaction strength. As with the other potentials, we employ a cutoff when using the P2 potential in a simulation. Since the P2 potential is not spherically symmetric, we set $r_{\text{cutoff}} = 4.5\sigma$.

Having chosen one of the above potentials, we must determine the force on each particle, in order to integrate our equations of motion. This is achieved in the simulation by summing over each pair of particles. Each pair of particles is tested to see whether their

separation is less than the relevant cutoff radius. The potential energy and corresponding force of each such pair interaction is then calculated. The force on each particle can thus be determined by summing up the contributions from each pair.

If each pair of particles must be tested in turn, then we have $N(N - 1)/2 = \mathcal{O}(N^2)$ tests to perform. If the length of the **simulation box** — the cubic (in our case) volume that our molecular system occupies — is greater than three cutoff radii, we employ the **cell code** technique, which reduces the problem to $\mathcal{O}(N)$. We divide the simulation box into a collection of **cells** of equal size, such that the width of each cell is greater than one-half the cutoff radius. If we draw a circle (in 2D, or sphere in 3D) of radius r_{cutoff} around any particle in a given cell, the resultant sphere is confined to this given cell, and its neighbours (8 in 2D, 26 in 3D). Consequently, it is only necessary to check for possible pair interactions either within cells, or between neighbouring cells. In the thermodynamic limit, as we keep the density constant but increase the volume of our system, the average number of checks per particle that we must make remains constant (rendering it $\mathcal{O}(N)$).

Clearly, the smaller we can make our cell-size (given the restriction due to r_{cutoff}), the more efficient our code will be. Systems of LJ particles are often not large enough to gain from this technique, due to the large cutoff radius. However, a similarly sized WCA system, with its much shorter cutoff radius, can gain considerably.

So far we have only considered forces due to interactions between particles. In both thermodynamics and statistical mechanics, however, particles interact not only with other particles, but also with the walls of their container. In our simulations we do not use external forces to contain our system. In section §1.4.4 we will look at the boundary of our system. For the moment, we will consider how to go about solving our equations of motion.

1.4.3 Integration Methods

At the heart of any MD simulation is a numerical integration scheme, or **integrator**, used in order to solve the first-order ordinary differential equations that result from our Hamiltonian formalism. Based on information about the system at a particular time t , the integrator determines an approximate value to the solution of these differential equations at a time $t + \delta t$. This step from values at time t to values at time $t + \delta t$ is called a **timestep**. We shall also use the word **timestep** to refer to the period of time δt between these jumps — the meaning will be clear from the context.

There are several options for our choice of integrator, including the Runge-Kutta method, various Verlet methods and the Gear

predictor-corrector method (for an overview and comparison of these methods, see (Allen and Tildesley 1987; Berendsen and van Gunsteren 1985)). For our work in this thesis we choose the Gear method, partly because it requires only one force calculation per timestep (unlike the Runge-Kutta method), and partly because it can be more easily adapted to non-Hamiltonian equations of motion such as the Nose-Hoover[‡] (§3.2) and isokinetic (§3.5) schemes than can the Verlet methods, which require iterative schemes when the $\dot{\mathbf{p}}$ equation of motion depends on the momenta (Frenkel and Smit 1996). We choose a **fourth-order method**, meaning that the \mathbf{r}_i and \mathbf{p}_i are accurate to $\mathcal{O}((\delta t)^4)$. We note that, for this method, the timestep is constant, and chosen at the beginning of a simulation run.

The Gear method is a **predictor-corrector** method, consisting of three separate stages. The first (predictor) advances the system, based on information gathered on the derivatives (up to 4th order, in our case) of each of the coordinates and momenta being integrated. These predictions are not based on the equations of motion, but rather on the stored derivatives of the coordinates and momenta, utilising the ‘magic numbers’ prescribed by Gear (Gear 1971) to optimize the stability and accuracy of our solution. At the intermediate stage, the derivatives that need to be included in the equations of motion (momenta and forces in the case of the usual Hamiltonian model) are calculated, and used to determine an error in the predicted values. This information is fed in to the final (corrector) stage, which corrects the intermediate values to the final ones. It is these final values that are used to collect information about the system in its travels through phase space.

1.4.4 The Theory of Periodic Boundary Systems

In the systems that we shall examine, what interests us is the **bulk behaviour** of the gas — the interactions between particles away from the influence of the walls of the system. However, these walls, or limits, of the system play an essential role of containment. A system of N particles with no walls would have no hope of being ergodic, and would soon become a collection of particles moving at constant velocity towards infinity.

Empirically, the laws of thermodynamics do not depend on the manner in which particles are kept within the confines of a system, only the confining volume. For a system of diameter L ,[§] this is reasonable when we realise that the interactions with the wall increase

[‡]Strictly speaking, Nose-Hoover is a Hamiltonian scheme, but the energy of the real degrees of freedom is not constant.

[§]ie a system such that, for any two allowed \mathbf{r}_i and \mathbf{r}_j , $|\mathbf{r}_i - \mathbf{r}_j| < L$

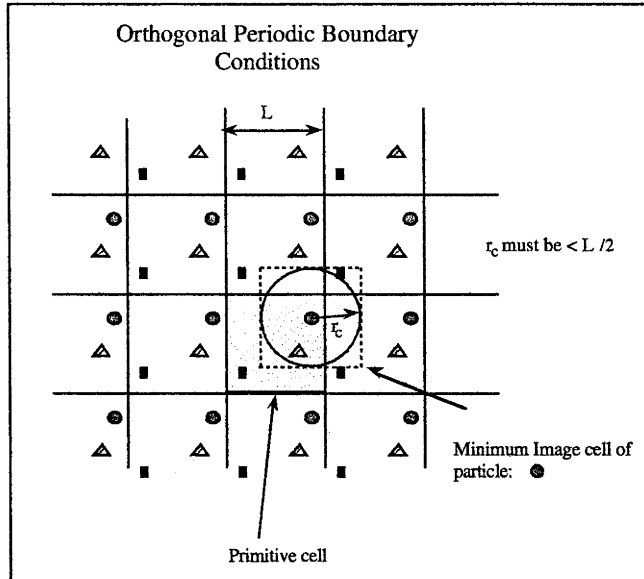


Figure 1.1: The implementation of periodic boundary conditions is tantamount to replicating our system in the x -, y - and z -directions (picture courtesy of (Evans and Morriss 1990)).

in the thermodynamic limit as L^2 — that is, in proportion with the surface area of the confining walls — whereas the interactions within the bulk of the gas increase as L^3 — that is, in proportion with the volume. Thus, although they are essential for maintaining the system, the effects of the walls on the system are, if anything, a distraction from the significant thermodynamic results that we expect from our experiments.

Due to limitations in computational power, it is simply not possible to increase the size of our system sufficiently to remove these[†] finite-size effects from our simulation results (which can converge as slowly as $N^{-1/3}$ (Ladd 1990)). One device that we can employ to reduce these effects, however, is the use of **periodic boundary conditions**. When using periodic boundary conditions, we no longer confine our particles to a volume V by means of a repulsive potential at the walls. Instead, we imagine that the system we are examining is in fact an infinite system of particles, created by the replication of a finite cubic **box** of particles in the x -, y - and z -directions (see Fig. 1.1). As there is now no prohibitive barrier, particles can pass through the imagined boundary of our system. However, when they do so, one of their image particles from an adjacent box will pass into the original cell. Thus, at any point in time, we will have a fixed number of particles in this original box.

There are several different ways of considering **periodic bound-**

[†]or other

ary systems — systems with periodic boundary conditions. They can be thought of as an infinite system with a particular initial configuration that is replicated on a grid throughout space. We can also think of them in terms of a finite system such that when one particle leaves, another is put in with the same velocity, on the opposite wall. This is tantamount to a jump in phase space to a new trajectory. Finally, we can think of them as a set of particles with no boundary, but whose interaction potential is periodic through all of space. We shall revisit this last interpretation in §2.1.

The size of a periodic boundary system has important implications for the force calculations. Clearly the force on any particle is identical to the force on one of its images, so we have N different forces to evaluate. However, each particle effectively interacts with an infinity of other particles (and images). This is indeed a problem for potential energies which do not converge, such as the Coulomb potential^{||}. However, all of the potential energies outlined in the previous section *do* converge^{**}.

Where cutoff radii are employed, the system will not interact with its images provided the cutoff radius is less than one-half the box length. Consequently, we will always ensure that the system size is large enough with respect to the cutoff radius, so that particles can not interact with their images. This condition has an additional feature regarding the interaction of any two particles i and j . For any two such particles, there is a family of vectors $\mathbf{r}_{i'j''} = \mathbf{r}_{j''} - \mathbf{r}_{i'}$ that correspond to the difference between images i' and j'' of the two particles i and j . Only one of these vectors will be less in magnitude than the cutoff radius, however. We call this vector, for a given i and j , the **minimum image displacement** $\tilde{\mathbf{r}}_{ij}$, and we call its magnitude the **minimum image separation** \tilde{r}_{ij} . In Fig. 1.1, the circle and square particles have a minimum image separation of (approximately) r_c , although their separation within the replicated box is much greater.

Finally, we note a special set of boundary conditions that are employed for simulations of Couette flow. We imagine our infinite array of simulation boxes at time t_0 , replicated through space, and then step the Couette flow simulation through time. It is clear that there will be a discontinuity in the velocity profile — as we move in the positive y -direction, the streaming velocity will suffer a jump-discontinuity of γL as we move from one simulation box to the next. This undesirable effect can be corrected by employing **Lees-Edwards boundary conditions** (Lees and Edwards 1972). Under these conditions, the image of the simulation box *above* our central box is moved $\gamma L \delta t$ in the positive x -direction, and the image of the

^{||}which must be dealt with using the theory of Ewald summations

^{**}with or without the use of a cutoff radius

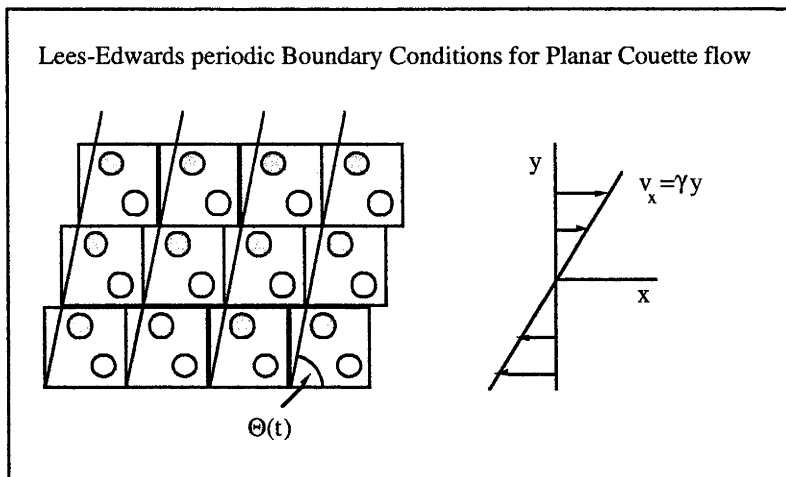


Figure 1.2: Lees-Edwards boundary conditions are consistent with the extension of the linear velocity profile generated by Couette flow into neighbouring images of the simulation box (picture courtesy of (Evans and Morriss 1990)).

simulation box *below* our central box is moved the same amount in the negative x -direction, before minimum-image displacements are determined (see Fig. 1.2). This approach corrects the discontinuity in the velocity profile, and thus permits the use of (skewed) periodic boundaries.

1.4.5 Collecting Averages

Having determined how we simulate our system in its time evolution, we now turn our attention to collecting the ‘results’ of our simulation. Our theoretical considerations lead us to equate the macroscopic observables of the systems we simulate with the infinite time averages of appropriate microscopic properties. We expect these time averages to be independent of the particular trajectory, for almost every^{††} trajectory. Thus, for a given simulation, we expect the average value of a particular function to converge to the macroscopic observable.

The values for a particular quantity that we report in this thesis will be the average of values determined at each time step of the simulation. In order to calculate the errors, we divide the simulation run into ten ‘blocks’, each of length one-tenth the whole simulation, and treat each of these values as ten separate measurements. The error reported is then the standard deviation of these values. This figure is potentially an over-estimate of the errors in the reported average. In order to consider whether this is indeed the case, the sta-

^{††}in a measure-theoretic sense

tistical inefficiency s was estimated using the expression (see Allen and Tildesley 1987)

$$s = \tau_b \left(\frac{\text{RMS}_b(B(t))}{\text{RMS}(B(t))} \right),$$

where τ_b is the number of timesteps per block, $\text{RMS}_b(B)$ is the root-mean-squared error in the block averages recorded for the function $B(t)$, and $\text{RMS}(B(t))$ is the root-mean-squared error in the instantaneous values of $B(t)$. We anticipate a value of $s \approx 22$, in agreement with (Allen and Tildesley 1987). The block errors appear to be a consistent measure of the error in the values for the macroscopic quantity.

1.5 Quaternions and Rigid-Body Dynamics

It is important, for the application of the Hamiltonian approach, that all of our coordinates be independent of one another. For a system of atoms, choosing the x , y , and z axis coordinates for each particle is suitable. If, however, some coordinates are constrained (such as by bond lengths), this independence of coordinates no longer holds. In §2.4.1 we shall look at how to handle such constraints in some detail. For now we simply remark that these constraints can be simulated by the determination of constraint forces, additional to the forces of the otherwise-unconstrained system. Alternatively, we can re-parametrise our system so that the number of coordinates corresponds to the number of degrees of freedom. This approach is generally much more difficult, if not intractable, whence it becomes easier to calculate supplemental forces of constraint.

In the case of molecules whose shape does not change, however, re-parametrisation is possible. When simulations allow motion that changes a molecule's shape (as with freely-jointed chain polymers), the number of degrees of freedom depends on the size and topology of the molecule. A **rigid body** — a molecule that cannot change shape — can be completely described, from a mechanical point of view, by knowing the position of its centre of mass, and its orientation in space.

We have already described a simple potential that we shall consider in testing our theory on rigid bodies. There are technical difficulties in representing orientations in three dimensions, so we shall outline our approach below. Starting briefly with Euler angles, we shall move on to the quaternion, which lends itself more practically to the computer simulation of rigid bodies. We shall then consider how we might formulate a Hamiltonian from the quaternion coordinates, for application in later chapters.

1.5.1 Representing Rotation - Euler Angles

Although the position of the centre of mass of a rigid body in our system will change in time, the axes that we use to define this position do not change. This is the case when, for example, we perform an experiment in a laboratory. Although our laboratory is rotating about a planet rotating about a sun moving through our galaxy at high speed, we consider for the purposes of our experiment that our laboratory forms an inertial frame of reference by which we can measure positions. Consequently, we refer to the system frame of reference as the **laboratory frame**, and the axes of this frame as the **laboratory axes** — the x , y , and z axes.

For a single rigid body, we define the **momenta of inertia tensor** about a set of axes xyz as (MacQuarrie 1976)

$$\begin{aligned}\Theta_{xx} &= \sum_j m_j [(y_j - y_{CM})^2 + (z_j - z_{CM})^2], \\ \Theta_{yy} &= \sum_j m_j [(x_j - x_{CM})^2 + (z_j - z_{CM})^2], \\ \Theta_{zz} &= \sum_j m_j [(x_j - x_{CM})^2 + (y_j - y_{CM})^2], \\ \Theta_{\alpha\beta} &= \sum_j m_j (\alpha_j - \alpha_{CM})(\beta_j - \beta_{CM}) \quad (\alpha, \beta \in \{x, y, z\}, \alpha \neq \beta),\end{aligned}$$

where the sum is over the atoms of the rigid body, and the centre of mass of the body has coordinates (x_{CM}, y_{CM}, z_{CM}) . For each body, we can define the set of **principal axes** as that set of axes $x'y'z'$ for which the moment of inertia tensor is diagonal, and for which $\Theta_{xx} = \Theta_{yy} \neq \Theta_{zz}$ (since we are dealing with bodies with one axis of symmetry)^{‡‡}. Since we will use the principal axes to define a set of axes on each individual rigid body, we also refer to this axis set as the **body axes** for the particular rigid body — the x' , y' , and z' axes. These axes form the **body frame** of reference, for each body. In this frame, $\Theta = \Theta^P$, the principal axis momenta of inertia.

As the body moves in space, the body axes will retain their chirality, but will change their orientation. The new position of the x' axis is a two-parameter problem, corresponding to the position of a point on the unit sphere. Once this position is determined, the new position of the y' axis is a one-parameter problem, corresponding to the position of a point on a unit circle (the great circle forming an equator to the intersection of the x' axis and the unit sphere). Due to the constant chirality, this entirely determines the z' axis, so our new orientation is defined by $2 + 1 = 3$ parameters.

The three parameters that are most pervasively used to describe orientation are the **Euler angles** θ, ϕ, ψ . These angles represent a

^{‡‡}such a set of Cartesian coordinate axes always exists (MacQuarrie 1976)

sequence of three rotations from the laboratory frame to the body frame, about the axes of the intermediate body frames. For each triplet of angles, there are twelve possible resultant transformations (three axes for the first choice, then two on each subsequent choice, since the same axis cannot be rotated twice in a row). The sequence of axes must therefore be chosen in advance. As there is no inherently preferable order, there are several standard conventions (Goldstein 1980).

While this formalism provides a formally exact framework for rigid bodies, it also provides many difficulties. The construction of a Hamiltonian is a tedious but straightforward algebraic problem (Evans 1975), and most applications of Euler angles to simulation avoid this altogether. The standard approaches are to use the angles (θ, ϕ, ψ) and either the body-frame or laboratory-frame angular velocities. Even here, there are problems. The equations of motion for the Euler angles are given by (Allen and Tildesley 1987)

$$\begin{aligned}\dot{\phi} &= -\omega'_x \frac{\sin \phi \cos \theta}{\sin \theta} + \omega'_y \frac{\cos \phi \cos \theta}{\sin \theta} + \omega'_z, \\ \dot{\theta} &= \omega'_x \cos \phi + \omega'_y \sin \phi, \\ \dot{\psi} &= \omega'_x \frac{\sin \phi}{\sin \theta} - \omega'_y \frac{\cos \phi}{\sin \theta} + \omega'_z.\end{aligned}$$

Whilst integration of these equations will lead to exact solutions, numerical integration becomes problematic as $\sin \phi \rightarrow 0$. Efforts to circumvent this problem include switching between two coordinate frames, so that in the new coordinate frame $\sin \phi$ is not zero (Barojas, Levesque, and Quentrec 1973). These methods are not continuous, as well as being computationally cumbersome and inelegant. An alternative, efficient*, and elegant approach to this problem (Evans 1977) is to use quaternions.

1.5.2 Hamilton's Quaternion

The history of the quaternion includes contributions from luminaries such as Euler (Euler 1776) and Gauss. However, the 'lion's share' of their development occurred at the hands of Hamilton (Bell 1965). Hamilton's quaternion originated from a study of vectors. If we consider two points in real space, then the position of the second with respect to the first (origin) can be given using three parameters (such as x , y , and z positions). Similarly, Hamilton reasoned that the relative position of two vectors can be determined using *four* parameters (Hamilton 1969). These four parameters essentially determine a unit vector about which to rotate, an amount to rotate, and a rescaling factor.

*Evans and Murad 1977

It is interesting to note that only three parameters are required to perform this transformation. The Euler angles θ, ϕ, ψ will take us to the new frame of reference, and a scaling factor will change the size of the vector. However, a vector is symmetric about one axis, so that by choosing this axis as our body frame z' -axis, the Euler angle ψ is redundant. The process thus requires $4 - 1 = 3$ parameters.

If the question had been to rotate a body with no axis of symmetry (such as a potato) from one position to another, and rescale, then the problem would indeed require four parameters. In this case, Hamilton's quaternion provides a convenient formalism. Furthermore, even if we remove the need to rescale (as is the case for describing the motion of rigid bodies), the mathematical properties of the formalism avoid the difficulties of integrating the equations of motion, as we shall see. To begin with, we define the quaternion — the '4-vector' representing the four parameters — along the same lines as was done by Hamilton.

Imagine that we wish to rotate a vector \mathbf{r} through an angle Φ , about an axis \mathbf{n} . What is the new vector \mathbf{r}' ? We can solve this problem (Goldstein 1980) by decomposing the vector \mathbf{r} into two parts — the part parallel to \mathbf{n} and the part perpendicular to it. Clearly the parallel part will not change, and the perpendicular part will swing around \mathbf{n} . The new vector \mathbf{r}' can be written in terms of $\mathbf{r}, \hat{\mathbf{n}}$ (where $\hat{\mathbf{n}} = \mathbf{n}/|\mathbf{n}|$) and Φ as follows:

$$\mathbf{r}' = \hat{\mathbf{n}}(\hat{\mathbf{n}} \cdot \mathbf{r}) + [\mathbf{r} - \hat{\mathbf{n}}(\hat{\mathbf{n}} \cdot \mathbf{r})] \cos \Phi + (\mathbf{r} \times \hat{\mathbf{n}}) \sin \Phi. \quad (1.10)$$

If we define a **quaternion** $\mathbf{Q} = (q_0, q_1, q_2, q_3)$ such that

$$\begin{aligned} q_0 &= \cos \frac{\Phi}{2}, \\ \mathbf{q} &= (q_1, q_2, q_3) = \hat{\mathbf{n}} \sin \frac{\Phi}{2}, \end{aligned} \quad (1.11)$$

then we have

$$\mathbf{r}' = \mathbf{r}(q_0^2 - q_1^2 - q_2^2 - q_3^2) + 2\mathbf{q}(\mathbf{q} \cdot \mathbf{r}) + 2(\mathbf{r} \times \mathbf{q})q_0. \quad (1.12)$$

From this relationship we can define a rotation matrix \mathbf{R} which represents this transformation in Cartesian coordinates, so that $\mathbf{r}' = \mathbf{R}(\mathbf{Q})\mathbf{r}$ for the Cartesian representation of \mathbf{r}' and \mathbf{r} . \mathbf{R} has the form

$$\mathbf{R}(\mathbf{Q}) := \begin{bmatrix} q_0^2 + q_1^2 - q_2^2 - q_3^2 & 2q_1q_2 + 2q_0q_3 & 2q_1q_3 - 2q_0q_2 \\ 2q_1q_2 - 2q_0q_3 & q_0^2 - q_1^2 + q_2^2 - q_3^2 & 2q_2q_3 + 2q_0q_1 \\ 2q_1q_3 + 2q_0q_2 & 2q_2q_3 - 2q_0q_1 & q_0^2 - q_1^2 - q_2^2 + q_3^2 \end{bmatrix}. \quad (1.13)$$

The **determinant** of $\mathbf{R}(\mathbf{Q})$, denoted by $R(\mathbf{Q})$, is therefore

$$R(\mathbf{Q}) = (q_0^2 + q_1^2 + q_2^2 + q_3^2)^3 = \left(\cos^2 \frac{\Phi}{2} + |\hat{\mathbf{n}}|^2 \sin^2 \frac{\Phi}{2}\right)^3 = 1, \quad (1.14)$$

as expected of a rotation matrix.

Clearly, we have used four parameters to present this three-parameter problem — the additional degree of freedom is lost when we constrain $|\mathbf{\Omega}| \equiv 1$. What happens when we remove this constraint? We obtain $\mathbf{R}(\mathbf{\Omega}) = \mathbf{R}(\hat{\mathbf{\Omega}}|\mathbf{\Omega}|) = \mathbf{R}(\hat{\mathbf{\Omega}})|\mathbf{\Omega}^2|$. $\mathbf{R}(\hat{\mathbf{\Omega}})$ is a rotation matrix, since $|\hat{\mathbf{\Omega}}| \equiv 1$. The additional degree of freedom corresponds to a dilation of space by a factor of $|\mathbf{\Omega}^2|$.

It is worth noting that this extension will conserve the chirality of the object acted upon by $\mathbf{R}(\mathbf{\Omega})$, since $R(\mathbf{\Omega}) > 0 \forall \mathbf{\Omega}$. Indeed, $\mathbf{R}(\mathbf{\Omega}) = \mathbf{R}(-\mathbf{\Omega})$.

1.5.3 Quaternion Mathematics

Quaternions[†] are extremely interesting mathematical objects. Although it is not appropriate here to go into the details of this mathematics at length, several of these properties will be useful in our representation of the orientation of a molecule by quaternions. At this point, then, we will highlight these properties.

It is well known that the set of rotations forms a (non-Abelian) group, where the group operation represents the application of consecutive rotations. When represented by matrices, this operation is simply the usual matrix product (which is not commutative). Since the (normalised) quaternion is merely another way of representing rotations, there must be a (non-commutative) product of quaternions such that, under this product, the quaternion group is isomorphic to the group of rotations.

Thus the form of the quaternion product, which we shall denote by \otimes , must be such that $\mathbf{R}(\mathbf{\Omega}_2 \otimes \mathbf{\Omega}_1) = \mathbf{R}(\mathbf{\Omega}_2)\mathbf{R}(\mathbf{\Omega}_1)$. This product is not trivially deduced by multiplying two rotation matrices and determining the form of the new quaternion from the elements of the product matrix. The quadratic form of the elements of $\mathbf{R}(\mathbf{\Omega})$ exacerbates this problem. By using the properties of the determinant and trace of the matrix, and taking the special cases when either of the rotations is the identity, one can derive the quaternion product, which has the following form, for quaternions $\mathbf{\Omega}_A = [\mathbf{a}_0, \mathbf{a}_1, \mathbf{a}_2, \mathbf{a}_3] = [\mathbf{a}_0, \mathbf{a}]$ and $\mathbf{\Omega}_B = [\mathbf{b}_0, \mathbf{b}]$:

$$\mathbf{\Omega}_B \otimes \mathbf{\Omega}_A = [\mathbf{b}_0\mathbf{a}_0 - \mathbf{b} \cdot \mathbf{a}, \mathbf{b}_0\mathbf{a} + \mathbf{a}_0\mathbf{b} - \mathbf{b} \times \mathbf{a}]. \quad (1.15)$$

The cross product term ensures that the quaternion product is indeed non-commutative. It is bi-linear, and can thus be re-written in the following form, which shall prove useful in the next section:

$$\mathbf{\Omega}_B \otimes \mathbf{\Omega}_A = \Xi(\mathbf{\Omega}_A)\mathbf{\Omega}_B, \quad (1.16)$$

[†]or more strictly, real quaternions, where each element is a real number.

where

$$\Xi(\mathbf{Q}) = \begin{bmatrix} q_0 & -q_1 & -q_2 & -q_3 \\ q_1 & q_0 & q_3 & -q_2 \\ q_2 & -q_3 & q_0 & q_1 \\ q_3 & q_2 & -q_1 & q_0 \end{bmatrix}. \quad (1.17)$$

We can easily extend this group isomorphism over the set of all quaternions under this product, corresponding to the group of rotations with (positive) dilation. Being a group ensures us of closure, a multiplicative identity $(1, 0, 0, 0)$, and the unique definition of an inverse \mathbf{Q}^{-1} for each \mathbf{Q} .

Indeed, the set of quaternions is a non-commutative field[†] under the operations of multiplication, thus defined, and addition, where elements are summed in the usual fashion for vectors. A similar extension can be applied to the set of rotations with dilation matrices, with addition defined in the usual way — however, the isomorphism between the two breaks down if addition is defined in this manner[§]. Thus, when we consider the equations of motion for the quaternion in terms of consecutive rotations, we must confine ourselves to the quaternion group, rather than the quaternion field.

We note in conclusion that $\Xi(\mathbf{Q})$ has some useful properties:

$$\begin{aligned} \det(\Xi(\mathbf{Q})) &= \mathbf{Q}^4, \\ \Xi(\mathbf{Q})\Xi^T(\mathbf{Q}) &= \mathbf{Q}^2\mathbf{I}, \end{aligned} \quad (1.18)$$

where \mathbf{I} is the identity matrix.

1.5.4 Quaternion Dynamics

Suppose at time $t = 0$ a molecule is in an orientation described by the quaternion $\mathbf{Q}(0)$. This could, for example, be the quaternion describing the body axes as a rotation from the laboratory axes. After a short time δt it is now in a new configuration. This new configuration can be considered to be a re-orientation of the previous system - that is, $\mathbf{Q}(\delta t) = \mathbf{Q}_\delta \otimes \mathbf{Q}(0)$, for some (small) re-orientation quaternion \mathbf{Q}_δ . From Taylor's Theorem, we have that

$$\begin{aligned} \mathbf{Q} + \dot{\mathbf{Q}} \cdot \delta t &= \mathbf{Q}_\delta \otimes \mathbf{Q} \\ \dot{\mathbf{Q}} \cdot \delta t &= (\mathbf{Q}_\delta \otimes \mathbf{Q}) - \mathbf{Q} \\ &= (\mathbf{Q}_\delta - 1) \otimes \mathbf{Q}, \end{aligned} \quad (1.19)$$

since distributivity is a quaternions field property.

[†]sometimes called a corpus - see (Val 1964)

[§]A simple example is when $\mathbf{Q}_A = (1, 0, 0, 0)$ and $\mathbf{Q}_B = (2, 0, 0, 0)$. Interestingly, an isomorphism can be constructed between the field of (real) quaternions and a subset of the complex 2×2 matrices, with the usual multiplication and addition.

Clearly $\mathbf{\Omega}_\delta(0) = 1$, since in this limit the original quaternion does not change. We therefore assume that $\mathbf{\Omega}_\delta$ has the following form :

$$\mathbf{\Omega}_\delta(t) = \left[(1 + a(t)) \cos \frac{\delta(t)}{2}, (1 + a(t)) \hat{\mathbf{n}}(t) \sin \frac{\delta(t)}{2} \right], \quad (1.20)$$

where $a(0) = 0, \delta(0) = 0$. Written as a Taylor expansion in δt , we have, to first order

$$\begin{aligned} \mathbf{\Omega}_\delta(t) - 1 &= \left[(1 + \dot{a}t) \left(1 - \frac{\dot{\delta}^2 t^2}{8} \right) - 1, (1 + \dot{a}t) \frac{\dot{\delta}t}{2} (\hat{\mathbf{n}} + \dot{\hat{\mathbf{n}}}t) \right] \\ &= \left[\dot{a}, \hat{\mathbf{n}} \frac{\dot{\delta}}{2} \right] t + \mathcal{O}(t^2). \end{aligned} \quad (1.21)$$

We notice that \dot{a} is the rate of change of $|\mathbf{\Omega}|$, and that $\hat{\mathbf{n}}\dot{\delta}/2$ is simply $\boldsymbol{\omega}'/2 = (\omega'_x, \omega'_y, \omega'_z)/2$: one half the body-axes angular velocities. Consequently we denote this quaternion by $\mathbf{\Omega}/2$. Substituting Eqn.(1.21) into Eqn.(1.19) in the limit $t \rightarrow 0$ gives us

$$\dot{\mathbf{\Omega}} = \frac{1}{2} \mathbf{\Omega} \otimes \mathbf{\Omega} = \frac{1}{2} \Xi(\mathbf{\Omega}) \mathbf{\Omega}. \quad (1.22)$$

During a computer simulation, the angular velocities are calculated in the body frame. Thus the elements of $\mathbf{\Omega}$, and consequently the elements of $\dot{\mathbf{\Omega}}$, are straightforward to determine. Furthermore, we know from Eqn.(1.18) that these equations will not be singular as long as $|\mathbf{\Omega}| \neq 0$.

Having determined the equations of motion for $\dot{\mathbf{\Omega}}$, we must also determine the equations of motion for the body-frame angular velocities, to incorporate the intermolecular torques into our simulation. In the laboratory frame, we have the rotational equivalent of Newton's equation, $\boldsymbol{\tau} = \dot{\mathbf{L}}$, where \mathbf{L} represents the angular momentum of a molecule, and $\boldsymbol{\tau}$ the torque applied to it. In the body frame, we must take coriolis effects into account, resulting in the relation $\boldsymbol{\tau}' = \boldsymbol{\omega}' \times \mathbf{L}' + \dot{\mathbf{L}}' = \boldsymbol{\omega}' \times \Theta^P \boldsymbol{\omega}' + \Theta^P \dot{\boldsymbol{\omega}}'$. This equation, along with Eqn.(1.22), form the first-order differential equations that we must solve to determine the dynamics of our system.

1.5.5 The Hamiltonian Formalism with Quaternions

It would seem appropriate, given that we are going to use Hamilton's quaternions to represent orientations in our model, to use Hamilton's formalism for their mechanics. It is also appropriate, given that we

will use the Hamiltonian formalism to develop our theories on different expressions for the temperature of a system. This approach has some difficulties, however, stemming from the over-parametrisation of our problem that results from using quaternions to model the orientation of molecules. We will outline these difficulties in this section.

Given that the introduction of quaternions was primarily to remove the difficulty in integrating the Euler angle equations of motion, one could conceivably dispense with the quaternions once they had served that purpose, and return to the Euler angle description of the problem for matters such as the calculation of temperatures. There are two main objections to this approach, however. First, the conjugate momenta of the Euler angles are algebraically complex, as is the final form of the Hamiltonian. The expressions that must be averaged would become very complicated — indeed, it is possible that they would suffer from the same singularities as the equations of motion when integrated — and it is desirable to find a simpler alternative. Second, the transformation from quaternions to Euler angles is not as simple as the reverse process, by which the quaternions are defined. Great care must be taken with the inverse trigonometric functions, with the added difficulty that there are two (equal but opposite) quaternions that represent each rotation. We hope, in developing a Hamiltonian formalism using quaternions, to avoid the complicated and unifying algebra surrounding the Euler angle approach.

The difficulty with developing a Hamiltonian formalism for quaternions lies in the need of a physically meaningful interpretation of all four parameters. We recall that one of the conditions of being able to use a Hamiltonian approach was that the number of coordinates matches the number of degrees of freedom (§1.2.1). Clearly, three of the four quaternionic degrees of freedom represent rotations in three dimensions. Dilation, however, is not a commonly observed physical phenomenon for rigid bodies! We must find a meaning for this additional degree of freedom within our formalism, so that, when we choose to remove it, we can do so in a way that is consistent with this formalism.

The four-parameter problem that we shall model using the quaternion is a ‘potato-on-a-wire’ problem. Suppose we have a body with no axis of symmetry that is ‘skewered’ on a wire, rotating freely in space about an origin in space. This is a four parameter problem — three describe the orientation of the wire (and potato) in space, and the fourth describes how far along the wire the potato is from the origin. At first glance, this problem seems to be perfectly suited to description via quaternions. There are problems, however.

Let us consider the ‘potato-on-a-wire’ problem when the potato

is at the origin. Here there are three degrees of freedom — the wire (and potato) are still free to rotate. However, the quaternion representation at this point must be $(0,0,0,0)$ *no matter what the orientation*. This arises from the dilation model — the rotation with dilation corresponding to $(0,0,0,0)$ reduces any body to a point at the origin. Having no degrees of freedom at the origin implies that we no longer have a rigid body, but a point — finding a physical system with these properties is seemingly impossible.

However, it is not crucial that our model work in a neighbourhood of the zero quaternion. While the four parameters must be free to vary independently, we are able to place arbitrary restrictions on their ranges. If we were to model a potato constrained between two points distance $d_1, d_2 > 0$ along the wire, then we would be free to use quaternions such that $d_1 < |\mathbf{\Omega}| < d_2$, for example. Using this model, then, we will construct a Hamiltonian for our system.

We begin by considering the Lagrangian for the system. The kinetic term consists of four contributions — three from the rotation of the wire (and potato), the fourth from the potato's motion along the wire. In our model, the position of the potato along the wire is given by $a = |\mathbf{\Omega}|$. The potential term is arbitrary. Hence we obtain the Lagrangian

$$\begin{aligned}
 \mathcal{L} &= \sum_i \frac{1}{2} (\Theta_{xx}^P + ma^2) \omega_{xi}'^2 + \frac{1}{2} (\Theta_{yy}^P + ma^2) \omega_{yi}'^2 + \frac{1}{2} \Theta_{zz}^P \omega_{zi}'^2 + \frac{1}{2} m \dot{a}^2 - \Phi(\mathbf{\Omega}) \\
 &= 2 \sum_i \mathbf{\Omega}_i^T \mathbf{M} \mathbf{\Omega}_i - \Phi(\mathbf{\Omega}) \\
 &= 2 \sum_i (\Xi^{-1}(\mathbf{\Omega}_i) \dot{\mathbf{\Omega}}_i)^T \mathbf{M} (\Xi^{-1}(\mathbf{\Omega}_i) \dot{\mathbf{\Omega}}_i) - \Phi(\mathbf{\Omega}) \\
 &= 2 \sum_i \dot{\mathbf{\Omega}}_i^T \Xi^{-1T}(\mathbf{\Omega}_i) \mathbf{M} \Xi^{-1}(\mathbf{\Omega}_i) \dot{\mathbf{\Omega}}_i - \Phi(\mathbf{\Omega}),
 \end{aligned} \tag{1.23}$$

where

$$\mathbf{M} = \begin{bmatrix} m & 0 & 0 & 0 \\ 0 & \Theta_{xx}^P + ma^2 & 0 & 0 \\ 0 & 0 & \Theta_{yy}^P + ma^2 & 0 \\ 0 & 0 & 0 & \Theta_{zz}^P \end{bmatrix}. \tag{1.24}$$

The Hamiltonian formulation replaces $\dot{\mathbf{\Omega}}_i$ with

$$\begin{aligned}
 \mathfrak{P}_i &= \frac{\partial \mathcal{L}(\mathbf{\Omega}, \dot{\mathbf{\Omega}})}{\partial \dot{\mathbf{\Omega}}_i} \\
 &= 4 \Xi^{-1T}(\mathbf{\Omega}_i) \mathbf{M} \Xi^{-1}(\mathbf{\Omega}_i) \dot{\mathbf{\Omega}}_i.
 \end{aligned} \tag{1.25}$$

The Lagrangian \mathcal{L} is replaced with the Hamiltonian[¶]

$$\begin{aligned} h &= \dot{\mathbf{q}}_i^T \mathfrak{P}_i - \mathcal{L} \\ &= 2 \sum_i \dot{\mathbf{q}}_i^T \Xi^{-1T}(\mathbf{q}_i) \mathbf{M} \Xi^{-1}(\mathbf{q}_i) \dot{\mathbf{q}}_i + \Phi(\mathbf{q}). \end{aligned} \quad (1.26)$$

By definition, however, the Hamiltonian must be a function of the \mathfrak{P}_i and \mathbf{q}_i . We therefore invert Eqn.(1.25) in the usual fashion, to give

$$\dot{\mathbf{q}}_i = \frac{1}{4} \Xi(\mathbf{q}_i) \mathbf{M}^{-1} \Xi^T(\mathbf{q}_i) \mathfrak{P}_i. \quad (1.27)$$

Thus the Hamiltonian can be written as

$$\begin{aligned} \mathcal{H} &= 2 \sum_i \left(\frac{1}{4} \Xi(\mathbf{q}_i) \mathbf{M}^{-1} \Xi^T(\mathbf{q}_i) \mathfrak{P}_i \right)^T \Xi^{-1T}(\mathbf{q}_i) \mathbf{M} \Xi^{-1}(\mathbf{q}_i) \frac{1}{4} \Xi(\mathbf{q}_i) \mathbf{M}^{-1} \Xi^T(\mathbf{q}_i) \mathfrak{P}_i + \Phi(\mathbf{q}) \\ &= \frac{1}{8} \sum_i \mathfrak{P}_i^T \Xi(\mathbf{q}_i) \mathbf{M}^{-1} \Xi^T(\mathbf{q}_i) \Xi^{-1T}(\mathbf{q}_i) \mathbf{M} \Xi^{-1}(\mathbf{q}_i) \Xi(\mathbf{q}_i) \mathbf{M}^{-1} \Xi^T(\mathbf{q}_i) \mathfrak{P}_i + \Phi(\mathbf{q}) \\ &= \frac{1}{8} \sum_i \mathfrak{P}_i^T \Xi(\mathbf{q}_i) \mathbf{M}^{-1} \Xi^T(\mathbf{q}_i) \mathfrak{P}_i + \Phi(\mathbf{q}). \end{aligned} \quad (1.28)$$

[¶]denoted h , as it is not yet written in terms of canonical pairs

Chapter 2

Generalised Temperature Expressions

This chapter will focus on the derivation of expressions that can be used to determine the temperature of a system. It will be broken into five parts. Initially, we will examine temperature expressions that appear in the literature (§2.1). We will then focus on the recent work of Rugh, who has furnished a family of expressions for the thermodynamic temperature of a microcanonical ensemble. In §2.2 we explore his derivation, as well as looking at two extensions of his work. After this, we derive a more general expression for the temperature (§2.3), demonstrating that it can be used to derive the temperature expressions in §2.1 and §2.2, as well as generating others. We will then examine some extensions of this work, in order to determine under what conditions the use of this more general result can be justified (§2.4). Finally, in §2.5, we derive the **microscopic temperature expressions** — temperature expressions written explicitly as a function of the chosen coordinate system — that we will test in Chapter 4 of this thesis.

2.1 Existing Temperature Expressions

Until recently, there have been few different expressions for the temperature of a system, in terms of its microscopic variables. The predominant expression, almost universally employed, comes about from the **Equipartition theorem**. The Equipartition theorem is so called because it demonstrates that the average energy of an ideal gas is equally distributed among its degrees of freedom. The nominal emphasis is in this isotropy among the degrees of freedom. However, its main use lies in the association with the temperature of the system.

The simplest derivation of the Equipartition theorem — the result $K = \frac{3}{2}NkT$, where K represents the (kinetic) energy of an ideal

gas — is recognizable even to students of high school physics. In this form, it is usually derived from the ideal gas law $PV = NkT$ by invoking Newton's laws of motion, in particular $\dot{p} = F$. The pressure term in the ideal gas law can then be related to the momenta of particles, by considering the force per unit area exerted on particles by the wall.

In 1918, Tolman generalised this result to systems whose energy includes a non-zero potential (Tolman 1918). This Generalised Equipartition theorem is proven for the canonical ensemble by an elegant consideration of the energy of the system.

From the product rule for differentiation we have

$$\frac{d}{d\Gamma_i} \Gamma_i e^{-\beta\mathcal{H}(\Gamma)} = e^{-\beta\mathcal{H}(\Gamma)} - \Gamma_i e^{-\beta\mathcal{H}(\Gamma)} \beta \frac{\partial\mathcal{H}}{\partial\Gamma_i}.$$

for a single phase variable Γ_i^* . Integrating this with respect to Γ_i over its range of possible values (a, b) gives us

$$\Gamma_i e^{-\beta\mathcal{H}(\Gamma)} \Big|_{\Gamma_i=a}^{\Gamma_i=b} = \int_a^b e^{-\beta\mathcal{H}(\Gamma)} d\Gamma_i - \int_a^b \Gamma_i e^{-\beta\mathcal{H}(\Gamma)} \beta \frac{\partial\mathcal{H}(\Gamma)}{\partial\Gamma_i} d\Gamma_i. \quad (2.1)$$

The surface term on the left becomes the focus of our analysis. If the phase variable Γ_i is a momentum, then $(a, b) = (-\infty, +\infty)$. Since the kinetic energy is a quadratic form (Goldstein 1980), $\mathcal{H} \rightarrow \infty$ much faster than $\Gamma_i \rightarrow \infty$. Consequently, the left hand side of Eqn.(2.1) is zero for any momentum variable.

If, on the other hand, Γ_i is a coordinate, then the range (a, b) will be an interval of finite length[†]. It may seem, at first glance, that we can go no further in evaluating the surface term. But what does it mean for particles to be bound so that a position coordinate lies within (a, b) ? How is this achieved? It is achieved by stopping particles from straying beyond this interval, which is done in the real world by some force field which does not permit particles to leave the system. These forces must be large enough to stop any particle from crossing this barrier, and are represented by a potential that goes to infinity as the wall is approached[‡]. Thus, as with the momenta, the energy goes to infinity at the limits of integration. Since a and b are finite, the surface term is zero for any coordinate.

We therefore have that

$$\int_a^b e^{-\beta\mathcal{H}(\Gamma)} d\Gamma_i = \beta \int_a^b e^{-\beta\mathcal{H}(\Gamma)} \Gamma_i \frac{\partial\mathcal{H}}{\partial\Gamma_i} d\Gamma_i.$$

*No summation convention is being used here.

[†]There are subtleties in this argument with regard to the thermodynamic limit. We must either assert that our finite system is close enough to the thermodynamic limit for the canonical distribution to be substantially correct — a reasonable assertion — or consider some limiting process as $N \rightarrow \infty$.

[‡]In principle, it is not necessary to have a barrier of *infinite* potential energy, but certainly large enough to stop any particle from passing this point.

Integrating over the other coordinates yields

$$\frac{1}{\beta} = kT = \frac{\int e^{-\beta\mathcal{H}(\Gamma)} \Gamma_i \frac{\partial \mathcal{H}}{\partial \Gamma_i} d\Gamma}{\int e^{-\beta\mathcal{H}(\Gamma)} d\Gamma} = \left\langle \Gamma_i \frac{\partial \mathcal{H}(\Gamma)}{\partial \Gamma_i} \right\rangle_{\beta}. \quad (2.2)$$

The Equipartition theorem is also proven for the microcanonical ensemble (Münster 1969; Huang 1963). Such proofs use the equivalence of the various definitions of the entropy in the microcanonical ensemble.

In the case where Γ_i is known to be a momentum, this result becomes $kT = \langle p_i^2/m \rangle^{\S}$, and we shall refer to it as the **Equipartition theorem**. In the case where Γ_i is known to be a coordinate, this result becomes $kT = \langle -q_i F_i \rangle$, and we shall refer to it as the **Clausius virial theorem**[¶]. In the case where it is not known whether Γ_i is a momentum or a coordinate, we shall call this result the **Generalised Equipartition theorem**.

The above proof does not hold in period boundary systems, where the potential energy does not go to infinity at the limits of the system. Indeed, from the above argument, it is trivial that the left hand side does not go to zero. Should a particle be at a^+ or at b^- (ie just inside the boundaries of the system), then the Hamiltonian will be the same value, but $ae^{-\beta\mathcal{H}} \neq be^{-\beta\mathcal{H}}$ unless $a = b$, which is clearly not the case. A similar problem arises in the microcanonical case.

Given the importance of the boundary conditions for the Clausius virial theorem, it is generally only used by practitioners of molecular simulations to determine the *pressure* of the system (Allen and Tildesley 1987). For a real system, we can break the force contributions into two parts — interactions between particles, and interactions between particles and the wall. These contributions are known as **internal forces** and **external forces** respectively. For the periodic system, we can apply a similar breakdown, between interactions which act *through* the boundaries of our system, and those which do not. Here, the interactions through the walls constitute *external forces*.

In the real system, the external forces are associated with the pressure of the system. We can define (Allen and Tildesley 1987, p.47-8) an ‘internal’ virial and an ‘external’ virial (associated with the internal and external forces respectively). The temperature is associated with the total virial, while the pressure is associated with the external virial only. Consequently, by calculating the temperature through other means (such as the Equipartition theorem) and

[§]Note that we omit a subscript β or E , indicating that the result is generally applicable in either ensemble.

[¶]since $\sum_i q_i \dot{p}_i$ is known as the **virial** in classical mechanics (Goldstein 1980)

calculating the internal virial during a computer simulation of the real system, one can determine the pressure of the real system.

This result is most easily derived in the canonical ensemble, where the thermodynamic pressure $p = -\partial A/\partial V$. The partition function's dependence on V can be made explicit through a clever rescaling of the coordinates (Green 1969), whereby the above result can be made rigorous. By the nature of the rescaling, this result can be applied in periodic boundary systems.

For a microcanonical system, the existing derivations are more complicated. The extension to period boundary systems is fraught with difficulty, sometimes leading to error^{||}. Erpenbeck and Wood's proof uses the 'infinite checkerboard' model, where particles stray through all of space, but interact through periodic potentials. This translates easily to periodic boundary systems, as the total momentum is zero** (Erpenbeck and Wood 1977). Such derivations equate the microscopic concept of pressure — the average momentum flux through a unit area of surface — with the thermodynamic concept. Using Rugh's dynamical approach to determining thermodynamic properties, we will give a simple, direct proof — valid for periodic boundary systems — that gives the same resultant expression for the thermodynamic pressure (§2.2.3). This proof, however, is restricted to equilibrium systems.

Outside the Equipartition result, there are few additional expressions for the temperature of a system in terms of its microscopic variables in the literature, and their application is extremely limited.

The Hypervirial theorems (Gray and Gubbins 1984, App. E) are based on the result that, for a system in thermal equilibrium, $\dot{\bar{\mathcal{A}}} = 0$ for a phase function \mathcal{A} . This result leads to (Gray and Gubbins 1984, Eqn E.27)

$$\overline{\sum_i \frac{\partial \mathcal{A}}{\partial q_i} \frac{\partial \mathcal{H}}{\partial p_i}} = \overline{\sum_i \frac{\partial \mathcal{A}}{\partial p_i} \frac{\partial \mathcal{H}}{\partial q_i}}.$$

For a particular choice of \mathcal{A} , we can separate out terms involving $\overline{\sum_i p_i^2/m}$, which we can associate with the temperature of the system. For example, choosing $\mathcal{A} = \sum_i m_i F_i p_i$ leads to the expression

$$\overline{\mathbf{F} \cdot \mathbf{F}} = kT \overline{\nabla \cdot \mathbf{F}}, \quad (2.3)$$

^{||}Ladd, for example, begins his proof by showing that $\sum_i r_i p_i$ is bounded, since the \mathbf{r} are bounded by the size of the system, and the \mathbf{p} are bounded by its energy (Ladd 1990). He then claims that $\overline{\sum_i p_i^2/m - r_i F_i} = \frac{\partial}{\partial t} \overline{\sum_i r_i p_i} = 0$, since the time average of the derivative of a bounded function must be zero. However, $\frac{\partial}{\partial t} \overline{\sum_i r_i p_i} \neq \overline{\sum_i (p_i^2/m - r_i F_i)}$ in a periodic boundary system, due to the discontinuity in the \mathbf{r} . Further proof, regarding time average of these discontinuities is required in order for this assertion to be true.

**and hence the centre of gravity of the 'checkerboard' is constant.

which we will encounter later on. This form, and the Equipartition result are the only ones that appear in the text, where the former is used to defend the classical-mechanics approximation in the theory of rigid-body molecular fluids (Gray and Gubbins 1984, §1.2.2).

The advantage of this style of derivation is that it makes no comment on the type of system that is being considered. It may be at constant pressure or volume, temperature or energy — all that matters is that it be at thermal equilibrium. The disadvantage of this approach is the difficulty in knowing what functions will lead to a useful expression. It is difficult to determine phase functions that contain mixtures of momenta and coordinates, for example, without choosing at least two different functions \mathcal{A}_1 and \mathcal{A}_2 , and combining results.

Another generalised result appears without proof in Allen and Tildesley, in the paragraph under Eqns.(2.47) — “... the general form $\langle \mathcal{A} \partial \mathcal{H} / \partial q_k \rangle = k_B T \langle \partial \mathcal{A} / \partial q_k \rangle$... may be easily derived in the canonical ensemble. They are valid (to $\mathcal{O}(N^{-1})$) in any ensemble.” (Allen and Tildesley 1987, p.46). Only the Generalised equipartition theorem forms of this equation (ie $\mathcal{A} = \Gamma_i$) appear in the text, however.

2.2 Rugh's Temperature Expressions

Rugh's derivation of temperature expressions in the microcanonical ensemble deserves special attention. Rugh first derived the following expression for the thermodynamic temperature of a microcanonical ensemble (Rugh 1997)

$$\frac{1}{kT} = \left\langle \nabla \cdot \frac{\nabla \mathcal{H}}{|\nabla \mathcal{H}|^2} \right\rangle_E. \quad (2.4)$$

The paper also alludes to the possibility of generalising this derivation to encompass a family of expressions, all of whose averages yield the temperature. This generalisation, in the form

$$\frac{1}{kT} = \left\langle \nabla \cdot \frac{\mathbf{B}}{\nabla \mathcal{H} \cdot \mathbf{B}} \right\rangle_E, \quad (2.5)$$

is achieved in a later publication (Rugh 1998, Eq.(14))^{††}. Rugh's derivation appears in the rigorous language of measure theory. However, rather than reproduce that here, we consider a more intuitive flavour of the proof.

We will also introduce two simple extensions to Rugh's approach, which do not appear in his work — a general expression for the heat capacity, and the determination of the thermodynamic pressure.

^{††}and has been recently rederived with a different approach (Rickayzen and Powles 2001).

2.2.1 Derivation

From the thermodynamic definition $1/T = \partial S/\partial E$, we know that the temperature is given by the derivative of the *logarithm of the microcanonical ensemble partition function*, with respect to the *energy* defining the ensemble (§1.2.3). This partition function \mathcal{Z}^E can be written as an integral over the hypersurface of constant energy $A(E)$. Therefore we are interested in the function

$$\begin{aligned} \frac{1}{T} &= \lim_{\delta \rightarrow 0} \frac{S(E + \delta) - S(E)}{\delta} = \lim_{\delta \rightarrow 0} \frac{\ln \mathcal{Z}^{E+\delta} - \ln \mathcal{Z}^E}{\delta} \\ &= \lim_{\delta \rightarrow 0} \frac{1}{\delta} \ln \frac{\mathcal{Z}^{E+\delta}}{\mathcal{Z}^E}. \end{aligned} \quad (2.6)$$

If we can write $\mathcal{Z}^{E+\delta}$ as the integral of some function over $A(E)$, then this last ratio becomes the average of such a function on the hypersurface $A(E)$. But how can such a function be determined? Rugh achieves this by creating a mapping from $A(E)$ to $A(E + \delta)$, through the concept of a flow.

Imagine observing water flowing down a river. At any instant in time we can associate with each point in the river a velocity, corresponding to how fast, and in which direction, water is moving at that point. If the river isn't flowing too turbulently, we can imagine that these local velocities do not change over time. Consequently, if we drop a paper boat into the water, which moves with the water around it, we can trace the path of the water by following the boat. If we drop another boat into the water at exactly the same point, we would expect it to follow exactly the same path.

Suppose at each point in phase space we have a vector $\boldsymbol{\eta}(\boldsymbol{\Gamma})$. $\boldsymbol{\eta}$ is a vector-valued function, or **vector field**, of our phase space. We could imagine that this vector field is a velocity field, representing the velocity of points moving through our space, like the water down the river. Such a vector field defines a **flow**, and the trajectory of any point is defined as the solution of the first-order differential equation $\dot{\boldsymbol{\Gamma}} = \boldsymbol{\eta}(\boldsymbol{\Gamma})$. For example, the evolution of a system of particles, under Newtonian mechanics, corresponds to the flow $\boldsymbol{\eta}(\boldsymbol{\Gamma}) = \mathbf{J}\nabla\mathcal{H}(\boldsymbol{\Gamma})$ for

$$\mathbf{J} = \begin{bmatrix} 0 & \mathbf{I} \\ -\mathbf{I} & 0 \end{bmatrix},$$

where \mathbf{I} is the $M \times M$ identity matrix^{‡‡}.

For this problem, we wish to define a transformation from the hypersurface $A(E)$ to the hypersurface $A(E + \delta)$. Therefore we define a flow $\boldsymbol{\eta}$ outward from $A(E)$, ie such that $\boldsymbol{\eta} \cdot \nabla\mathcal{H} \neq 0$. Let us define by $g_{\boldsymbol{\eta}}^t(\boldsymbol{\Gamma})$ the position of a point, starting at $\boldsymbol{\Gamma}$, that has moved under the action of the flow $\boldsymbol{\eta}$ for time t .

^{‡‡}Recall that M is the number of coordinates or momenta.

By definition, the motion of the point Γ through phase space is given by

$$g_{\eta}^t(\Gamma) = \Gamma + t\eta(\Gamma) + \mathcal{O}(t^2). \quad (2.7)$$

The change in energy along this path will be

$$\begin{aligned} \mathcal{H}(t) - \mathcal{H}(0) &= \int_0^t \frac{d\mathcal{H}}{d\xi} d\xi = \int_0^t \nabla\mathcal{H}(\Gamma(\xi)) \cdot \dot{\Gamma}(\xi) d\xi \\ &= \int_0^t \nabla\mathcal{H}(\Gamma(\xi)) \cdot \eta(\Gamma(\xi)) d\xi. \end{aligned}$$

For an arbitrary vector field \mathbf{B} , suppose we define $\eta = \mathbf{B}/\nabla\mathcal{H} \cdot \mathbf{B}$. In this instance, we obtain

$$\mathcal{H}(t) - \mathcal{H}(0) = \int_0^t \nabla\mathcal{H}(\Gamma(\xi)) \cdot \frac{\mathbf{B}(\Gamma(\xi))}{\nabla\mathcal{H}(\Gamma(\xi)) \cdot \mathbf{B}(\Gamma(\xi))} d\xi = t.$$

Consequently, a flow of this form will have the property that *all points* on the hypersurface $A(E)$ will be transformed to the hypersurface $A(E + \delta)$, after having travelled along the flow η for time δ . A similar argument shows that the time reversal of this flow will transform *all points* on the hypersurface $A(E + \delta)$ to the hypersurface $A(E)$ after time δ . For this argument to hold, it is essential that $\nabla\mathcal{H} \cdot \mathbf{B} \neq 0$ — if $\nabla\mathcal{H} \cdot \mathbf{B} = 0$, the flow runs *tangentially* to the hypersurface of constant energy, and cannot be used to transform each point on the hypersurface monotonically (with respect to the energy). We shall revisit this problem after the proof is complete.

But how does the mapping from $A(E)$ to $A(E + \delta)$ help? It helps us to re-write the partition function of $\mathcal{Z}^{E+\delta}$ in the following manner:

$$\mathcal{Z}^{E+\delta} = \int_{A(E+\delta)} \mu(dA_{E+\delta}) = \lim_{\Delta \rightarrow 0} \frac{1}{\Delta} \int_{A(E+\delta)}^{A(E+\delta+\Delta)} d\Gamma \quad (2.8)$$

$$= \lim_{\Delta \rightarrow 0} \frac{1}{\Delta} \int_{A(E)}^{A(E+\Delta)} d(g_{\eta}^{\delta}(\Gamma^*)) \quad (2.9)$$

$$= \lim_{\Delta \rightarrow 0} \frac{1}{\Delta} \int_{A(E)}^{A(E+\Delta)} \mathcal{J}(g_{\eta}^{\delta}) d\Gamma^* \quad (2.10)$$

$$= \int_{A(E)} \mathcal{J}(g_{\eta}^{\delta}) \mu(dA_E). \quad (2.11)$$

Eqn.(2.8) is simply a statement of definition (§1.2.3). In getting to Eqn.(2.9), we have changed coordinates from the set of phase

points $\{\Gamma : E + \delta < \mathcal{H}(\Gamma) < E + \delta + \Delta\}$ to the set of phase points $\{\Gamma^* : E < \mathcal{H}(\Gamma^*) < E + \Delta\}$, so must apply the mapping g_η^δ to these points in order to be integrating over the same set in phase space.

Since we have changed coordinates, we can rewrite this as an integral over our new coordinates, multiplying the integrand by the **Jacobian** of the transformation, $\mathcal{J}(g_\eta^\delta)$, defined as

$$\mathcal{J} = \det \left(\frac{\partial g_\eta^\delta(\Gamma)}{\partial \Gamma} \right).$$

Thus we obtain Eqn.(2.10). Eqn.(2.11) follows in the limit $\Delta \rightarrow 0$. Substituting this back in to Eqn.(2.6) gives us

$$\frac{1}{T} = \lim_{\delta \rightarrow 0} \frac{1}{\delta} \ln \frac{\int_{A(E)} \mathcal{J}(g_\eta^\delta) \mu(dA_E)}{\mathcal{Z}^E} = \lim_{\delta \rightarrow 0} \frac{1}{\delta} \ln \langle \mathcal{J}(g_\eta^\delta) \rangle_E,$$

so we must expand $\mathcal{J}(g_\eta^\delta)$ in terms of δ to find the temperature. For if*

$$\langle \mathcal{J}(g_\eta^\delta) \rangle_E = 1 + \delta \langle J_1 \rangle_E + \mathcal{O}(\delta^2),$$

then

$$\frac{1}{T} = \lim_{\delta \rightarrow 0} \frac{\ln(1 + \delta \langle J_1 \rangle_E + \mathcal{O}(\delta^2))}{\delta} = \lim_{\delta \rightarrow 0} \frac{(\delta \langle J_1 \rangle_E + \mathcal{O}(\delta^2))}{\delta} = \langle J_1 \rangle_E,$$

where we use the expansion $\ln(1 + x) = x - x^2/2 + \mathcal{O}(x^3)$. From Eqn.(2.7), we obtain

$$\frac{\partial g_{\eta_i}^\delta}{\partial \Gamma_j} = \delta_{ij} + \delta \frac{\partial \eta_i}{\partial \Gamma_j} + \mathcal{O}(\delta^2).$$

The only terms that can contribute to the determinant come from the product of the diagonal elements — all other contributions must be at least $\mathcal{O}(\delta^2)$ as they must contain at least two off-diagonal (and therefore $\mathcal{O}(\delta)$ each) elements. Thus

$$\begin{aligned} \langle \mathcal{J}(g_\eta^\delta) \rangle_E &= \left\langle \prod_i \left(1 + \delta \frac{\partial \eta_i}{\partial \Gamma_i} \right) + \mathcal{O}(\delta^2) \right\rangle_E \\ &= 1 + \left\langle \delta \sum \frac{\partial \eta_i}{\partial \Gamma_i} \right\rangle_E + \mathcal{O}(\delta^2) \\ &= 1 + \delta \langle \nabla \cdot \eta \rangle_E + \mathcal{O}(\delta^2). \end{aligned}$$

Matching the coefficient of order δ with the inverse temperature gives us the result

$$\frac{1}{T} = \frac{\partial S(E)}{\partial E} = \langle \nabla \cdot \eta \rangle_E. \quad (2.12)$$

*note that the leading term must be one, as $A(E) \mapsto A(E + \delta)$ is the identity transformation when $\delta = 0$

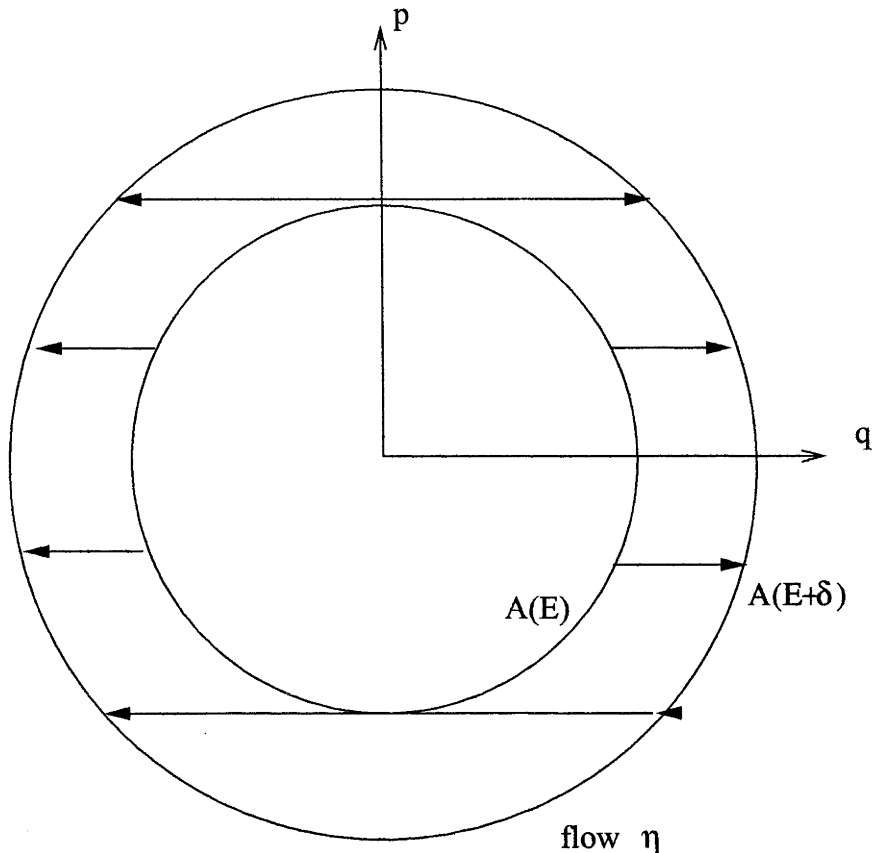


Figure 2.1: In the case of a harmonic oscillator (whose hypersurfaces of constant energy can be hyperspheres in phase space), the flow η 'tops and tails' the sphere $A(E+\delta)$. Only those points with momenta allowed on $A(E)$ will be generated.

The most certain choice for \mathbf{B} to avoid the situation $\nabla\mathcal{H} \cdot \mathbf{B} = 0$ is $\mathbf{B} = \nabla\mathcal{H}$. This leads us to Eqn.(2.4).

We note, once again, that the expression $|\nabla\mathcal{H}|^2$ involves the sum of dimensionally inconsistent quantities, so that the coordinate and momentum variables must be measured in a consistent set of units.

It is worth noting at this point that there are problems in finding appropriate η outside of the $\nabla\mathcal{H}/|\nabla\mathcal{H}|^2$. Suppose, for example, that we choose the vector field $\eta = \nabla K/|\nabla K|^2$. The vector field η will create trajectories which move all points from $A(E)$ at the same (constant) rate of energy increase. However, when $\mathbf{p} = 0$ (ie when the potential energy is maximum), $\nabla K \cdot \nabla\mathcal{H} = |\nabla K|^2 = 0$ — the field η is undefined, and hence the requirement in the proof is broken (see Fig. 2.1).

The effect of this underestimate of $\mathcal{Z}^{E+\delta}$ will vanish for certain choices of vector fields, in the limit $\delta \rightarrow 0$ and in the thermodynamic limit. Rather than consider how we might go about proving this

directly for a given $\boldsymbol{\eta}$, we shall prove a more general result using a different approach. As it turns out (Rugh 1998; Jepps, Ayton, and Evans 2000) it is possible to prove Eqn.(2.12), requiring only that $\boldsymbol{\eta}$ be defined almost everywhere[†]. Before we do this, however, we shall consider two extensions of the above proof. The first is a calculation of the thermodynamic heat capacity; the second is a calculation of the thermodynamic pressure.

2.2.2 Extension I — the Heat Capacity

The (isochoric) **heat capacity** is defined as the the rate of change of internal energy with respect to temperature at constant volume, ie

$$C_V = \left. \frac{\partial E}{\partial T} \right|_V.$$

Therefore we note that[‡]

$$\frac{1}{C_V} = \frac{\partial T}{\partial E} = \frac{\partial}{\partial E} \left[\frac{\partial S}{\partial E} \right]^{-1} = - \left[\frac{\partial S}{\partial E} \right]^{-2} \frac{\partial^2 S}{\partial E^2} = -T^2 \frac{\partial^2 S}{\partial E^2}.$$

It is a straight-forward extension of the previous proof to calculate this next derivative of entropy with respect to energy, and with it the heat capacity of our system. We have already derived an expansion of $\mathcal{J}(g_\eta^\delta)$ in powers of δ , although we have omitted terms of $\mathcal{O}(\delta^2)$ or higher. We must now go back and determine the $\mathcal{O}(\delta^2)$ term. Rugh does not do this explicitly in either of his papers, although the result can be obtained by using (Rugh 1998, Eq.(6)). Indeed, Rugh uses this approach to derive a kinetic expression for the heat capacity (Rugh 1998, Eq.(32)).

The first step is to determine g_η^δ to $\mathcal{O}(\delta^2)$. The second-order term comes about from noting that

$$\ddot{\Gamma} = \left(\sum_i \frac{d\Gamma_i}{dt} \frac{\partial}{\partial \Gamma_i} \right) \dot{\Gamma} = (\boldsymbol{\eta} \cdot \nabla) \boldsymbol{\eta},$$

so that

$$g_\eta^\delta(\boldsymbol{\Gamma}) = \boldsymbol{\Gamma} + \delta \boldsymbol{\eta}(\boldsymbol{\Gamma}) + \frac{1}{2} \delta^2 (\boldsymbol{\eta} \cdot \nabla) \boldsymbol{\eta} + \mathcal{O}(\delta^3),$$

and

$$\frac{\partial g_{\eta_i}^\delta}{\partial \Gamma_j} = \delta_{ij} + \delta \frac{\partial \eta_i}{\partial \Gamma_j} + \frac{\delta^2}{2} \frac{\partial (\boldsymbol{\eta} \cdot \nabla) \eta_i}{\partial \Gamma_j} + \mathcal{O}(\delta^3).$$

We need only consider contributions to the Jacobian [= $\det(\partial g_\eta^\delta / \partial \boldsymbol{\Gamma})$] up to $\mathcal{O}(\delta^2)$. As well as those terms included before, there will be

[†]in the measure theoretic sense

[‡]In this equation, and the following, it is understood that the partial derivatives are for constant volume.

additional contributions from the diagonal elements, of the forms $\partial(\boldsymbol{\eta} \cdot \nabla)\eta_i/\partial\Gamma_i$ and $(\partial\eta_i/\partial\Gamma_i)(\partial\eta_j/\partial\Gamma_j)$. Furthermore, the product of the first-order terms of non-diagonal elements will also produce second-order contributions, when they are multiplied by zero-order terms from the diagonal matrix elements. These terms will be of the form $(\partial\eta_i/\partial\Gamma_j)(\partial\eta_j/\partial\Gamma_i)$. Combining all these terms to $\mathcal{O}(\delta^2)$ gives

$$\begin{aligned}
\langle \mathcal{J}(g_\eta^\delta) \rangle_E &= \left\langle \prod_i \left(1 + \delta \frac{\partial\eta_i}{\partial\Gamma_i} + \frac{\delta^2}{2} \frac{\partial(\boldsymbol{\eta} \cdot \nabla)\eta_i}{\partial\Gamma_i} \right) - \sum_{i>j} \delta \frac{\partial\eta_i}{\partial\Gamma_i} \delta \frac{\partial\eta_j}{\partial\Gamma_j} + \mathcal{O}(\delta^3) \right\rangle_E \\
&= 1 + \left\langle \delta \sum_i \frac{\partial\eta_i}{\partial\Gamma_i} \right\rangle_E + \frac{\delta^2}{2} \left\langle \sum_i \frac{\partial(\boldsymbol{\eta} \cdot \nabla)\eta_i}{\partial\Gamma_i} \right\rangle_E \\
&\quad + \delta^2 \left\langle \sum_{i>j} \left[\frac{\partial\eta_i}{\partial\Gamma_i} \frac{\partial\eta_j}{\partial\Gamma_j} - \frac{\partial\eta_i}{\partial\Gamma_j} \frac{\partial\eta_j}{\partial\Gamma_i} \right] \right\rangle_E + \mathcal{O}(\delta^3) \\
&= 1 + \delta \langle \nabla \cdot \boldsymbol{\eta} \rangle_E + \frac{\delta^2}{2} \left\langle \sum_{ij} \eta_j \frac{\partial\eta_i}{\partial\Gamma_i \partial\Gamma_j} + \frac{\partial\eta_j}{\partial\Gamma_i} \frac{\partial\eta_i}{\partial\Gamma_j} \right\rangle_E \\
&\quad + \frac{\delta^2}{2} \left\langle \sum_{i \neq j} \left[-\frac{\partial\eta_i}{\partial\Gamma_j} \frac{\partial\eta_j}{\partial\Gamma_i} + \frac{\partial\eta_i}{\partial\Gamma_i} \frac{\partial\eta_j}{\partial\Gamma_j} \right] \right\rangle_E + \mathcal{O}(\delta^3) \\
&= 1 + \delta \langle \nabla \cdot \boldsymbol{\eta} \rangle_E + \frac{\delta^2}{2} \left\langle \sum_{ij} \eta_j \frac{\partial\eta_i}{\partial\Gamma_j \partial\Gamma_i} \right\rangle_E + \frac{\delta^2}{2} \left\langle \sum_i \frac{\partial\eta_i}{\partial\Gamma_i} \frac{\partial\eta_i}{\partial\Gamma_i} \right\rangle_E \\
&\quad + \frac{\delta^2}{2} \left\langle \sum_{i \neq j} \left[\frac{\partial\eta_i}{\partial\Gamma_i} \frac{\partial\eta_j}{\partial\Gamma_j} \right] \right\rangle_E + \mathcal{O}(\delta^3) \\
&= 1 + \delta \langle \nabla \cdot \boldsymbol{\eta} \rangle_E + \frac{\delta^2}{2} \left\langle \sum_{ij} \eta_j \frac{\partial\eta_i}{\partial\Gamma_j \partial\Gamma_i} + \sum_{ij} \left[\frac{\partial\eta_i}{\partial\Gamma_i} \frac{\partial\eta_j}{\partial\Gamma_j} \right] \right\rangle_E + \mathcal{O}(\delta^3) \\
&= 1 + \delta \langle \nabla \cdot \boldsymbol{\eta} \rangle_E + \frac{\delta^2}{2} \langle (\nabla \cdot \boldsymbol{\eta})^2 + (\boldsymbol{\eta} \cdot \nabla)(\nabla \cdot \boldsymbol{\eta}) \rangle_E + \mathcal{O}(\delta^3).
\end{aligned}$$

Using the expansion $\ln(1+x) = x - x^2/2 + \mathcal{O}(x^3)$, we obtain

$$\begin{aligned}
S(E+\delta) - S(E) &= \ln \left(1 + \delta \langle J_1 \rangle_E + \frac{\delta^2}{2} \langle J_2 \rangle_E + \mathcal{O}(\delta^3) \right) \\
&= \left(\delta \langle J_1 \rangle_E + \frac{\delta^2}{2} \langle J_2 \rangle_E - \frac{\delta^2}{2} \langle J_1 \rangle_E^2 + \mathcal{O}(\delta^3) \right).
\end{aligned}$$

Therefore

$$\boxed{\frac{1}{C_V} = -T^2 \frac{\partial^2 S}{\partial E^2} = 1 - \frac{\langle (\nabla \cdot \boldsymbol{\eta})^2 + (\boldsymbol{\eta} \cdot \nabla)(\nabla \cdot \boldsymbol{\eta}) \rangle_E}{\langle \nabla \cdot \boldsymbol{\eta} \rangle_E^2}} \quad (2.13)$$

2.2.3 Extension II — the Thermodynamic Pressure

Much of the preceding argument regarding the calculation of $\partial S/\partial E$ holds for the calculation of $\partial S/\partial V$ as well. If we can find a flow g_η^v that maps $A(E, V) \mapsto A(E, V + v)$, then $p/kT = \partial S/k\partial V|_E$ will be given by $\langle \nabla \cdot \eta \rangle_E$.

The transformation from a system of volume V to a system of volume $V + v$ is essentially a coordinate transformation, so let us imagine a transformation $\mathbf{q}_v(t)$ of our coordinates such that $\mathbf{q}_a(t) \in A(E, V + a) \Leftrightarrow \mathbf{q}_b(t) \in A(E, V + b) \forall a, b, V$. Consequently the vector field $\boldsymbol{\eta}_q = \mathbf{q}'_v(t) = \partial \mathbf{q}_v(t)/\partial v$ will form the configurational part of the flow that takes us through the $A(E, V + v)$ at unit rate. The momentum part $\boldsymbol{\eta}_p$ can be chosen so that $\mathcal{H}(\Gamma_v) = \mathcal{H}(\Gamma)$ — the thermodynamic pressure is defined as the partial derivative *at constant E*. We will choose it to be parallel to \mathbf{p} . If we define $\boldsymbol{\eta} = [\boldsymbol{\eta}_q, \boldsymbol{\eta}_p]$, then $p/T = \langle \nabla \cdot \boldsymbol{\eta} \rangle_E$.

The simplest choice for $\mathbf{q}_v(t)$ for a system of interacting particles is the transformation that rescales all Cartesian coordinates \mathbf{r} by a factor $(1 + v/V)^{1/3}$, ie $\mathbf{r}_v = \mathbf{r}(1 + v/V)^{1/3}$. Thus

$$\boldsymbol{\eta}_q = \boldsymbol{\eta}_r = \mathbf{r}'_v = \mathbf{r}_v/3V.$$

If we define $\Phi_v(\mathbf{r}) = \Phi(\mathbf{r}_v)$, then

$$\begin{aligned} \Phi'_0(\mathbf{r}) &= \nabla \Phi(\mathbf{r}) \cdot \mathbf{r}'_0 = -\mathbf{F} \cdot \mathbf{r}/3V \\ \Rightarrow \mathcal{H}'_0 &= \frac{\mathbf{p} \cdot \boldsymbol{\eta}_p}{m} + \Phi'_0 = 0 \\ \Rightarrow \boldsymbol{\eta}_p &= \frac{m\mathbf{F} \cdot \mathbf{r}}{3V\mathbf{p} \cdot \mathbf{p}}\mathbf{p}. \end{aligned}$$

We can therefore calculate

$$\begin{aligned} \nabla \cdot \boldsymbol{\eta} &= \frac{\partial}{\partial \mathbf{r}} \cdot \frac{\mathbf{r}}{3V} + \frac{\partial}{\partial \mathbf{p}} \cdot \frac{m\mathbf{F} \cdot \mathbf{r}}{3V\mathbf{p} \cdot \mathbf{p}}\mathbf{p} \\ &= \frac{3N}{3V} + \frac{m\mathbf{F} \cdot \mathbf{r}}{3V} \nabla_{\mathbf{p}} \cdot (\mathbf{p} \cdot \mathbf{p})^{-1}\mathbf{p} \\ &= \frac{N}{V} + \frac{m\mathbf{F} \cdot \mathbf{r}}{3V} \frac{(3N - 2)}{\mathbf{p} \cdot \mathbf{p}}, \end{aligned}$$

so that

$$\frac{pV}{NkT} = \frac{V}{N} \langle \nabla \cdot \boldsymbol{\eta} \rangle_E = 1 + \frac{(3N - 2)}{3N} \left\langle \frac{m\mathbf{F} \cdot \mathbf{r}}{\mathbf{p} \cdot \mathbf{p}} \right\rangle_E. \quad (2.14)$$

The above does not hold for periodic boundary systems. In such systems, the potential energy is of the form $\Phi(\mathbf{r}) = 1/2 \sum_{ij} \phi(\tilde{r}_{ij})$, where the \tilde{r}_{ij} represent the minimum-image displacements between

particles i and j (§1.4.4). These minimum-image displacements are a function of, among other things, the size of the periodic system. Consequently, the \tilde{r}_{ij} depend on V , so that $\Phi'_v(\mathbf{r}(t)) \neq -\mathbf{F} \cdot \mathbf{r}'_v(t)$ when the size of the system changes.

We therefore modify our approach as follows: under the rescaling transformation, $\Phi(\mathbf{r}) \mapsto \Phi_v(\mathbf{r}) = 1/2 \sum_{ij} \phi(\tilde{r}_{ij}(1 + v/V)^{1/3})$. Consequently Φ'_0 is given by

$$\begin{aligned} \frac{\partial \Phi_0(\mathbf{r})}{\partial v} &= \frac{1}{2} \sum_{ij} \frac{\partial}{\partial v} \phi(\tilde{r}_{ij}(1 + v/V)^{1/3}) \Big|_{v=0} \\ &= \frac{1}{2} \sum_{ij} \frac{\partial}{\partial X_{ij}} \phi(X_{ij}) \frac{\partial X_{ij}}{\partial v} \Big|_{v=0} \quad \text{where } X_{ij} = (\tilde{r}_{ij}(1 + v/V)^{1/3}) \\ &= -\frac{1}{2} \sum_{ij} F(X_{ij}) \tilde{r}_{ij} (1 + v/V)^{-2/3} \cdot \frac{1}{3} \cdot \frac{1}{V} \Big|_{v=0} \\ &= -\frac{1}{3V} \frac{1}{2} \sum_{ij} F(\tilde{r}_{ij}) \tilde{r}_{ij} = -\frac{1}{3V} \sum_{i>j} \mathbf{F}_{ij} \cdot \tilde{\mathbf{r}}_{ij}. \end{aligned}$$

Comparing this expression with Eqn.(2.14), we note that the only difference is that $\mathbf{F} \cdot \mathbf{r}$ has been replaced with $\sum_{i>j} \mathbf{F}_{ij} \cdot \tilde{\mathbf{r}}_{ij}$. While these two expressions are not equal for periodic boundary systems, they are identical for systems with real walls[§]. Thus, the final expression, valid for real or periodic boundary systems, is

$$\boxed{\frac{pV}{NkT} = \langle \nabla \cdot \boldsymbol{\eta} \rangle_E = 1 + \frac{(3N - 2)}{3N} \left\langle \frac{m \sum_{i>j} \mathbf{F}_{ij} \cdot \tilde{\mathbf{r}}_{ij}}{\mathbf{p} \cdot \mathbf{p}} \right\rangle_E} \quad (2.15)$$

Thus we recover the usual microscopic expression for the temperature, apart from the factor $(3N - 2)/3N$. We shall come across further similar $\mathcal{O}(1/N)$ discrepancies between traditional microcanonical results and those obtained taking the approach due to Rugh. We note, in conclusion, that Eqn.(2.15) is only one of an infinite family of possible expressions for the pressure, determined by our particular choice of $\boldsymbol{\eta}$.

2.3 A More Generalised Temperature Expression

While Rugh has developed a generalised temperature expression for the microcanonical ensemble, it is possible to produce a more general

[§]as long as the potential can be written in the form $\Phi(\mathbf{r}) = \sum_i v_i(l_i)$ for variables l_i that rescale according to our transformation

result, valid in both canonical and microcanonical ensembles[¶], which we shall prove in the following section:

$$kT = \frac{\langle \nabla \mathcal{H}(\mathbf{\Gamma}) \cdot \mathbf{B}(\mathbf{\Gamma}) \rangle}{\langle \nabla \cdot \mathbf{B}(\mathbf{\Gamma}) \rangle} \quad (2.16)$$

The proof is most easily seen in the canonical ensemble, so we shall begin our derivation there. We will then move to the case of the microcanonical ensemble, where our argument will be of a similar nature to that found in (Rugh 1998). Indeed, the results of §2.3.2 are contained within (Rugh 1998, Eq.(6)) — however, where Rugh focusses on the case where $\nabla \mathcal{H} \cdot \mathbf{B} \equiv 1$, in this thesis we will investigate the broader class of flows where this equality holds only in the thermodynamic limit.

The result that we shall prove is the following: Suppose we choose any vector field $\mathbf{B}(\mathbf{\Gamma})$ such that $0 < |\langle \nabla \mathcal{H} \cdot \mathbf{B}(\mathbf{\Gamma}) \rangle| < \infty$, $0 < |\langle \nabla \cdot \mathbf{B}(\mathbf{\Gamma}) \rangle| < \infty$ and $\nabla \mathcal{H} \cdot \mathbf{B}(\mathbf{\Gamma})$ grows more slowly than e^N in the thermodynamic limit. Then the temperature of the system will be given by Eqn.(2.16).

In §2.3.1 and §2.3.2 we will prove Eqn.(2.16) for the canonical and microcanonical ensembles. In §2.3.4 we will show the consistency of this result with those discussed earlier, before going on to consider how to extend this result to systems of non-canonical variables (§2.4.1), systems with constraints (§2.4.2) and periodic boundary systems (§2.4.3). Finally, we will derive some expressions for the temperature, in terms of the variables we will use in our simulations (§2.5).

Parts of the following sections — in particular, §1.2.4, §1.2.3, §2.3.3, §2.3.4, §2.4.3 and the atomic temperature expressions in §2.5 — appear in (Jepps, Ayton, and Evans 2000).

2.3.1 Canonical Ensembles

We begin with a proof of Eqn.(2.16) in the canonical ensemble. Consider an N -particle system, whose physical volume V is determined by a set of barriers or walls. If we denote by Ω the set of all allowed microstates $\mathbf{\Gamma}$ (for a given N and V) within our phase space^{||}, then the extent of Ω in the coordinate variables is limited by the physical size of the system. The momenta are unbounded in Ω , so that Ω forms a cylinder in phase space.

Our proof is essentially an extension of Tolman's proof of the Equipartition theorem^{**}. We invoke Gauss' theorem over $\Omega(E)$ for

[¶]and in the Grand Canonical Ensemble as well (Baranyai 2000)

^{||}recalling our definition of Ω from §1.2.3

^{**}as anticipated by (Allen and Tildesley 1987), §2.1

an arbitrary vector field in phase space $\mathbf{B}(\Gamma)e^{-\beta\mathcal{H}(\Gamma)\dagger\dagger}$ (where we assume a finite, positive β), ie

$$\begin{aligned} \int_{A(E)} e^{-\beta\mathcal{H}(\Gamma)} \mathbf{B}(\Gamma) \cdot \hat{\mathbf{n}}(\Gamma) dA_E &= \int_{\Omega(E)} \nabla \cdot (\mathbf{B}(\Gamma)e^{-\beta\mathcal{H}(\Gamma)}) d\Gamma \\ &= \int_{\Omega(E)} e^{-\beta\mathcal{H}(\Gamma)} \nabla \cdot \mathbf{B}(\Gamma) d\Gamma - \beta \int_{\Omega(E)} e^{-\beta\mathcal{H}(\Gamma)} \nabla \mathcal{H}(\Gamma) \cdot \mathbf{B}(\Gamma) d\Gamma. \end{aligned}$$

In the limit as $E \rightarrow \infty$, we obtain

$$\begin{aligned} \lim_{E \rightarrow \infty} e^{-\beta E} \int_{A(E)} \mathbf{B}(\Gamma) \cdot \hat{\mathbf{n}}(\Gamma) dA_E &= \\ \int_{\Omega} e^{-\beta\mathcal{H}(\Gamma)} \nabla \cdot \mathbf{B}(\Gamma) d\Gamma - \beta \int_{\Omega} e^{-\beta\mathcal{H}(\Gamma)} \nabla \mathcal{H}(\Gamma) \cdot \mathbf{B}(\Gamma) d\Gamma. \end{aligned} \quad (2.17)$$

If $\langle \nabla \mathcal{H} \cdot \mathbf{B} \rangle_{\beta}$ exists, then

$$\begin{aligned} \left| \int_{\Omega} e^{-\beta\mathcal{H}(\Gamma)} \nabla \mathcal{H}(\Gamma) \cdot \mathbf{B}(\Gamma) d\Gamma \right| < \infty &\Rightarrow \left| \int_0^{\infty} \int_{A(E)} e^{-\beta E} \nabla \mathcal{H}(\Gamma) \cdot \mathbf{B}(\Gamma) \frac{dA_E}{|\nabla \mathcal{H}|} dE \right| < \infty \\ &\Rightarrow \lim_{E \rightarrow \infty} \int_{A(E)} e^{-\beta E} \mathbf{B}(\Gamma) \cdot \hat{\mathbf{n}}(\Gamma) dA_E = 0. \end{aligned}$$

This means that whenever $\langle \nabla \mathcal{H} \cdot \mathbf{B} \rangle_{\beta}$ exists, the left hand side of Eqn.(2.17) must be identically zero^{††}. It follows by rearrangement that

$$\frac{1}{kT} = \beta = \frac{\int_{\Omega} e^{-\beta\mathcal{H}(\Gamma)} \nabla \cdot \mathbf{B}(\Gamma) d\Gamma}{\int_{\Omega} e^{-\beta\mathcal{H}(\Gamma)} \nabla \mathcal{H}(\Gamma) \cdot \mathbf{B}(\Gamma) d\Gamma} = \frac{\langle \nabla \cdot \mathbf{B}(\Gamma) \rangle_{\beta}}{\langle \nabla \mathcal{H}(\Gamma) \cdot \mathbf{B}(\Gamma) \rangle_{\beta}}, \quad (2.18)$$

in agreement with Eqn.(2.16).

A further consequence of the existence of $\langle \nabla \mathcal{H} \cdot \mathbf{B} \rangle_{\beta}$ is that the integral

$$e^{-\beta E} \int_{A(E)} \mathbf{B}(\Gamma) \cdot \hat{\mathbf{n}}(\Gamma) dA_E = e^{\beta[TS(E)-E]} \langle \nabla \mathcal{H} \cdot \mathbf{B}(\Gamma) \rangle_E$$

converges. When we consider that $e^{\beta[TS(E)-E]}$ also converges, but that $e^{S(E)}$ does not, we immediately obtain the third condition on $\mathbf{B}(\Gamma)$.

^{††}The application of Gauss' Theorem is valid, since all points of energy less than E are in the *interior* of the set $\Omega(E)$, and the hypersurface $A(E)$ forms the *boundary* of Ω . This is a reflection of the quadratic form of the kinetic energy — the point Γ' , $\mathcal{H}(\Gamma') < E$ is contained within the hyperellipsoid $\{\Gamma : \Phi(\Gamma) = \Phi(\Gamma'), K(\Gamma) = E - \Phi(\Gamma)\}$. This can be extended under canonical transformation.

^{†††}and hence the existence of $\langle \nabla \cdot \mathbf{B} \rangle_{\beta}$ is guaranteed, for finite β

2.3.2 Microcanonical Ensembles

The proof of Eqn.(2.16) in the microcanonical ensemble is not a straightforward extension of the microcanonical Equipartition theorem proof, as was the case for the canonical ensemble. Let us consider the same physical system as in the canonical ensemble proof, in energetic isolation from its surroundings, rather than being in thermal equilibrium. Suppose, for an arbitrary vector field $\mathbf{B}(\Gamma)$, we define

$$\mathcal{Z}_{\mathbf{B}}^E(E) = e^{S_{\mathbf{B}}(E)/k} = \frac{1}{h^{3N}N!} \int_{A(E)} \nabla \mathcal{H}(\Gamma) \cdot \mathbf{B}(\Gamma) \, d\mu_E, \quad (2.19)$$

where we assume $\langle \nabla \mathcal{H} \cdot \mathbf{B} \rangle_E$ is positive and finite (since $e^{S_{\mathbf{B}}(E)/k}$ must be). From first principles,

$$\begin{aligned} h^{3N}N! \frac{\partial \mathcal{Z}_{\mathbf{B}}^E(E)}{\partial E} &= \lim_{\delta \rightarrow 0} h^{3N}N! \frac{\mathcal{Z}_{\mathbf{B}}^E(E + \delta) - \mathcal{Z}_{\mathbf{B}}^E(E)}{\delta} \\ &= \lim_{\delta \rightarrow 0} \frac{1}{\delta} \left[\int_{A(E+\delta)} \nabla \mathcal{H} \cdot \mathbf{B} \, d\mu_{E+\delta} - \int_{A(E)} \nabla \mathcal{H} \cdot \mathbf{B} \, d\mu_E \right] \\ &= \lim_{\delta \rightarrow 0} \frac{1}{\delta} \left[\int_{A(E+\delta)} \mathbf{B}(\Gamma) \cdot \hat{\mathbf{n}}(\Gamma) \, dA_{E+\delta} - \int_{A(E)} \mathbf{B}(\Gamma) \cdot \hat{\mathbf{n}}(\Gamma) \, dA_E \right], \end{aligned}$$

where $\hat{\mathbf{n}}(\Gamma)$ is a unit normal vector to the hypersurface $A(E)$ at Γ . We apply Gauss' theorem to obtain

$$\begin{aligned} h^{3N}N! \frac{\partial \mathcal{Z}_{\mathbf{B}}^E(E)}{\partial E} &= \lim_{\delta \rightarrow 0} \frac{1}{\delta} \int_E^{E+\delta} \int_{A(\xi)} \nabla \cdot \mathbf{B}(\Gamma) \, dA_{\xi} \, d\xi \\ &= \int_{A(E)} \nabla \cdot \mathbf{B}(\Gamma) \, d\mu_E. \end{aligned}$$

Therefore it follows that

$$\frac{1}{kT_{\mathbf{B}}(E)} := \frac{1}{k} \frac{\partial S_{\mathbf{B}}(E)}{\partial E} = \frac{\langle \nabla \cdot \mathbf{B}(\Gamma) \rangle_E}{\langle \nabla \mathcal{H} \cdot \mathbf{B}(\Gamma) \rangle_E}. \quad (2.20)$$

From Eqn.(2.19), we have that $S_{\mathbf{B}}(E) = S(E) + k \ln \langle \nabla \mathcal{H} \cdot \mathbf{B}(\Gamma) \rangle_E$. Now, as long as $\langle \nabla \mathcal{H} \cdot \mathbf{B}(\Gamma) \rangle_E$ grows more slowly than e^N in the thermodynamic limit, $\partial S_{\mathbf{B}}(E)/\partial E \asymp \partial S(E)/\partial E$. Consequently, $T_{\mathbf{B}}(E) \asymp T(E)$, and we recover the same result as Eqn.(2.16). Furthermore, we may drop the condition that $\langle \nabla \mathcal{H} \cdot \mathbf{B}(\Gamma) \rangle_E$ be positive, since from Eqn.(2.20) $T_{(-\mathbf{B})} = T_{\mathbf{B}}$.

2.3.3 Conditions for \mathcal{H} and \mathbf{B}

In the canonical ensemble proof, we apply Gauss' theorem to $\mathbf{B}e^{-\beta\mathcal{H}}$ on the surface $A(E)$, defined by \mathcal{H} . In the microcanonical ensemble proof, we apply Gauss' theorem to \mathbf{B} on the surface $A(E)$. In order to do this, we require that $\mathbf{B}e^{-\beta\mathcal{H}}$ and \mathbf{B} be **absolutely continuous***. We also require that \mathcal{H} be absolutely continuous, so that the surfaces $A(E)$ are sufficiently smooth so that Gauss' theorem can be applied on them.

The set of vector fields for which $0 < |\langle \nabla \cdot \mathbf{B} \rangle| < \infty$, $0 < |\langle \nabla \mathcal{H} \cdot \mathbf{B} \rangle| < \infty$, and $(\ln |\langle \nabla \mathcal{H} \cdot \mathbf{B} \rangle|)/N \simeq 0$ is more easily determined in the canonical ensemble, where the range of the integrals involved is independent of the Hamiltonian. Determining the members of this set is a difficult problem. We simply note that the last condition allows all finite-order polynomials and bounded functions of the p_i and q_i , as well as ratios of finite-order polynomials.

Thus the conditions for Eqn.(2.16) to hold in the microcanonical ensemble are the same as those for the canonical ensemble.

2.3.4 Consistency with Earlier Expressions

Having proven Eqn.(2.16) in the canonical and microcanonical ensembles, we now demonstrate its consistency with the existing expressions for the thermodynamic temperature, outlined in §2.1-§2.2.

If we choose $\mathbf{B}(\boldsymbol{\Gamma}) = (0, \dots, \Gamma_i, \dots, 0)$, so that only the i -th component is non-zero, then we obtain

$$kT = \frac{\langle \nabla \mathcal{H}(\boldsymbol{\Gamma}) \cdot \mathbf{B}(\boldsymbol{\Gamma}) \rangle}{\langle \nabla \cdot \mathbf{B}(\boldsymbol{\Gamma}) \rangle} = \left\langle \Gamma_i \frac{\partial \mathcal{H}}{\partial \Gamma_i} \right\rangle,$$

which we recognise as the Generalised equipartition theorem, Eqn.(2.2). Setting this component to an arbitrary function \mathcal{A} instead of simply Γ_i gives us the result cited in (Allen and Tildesley 1987). If we choose \mathbf{B} to have the form

$$\mathbf{B}(\boldsymbol{\Gamma}) = \frac{\mathbf{X}(\boldsymbol{\Gamma})}{\nabla \mathcal{H}(\boldsymbol{\Gamma}) \cdot \mathbf{X}(\boldsymbol{\Gamma})} \quad (2.21)$$

for an arbitrary vector field $\mathbf{X}(\boldsymbol{\Gamma})$, then $\nabla \mathcal{H} \cdot \mathbf{B} \equiv 1$ for *all* choices of $\mathbf{X}(\boldsymbol{\Gamma})$. This choice leads us to Rugh's more general result Eqn.(2.5). Substituting $\mathbf{X}(\boldsymbol{\Gamma}) = \nabla \mathcal{H}(\boldsymbol{\Gamma})$, we obtain Rugh's original expression for the temperature Eqn.(2.4). Finally, if we choose $\mathbf{B}(\boldsymbol{\Gamma}) = (\mathbf{F}, 0)$ (ie all momentum components are set to zero), then we obtain Eqn.(2.3), as per (Gray and Gubbins 1984).

*the set of absolutely continuous functions are those for which the fundamental theorem of calculus holds. Absolute continuity implies differentiability almost everywhere (Rudin 1987).

2.4 Extensions to Eqn.(2.16)

We have now derived a general expression for the temperature of a system, in terms of the phase variables used to describe the system. However, there are situations where we prefer not to use a set of canonical variables in order to describe the system we are studying.

For example, we may have a set of constraints on the system (such as bond lengths) that are accounted for in other ways during the simulation (such as a Gaussian constraint — see §3.4). This approach is often much less complicated than recasting the entire problem into a reduced set of variables, in order to determine the system's dynamics. In rigid-body simulations, system orientations can be described using Euler angles or quaternions, but the dynamics of these orientations is rarely determined using the appropriate conjugate momenta. Instead, the body-frame angular velocities are used. Furthermore, the use of quaternions means that four parameters are used to determine a three-parameter orientation of bodies in real space (or sometimes, in the case of spherically symmetric systems, a two-parameter orientation).

Thus, non-canonical descriptions of systems are relatively common when they provide simpler equations of motion. It is therefore useful to consider how one might apply the Eqn.(2.16) to systems whose descriptions are non-canonical. In this section, we will consider how to amend our result to allow for non-canonical descriptions of our system. This will include the use of variables that do not form a set of conjugate pairs (§2.4.1), and the inclusion of constraints (§2.4.2).

We have already noted that the Generalised equipartition theorem breaks down in periodic boundary systems. As most computer simulations employ periodic boundary conditions, it is important to re-examine our derivation to determine what conditions will ensure that Eqn.(2.16) holds in periodic boundary systems. This is done in §2.4.3.

2.4.1 Non-Canonical Variables

It is not uncommon for systems to be described in non-canonical coordinate pairs. The use of Euler angles and angular velocities, rather than conjugate momenta, is a common example. Consequently, we would like to recast Eqn.(2.16) for systems of non-canonical coordinate pairs.

Therefore, rather than representing our system by the point $\mathbf{\Gamma}$ in phase space, we represent it by the point $\mathbf{G} = \mathbf{G}(\mathbf{\Gamma})$ in a new 'phase' space of microstates[†]. This mapping should be one-one, onto and

[†]While being a space of all microstates, it lacks many of the useful properties

continuous, so that this transformation has an inverse, ie so that $\Gamma = \Gamma(\mathbf{G})$ for some \mathbf{G} . Thus the function $\mathcal{A}(\Gamma)$ can be re-written as the function $\tilde{\mathcal{A}}(\mathbf{G}(\Gamma)) = \tilde{\mathcal{A}}(\mathbf{G}) = \mathcal{A}(\Gamma)$. The energy of the system is given by the function $\tilde{H}(\mathbf{G}) = \mathcal{H}(\Gamma(\mathbf{G}))^\dagger$, and we can define $\tilde{A}(E)$ as the set of points \mathbf{G} such that $\tilde{H}(\mathbf{G}) = E$. We must also define a new gradient vector operator, $\tilde{\nabla} = [\frac{\partial}{\partial G_1}, \dots, \frac{\partial}{\partial G_{2M}}]$.

A crucial point here is that infinite time averages and ensemble averages are no longer equal in this new 'phase' space. A simple example demonstrating this point is by choosing $\mathbf{G} = (q_1, \dots, q_M, \dot{q}_1, \dots, \dot{q}_M)$. The 'phase' averages of quantities in the non-canonical description will not correspond to the phase averages in the canonical description, yet by ergodic theory we claim that the real phase averages and infinite time averages are equal.

Consequently, ensemble averages must be written in terms of Γ rather than \mathbf{G} , so that $\overline{\tilde{\mathcal{A}}(\mathbf{G})} = \overline{\mathcal{A}(\Gamma(\mathbf{G}))} = \langle \mathcal{A}(\Gamma) \rangle$. We convert between these coordinate systems using the Jacobian of the transformation — $\mathcal{A}(\Gamma) d\Gamma = \tilde{\mathcal{A}}(\mathbf{G}) \tilde{\mathcal{J}}(\mathbf{G}) d\mathbf{G}$.

The effect of non-canonical coordinate pairs can be most easily seen in the canonical ensemble, where we begin by considering

$$\begin{aligned} \beta \langle \tilde{\nabla} \tilde{H} \cdot \tilde{\mathbf{B}} \rangle_\beta &= \frac{\beta}{\mathcal{Z}^\beta} \int_\Omega [\tilde{\nabla} \tilde{H} \cdot \tilde{\mathbf{B}}](\mathbf{G}) e^{-\beta \mathcal{H}(\Gamma)} d\Gamma \\ &= \frac{\beta}{\mathcal{Z}^\beta} \int_{\tilde{\Omega}} [\tilde{\nabla} \tilde{H} \cdot \tilde{\mathbf{B}}](\mathbf{G}) e^{-\beta \tilde{H}(\mathbf{G})} \tilde{\mathcal{J}}(\mathbf{G}_\Gamma) d\mathbf{G} \\ &= \frac{\beta}{\mathcal{Z}^\beta} \int_{\tilde{\Omega}} [\tilde{\nabla} \tilde{H} \cdot (\tilde{\mathbf{B}} \tilde{\mathcal{J}})](\mathbf{G}) e^{-\beta \tilde{H}(\mathbf{G})} d\mathbf{G}. \end{aligned}$$

By the same argument used in §2.3.1, we invoke Gauss' theorem to obtain

$$\beta \int_{\tilde{\Omega}} (\tilde{\nabla} \tilde{H} \cdot (\tilde{\mathbf{B}} \tilde{\mathcal{J}}))(\mathbf{G}) e^{-\beta \tilde{H}(\mathbf{G})} d\mathbf{G} = \int_{\tilde{\Omega}} (\tilde{\nabla} \cdot (\tilde{\mathbf{B}} \tilde{\mathcal{J}}))(\mathbf{G}) e^{-\beta \tilde{H}(\mathbf{G})} d\mathbf{G},$$

as long as $\beta \langle \tilde{\nabla} \tilde{H} \cdot \tilde{\mathbf{B}} \rangle_\beta$ exists. Thus we conclude that

$$\begin{aligned} \beta \langle \tilde{\nabla} \tilde{H} \cdot \tilde{\mathbf{B}} \rangle_\beta &= \frac{\beta}{\mathcal{Z}^\beta} \int_{\tilde{\Omega}} (\tilde{\nabla} \tilde{H} \cdot (\tilde{\mathbf{B}} \tilde{\mathcal{J}}))(\mathbf{G}) e^{-\beta \tilde{H}(\mathbf{G})} d\mathbf{G} \\ &= \frac{1}{\mathcal{Z}^\beta} \int_{\tilde{\Omega}} (\tilde{\nabla} \cdot (\tilde{\mathbf{B}} \tilde{\mathcal{J}}))(\mathbf{G}) e^{-\beta \tilde{H}(\mathbf{G})} d\mathbf{G} \\ &= \frac{1}{\mathcal{Z}^\beta} \int_\Omega \left(\frac{1}{\tilde{\mathcal{J}}} \tilde{\nabla} \cdot (\tilde{\mathbf{B}} \tilde{\mathcal{J}}) \right)(\mathbf{G}) e^{-\beta \mathcal{H}(\Gamma)} d\Gamma \\ &= \left\langle \frac{1}{\tilde{\mathcal{J}}} \tilde{\nabla} \cdot \tilde{\mathbf{B}} \tilde{\mathcal{J}} \right\rangle_\beta = \langle \tilde{\nabla} \cdot \tilde{\mathbf{B}} \rangle_\beta + \langle \tilde{\mathbf{B}} \cdot \tilde{\nabla} \ln \tilde{\mathcal{J}} \rangle_\beta. \end{aligned}$$

of a phase space because of the arbitrariness of the choice of variables.

[†]We avoid the notation $\tilde{\mathcal{H}}$, to emphasise that a Hamiltonian is only ever a function of canonical variables.

Thus for non-canonical variables, Eqn.(2.16) is corrected by a term related to the rescaling of our phase space due to a change in coordinates. We note that this is consistent with the transformation from one set of canonical variables to another, where $\mathcal{J} \equiv 1$.

The proof in the microcanonical ensemble contains a similar adjustment. This time, the definition of the entropy is the source of variation. We observe that

$$\begin{aligned}
 \frac{1}{h^{3N}N!} \int_{A(E)} \frac{dA_E}{|\nabla\mathcal{H}|} &= \frac{1}{h^{3N}N!} \int \delta(\mathcal{H}(\mathbf{\Gamma}) - E) d\mathbf{\Gamma} \\
 &= \lim_{\delta E \rightarrow 0} \frac{1}{h^{3N}N!} \int_{\Omega(E, E+\delta E)} d\mathbf{\Gamma} \\
 &= \lim_{\delta E \rightarrow 0} \frac{1}{h^{3N}N!} \int_{\tilde{\Omega}(E, E+\delta E)} \tilde{\mathcal{J}} d\mathbf{G} \\
 &= \frac{1}{h^{3N}N!} \int \delta(\tilde{H}(\mathbf{G}) - E) \tilde{\mathcal{J}} d\mathbf{G} \\
 &= \frac{1}{h^{3N}N!} \int_{\tilde{A}(E)} \frac{\tilde{\mathcal{J}} d\tilde{A}_E}{|\tilde{\nabla}\tilde{H}|},
 \end{aligned}$$

where $\tilde{\Omega}(a, b) = \{\mathbf{G} : a < \tilde{H}(\mathbf{G}) < b\}$. Consequently we define

$$Z_{\tilde{\mathbf{B}}}^E(E) = e^{S_{\tilde{\mathbf{B}}}^E(E)} = \frac{1}{h^{3N}N!} \int_{\tilde{A}(E)} \tilde{\mathcal{J}}\tilde{\mathbf{B}} \cdot \tilde{\nabla}\tilde{H} \frac{d\tilde{A}_E}{|\tilde{\nabla}\tilde{H}|},$$

whence we obtain

$$\begin{aligned}
 h^{3N}N! \frac{\partial Z_{\tilde{\mathbf{B}}}^E(E)}{\partial E} &= \lim_{\delta \rightarrow 0} h^{3N}N! \frac{Z_{\tilde{\mathbf{B}}}^E(E+\delta) - Z_{\tilde{\mathbf{B}}}^E(E)}{\delta} \\
 &= \lim_{\delta \rightarrow 0} \frac{1}{\delta} \left[\int_{\tilde{A}(E+\delta)} \tilde{\mathcal{J}}\tilde{\mathbf{B}} \cdot \tilde{\nabla}\tilde{H} \frac{d\tilde{A}_{E+\delta}}{|\tilde{\nabla}\tilde{H}|} - \int_{\tilde{A}(E)} \tilde{\mathcal{J}}\tilde{\mathbf{B}} \cdot \tilde{\nabla}\tilde{H} \frac{d\tilde{A}_E}{|\tilde{\nabla}\tilde{H}|} \right] \\
 &= \lim_{\delta \rightarrow 0} \frac{1}{\delta} \left[\int_{\tilde{A}(E+\delta)} \tilde{\mathcal{J}}\tilde{\mathbf{B}}(\mathbf{G}) \cdot \hat{\mathbf{n}}(\mathbf{G}) d\tilde{A}_{E+\delta} - \int_{\tilde{A}(E)} \tilde{\mathcal{J}}\tilde{\mathbf{B}}(\mathbf{G}) \cdot \hat{\mathbf{n}}(\mathbf{G}) d\tilde{A}_E \right],
 \end{aligned}$$

where $\hat{\mathbf{n}}(\mathbf{G})$ is a unit normal vector to the hypersurface $\tilde{A}(E)$ at \mathbf{G} .

We apply Gauss' theorem to obtain

$$\begin{aligned}
 h^{3N} N! \frac{\partial Z_{\tilde{\mathbf{B}}}^E(E)}{\partial E} &= \lim_{\delta \rightarrow 0} \frac{1}{\delta} \int_E^{E+\delta} \int_{\tilde{A}(\xi)} \tilde{\nabla} \cdot (\tilde{\mathcal{J}} \tilde{\mathbf{B}}) d\tilde{A}_\xi d\xi \\
 &= \int_{\tilde{A}(E)} \tilde{\nabla} \cdot (\tilde{\mathcal{J}} \tilde{\mathbf{B}}) \delta(\tilde{H}(\mathbf{G}) - E) d\mathbf{G} \\
 &= \int_{A(E)} \frac{\tilde{\nabla} \cdot (\tilde{\mathcal{J}} \tilde{\mathbf{B}})}{\tilde{\mathcal{J}}} \delta(\mathcal{H}(\mathbf{\Gamma}) - E) d\mathbf{\Gamma}.
 \end{aligned}$$

Therefore it follows that

$$\frac{1}{kT_{\tilde{\mathbf{B}}}(E)} := \frac{1}{k} \frac{\partial S_{\tilde{\mathbf{B}}}(E)}{\partial E} = \frac{\langle \tilde{\nabla} \cdot \tilde{\mathbf{B}} \rangle_E + \langle \tilde{\mathbf{B}} \cdot \tilde{\nabla} \ln \tilde{\mathcal{J}} \rangle_E}{\langle \tilde{\nabla} \tilde{H} \cdot \tilde{\mathbf{B}} \rangle_E}, \quad (2.22)$$

in agreement with the canonical ensemble result.

2.4.2 Over-Parametrised Descriptions

It is quite common to describe a system using more coordinates than there are spatial degrees of freedom in the system being described. We call such descriptions **over-parametrised**. Examples include the use of Cartesian coordinates to describe molecular systems, and the use of quaternions to describe rotations. An important part of the Hamiltonian formalism, on which Eqn.(2.16) is based, is that each coordinate is free to vary independently of the others. In over-parametrised descriptions, this condition is not obeyed, so we cannot automatically expect Eqn.(2.16) to hold. In this subsection we will consider what conditions are required so that Eqn.(2.16) does hold for such models.

Typically, over-parametrisation is used to describe a system whose behaviour is **constrained** in some fashion (as with the bond lengths in molecular systems). We shall consider constraints of the form $g(\mathbf{\Gamma}) = k$ for some constant k . Dealing with such constraints usually involves the introduction of additional terms into the equations of motion, in order to keep $g(\mathbf{\Gamma})$ constant. The conditions under which our generalised temperature expression Eqn.(2.16) holds in over-parametrised systems appear in Lue and Evans 2000 — however, Lue's claim that the entropy of the constrained system is the logarithm of the extent of the constrained ensemble[§], although crucial to his argument, is not justified. We will therefore focus on

[§]determined using a measure of the appropriate dimension

this matter, and in the process consider for what constraints these conditions are sufficient.

Eqn.(2.16) can only be applied to a system which has a canonical description, where all variables are free to vary independently. We can achieve this for a constrained system by transforming our coordinates Γ to a new set Γ' , where one of these new coordinates (Γ'_1 , say) is equal to $g(\Gamma)$. This coordinate, and its conjugate momentum, therefore become redundant, and can be removed from this new set of canonical variables. We will be left with a (canonical) subset, to which Eqn.(2.16) can be applied.[¶]

Finding such a transformation is not trivial, however. Indeed, there is an immediate problem. Canonical variables come in pairs — for each coordinate, there is a corresponding momentum. Consequently, phase space must be even in dimension. A single constraint $g(\Gamma)$ in this space is obeyed on a hypersurface of dimension one less than the space it is embedded in, and is therefore odd in dimension. As it requires an odd number of variables to describe a point on this hypersurface uniquely, it cannot be described using canonical variables.

A special case, however, is the class of **holonomic** constraints — constraints of the form $h(\mathbf{q}) = k$. Holonomic constraints are constraints on the coordinates, and not the momenta. For such constraints, $\dot{h} = \nabla h \cdot \dot{\mathbf{q}} = \nabla h \cdot \mathbf{M}^{-1} \mathbf{p} = 0$, which constitutes a second constraint on our system, involving both positions and momenta. The time evolution of a system in which $h(\mathbf{q})$ is held constant must therefore obey *both* constraints. The hypersurface on which these two constraints are obeyed is therefore of dimension *two* less than the space it is embedded in, opening the possibility of a new canonical description.

Indeed, the theory of canonical transformations involving a change of coordinate systems is well understood. Furthermore, they constitute a common type of constraint that we shall encounter in our application of Eqn.(2.16). We will therefore restrict our discussion to the application of holonomic constraints.

Thus we transform our set \mathbf{q} to a new set, \mathbf{q}' , where $q'_1 = h(\mathbf{q})$. By rewriting the Lagrangian in terms of \mathbf{q}' and $\dot{\mathbf{q}}'$, we can determine a new Hamiltonian \mathcal{H}' for our system in terms of the \mathbf{q}' and \mathbf{p}' . Furthermore, the Hamiltonian for our reduced set of canonical variables $\Gamma'' = (q'_2, \dots, p'_2, \dots)$ will be obtained by setting $q'_1 = k$ and $p'_1 = -\sum_{i>2} M'^{-1}_{1i} p'_i / M'^{-1}_{11}$ (so that $\dot{q}'_1 = 0$) in the Hamiltonian

[¶]In the case of describing rotations using quaternions, the magnitude of the quaternion is already a redundant quantity. While it is typically constrained so that $|\mathbf{\Omega}| \equiv 1$ for numerical reasons, the equations of motion can be made independent of the quaternion magnitude. Its rate of change does not feature in the kinetic energy of our system, which is written as the usual product of moments of inertia and angular velocities.

\mathcal{H}' . Since Γ'' forms a set of canonical variables that describe our system, we know that $\beta \langle \nabla'' \mathcal{H}'' \cdot \mathbf{B}'' \rangle'' = \langle \nabla'' \cdot \mathbf{B}'' \rangle''$.

The problem, however, is that the variables of our simulation will not be this proper canonical set. Is it possible, however, to relate $\overline{\nabla \mathcal{H} \cdot \mathbf{B}}$ and $\overline{\nabla \cdot \mathbf{B}}$, given that these are functions of the over-parametrised description Γ , and not the proper one Γ'' ? In this subsection, we will show that it is indeed possible.

We start in the canonical ensemble, where $\overline{\nabla \mathcal{H} \cdot \mathbf{B}} = \langle \nabla \mathcal{H} \cdot \mathbf{B} \rangle''_{\beta}$. For convenience, we define $g(\Gamma) = \nabla_{\mathbf{q}} h \cdot \mathbf{M}^{-1} \mathbf{p} / M_{11}^{-1}$, so that $g'(\Gamma') = \sum_i M_{1i}^{-1} p'_i / M_{11}^{-1}$

$$\begin{aligned} \beta \langle \nabla \mathcal{H} \cdot \mathbf{B} \rangle''_{\beta} &= \frac{\beta}{Z^{\beta}} \int \nabla \mathcal{H} \cdot \mathbf{B} e^{-\beta \mathcal{H}''} d\Gamma'' \\ &= \frac{\beta}{Z^{\beta}} \int \nabla \mathcal{H} \cdot \mathbf{B} e^{-\beta \mathcal{H}'} \delta(q'_1 - k) \delta(p'_1 + \sum_{i>2} M_{1i}^{-1} p'_i / M_{11}^{-1}) d\Gamma' \\ &= \frac{\beta}{Z^{\beta}} \int \nabla \mathcal{H} \cdot \mathbf{B} e^{-\beta \mathcal{H}'} \delta(q'_1 - k) \delta(g'(\Gamma')) d\Gamma' \\ &= \frac{\beta}{Z^{\beta}} \int \nabla \mathcal{H} \cdot \mathbf{B} e^{-\beta \mathcal{H}} \delta(h(\mathbf{q}) - k) \delta(g(\Gamma)) d\Gamma, \end{aligned}$$

where we have transformed coordinates from Γ' to Γ , knowing that the Jacobian of this transformation is unity as the transformation is canonical.

We recall from §2.3.1 that we invoked Gauss' theorem with the vector field $\mathbf{B} e^{-\beta \mathcal{H}}$, showing that the surface term goes to zero. However, whereas earlier we applied Gauss' theorem over a volume of the same dimension as our space, in our current situation we must apply it over the hypersurface in that space where $\delta(h(\mathbf{q}) - k) \delta(g(\Gamma))$ is non-zero — the **hypersurface of constraint**. Consequently, Gauss' theorem will only hold if the vector field $\mathbf{B} e^{-\beta \mathcal{H}}$ — and therefore the vector field \mathbf{B} — is orthogonal to the hypersurface of constraint. This implies that $\mathbf{B} \cdot \nabla h = 0$ and $\mathbf{B} \cdot \nabla g = 0$.

If this condition holds, we can invoke Gauss' theorem, obtaining

$$\begin{aligned} \beta \langle \nabla \mathcal{H} \cdot \mathbf{B} \rangle'' &= \frac{1}{Z^{\beta}} \int \nabla \cdot \mathbf{B} e^{-\beta \mathcal{H}} \delta(h(\mathbf{q}) - k) \delta(g(\Gamma) - 0) d\Gamma \\ &= \langle \nabla \cdot \mathbf{B} \rangle'', \end{aligned}$$

and we are done.

A similar extension must be made in the microcanonical ensem-

ble. We start with

$$\begin{aligned}
 \frac{1}{h^{3N}N!} \int_{A''(E)} \frac{dA''_E}{|\nabla\mathcal{H}''|} &= \frac{1}{h^{3N}N!} \int \delta(\mathcal{H}'(\mathbf{\Gamma}') - E) \delta(q'_1 - k) \delta(g'(\mathbf{\Gamma}')) d\mathbf{\Gamma}' \\
 &= \lim_{\delta \rightarrow 0} \frac{1}{h^{3N}N!} \int_{A'(E+\delta)} \int_{q'_1=k} \int_{g'(\mathbf{\Gamma}')=0}^{q'_1=k+\delta} d\mathbf{\Gamma}' \\
 &= \lim_{\delta \rightarrow 0} \frac{1}{h^{3N}N!} \int_{A(E)} \int_{h(\mathbf{q})=k} \int_{g(\mathbf{\Gamma})=0}^{h(\mathbf{q})=k+\delta} d\mathbf{\Gamma} \\
 &= \frac{1}{h^{3N}N!} \int_{A(E)} \delta(h(\mathbf{q}) - k) \delta(g(\mathbf{\Gamma})) \frac{dA_E}{|\nabla\mathcal{H}|},
 \end{aligned}$$

and

$$\begin{aligned}
 \mathcal{Z}_{\mathbf{B}}^E(E) = e^{S_{\mathbf{B}}(E)} &= \frac{1}{h^{3N}N!} \int_{A''(E)} \mathbf{B} \cdot \nabla\mathcal{H} \frac{dA''_E}{|\nabla\mathcal{H}''|} \\
 &= \frac{1}{h^{3N}N!} \int_{A(E)} \mathbf{B} \cdot \nabla\mathcal{H} \delta(h(\mathbf{q}) - k) \delta(g(\mathbf{\Gamma})) \frac{dA_E}{|\nabla\mathcal{H}|},
 \end{aligned}$$

so that

$$\begin{aligned}
 h^{3N}N! \frac{\partial \mathcal{Z}_{\mathbf{B}}^E(E)}{\partial E} &= \lim_{\delta \rightarrow 0} \frac{1}{\delta} \left[\int_{A(E+\delta)} \mathbf{B}(\mathbf{\Gamma}) \cdot \hat{\mathbf{n}}(\mathbf{\Gamma}) \delta(h(\mathbf{q}) - k) \delta(g(\mathbf{\Gamma})) dA_{E+\delta} - \right. \\
 &\quad \left. \int_{A(E)} \mathbf{B}(\mathbf{\Gamma}) \cdot \hat{\mathbf{n}}(\mathbf{\Gamma}) \delta(h(\mathbf{q}) - k) \delta(g(\mathbf{\Gamma})) dA_E \right],
 \end{aligned}$$

At this point we make the same amendment to our application of Gauss' theorem as for the microcanonical ensemble. We do not apply Gauss' theorem to the entire volume of phase space between $A(E)$ and $A(E + \delta)$, but only on the hypersurface of constraint. Consequently, we can only apply Gauss' theorem if $\mathbf{B} \cdot \nabla h = 0$ and $\mathbf{B} \cdot \nabla g = 0$ — the same conditions as in the canonical ensemble case. From the point of view of Rugh's derivation, we can interpret this condition as a requirement to choose a vector field \mathbf{B} so that the generated flow lies on the hypersurface of constraint — the constraints are conserved as we move from $A(E)$ to $A(E + \delta)$.

Given that these conditions are obeyed, we obtain

$$\begin{aligned}
 h^{3N}N! \frac{\partial \mathcal{Z}_{\mathbf{B}}^E(E)}{\partial E} &= \int_{A(E)} \nabla \cdot \mathbf{B} \delta(h(\mathbf{q}) - k) \delta(g(\mathbf{\Gamma})) \delta(\mathcal{H}(\mathbf{\Gamma}) - E) d\mathbf{\Gamma} \\
 &= \int_{A''(E)} \nabla \cdot \mathbf{B} \frac{dA''_E}{|\nabla\mathcal{H}''|},
 \end{aligned}$$

whence we see that

$$\frac{1}{kT_{\mathbf{B}}(E)} := \frac{1}{k} \frac{\partial S_{\mathbf{B}}(E)}{\partial E} = \frac{\langle \nabla \cdot \mathbf{B}(\Gamma) \rangle_E''}{\langle \nabla \mathcal{H}(\Gamma) \cdot \mathbf{B}(\Gamma) \rangle_E''}. \quad (2.23)$$

We therefore see that Eqn.(2.16) will hold for constrained systems, provided that \mathbf{B} lies in the tangent space of the constraints. This is in agreement with the conclusions of Lue (Lue and Evans 2000). In the case of a holonomic constraint, this requirement is two-fold —

$$\mathbf{B} \cdot \nabla h(\mathbf{q}) = 0 \text{ and } \mathbf{B} \cdot \nabla g(\Gamma) = 0. \quad (2.24)$$

It remains a point of further work to extend this to systems with non-holonomic constraints. The current argument relies on the assumption that the constrained system is still Hamiltonian. For many constraints, this assumption cannot be accommodated — even if Eqn.(2.16) were still to hold, an entirely different approach would be required.

2.4.3 Periodic Boundary Conditions

Having already outlined the usefulness of periodic boundary conditions (§1.4.4), we turn our attention to examining under what conditions Eqn.(2.16) will hold when such conditions are employed. We will restrict our attention to Cartesian descriptions, because this is the representation that we shall adopt, and we will thereby avoid the additional difficulties of a more general theoretical approach.

For periodic systems, the extent of Ω in the coordinates is no longer determined by boundary walls, but by the size and shape of the simulation box. If the simulation box is the same size and shape as the bounded system, then Ω will be the same in both cases.

The difference between the bounded and periodic systems is that particles cannot pass through the walls of the bounded system. This implies that the potential energy goes to infinity at the walls, so that our surfaces of constant energy lie entirely *within* Ω , and do not pass through the boundary, which we denote by $\partial\Omega$. This assumption is implicit in our application of Gauss' theorem, and is an essential part of the proofs of the canonical and microcanonical-ensemble Equipartition theorem.

In the periodic system, particles *can* (and do) pass through the boundaries of our simulation box, reappearing on the other side of the cell. Therefore hypersurfaces of constant energy must pass through $\partial\Omega$. Thus, when we use Gauss' theorem, our Gaussian surface consists not only of constant-energy hypersurfaces, but of subsets of $\partial\Omega$ as well.

We begin by considering the canonical ensemble, where our proof of Eqn.(2.16) began by applying Gauss' theorem in the volume

$\Omega(E)$. With periodic boundary conditions, our Gaussian surface consists not only of $A(E)$, but of $\partial\Omega(E) = \partial\Omega \cap \Omega(E)$ as well, and the left hand side of Eqn.(2.17) becomes

$$\lim_{E \rightarrow \infty} \int_{A(E) \cup \partial\Omega(E)} e^{-\beta\mathcal{H}(\Gamma)} \mathbf{B}(\Gamma) \cdot \hat{\mathbf{n}}(\Gamma) dA.$$

where dA is the hypersurface measure in our phase space, and $\hat{\mathbf{n}}(\Gamma)$ is the unit normal on our surface. Note that $\hat{\mathbf{n}}(\Gamma)$ does not necessarily point in the same direction as $\nabla\mathcal{H}(\Gamma)$, since the walls of the simulation box are independent by the energy surfaces. We have already seen that the integral over $A(E)$ must go to zero in order for $\langle \nabla\mathcal{H} \cdot \mathbf{B} \rangle_\beta$ to exist, so we only require that

$$\int_{\partial\Omega} e^{-\beta\mathcal{H}(\Gamma)} \mathbf{B}(\Gamma) \cdot \hat{\mathbf{n}}(\Gamma) dA = 0 \quad \forall \beta.$$

In the microcanonical case, we apply Gauss' theorem in the volume between surfaces $A(E)$ and $A(E + \delta)$. With periodic boundary conditions, the bounds of this volume must also include all points on $\partial\Omega$ whose energies lie between E and $E + \delta$. This extra term is of the form

$$\lim_{\delta \rightarrow 0} \frac{1}{\delta} \left[\int_{\partial\Omega(E+\delta)} \mathbf{B}(\Gamma) \cdot \hat{\mathbf{n}}(\Gamma) dA - \int_{\partial\Omega(E)} \mathbf{B}(\Gamma) \cdot \hat{\mathbf{n}}(\Gamma) dA \right] = \int_{\partial A(E)} \mathbf{B}(\Gamma) \cdot \hat{\mathbf{n}}(\Gamma) dL_E,$$

where $\partial A(E) = \partial\Omega \cap A(E)$, and dL_E is the volume measure on $\partial A(E)$. From the properties of the Laplace transform we see that

$$\int_{\partial\Omega} e^{-\beta\mathcal{H}(\Gamma)} \mathbf{B}(\Gamma) \cdot \hat{\mathbf{n}}(\Gamma) dA = 0 \quad \forall \beta \quad \Leftrightarrow \quad \int_{\partial A(E)} \mathbf{B}(\Gamma) \cdot \hat{\mathbf{n}}(\Gamma) dL_E = 0 \quad \forall E,$$

so that the condition under which Eqn.(2.16) will hold for all canonical ensembles is the same as the condition under which it will hold in all microcanonical ensembles. But what vector fields satisfy this condition?

Let us consider a system where one of the particles is at one of the walls of the simulation box^{||}, corresponding to a phase point Γ_a . There is an equivalent system where this particle is placed on the 'opposite' wall of the simulation box, represented by Γ_b . It follows that $\hat{\mathbf{n}}(\Gamma_a) = -\hat{\mathbf{n}}(\Gamma_b)$ in phase space. Therefore, since Γ_a and Γ_b must lie in the same microcanonical ensemble, if $\mathbf{B}(\Gamma_a) =$

^{||}If two or more particles are at the wall, or if the particle is in a corner, then this corresponds to a subset of $\partial\Omega$ of measure zero.

$\mathbf{B}(\Gamma_b)$, then the condition for periodic boundary systems is satisfied. Therefore any vector field which is **periodic** in the simulation box — that is, $\mathbf{B}(\Gamma_a) = \mathbf{B}(\Gamma_b)$ whenever Γ_a and Γ_b describe the same state — will satisfy Eqn.(2.16) for periodic boundary systems. Note that this is a sufficient condition, but not a necessary one for a given Hamiltonian (by which the $\partial A(E)$ are defined). It is a necessary condition, however, if Eqn.(2.16) is to hold independently of the choice of Hamiltonian.

In relation to this point, we note that Gray and Gubbin's starting premise for their hypervirial relations (that $\overline{\dot{\mathcal{A}}} = 0$) is not always true in periodic boundary systems if \mathcal{A} is not periodic in the simulation box. We also note that the configurational part of Γ is not periodic in our cell, from which we (correctly) conclude that the Clausius virial theorem will not hold in periodic boundary systems. Interestingly, since the Hamiltonian is periodic in periodic boundary systems, $\nabla\mathcal{H}/|\nabla\mathcal{H}|^2$ will also be periodic, so that Rugh's result holds in periodic systems.

There is a final, important consequence of using periodic boundary conditions that we must remember to take into account. We recall that the inverse temperature is defined as the derivative of the entropy with respect to the *internal* energy of a system. It is important, therefore, that we choose a frame of reference such that the kinetic energy in our Hamiltonian represents the internal kinetic energy of the system.

For a bounded system, this is quite simply achieved by choosing the frame of reference of the box containing the particles**. In the periodic boundary system, we must use the centre-of-mass frame of the particles. Consequently, we have an over-parametrised system, since we must have $\sum_i m_i x_i = k_x$ and $\sum_i m_i \dot{x}_i = 0$, with similar constraints in the y - and z -directions††. We call a periodic boundary system with these conditions the **MD ensemble**, since it is commonly used in molecular dynamics. Thus we have a canonical MD ensemble, a microcanonical MD ensemble, and so on. We can therefore apply the work of the previous section to calculate the

**Technically, this frame of reference is inertial, so we should choose the centre-of-mass frame of whole system (ie particles and box). However, we assume that the box is massive enough that the kinetic contribution of the box will be well approximated by zero, and the positions of the walls, as required in the calculation of the external forces, can be assumed constant.

††Note that these position coordinates are not the periodic coordinates we use in our simulations, but the continuous ones that follow the particles as they diverge from the initial simulation box. The forces in this representation must be periodic throughout all space. The condition on the coordinate derivatives is identical in our simulation, but the condition on the coordinates themselves must be appropriately amended. Ultimately, however, this difference does not affect our conclusions in this subsection.

temperature, as these constraints are holonomic. We find that the temperature of the system will be given by Eqn.(2.16) for any vector field \mathbf{B} such that $\mathbf{B} \cdot \nabla(\sum_i m_i x_i) = 0$, $\mathbf{B} \cdot \nabla(\sum_i p_{x_i}) = 0$, and similar conditions for y and z directions.

Interestingly, the Equipartition theorem ($\mathbf{B} = \nabla K$) obeys these conditions, and therefore holds in the MD ensembles. We will consider which other temperature expressions can also be used in the MD ensembles in the next section.

2.5 Microscopic Temperature Expressions

We conclude this chapter by using the work of the previous sections, to produce a series of temperature expressions that we will test in Chapter 4. We will begin with the expressions for atomic systems, and then look at rigid-body temperature expressions. Finally, we will derive two expressions for the heat capacity, from our work in §2.2.2.

To begin, we will simulate a system of N identical atoms (ie of equal mass) in a cubic box, using a description of Cartesian coordinates \mathbf{r} and momenta \mathbf{p} . We will use periodic boundary conditions during our simulation, and will therefore be in the canonical or microcanonical MD ensembles. Furthermore, the potential energy in our system will consist of a sum of pairwise interactions, according to a short-ranged pair potential $\phi(r)$. We will use either the LJ or WCA potentials, as defined in §1.4.2. The Hamiltonian \mathcal{H} for this system will be the sum of a kinetic term K and a configurational term Φ :

$$\mathcal{H}(\Gamma) = K(\mathbf{p}) + \Phi(\mathbf{q}) = \sum_{i=1}^{3N} \frac{p_i^2}{2m} + \sum_{j < i} \phi(\tilde{r}_{ij}), \quad (2.25)$$

where \tilde{r}_{ij} is the minimum-image separation between particles i and j (§1.4.4). We therefore obtain equations of motion

$$\dot{\mathbf{r}} = \nabla_{\mathbf{p}} \mathcal{H} = \frac{\mathbf{p}}{m}, \quad \dot{\mathbf{p}} = \nabla_{\mathbf{r}} \mathcal{H} = \mathbf{F}.$$

We are interested in determining vector fields \mathbf{B} for which Eqn.(2.16) will hold. As our system uses periodic boundary conditions, the forces F_i acting on a body are not correlated with the coordinates of the particles r_i , but only with their minimum-image separations. Consequently, many of the simple vector fields \mathbf{B} that we might otherwise test are uncorrelated with the forces, so that $\langle \nabla \mathcal{H} \cdot \mathbf{B} \rangle = 0$. In general, it is difficult to find functions that are correlated with the inter-particle forces, and the calculation of their divergences is also difficult (and computationally expensive). Due to this difficulty,

from this point on we restrict ourselves to choices of $\mathbf{B}(\Gamma)$ which are directly related to $\nabla\mathcal{H}$, to ensure that this condition is met.

Based on the results in this chapter, we shall examine six expressions for the temperature of our system:

$$\frac{1}{kT_{\text{NR}}} = \left\langle \nabla \cdot \frac{\nabla\mathcal{H}}{|\nabla\mathcal{H}|^2} \right\rangle, \quad \frac{1}{kT_{\text{NF}}} = \frac{\langle \nabla \cdot \nabla\mathcal{H} \rangle}{\langle |\nabla\mathcal{H}|^2 \rangle}, \quad (2.26)$$

$$\frac{1}{kT_{\text{CR}}} = \left\langle \nabla \cdot \frac{\nabla\Phi}{|\nabla\Phi|^2} \right\rangle, \quad \frac{1}{kT_{\text{CF}}} = \frac{\langle \nabla \cdot \nabla\Phi \rangle}{\langle |\nabla\Phi|^2 \rangle}, \quad (2.27)$$

$$\frac{1}{kT_{\text{KR}}} = \left\langle \nabla \cdot \frac{\nabla K}{|\nabla K|^2} \right\rangle, \quad \frac{1}{kT_{\text{KF}}} = \frac{\langle \nabla \cdot \nabla K \rangle}{\langle |\nabla K|^2 \rangle}. \quad (2.28)$$

Here, the letters N, C, and K stand for ‘Normal’ (or ‘Natural’), ‘Configurational’ and ‘Kinetic’ respectively, and the letters R and F stand for ‘Rough’ and ‘Fractional’ respectively. We also denote the **instantaneous values** of these expressions by the symbols $T_{\text{NR}}, T_{\text{CF}}$, etc. Of particular interest are the configurational temperatures — these permit the measurement of the temperature of a system without reference to the momenta of its molecules.

Thus, the Rough temperatures are of the form appearing in (Rugh 1997; Rugh 1998), and the fractional temperatures are the similar, fractional forms appearing in Eqn.(2.16). We note immediately that T_{KF} is none other than the Equipartition temperature — that is, the temperature expression as determined by the Equipartition theorem.

Before we expand these temperature expressions in terms of the coordinate and momenta, however, we should ensure that they meet the criteria determined in the previous section for periodic boundary systems and the MD ensemble, as well as the continuity requirement in our application of Gauss’ theorem.

If the potential has a continuous first derivative, then $\nabla\mathcal{H}$ satisfies the requirements of Gauss’ Theorem. The WCA has a continuous first derivative, and while the LJ potential is discontinuous at its cutoff, the numerical error in setting the potential and its derivative to zero at the cutoff is very small. Furthermore, Φ and K both grow as N in the thermodynamic limit, so these expressions obey the conditions for Eqn.(2.16) to hold, provided the averages exist. We note that Φ is periodic in the spatial coordinates, so that $\nabla\Phi$, ∇K and $\nabla\mathcal{H}$ will be periodic vector fields in our simulation box. Thus our six temperature expressions meet the criteria for Eqn.(2.16) to hold in periodic boundary systems.

The requirements for the MD ensemble are that $\mathbf{B} \cdot \nabla(\sum_i m_i x_i) = 0$, $\mathbf{B} \cdot \nabla(\sum_i p_{x_i}) = 0$, and similarly for the other y - and z -directions. These conditions become $\sum_i F_{x_i} m_i = m \sum_i F_{x_i}$ for the configuration temperatures, $\sum_i p_{x_i} = 0$ for the kinetic temperatures, and both for the normal temperatures. Each of these conditions is satisfied in the

periodic system. We note, however, that if the masses were unequal, the configurational condition would no longer hold.

Since they obey all the conditions required, we can expect each of the six temperature expressions to hold during our simulations. In terms of the generalised coordinates, momenta and forces, they become

$$\frac{1}{kT_{\text{NR}}} = \left\langle \frac{\frac{3N}{m} - \sum_i \frac{\partial F_i}{\partial q_i}}{\sum_i \frac{p_i^2}{m^2} + F_i^2} - \frac{2 \sum_i \frac{p_i^2}{m^3} + 2 \sum_{ij} F_i F_j \frac{\partial F_j}{\partial q_i}}{(\sum_i \frac{p_i^2}{m^2} + F_i^2)^2} \right\rangle, \quad (2.29)$$

$$\frac{1}{kT_{\text{CR}}} = \left\langle \frac{-\sum_i \frac{\partial F_i}{\partial q_i}}{\sum_i F_i^2} - \frac{2 \sum_{ij} F_i F_j \frac{\partial F_j}{\partial q_i}}{(\sum_i F_i^2)^2} \right\rangle, \quad (2.30)$$

$$\frac{1}{kT_{\text{KR}}} = \left\langle \frac{\frac{3N}{m}}{\sum_i \frac{p_i^2}{m^2}} - \frac{2 \sum_i \frac{p_i^2}{m^3}}{(\sum_i \frac{p_i^2}{m^2})^2} \right\rangle = \left\langle \frac{3N - 2}{\sum_i \frac{p_i^2}{m}} \right\rangle, \quad (2.31)$$

$$\frac{1}{kT_{\text{NF}}} = \frac{\left\langle \frac{3N}{m} - \sum_i \frac{\partial F_i}{\partial q_i} \right\rangle}{\left\langle \sum_i \frac{p_i^2}{m^2} + F_i^2 \right\rangle}, \quad (2.32)$$

$$\frac{1}{kT_{\text{CF}}} = \frac{\left\langle -\sum_i \frac{\partial F_i}{\partial q_i} \right\rangle}{\left\langle \sum_i F_i^2 \right\rangle}, \quad (2.33)$$

$$\frac{1}{kT_{\text{KF}}} = \frac{\left\langle \frac{3N}{m} \right\rangle}{\left\langle \sum_i \frac{p_i^2}{m^2} \right\rangle} = \frac{3N}{\left\langle \sum_i \frac{p_i^2}{m} \right\rangle}. \quad (2.34)$$

If we consider the second term on the right hand side of Eqn.(2.29) and Eqn.(2.30), the numerator increases as N for a short-ranged potential (since $F_i F_j \partial F_j / \partial q_i$ is zero unless particles i and j interact), and the denominator increases as N^2 . Therefore this second term becomes negligible in the thermodynamic limit, and the $\mathcal{O}(1)$ term for the temperature is contained in the first term of Eqn.(2.29) and Eqn.(2.30). We will denote by T_{N1} and T_{C1} the temperature expressions consisting of these $\mathcal{O}(1)$ expressions:

$$\frac{1}{kT_{\text{N1}}} = \left\langle \frac{\frac{3N}{m} - \sum_i \frac{\partial F_i}{\partial q_i}}{\sum_i \frac{p_i^2}{m^2} + F_i^2} \right\rangle, \quad (2.35)$$

$$\frac{1}{kT_{\text{C1}}} = \left\langle \frac{-\sum_i \frac{\partial F_i}{\partial q_i}}{\sum_i F_i^2} \right\rangle. \quad (2.36)$$

For completeness, we also define the temperature

$$\frac{1}{kT_{\text{K1}}} = \left\langle \frac{\frac{3N}{m}}{\sum_i \frac{p_i^2}{m^2}} \right\rangle, \quad (2.37)$$

and we will call this form of the temperature expressions the ' $\mathcal{O}(1)$ ' temperature.

We expect each of these nine expressions to be equal, to $\mathcal{O}(1/N)$, to the thermodynamic temperature of our system. Collectively, we call the various \mathcal{T} . the **instantaneous temperature expressions**, or **instantaneous temperatures**, and we call the various T . the **temperatures** of our system.

At a given phase point, the only difference between the instantaneous configurational temperatures for WCA and LJ systems arises from the attractive forces in the LJ potential. We note, however, from the form of the configurational temperatures, that the contributions for the short-range repulsive part of the potential are orders of magnitude larger than the contributions from the attractive tail. These contributions, which dominate in the range of state points usually examined for LJ and WCA systems, are essentially identical at a given phase point, for either potential.

Given the structural similarity between WCA and LJ fluids in the range of state points we shall consider (Weeks, Chandler, and Andersen 1971) — particularly at short-range — we would expect to observe similar behaviour trends in the configurational temperatures of WCA and LJ fluids, as simulation parameters vary. Certainly we do not expect identical temperatures for identical initial conditions. However, we would expect similar time-behaviour of the fluctuations and cumulating average of the instantaneous configuration temperatures, similar convergence of the configurational temperatures in the thermodynamic limit, and so on. The shorter times required for simulations of WCA systems, due to the short range of the potential, leads us to examine these systems in Chapter 4.

We will also test our theory on rigid-body systems. We will simulate a system of N identical rigid bodies (ie of equal mass) in a cubic box, using a description of Cartesian coordinates \mathbf{r} and momenta \mathbf{p} to describe translational behaviour, and $\mathbf{\Omega}_i$ and $\boldsymbol{\omega}'_i$ to describe rotational behaviour. We will again use periodic boundary conditions during our simulation. The potential energy in our system will be the sum of pairwise P2 potential (§1.4.2) interactions. Consequently, the description we have chosen over-parametrises our system — we are using four parameters to describe a two-parameter problem, since the P2 potential represents an interaction between two (unit) vectors in space. We will denote by $\hat{\mathbf{n}}_i$ the (unit) vector associated particle i , which we choose to be the z -axis of the body frame representing the orientation of particle i . The energy E for this system will therefore be

$$E = \sum_i \frac{p_i^2}{2m} + \boldsymbol{\omega}'_i \Theta^P \boldsymbol{\omega}'_i + \sum_{j < i} \phi_{P2}(\tilde{r}_{ij}, \theta_{ij}),$$

where θ_{ij} represents the angle between $\hat{\mathbf{n}}_i$ and $\hat{\mathbf{n}}_j$. At this point we define $\mathbf{Q} = (\mathbf{q}_{10}, \mathbf{q}_{11}, \mathbf{q}_{12}, \mathbf{q}_{13}, \mathbf{q}_{20}, \dots, \mathbf{q}_{N3})$, where $\mathbf{q}_{i\alpha}$ represents

the α -th component ($\alpha \in \{0, 1, 2, 3\}$) of the i -th quaternion, as the vector of all quaternion coordinates. Thus we can define two coordinate-based temperatures, based on the vector fields $\nabla_{\mathbf{r}}\Phi$ and $\nabla_{\mathbf{Q}}\Phi$. The former will have exactly the same form as Eqn.(2.33). We will now examine the latter form, from which we will obtain **quaternionic** fractional and $\mathcal{O}(1)$ temperatures T_{QF} and T_{Q1} respectively. We recall that

$$\begin{aligned}\phi_{\text{P2}}(\tilde{r}_{ij}, \theta_{ij}) &= 4\epsilon \left[\left(\frac{\sigma}{\tilde{r}_{ij}} \right)^{12} - \left(1 + \lambda \frac{3 \cos^2 \theta_{ij} - 1}{2} \right) \left(\frac{\sigma}{\tilde{r}_{ij}} \right)^6 \right] \\ &= 4\epsilon \left[\left(\frac{\sigma}{\tilde{r}_{ij}} \right)^{12} - \left(1 - \frac{\lambda}{2} \right) \left(\frac{\sigma}{\tilde{r}_{ij}} \right)^6 \right] - 4\epsilon \lambda \frac{3(\hat{\mathbf{n}}_i \cdot \hat{\mathbf{n}}_j)^2}{2} \left(\frac{\sigma}{\tilde{r}_{ij}} \right)^6.\end{aligned}$$

We call this last term $\phi_{\text{rot}}(\tilde{r}_{ij}, \hat{\mathbf{n}}_i, \hat{\mathbf{n}}_j)$, and we define

$$\Phi_{\text{rot}} = \sum_{\{ij\}} \phi_{\text{rot}}(\tilde{r}_{ij}, \hat{\mathbf{n}}_i, \hat{\mathbf{n}}_j) = -6\epsilon\lambda\sigma^6 \sum_{\{ij\}} (\hat{\mathbf{n}}_i \cdot \hat{\mathbf{n}}_j)^2 \left(\frac{1}{\tilde{r}_{ij}} \right)^6 = \kappa \sum_{\{ij\}} (\hat{\mathbf{n}}_i \cdot \hat{\mathbf{n}}_j)^2 \tilde{r}_{ij}^{-6},$$

where $\kappa = -6\epsilon\lambda\sigma^6$. In order to determine T_{QF} , we must calculate $\partial_{i\alpha}V = \partial_{i\alpha}\Phi_{\text{rot}}$ and $\partial_{i\alpha}\partial_{i\alpha}V = \partial_{i\alpha}\partial_{i\alpha}\Phi_{\text{rot}}$, where $\partial_{i\alpha} = \partial/\partial q_{i\alpha}$. Therefore the quaternionic temperature $kT_{\text{QF}} = \langle \sum_{i\alpha} (\partial_{i\alpha}\Phi_{\text{rot}})^2 \rangle / \langle \sum_{i\alpha} \partial_{i\alpha}^2 \Phi_{\text{rot}} \rangle$, and the rest of this section is dedicated to determining the two sums in this expression, for which we must calculate averages.

We have

$$\begin{aligned}\partial_{i\alpha}\Phi_{\text{rot}} &= \partial_{i\alpha} \left(\kappa \sum_j (\hat{\mathbf{n}}_i \cdot \hat{\mathbf{n}}_j)^2 \tilde{r}_{ij}^{-6} \right) \\ &= \kappa \sum_j \tilde{r}_{ij}^{-6} \partial_{i\alpha} (\hat{\mathbf{n}}_i \cdot \hat{\mathbf{n}}_j)^2 \\ &= 2\kappa \sum_j \tilde{r}_{ij}^{-6} (\hat{\mathbf{n}}_i \cdot \hat{\mathbf{n}}_j) (\partial_{i\alpha} \hat{\mathbf{n}}_i \cdot \hat{\mathbf{n}}_j), \\ \partial_{i\alpha}^2 \Phi_{\text{rot}} &= 2\partial_{i\alpha} \left(\kappa \sum_j \tilde{r}_{ij}^{-6} (\hat{\mathbf{n}}_i \cdot \hat{\mathbf{n}}_j) (\partial_{i\alpha} \hat{\mathbf{n}}_i \cdot \hat{\mathbf{n}}_j) \right) \\ &= 2\kappa \sum_j \tilde{r}_{ij}^{-6} [(\partial_{i\alpha} \hat{\mathbf{n}}_i \cdot \hat{\mathbf{n}}_j) (\partial_{i\alpha} \hat{\mathbf{n}}_i \cdot \hat{\mathbf{n}}_j) + (\hat{\mathbf{n}}_i \cdot \hat{\mathbf{n}}_j) (\partial_{i\alpha}^2 \hat{\mathbf{n}}_i \cdot \hat{\mathbf{n}}_j)],\end{aligned}$$

and

$$\begin{aligned}(\partial_{i\alpha}\Phi_{\text{rot}})^2 &= \left(2\kappa \sum_j \tilde{r}_{ij}^{-6} (\hat{\mathbf{n}}_i \cdot \hat{\mathbf{n}}_j) (\partial_{i\alpha} \hat{\mathbf{n}}_i \cdot \hat{\mathbf{n}}_j) \right) \left(2\kappa \sum_k \tilde{r}_{ik}^{-6} (\hat{\mathbf{n}}_i \cdot \hat{\mathbf{n}}_k) (\partial_{i\alpha} \hat{\mathbf{n}}_i \cdot \hat{\mathbf{n}}_k) \right) \\ &= 4\kappa^2 \sum_{jk} \tilde{r}_{ij}^{-6} \tilde{r}_{ik}^{-6} (\hat{\mathbf{n}}_i \cdot \hat{\mathbf{n}}_j) (\hat{\mathbf{n}}_i \cdot \hat{\mathbf{n}}_k) (\partial_{i\alpha} \hat{\mathbf{n}}_i \cdot \hat{\mathbf{n}}_j) (\partial_{i\alpha} \hat{\mathbf{n}}_i \cdot \hat{\mathbf{n}}_k).\end{aligned}$$

Therefore

$$\begin{aligned}
\sum_{i\alpha} (\partial_{i\alpha} \Phi_{\text{rot}})^2 &= 4\kappa^2 \sum_{i\alpha jk} \tilde{r}_{ij}^{-6} \tilde{r}_{ik}^{-6} (\hat{\mathbf{n}}_i \cdot \hat{\mathbf{n}}_j) (\hat{\mathbf{n}}_i \cdot \hat{\mathbf{n}}_k) (\partial_{i\alpha} \hat{\mathbf{n}}_i \cdot \hat{\mathbf{n}}_j) (\partial_{i\alpha} \hat{\mathbf{n}}_i \cdot \hat{\mathbf{n}}_k), \\
&= 4\kappa^2 \sum_{ijk} \tilde{r}_{ij}^{-6} \tilde{r}_{ik}^{-6} (\hat{\mathbf{n}}_i \cdot \hat{\mathbf{n}}_j) (\hat{\mathbf{n}}_i \cdot \hat{\mathbf{n}}_k) \sum_{\alpha} (\partial_{i\alpha} \hat{\mathbf{n}}_i \cdot \hat{\mathbf{n}}_j) (\partial_{i\alpha} \hat{\mathbf{n}}_i \cdot \hat{\mathbf{n}}_k), \\
\sum_{i\alpha} \partial_{i\alpha}^2 \Phi_{\text{rot}} &= 2\kappa \sum_{i\alpha j} \tilde{r}_{ij}^{-6} [(\partial_{i\alpha} \hat{\mathbf{n}}_i \cdot \hat{\mathbf{n}}_j) (\partial_{i\alpha} \hat{\mathbf{n}}_i \cdot \hat{\mathbf{n}}_j) + (\hat{\mathbf{n}}_i \cdot \hat{\mathbf{n}}_j) (\partial_{i\alpha}^2 \hat{\mathbf{n}}_i \cdot \hat{\mathbf{n}}_j)] \\
&= 2\kappa \sum_{ij} \tilde{r}_{ij}^{-6} \left[\sum_{\alpha} (\partial_{i\alpha} \hat{\mathbf{n}}_i \cdot \hat{\mathbf{n}}_j) (\partial_{i\alpha} \hat{\mathbf{n}}_i \cdot \hat{\mathbf{n}}_j) + (\hat{\mathbf{n}}_i \cdot \hat{\mathbf{n}}_j) (\hat{\mathbf{n}}_j \cdot \sum_{\alpha} \partial_{i\alpha}^2 \hat{\mathbf{n}}_i) \right].
\end{aligned}$$

From the results of §2.6, we know that

$$\begin{aligned}
\sum_{\alpha} (\partial_{i\alpha} \hat{\mathbf{n}}_i \cdot \hat{\mathbf{n}}_j) (\partial_{i\alpha} \hat{\mathbf{n}}_i \cdot \hat{\mathbf{n}}_k) &= \frac{4\hat{\mathbf{n}}_j \cdot \hat{\mathbf{n}}_k}{|\mathbf{n}_i|} - \frac{4(\hat{\mathbf{n}}_j \cdot \mathbf{n}_i)(\hat{\mathbf{n}}_k \cdot \mathbf{n}_i)}{|\mathbf{n}_i|^3} \\
&= \frac{4}{|\mathbf{n}_i|} [\hat{\mathbf{n}}_j \cdot \hat{\mathbf{n}}_k - (\hat{\mathbf{n}}_j \cdot \hat{\mathbf{n}}_i)(\hat{\mathbf{n}}_k \cdot \hat{\mathbf{n}}_i)], \\
\sum_{\alpha} (\partial_{i\alpha} \hat{\mathbf{n}}_i \cdot \hat{\mathbf{n}}_j) (\partial_{i\alpha} \hat{\mathbf{n}}_i \cdot \hat{\mathbf{n}}_j) &= \frac{4}{|\mathbf{n}_i|} [1 - (\hat{\mathbf{n}}_j \cdot \hat{\mathbf{n}}_i)^2], \\
\hat{\mathbf{n}}_j \cdot \sum_{\alpha} \partial_{i\alpha}^2 \hat{\mathbf{n}}_i &= \hat{\mathbf{n}}_j \cdot \frac{-8\mathbf{n}_i}{|\mathbf{n}_i|^2} \\
&= \frac{-8}{|\mathbf{n}_i|} (\hat{\mathbf{n}}_j \cdot \hat{\mathbf{n}}_i).
\end{aligned}$$

Therefore, setting $|\mathbf{n}_i| \equiv 1$ (as will be the case in our simulation), we have

$$\begin{aligned}
\sum_{i\alpha} (\partial_{i\alpha} \Phi_{\text{rot}})^2 &= 4\kappa^2 \sum_{ijk} \tilde{r}_{ij}^{-6} \tilde{r}_{ik}^{-6} (\hat{\mathbf{n}}_i \cdot \hat{\mathbf{n}}_j) (\hat{\mathbf{n}}_i \cdot \hat{\mathbf{n}}_k) \sum_{\alpha} (\partial_{i\alpha} \hat{\mathbf{n}}_i \cdot \hat{\mathbf{n}}_j) (\partial_{i\alpha} \hat{\mathbf{n}}_i \cdot \hat{\mathbf{n}}_k) \\
&= 4\kappa^2 \sum_{ijk} \tilde{r}_{ij}^{-6} \tilde{r}_{ik}^{-6} (\hat{\mathbf{n}}_i \cdot \hat{\mathbf{n}}_j) (\hat{\mathbf{n}}_i \cdot \hat{\mathbf{n}}_k) 4 [\hat{\mathbf{n}}_j \cdot \hat{\mathbf{n}}_k - (\hat{\mathbf{n}}_j \cdot \hat{\mathbf{n}}_i)(\hat{\mathbf{n}}_k \cdot \hat{\mathbf{n}}_i)] \\
&= 16\kappa^2 \sum_{ijk} \tilde{r}_{ij}^{-6} \tilde{r}_{ik}^{-6} [(\hat{\mathbf{n}}_i \cdot \hat{\mathbf{n}}_j) (\hat{\mathbf{n}}_i \cdot \hat{\mathbf{n}}_k) (\hat{\mathbf{n}}_j \cdot \hat{\mathbf{n}}_k) - (\hat{\mathbf{n}}_j \cdot \hat{\mathbf{n}}_i)^2 (\hat{\mathbf{n}}_k \cdot \hat{\mathbf{n}}_i)^2] \\
&= 16\kappa^2 \sum_i \left(\left| \sum_j \tilde{r}_{ij}^{-6} (\hat{\mathbf{n}}_i \cdot \hat{\mathbf{n}}_j) \hat{\mathbf{n}}_j \right|^2 - \left| \sum_j \tilde{r}_{ij}^{-6} (\hat{\mathbf{n}}_i \cdot \hat{\mathbf{n}}_j)^2 \right|^2 \right),
\end{aligned}$$

and

$$\begin{aligned}
\sum_{i\alpha} \partial_{i\alpha}^2 \Phi_{\text{rot}} &= 2\kappa \sum_{ij} \tilde{r}_{ij}^{-6} \left[\sum_{\alpha} (\partial_{i\alpha} \hat{\mathbf{n}}_i \cdot \hat{\mathbf{n}}_j) (\partial_{i\alpha} \hat{\mathbf{n}}_i \cdot \hat{\mathbf{n}}_j) + (\hat{\mathbf{n}}_i \cdot \hat{\mathbf{n}}_j) (\hat{\mathbf{n}}_j \cdot \sum_{\alpha} \partial_{i\alpha}^2 \hat{\mathbf{n}}_i) \right] \\
&= 2\kappa \sum_{ij} \tilde{r}_{ij}^{-6} [4 [1 - (\hat{\mathbf{n}}_j \cdot \hat{\mathbf{n}}_i)^2] - 8(\hat{\mathbf{n}}_i \cdot \hat{\mathbf{n}}_j)(\hat{\mathbf{n}}_j \cdot \hat{\mathbf{n}}_i)] \\
&= 8\kappa \sum_{ij} \tilde{r}_{ij}^{-6} [1 - 3(\hat{\mathbf{n}}_j \cdot \hat{\mathbf{n}}_i)^2],
\end{aligned}$$

and therefore

$$\frac{1}{kT_{\text{QF}}} = \frac{2\kappa \sum_i \left\langle \left(\left| \sum_j \tilde{r}_{ij}^{-6} (\hat{\mathbf{n}}_i \cdot \hat{\mathbf{n}}_j) \hat{\mathbf{n}}_j \right|^2 - \left| \sum_j \tilde{r}_{ij}^{-6} (\hat{\mathbf{n}}_i \cdot \hat{\mathbf{n}}_j)^2 \right|^2 \right) \right\rangle}{\left\langle \sum_{ij} \tilde{r}_{ij}^{-6} [1 - 3(\hat{\mathbf{n}}_j \cdot \hat{\mathbf{n}}_i)^2] \right\rangle}, \quad (2.38)$$

and

$$\frac{1}{kT_{\text{Q1}}} = \left\langle \frac{2\kappa \sum_i \left(\left| \sum_j \tilde{r}_{ij}^{-6} (\hat{\mathbf{n}}_i \cdot \hat{\mathbf{n}}_j) \hat{\mathbf{n}}_j \right|^2 - \left| \sum_j \tilde{r}_{ij}^{-6} (\hat{\mathbf{n}}_i \cdot \hat{\mathbf{n}}_j)^2 \right|^2 \right)}{\sum_{ij} \tilde{r}_{ij}^{-6} [1 - 3(\hat{\mathbf{n}}_j \cdot \hat{\mathbf{n}}_i)^2]} \right\rangle. \quad (2.39)$$

Although we are applying T_{QF} and T_{Q1} in a periodic boundary system, there are no relevant constraints that need to be applied, as the quaternion expressions are independent of the Cartesian coordinates. We note, though, that our energy expression is not in terms of canonical variables. In principle, however, the energy can be written as a Hamiltonian, based on quaternions and their conjugate momenta. In doing so, our expressions for the quaternionic temperatures would remain unchanged. Thus, provided $\nabla_{\mathbf{Q}}\Phi$ obeys the conditions due to our over-parametrised representation, T_{QF} and T_{Q1} will yield the correct temperature. These conditions are that $\nabla_{\mathbf{Q}}\Phi$ is orthogonal to the constraint surfaces where $|\mathbf{Q}_i| = 1$ and where the $\omega_{zi} = 0^{\ddagger}$, for each i . However, the form $\hat{\mathbf{n}}_i \cdot \hat{\mathbf{n}}_j$ of the potential is independent of both $|\mathbf{Q}_i|$ and of the orientation about the z -axis for each particle, so that this condition is automatically obeyed. Consequently, we can expect Eqn.(2.38) to hold.

2.5.1 Microscopic Heat Capacity Expressions

Suppose we choose $\boldsymbol{\eta} = \nabla K / |\nabla K|^2$. Then we obtain the following expression for the kinetic heat capacity C_{VK}

$$\begin{aligned} \frac{1}{C_{VK}} &= 1 - \frac{\left\langle (\nabla \cdot \frac{\nabla K}{|\nabla K|^2})^2 + (\frac{\nabla K}{|\nabla K|^2} \cdot \nabla)(\nabla \cdot \frac{\nabla K}{|\nabla K|^2}) \right\rangle}{\left\langle (\nabla \cdot \frac{\nabla K}{|\nabla K|^2}) \right\rangle^2} \\ &= 1 - \frac{\left\langle (\frac{3N-2}{2K})^2 - \frac{3N-2}{2K^2} \right\rangle}{\left\langle \frac{3N-2}{2K} \right\rangle^2} \\ &= 1 - \frac{\langle K^{-2} \rangle (\frac{3N-2}{2})^2 - \frac{3N-2}{2}}{\langle K^{-1} \rangle^2 \left\langle \frac{3N-2}{2} \right\rangle^2} \\ &= 1 - \frac{3N-4 \langle K^{-2} \rangle}{3N-2 \langle K^{-1} \rangle^2}. \end{aligned} \quad (2.40)$$

[‡]Strictly speaking, it is not this condition, but its time integral that forms the constraint surface. This does not affect the validity our conclusions, however.

This result appears in (Rugh 1998, Eq.(32)). If we choose $\boldsymbol{\eta} = \nabla\Phi/|\nabla\Phi|^2$, then we obtain the **configurational heat capacity**

$$\begin{aligned} \frac{1}{C_{VC}} &= 1 - \frac{\left\langle \left(\nabla \cdot \frac{\nabla\Phi}{|\nabla\Phi|^2} \right)^2 + \left(\frac{\nabla\Phi}{|\nabla\Phi|^2} \cdot \nabla \right) \left(\nabla \cdot \frac{\nabla\Phi}{|\nabla\Phi|^2} \right) \right\rangle}{\left\langle \left(\nabla \cdot \frac{\nabla\Phi}{|\nabla\Phi|^2} \right) \right\rangle^2} \\ &= 1 - \frac{\left\langle (\mathcal{T}_{CR})^2 + \left(\frac{\nabla\Phi}{|\nabla\Phi|^2} \cdot \nabla \right) (\mathcal{T}_{CR}) \right\rangle}{T_{CR}^2}. \end{aligned} \quad (2.41)$$

Given that these two vector fields satisfy the necessary conditions such that Rugh's expression Eqn.(2.5) holds, we expect that these expressions for the heat capacity will also hold in our systems.

We will show the results of testing these expressions for the temperature and heat capacity in Chapter 4. Before we do so, however, we will consider the matter of how one can hold a system at constant temperature, in the following chapter.

2.6 Appendix: Useful Quaternion Results

We use the quaternion to determine the orientation of our molecule in space. The quaternion is a set of four variables which we use to describe a three-parameter problem. In our simulations, where we use the P2 potential as described in Eqn.(1.9), the orientation of the molecule about its axis of symmetry is excluded from the dynamics, removing yet a further degree of freedom. We therefore use four variables to describe a two-parameter system. As any axis may be chosen to represent this direction vector associated with our molecule, we have used the z -axis, as per the description in Goldstein (Goldstein 1980). Thus

$$\mathbf{n}_i(q_0, q_1, q_2, q_3) = [2q_0q_2 + 2q_1q_3, 2q_2q_3 - 2q_0q_1, q_0^2 - q_1^2 - q_2^2 + q_3^2],$$

and

$$\begin{aligned} \hat{\mathbf{n}}_i(q_0, q_1, q_2, q_3) &= \frac{\mathbf{n}_i(q_0, q_1, q_2, q_3)}{|\mathbf{n}_i|} \\ &= \left[\frac{2q_0q_2 + 2q_1q_3}{q_0^2 + q_1^2 + q_2^2 + q_3^2}, \frac{2q_2q_3 - 2q_0q_1}{q_0^2 + q_1^2 + q_2^2 + q_3^2}, \frac{q_0^2 - q_1^2 - q_2^2 + q_3^2}{q_0^2 + q_1^2 + q_2^2 + q_3^2} \right]. \end{aligned} \quad (2.42)$$

We define $\nabla\mathbf{n}$ such that $[\nabla\mathbf{n}]_{\beta\alpha} = \partial_{j\alpha}[\mathbf{n}_i]_{\beta}$, so that

$$\nabla_i \mathbf{n}_i = \begin{bmatrix} 2q_2 & 2q_3 & 2q_0 & 2q_1 \\ -2q_1 & -2q_0 & 2q_3 & 2q_2 \\ 2q_0 & -2q_1 & -2q_2 & 2q_3 \end{bmatrix}.$$

Therefore

$$\sum_{\alpha} (\mathbf{a} \cdot \partial_{i\alpha} \mathbf{n}_i) (\mathbf{b} \cdot \partial_{i\alpha} \mathbf{n}_i) = (\mathbf{a} \nabla_i \mathbf{n}_i) \cdot (\mathbf{b} \nabla_i \mathbf{n}_i) = \mathbf{a} \nabla_i \mathbf{n}_i [\nabla_i \mathbf{n}_i]^T \mathbf{b}^T.$$

However, $\nabla_i \mathbf{n}_i [\nabla_i \mathbf{n}_i]^T = 4|\mathbf{n}_i| \mathbf{I}$, when \mathbf{I} is the identity matrix. Therefore

$$\sum_{\alpha} (\mathbf{a} \cdot \partial_{i\alpha} \mathbf{n}_i) (\mathbf{b} \cdot \partial_{i\alpha} \mathbf{n}_i) = 4|\mathbf{n}_i| \mathbf{a} \cdot \mathbf{b}. \quad (2.43)$$

We also have

$$\begin{aligned} \sum_{\alpha} q_{i\alpha}^2 &= |\mathbf{Q}_i|^2 = |\mathbf{n}_i|, \\ \sum_{\alpha} q_{i\alpha} \partial_{i\alpha} \mathbf{n}_i &= \mathbf{Q}_i^T [\nabla_i \mathbf{n}_i]^T = 2\mathbf{n}_i, \\ \sum_{\alpha} \partial_{i\alpha}^2 \mathbf{n}_i &= 0. \end{aligned}$$

These results are useful for the \mathbf{n}_i — we need similar results now for the $\hat{\mathbf{n}}_i$. First of all, let us revisit the quotient rule for first and second derivatives.

$$\begin{aligned} \partial \frac{a}{b} &= \frac{b\partial a - a\partial b}{b^2} = \frac{\partial a}{b} - \frac{a\partial b}{b^2}, \\ \partial^2 \frac{a}{b} &= \partial \left(\frac{1}{b} \partial a + a \partial \frac{1}{b} \right) = \frac{1}{b} \partial^2 a + 2\partial a \partial \frac{1}{b} + a \partial^2 \frac{1}{b} \\ &= \frac{\partial^2 a}{b} - 2\partial a \frac{\partial b}{b^2} - a \partial \frac{\partial b}{b^2} \\ &= \frac{\partial^2 a}{b} - \frac{2\partial a \partial b}{b^2} - a \frac{b^2 \partial^2 b - \partial b \partial b^2}{b^4} \\ &= \frac{\partial^2 a}{b} - \frac{2\partial a \partial b}{b^2} - \frac{a \partial^2 b}{b^2} + \frac{2a(\partial b)^2}{b^3}. \end{aligned}$$

Therefore, noting that $\partial_{i\alpha} |\mathbf{n}_i| = 2q_{i\alpha}$ and $\partial_{i\alpha}^2 |\mathbf{n}_i| = 2$, we have

$$\begin{aligned} \partial_{i\alpha} \hat{\mathbf{n}}_i &= \partial_{i\alpha} \frac{\mathbf{n}_i}{|\mathbf{n}_i|} = \frac{\partial_{i\alpha} \mathbf{n}_i}{|\mathbf{n}_i|} - \frac{\mathbf{n}_i \partial_{i\alpha} |\mathbf{n}_i|}{|\mathbf{n}_i|^2} \\ &= \frac{\partial_{i\alpha} \mathbf{n}_i}{|\mathbf{n}_i|} - \frac{2q_{i\alpha} \mathbf{n}_i}{|\mathbf{n}_i|^2}, \\ \partial_{i\alpha}^2 \hat{\mathbf{n}}_i &= \partial_{i\alpha}^2 \frac{\mathbf{n}_i}{|\mathbf{n}_i|} = \frac{\partial_{i\alpha}^2 \mathbf{n}_i}{|\mathbf{n}_i|} - \frac{2\partial_{i\alpha} \mathbf{n}_i \partial_{i\alpha} |\mathbf{n}_i|}{|\mathbf{n}_i|^2} - \frac{\mathbf{n}_i \partial_{i\alpha}^2 |\mathbf{n}_i|}{|\mathbf{n}_i|^2} + \frac{2\mathbf{n}_i (\partial_{i\alpha} |\mathbf{n}_i|)^2}{|\mathbf{n}_i|^3} \\ &= \frac{\partial_{i\alpha}^2 \mathbf{n}_i}{|\mathbf{n}_i|} - \frac{2(\partial_{i\alpha} \mathbf{n}_i) 2q_{i\alpha}}{|\mathbf{n}_i|^2} - \frac{2\mathbf{n}_i}{|\mathbf{n}_i|^2} + \frac{2\mathbf{n}_i (2q_{i\alpha})^2}{|\mathbf{n}_i|^3} \\ &= \frac{\partial_{i\alpha}^2 \mathbf{n}_i}{|\mathbf{n}_i|} - \frac{4q_{i\alpha} \partial_{i\alpha} \mathbf{n}_i}{|\mathbf{n}_i|^2} - \frac{2\mathbf{n}_i}{|\mathbf{n}_i|^2} + \frac{8q_{i\alpha}^2 \mathbf{n}_i}{|\mathbf{n}_i|^3}. \end{aligned}$$

Thus

$$\begin{aligned}
& \sum_{\alpha} (\mathbf{a} \cdot \partial_{i\alpha} \hat{\mathbf{n}}_i) (\mathbf{b} \cdot \partial_{i\alpha} \hat{\mathbf{n}}_i) \\
&= \sum_{\alpha} (\mathbf{a} \cdot [\frac{\partial_{i\alpha} \mathbf{n}_i}{|\mathbf{n}_i|} - \frac{2q_{i\alpha} \mathbf{n}_i}{|\mathbf{n}_i|^2}]) (\mathbf{b} \cdot [\frac{\partial_{i\alpha} \mathbf{n}_i}{|\mathbf{n}_i|} - \frac{2q_{i\alpha} \mathbf{n}_i}{|\mathbf{n}_i|^2}]) \\
&= \sum_{\alpha} (\mathbf{a} \cdot \frac{\partial_{i\alpha} \mathbf{n}_i}{|\mathbf{n}_i|}) (\mathbf{b} \cdot \frac{\partial_{i\alpha} \mathbf{n}_i}{|\mathbf{n}_i|}) - \sum_{\alpha} (\mathbf{a} \cdot \frac{\partial_{i\alpha} \mathbf{n}_i}{|\mathbf{n}_i|}) (\mathbf{b} \cdot \frac{2q_{i\alpha} \mathbf{n}_i}{|\mathbf{n}_i|^2}) \\
&\quad - \sum_{\alpha} (\mathbf{a} \cdot \frac{2q_{i\alpha} \mathbf{n}_i}{|\mathbf{n}_i|^2}) (\mathbf{b} \cdot \frac{\partial_{i\alpha} \mathbf{n}_i}{|\mathbf{n}_i|}) + \sum_{\alpha} (\mathbf{a} \cdot \frac{2q_{i\alpha} \mathbf{n}_i}{|\mathbf{n}_i|^2}) (\mathbf{b} \cdot \frac{2q_{i\alpha} \mathbf{n}_i}{|\mathbf{n}_i|^2}) \\
&= \frac{4|\mathbf{n}_i| \mathbf{a} \cdot \mathbf{b}}{|\mathbf{n}_i|^2} - \frac{2\mathbf{b} \cdot \mathbf{n}_i}{|\mathbf{n}_i|^3} \mathbf{a} \cdot \sum_{\alpha} q_{i\alpha} \partial_{i\alpha} \mathbf{n}_i \\
&\quad - \frac{2\mathbf{a} \cdot \mathbf{n}_i}{|\mathbf{n}_i|^3} \mathbf{b} \cdot \sum_{\alpha} q_{i\alpha} \partial_{i\alpha} \mathbf{n}_i + \frac{4(\mathbf{a} \cdot \mathbf{n}_i)(\mathbf{b} \cdot \mathbf{n}_i)}{|\mathbf{n}_i|^4} \sum_{\alpha} q_{i\alpha}^2 \\
&= \frac{4\mathbf{a} \cdot \mathbf{b}}{|\mathbf{n}_i|} - \frac{2\mathbf{b} \cdot \mathbf{n}_i}{|\mathbf{n}_i|^3} 2\mathbf{a} \cdot \mathbf{n}_i - \frac{2\mathbf{a} \cdot \mathbf{n}_i}{|\mathbf{n}_i|^3} 2\mathbf{b} \cdot \mathbf{n}_i + \frac{4(\mathbf{a} \cdot \mathbf{n}_i)(\mathbf{b} \cdot \mathbf{n}_i)}{|\mathbf{n}_i|^4} |\mathbf{n}_i| \\
&= \frac{4\mathbf{a} \cdot \mathbf{b}}{|\mathbf{n}_i|} - \frac{8(\mathbf{a} \cdot \mathbf{n}_i)(\mathbf{b} \cdot \mathbf{n}_i)}{|\mathbf{n}_i|^3} + \frac{4(\mathbf{a} \cdot \mathbf{n}_i)(\mathbf{b} \cdot \mathbf{n}_i)}{|\mathbf{n}_i|^3} \\
&= \frac{4\mathbf{a} \cdot \mathbf{b}}{|\mathbf{n}_i|} - \frac{4(\mathbf{a} \cdot \mathbf{n}_i)(\mathbf{b} \cdot \mathbf{n}_i)}{|\mathbf{n}_i|^3}.
\end{aligned}$$

Similarly, we have

$$\begin{aligned}
\sum_{\alpha} \partial_{i\alpha}^2 \hat{\mathbf{n}}_i &= \sum_{\alpha} \frac{\partial_{i\alpha}^2 \mathbf{n}_i}{|\mathbf{n}_i|} - \frac{4q_{i\alpha} \partial_{i\alpha} \mathbf{n}_i}{|\mathbf{n}_i|^2} - \frac{2\mathbf{n}_i}{|\mathbf{n}_i|^2} + \frac{8q_{i\alpha}^2 \mathbf{n}_i}{|\mathbf{n}_i|^3} \\
&= 0 - \frac{8\mathbf{n}_i}{|\mathbf{n}_i|^2} - \frac{8\mathbf{n}_i}{|\mathbf{n}_i|^2} + \frac{8|\mathbf{n}_i| \mathbf{n}_i}{|\mathbf{n}_i|^3} \\
&= \frac{-8\mathbf{n}_i}{|\mathbf{n}_i|^2}.
\end{aligned}$$

Chapter 3

Thermostats

Due to our mechanical approach, the fundamental ensemble of statistical mechanics is the microcanonical ensemble, the ensemble of constant energy. However, in real life, it is very difficult to maintain a system in energetic isolation from its surroundings. More often, a system will be in thermal equilibrium with its surroundings — that is, at the same temperature as its environment. Assuming that this environment is at constant temperature, then our system will be a canonical ensemble. Since much of the data from real experiments comes from systems at constant temperature, we would like to be able to conduct computer experiments at constant temperature as well, to compare our results.

A simple way to run constant temperature simulations would be to use Metropolis Monte Carlo, where configuration space is sampled by random moves. However, the Monte Carlo method cannot simulate non-equilibrium systems, nor can it be used to simulate time-dependent behaviour. Thus, we would like a means of reproducing constant temperature (canonical) ensemble results using MD, where the natural ensemble is the constant-energy (microcanonical) ensemble. Certainly, constant-energy simulations will give us results that are correct to $\mathcal{O}(1/N)$. In this case, however, the temperature is not an input parameter, which is a significant impediment if we wish to run simulations at a constant, pre-defined temperature.

Computational experiments can simulate the canonical ensemble via the introduction of **thermostats**. A thermostat, in its most general sense, is a mechanism by which the temperature of a system is held constant. We begin our discussion of thermostats by a brief overview of the earliest thermostats (§3.1), before moving on to the ingenious method introduced by Shiuichi Nose* and developed by Nose and Hoover (§3.2). We then digress to introduce the Liouville theorem (§3.3), which will provide a useful tool as we propose new thermostats. Following this, we consider a lesser-known approach

*pronounced ‘no-zay’

to dynamics that is consistent with the treatment of constraints in Lagrangian dynamics — Gauss' principle of least constraint (§3.4). From this principle we will then examine the isokinetic thermostat of Hoover and Evans (§3.5).

All of these thermostats work by controlling $\sum_i p_i^2/m_i$ — the 'instantaneous' Equipartition temperature. Given the wealth of expressions available that can be used to determine the temperature, it is interesting to ask whether these new expressions can also be used to control the temperature of a system, and whether there is any advantage in choosing an alternative approach. In §3.6 we will consider how one might thermostat a system by controlling any of the expressions that were developed in Chapter 2, that are also associated with the temperature of the system.

3.1 The First Thermostats

The earliest thermostats[†] simply rescaled the momentum of each particle by $\sqrt{K_0/K_i}$, where K_i is the kinetic energy at a particular timestep, and $K_0 = 3NkT/2$ is the average kinetic energy for a system at the desired temperature T . The frequency of this rescaling depends on the desired accuracy. There are clearly issues about what ensemble is actually traced out by the trajectories of such a model, and hence whether this method does reproduce the results of a canonical ensemble. Furthermore, this method is not time-reversible, making comparisons of phase and (infinite) time averages difficult. Also, time-correlation functions will be effected by the fact that the velocities are discontinuous. However, application of this method (as early as (Woodcock 1971)) indicate that the method works quite well in equilibrium systems, for calculating time-independent behaviour. An alternative rescaling scheme (Andersen 1980) involves the random rescaling of the velocities of individual particles. Whilst giving good agreement for time-independent quantities, the dependence of time-dependent properties (such as the mean-square displacement) with the rate at which these random rescalings take place makes the method unreliable for such calculations (Frenkel and Smit 1996).

Various schemes have been suggested for incorporating the rescaling into the equations of motion, such as the popular Berendsen thermostat (Berendsen and van Gunsteren 1985). The rescaling therefore becomes a differential change in the equations of motion, rather than a discontinuous transformation. The advantage here is that the kinetic energy is not so rigidly constrained — the ther-

[†]See, for example, (Berendsen and van Gunsteren 1985; Evans and Holian 1985) and references therein.

mostat is **softer** inasmuch as it directs the kinetic energy to the desired value rather than forcing it to remain at a constant value. The problem of time irreversibility remains, however.

3.2 The Nose-Hoover Thermostat

The Nose-Hoover thermostat (Nose 1984; Hoover 1985; Evans and Holian 1985) was a revolution in constant-temperature simulation techniques. The Nose Hamiltonian

$$\mathcal{H}_N(\mathbf{\Gamma}) = \mathcal{H}_0(\mathbf{q}, \frac{\mathbf{P}}{s}) + gkT \ln s + \frac{p_S^2}{2Q}$$

supplements the Hamiltonian coordinates \mathbf{q} of the real system with an additional coordinate s , which can be thought of as representing an external thermal bath[‡]. Thus the usual Hamiltonian \mathcal{H}_0 of the real system, adjusted by the rescaling of the momenta, is augmented to include energy terms associated with the thermal bath — a “potential” term $gkT \ln s$ for some constant g , and a “kinetic” term $p_S^2/2Q$ for some fictitious mass (or friction term) Q .

By transforming to the scaled momenta \mathbf{p}' , scaled time t' , and friction constant ξ defined by

$$\mathbf{p}' = \frac{\mathbf{P}}{s} \quad t' = \int_0^t \frac{d\zeta}{s} \quad \xi = \frac{p_S}{Q},$$

we obtain the equations of motion (Hoover 1985)

$$\frac{d\mathbf{q}}{dt'} = \frac{\mathbf{p}'}{m}; \quad \frac{d\mathbf{p}'}{dt'} = \mathbf{F} - \xi\mathbf{p}'; \quad \frac{d\xi}{dt'} = \frac{1}{Q} \left[\frac{\mathbf{p}' \cdot \mathbf{p}'}{m} - gkT \right], \quad (3.1)$$

which provides a closed set of equations for the determination of $\mathbf{q}(t')$ and $\mathbf{p}'(t')$. The average along the trajectory of a quantity \mathcal{A} is therefore

$$\begin{aligned} \langle \mathcal{A} \rangle' &= \frac{\int_0^{T'} \mathcal{A}(\zeta) d\zeta}{T'} \\ &= \frac{\int_0^T \frac{\mathcal{A}(\zeta)}{s} d\zeta}{\int_0^T \frac{d\zeta}{s}} \\ &= \frac{\int \frac{\mathcal{A}(\mathbf{\Gamma}')}{s} \delta(\mathcal{H}_N - E) d\mathbf{q} d\mathbf{p}' ds dp_S}{\int \frac{1}{s} \delta(\mathcal{H}_N - E) d\mathbf{q} d\mathbf{p}' ds dp_S} \\ &= \frac{\int \mathcal{A}(\mathbf{\Gamma}') s^{3N-1} \delta(\mathcal{H}_N - E) d\mathbf{q} d\mathbf{p}' ds dp_S}{\int s^{3N-1} \delta(\mathcal{H}_N - E) d\mathbf{q} d\mathbf{p}' ds dp_S}, \end{aligned}$$

[‡]or the outside universe in general

where we equate the time and ensemble averages. Thus $\int s^{3N-1} \delta(\mathcal{H}_N - E) d\mathbf{q} d\mathbf{p}' ds dp_S$ represents the partition function for our scaled system. Integrating the integrand with respect to s , and using the result $\delta[\mathcal{H}_N(s) - E] = \delta(s - s_0)/\mathcal{H}'_N(s)$ (where $\mathcal{H}_N(s_0) = E$) we obtain

$$\begin{aligned} Z' &= \int (s^{3N-1} \delta(\mathcal{H}_N(\mathbf{q}, \mathbf{p}, s, p_S) - E) ds) d\mathbf{q} d\mathbf{p}' dp_S \\ &= \int (s^{3N-1} \frac{\delta(s - s_0)}{s} ds) d\mathbf{q} d\mathbf{p}' dp_S \\ &= \int \frac{s_0^{3N}}{gkT} d\mathbf{q} d\mathbf{p}' dp_S \\ &= \int \frac{\exp\left\{\frac{1}{gkT}(E - H_0(\mathbf{q}, \mathbf{p}') - \frac{p_S^2}{2Q})\right\}^{3N}}{gkT} d\mathbf{q} d\mathbf{p}' dp_S \\ &= \int \frac{Q}{gkT} \exp\left\{\frac{3N}{gkT}(E - H_0(\mathbf{q}, \mathbf{p}') - \frac{Q\xi^2}{2})\right\} d\mathbf{q} d\mathbf{p}' d\xi. \end{aligned}$$

Making the identifications $g = 3N$ and $Q = 3NkT\tau^2$, where τ represents the interaction strength between the system and the thermal bath, leads to the canonical ensemble partition function:

$$Z' = \left[\int e^{-\beta H_0(\mathbf{q}, \mathbf{p}')} d\mathbf{q} d\mathbf{p}' \right] \left[\int \tau^2 e^{-\beta E} e^{-\frac{3N\tau^2\xi^2}{2}} d\xi \right]. \quad (3.2)$$

Consequently, any average taken over a microcanonical simulation of the Nose Hamiltonian, using the Hoover scaled momenta and scaled time, will span phase space in such a way as to produce a canonical distribution in the coordinates and (scaled) momenta.

The advantages of the Nose-Hoover method are several. The equations of motion are time-reversible, which allows us to make an analysis of the ensemble. Like the Berendsen model, the temperature is an input variable in the equations of motion. Finally, it has been shown that equilibrium time correlation functions of Nose-Hoover dynamics are equivalent to those of Newtonian dynamics, in the thermodynamic limit (Evans and Holian 1985). Whilst this does not indicate that they are correct[§] to higher orders, equivalence in the thermodynamic limit is an important vindication of this method.

3.3 The Liouville Theorem

At this point we make use of one of the theorems of statistical mechanics, the Liouville theorem. It is essentially a law of conservation

[§]in the sense that they reproduce the results of real-life constant-temperature equilibrium time correlation functions

of probability — the total probability of being somewhere in phase space is 1, so the rate of change of the probability distribution at a point in phase space must be due to the ‘flow of probability’ to other parts of phase space. Consequently, the Liouville theorem is in the form of a balance relation (Münster 1969) —

$$\frac{\partial f}{\partial t} + \nabla \cdot (f\dot{\Gamma}) = 0. \quad (3.3)$$

We note that

$$\frac{\partial f}{\partial t} + \dot{\Gamma} \cdot \nabla f + f \nabla \cdot \dot{\Gamma} = \frac{df}{dt} + f \nabla \cdot \dot{\Gamma} = 0. \quad (3.4)$$

Eqs.(3.3) and (3.4) give us alternative ways of determining the probability distribution visited by a particular trajectory, as determined by the form of $\dot{\Gamma}(\Gamma)$. For example, consider the Nose-Hoover equations of motion Eqn.(3.1). Applying Eqn.(3.4), we obtain (Evans and Morriss 1990)

$$\frac{d \ln f}{dt} = \frac{1}{f} \frac{df}{dt} = -\nabla \cdot \dot{\Gamma} = \nabla_{\mathbf{p}'} \cdot \xi \mathbf{p}' = 3N\xi, \quad (3.5)$$

which we compare with

$$\begin{aligned} \frac{d -\beta(\mathcal{H}_0 + \frac{Q\xi^2}{2})}{dt} &= -\beta\dot{\mathcal{H}}_0 - \beta Q\xi\dot{\xi} \\ &= -\beta(\xi \frac{\mathbf{p}' \cdot \mathbf{p}'}{m}) - \beta\xi(\frac{\mathbf{p}' \cdot \mathbf{p}'}{m} - gkT) \\ &= g\xi \\ &= 3N\xi = \frac{d \ln f}{dt}, \end{aligned}$$

if we set $g = 3N$. Consequently

$$\ln f + c = -\beta(\mathcal{H}_0 + \frac{Q\xi^2}{2}) \Rightarrow f \propto e^{-\beta(\mathcal{H}_0 + \frac{Q\xi^2}{2})},$$

as expected. Of course, in order to determine f , we have had to make an ‘inspired guess’ as to the form of f — it is not at all obvious from Eqn.(3.5) what guess will lead to the correct answer. Nevertheless, the Liouville theorem will prove a useful analytical tool when we examine the effects of new equations of motion. If we can determine a probability distribution f that satisfies the Liouville theorem for a given $\dot{\Gamma}$, that distribution will be preserved by the dynamics. On the further assumption of ergodicity, the time average along a single trajectory will therefore be equal to the ensemble average.

3.4 Gauss' Principle of Least Constraint

The theory of Lagrangian and Hamiltonian mechanics derives from the treatment of Newtonian systems under constraints that do no work on the system (ie where the forces of constraint are orthogonal to the motion of particles). An alternative approach to this problem, which retains the Cartesian formalism, is **Gauss' principle of least constraint**. Gauss' principle states that the path a system will take is the one that minimises the function

$$C(\ddot{\mathbf{r}}) = \sum_{i=1}^N m_i \left(\ddot{\mathbf{r}}_i - \frac{\mathbf{F}_i(r_i)}{m_i} \right)^2,$$

for a given \mathbf{r} and \mathbf{F} . When the system is constrained in some manner (such as by bonds between atoms), then the function C must be minimised over the set of $\ddot{\mathbf{r}}$ that is consistent with this constraint. This can be achieved by using the method of Lagrange multipliers.

This ostensibly simple result, as well as its consistency with the formal treatment of constraints under Lagrangian mechanics, is elegantly proven in (Whittaker 1952). However, our application of Gauss' principle, in the derivation of the isokinetic ensemble, is to a system where the constraints necessarily perform work. The ultimate justification for this approach, therefore, will not be due to the 'correctness' of Gauss' principle (on which we do not comment, when considering constraints that perform work), but rather on further analysis of the equations of motion that result from using Gauss' principle. The framework of Gauss' principle will also be useful in considering alternative thermostating techniques. Thus, we shall consider how the principle can be applied, before looking at the isokinetic ensemble as a specific example.

3.4.1 Application of Gauss' Principle

Let us begin by considering the application of Gauss' principle to a system with a constraint $g(\mathbf{r}, \dot{\mathbf{r}}) = k$, a constant in time. We note that $\partial g / \partial t = 0$. The constraint can therefore be differentiated to give

$$\frac{d}{dt}g(\mathbf{r}, \dot{\mathbf{r}}) = \sum_j \frac{\partial g}{\partial r_j} \dot{r}_j + \sum_j \frac{\partial g}{\partial \dot{r}_j} \ddot{r}_j = 0. \quad (3.6)$$

This gives a form of the constraint in terms of $\ddot{\mathbf{r}}$. $C(\ddot{\mathbf{r}})$ can therefore be minimised with respect to the constraint $g(\mathbf{r}, \dot{\mathbf{r}}) = k$, giving

$$\begin{aligned} \frac{\partial}{\partial \ddot{r}_i} \left(\frac{1}{2} \sum_j m_j \left(\ddot{r}_j - \frac{F_j}{m_j} \right)^2 + \lambda \frac{d}{dt}g(\mathbf{r}, \dot{\mathbf{r}}) \right) &= 0 \\ \Rightarrow m_i \ddot{r}_i - F_i + \lambda \frac{\partial g}{\partial \dot{r}_i} &= 0. \end{aligned} \quad (3.7)$$

Substituting Eqn.(3.7) into Eqn.(3.6), we obtain the following expression for the Lagrange multiplier λ :

$$\begin{aligned} \sum_j \frac{\partial g}{\partial r_j} \dot{r}_j + \sum_j \frac{\partial g}{\partial \dot{r}_j} \frac{1}{m_j} (F_j - \lambda \frac{\partial g}{\partial \dot{r}_j}) &= 0 \\ \Rightarrow \sum_j \frac{\partial g}{\partial r_j} \dot{r}_j + \sum_j \frac{\partial g}{\partial \dot{r}_j} \frac{F_j}{m_j} &= \sum_j \frac{\partial g}{\partial \dot{r}_j} \frac{\lambda}{m_j} \frac{\partial g}{\partial \dot{r}_j} \\ \Rightarrow \lambda &= \frac{\sum_j \frac{\partial g}{\partial r_j} \dot{r}_j + \sum_j \frac{\partial g}{\partial \dot{r}_j} \frac{F_j}{m_j}}{\sum_j \frac{\partial g}{\partial \dot{r}_j} \frac{1}{m_j} \frac{\partial g}{\partial \dot{r}_j}}. \end{aligned}$$

As our simulations are performed in terms of phase space variables, it is convenient at this point to re-write these equations in terms of $(\mathbf{q}, \mathbf{p}) = (\mathbf{r}, \mathbf{M}\dot{\mathbf{r}})$. Thus we obtain

$$\lambda = \frac{\nabla_{\mathbf{r}}g \cdot \mathbf{M}^{-1}\mathbf{p} + \nabla_{\mathbf{p}}g \cdot \mathbf{F}}{\nabla_{\mathbf{p}}g \cdot \mathbf{M}\nabla_{\mathbf{p}}g},$$

so that our equations of motion become

$$\dot{\mathbf{q}} = \mathbf{M}^{-1}\mathbf{p}, \quad (3.8)$$

$$\dot{\mathbf{p}} = \mathbf{F} - \frac{\nabla_{\mathbf{r}}g \cdot \mathbf{M}^{-1}\mathbf{p} + \nabla_{\mathbf{p}}g \cdot \mathbf{F}}{\nabla_{\mathbf{p}}g \cdot \mathbf{M}\nabla_{\mathbf{p}}g} \mathbf{M}\nabla_{\mathbf{p}}g, \quad (3.9)$$

or, in terms of the Hamiltonian,

$$\dot{\mathbf{q}} = \nabla_{\mathbf{p}}\mathcal{H}, \quad (3.10)$$

$$\dot{\mathbf{p}} = -\nabla_{\mathbf{q}}\mathcal{H} - \frac{\nabla_{\mathbf{q}}g \cdot \nabla_{\mathbf{p}}\mathcal{H} - \nabla_{\mathbf{p}}g \cdot \nabla_{\mathbf{q}}\mathcal{H}}{\nabla_{\mathbf{p}}g \cdot \mathbf{M}\nabla_{\mathbf{p}}g} \mathbf{M}\nabla_{\mathbf{p}}g. \quad (3.11)$$

3.4.2 Holonomic Constraints

The above argument must be adapted in the case of **holonomic constraints** — constraints of the form $h(\mathbf{r}) = k$ — because the time derivative \dot{h} contains no terms in $\dot{\mathbf{r}}$, and therefore cannot be used in the method of Lagrange multipliers. Instead, we must take the second time-derivative of h in order to obtain these terms. Therefore let us define the holonomic constraint $h(\mathbf{r}) = k$, whose time derivative $\dot{h} = g(\mathbf{r}, \dot{\mathbf{r}}) = 0$. The results Eqns.(3.8-3.11) of the previous section are then identical for the constraint g . Furthermore, we note that

$$\begin{aligned} (0 =) g(\mathbf{r}, \dot{\mathbf{r}}) &= \nabla_{\mathbf{r}}h \cdot \dot{\mathbf{r}} = \nabla_{\mathbf{r}}\mathbf{M}^{-1}\mathbf{p} \\ &\Rightarrow \nabla_{\mathbf{p}}g = \mathbf{M}^{-1}\nabla_{\mathbf{q}}h, \end{aligned}$$

since \mathbf{M} is symmetric. Using this last result, the expression obtained in Eqns.(3.10-3.11) can be re-written

$$\dot{\mathbf{q}} = \nabla_{\mathbf{p}}\mathcal{H}, \quad (3.12)$$

$$\begin{aligned} \dot{\mathbf{p}} &= -\nabla_{\mathbf{q}}\mathcal{H} - \frac{\nabla_{\mathbf{q}}g \cdot \nabla_{\mathbf{p}}\mathcal{H} - \mathbf{M}^{-1}\nabla_{\mathbf{q}}h \cdot \nabla_{\mathbf{q}}\mathcal{H}}{\mathbf{M}^{-1}\nabla_{\mathbf{q}}h \cdot \mathbf{M}\mathbf{M}^{-1}\nabla_{\mathbf{q}}h} \mathbf{M}\mathbf{M}^{-1}\nabla_{\mathbf{q}}h \\ &= -\nabla_{\mathbf{q}}\mathcal{H} - \frac{\nabla_{\mathbf{q}}g \cdot \nabla_{\mathbf{p}}\mathcal{H} - \mathbf{M}^{-1}\nabla_{\mathbf{q}}h \cdot \nabla_{\mathbf{q}}\mathcal{H}}{\mathbf{M}^{-1}\nabla_{\mathbf{q}}h \cdot \nabla_{\mathbf{q}}h} \nabla_{\mathbf{q}}h. \end{aligned} \quad (3.13)$$

The vector $\dot{\mathbf{\Gamma}} = (\dot{\mathbf{q}}, \dot{\mathbf{p}})$ therefore lies in the tangent space of $\mathcal{H}(\Gamma)$, since

$$\begin{aligned} \nabla\mathcal{H} \cdot \dot{\mathbf{\Gamma}} &= \nabla_{\mathbf{q}}\mathcal{H} \cdot \nabla_{\mathbf{p}}\mathcal{H} + \nabla_{\mathbf{p}}\mathcal{H} \cdot \left[-\nabla_{\mathbf{q}}\mathcal{H} - \frac{\nabla_{\mathbf{q}}g \cdot \nabla_{\mathbf{p}}\mathcal{H} - \mathbf{M}^{-1}\nabla_{\mathbf{q}}h \cdot \nabla_{\mathbf{q}}\mathcal{H}}{\mathbf{M}^{-1}\nabla_{\mathbf{q}}h \cdot \nabla_{\mathbf{q}}h} \nabla_{\mathbf{q}}h \right] \\ &= \left(\frac{\mathbf{M}^{-1}\nabla_{\mathbf{q}}h \cdot \nabla_{\mathbf{q}}\mathcal{H} - \nabla_{\mathbf{q}}g \cdot \nabla_{\mathbf{p}}\mathcal{H}}{\mathbf{M}^{-1}\nabla_{\mathbf{q}}h \cdot \nabla_{\mathbf{q}}h} \right) \nabla_{\mathbf{p}}\mathcal{H} \cdot \nabla_{\mathbf{q}}h \\ &= \left(\frac{\mathbf{M}^{-1}\nabla_{\mathbf{q}}h \cdot \nabla_{\mathbf{q}}\mathcal{H} - \nabla_{\mathbf{q}}g \cdot \nabla_{\mathbf{p}}\mathcal{H}}{\mathbf{M}^{-1}\nabla_{\mathbf{q}}h \cdot \nabla_{\mathbf{q}}h} \right) g(\mathbf{r}, \dot{\mathbf{r}}) = 0, \end{aligned} \quad (3.14)$$

as $g(\mathbf{r}, \dot{\mathbf{r}}) = 0$ for the holonomic constraint. This implies that energy is conserved when Gauss' principle is applied to a holonomic constraint, by the following argument. The change in energy along the phase-space trajectory of the constrained system will be given by $\int d\mathcal{H}$, integrated over the trajectory. However

$$\int d\mathcal{H} = \int \nabla\mathcal{H} \cdot \dot{\mathbf{\Gamma}} = 0,$$

so the Hamiltonian is constant over the path taken. In conclusion, we note that this result holds for any constraint of the form $\mathbf{A}(\mathbf{r}) \cdot d\mathbf{r} = 0$, of which the holonomic constraints form a subset. Constraints of this form make up the set of constraints for which Gauss' principle, and the Lagrangian treatment of constraints, are consistent (Whittaker 1952; Goldstein 1980).

3.5 The Isokinetic Thermostat

The idea behind the isokinetic thermostat (Evans and Morriss 1983a; Evans and Morriss 1983b) is to keep the kinetic energy fixed, and thereby constrain the thermodynamic temperature of the system. Although it does not trivially follow that such a constraint should generate a constant-temperature ensemble, we shall see that this is indeed the case.

We therefore apply Gauss' principle to constrain our system such that $g(\mathbf{r}, \mathbf{p}) = \mathbf{p} \cdot \mathbf{M}^{-1}\mathbf{p}/2 = k$. It follows that

$$\nabla_{\mathbf{p}}g(\mathbf{q}, \mathbf{p}) = \mathbf{M}^{-1}\mathbf{p}, \quad \nabla_{\mathbf{q}}g(\mathbf{q}, \mathbf{p}) = 0,$$

so that

$$\dot{\mathbf{q}} = \mathbf{M}^{-1}\mathbf{p}, \quad (3.15)$$

$$\begin{aligned} \dot{\mathbf{p}} &= \mathbf{F} - \frac{0 + \mathbf{M}^{-1}\mathbf{p} \cdot \mathbf{F}}{\mathbf{M}^{-1}\mathbf{p} \cdot \mathbf{M}\mathbf{M}^{-1}\mathbf{p}} \mathbf{M}\mathbf{M}^{-1}\mathbf{p} \\ &= \mathbf{F} - \frac{\mathbf{M}^{-1}\mathbf{p} \cdot \mathbf{F}}{\mathbf{M}^{-1}\mathbf{p} \cdot \mathbf{p}} \mathbf{p} \\ &= \mathbf{F} - \alpha\mathbf{p}, \end{aligned} \quad (3.16)$$

where Eqn.(3.16) serves as a definition for α . These equations of motion correspond to a distribution function (Evans and Morriss 1990)

$$f_K(\mathbf{\Gamma}) = \frac{e^{-\beta\Phi(\mathbf{\Gamma})} \delta(K(\mathbf{\Gamma}) - K)}{\int e^{-\beta\Phi(\mathbf{\Gamma})} \delta(K(\mathbf{\Gamma}) - K) d\mathbf{\Gamma}}, \quad (3.17)$$

since we note that

$$\begin{aligned} -\nabla \cdot \dot{\mathbf{\Gamma}} &= -\nabla_{\mathbf{p}} \cdot \alpha\mathbf{p} = -\sum_i \frac{\partial}{\partial p_i} \left(\frac{\mathbf{M}^{-1}\mathbf{p} \cdot \mathbf{F}}{\mathbf{M}^{-1}\mathbf{p} \cdot \mathbf{p}} p_i \right) \\ &= -\sum_i \left(\frac{\mathbf{M}^{-1}F_i}{\mathbf{M}^{-1}\mathbf{p} \cdot \mathbf{p}} p_i - \alpha \frac{\mathbf{M}^{-1}2p_i}{\mathbf{M}^{-1}\mathbf{p} \cdot \mathbf{p}} p_i + \frac{\mathbf{M}^{-1}\mathbf{p} \cdot \mathbf{F}}{\mathbf{M}^{-1}\mathbf{p} \cdot \mathbf{p}} \right) \\ &= -(3N - 1)\alpha, \end{aligned}$$

and that

$$\begin{aligned} \frac{1}{f_K} \frac{df_K}{dt} &= \frac{d \ln f_K}{dt} = -\beta \dot{\Phi} \\ &= -\beta \mathbf{F} \cdot \mathbf{M}^{-1}\mathbf{p} \\ &= -\beta \alpha \mathbf{p} \cdot \mathbf{M}^{-1}\mathbf{p} \\ &= -(3N - 1)\alpha = -\nabla \cdot \dot{\mathbf{\Gamma}}, \end{aligned}$$

if we set $\beta = (3N - 1)/(\mathbf{p} \cdot \mathbf{M}^{-1}\mathbf{p})$ — a constant of the motion. For this choice of β , $df_K/dt = -f\nabla \cdot \dot{\mathbf{\Gamma}}$, and hence f_K is preserved by the dynamics. Consequently, β corresponds to the inverse temperature of our canonical ensemble, and is therefore consistent with our expectations through the equipartition theorem[¶].

Furthermore, we see that

$$\begin{aligned} \dot{\mathbf{\Gamma}} \cdot \nabla f &= f \dot{\mathbf{\Gamma}} \cdot \nabla \ln f = -f\beta \dot{\mathbf{\Gamma}} \cdot \nabla \mathcal{H} = -f\alpha(\beta\mathbf{p} \cdot \mathbf{M}^{-1}\mathbf{p}) \\ &= -(3N - 1)f\alpha = -f\nabla \cdot \dot{\mathbf{\Gamma}}, \end{aligned}$$

[¶]except for the difference of $\mathcal{O}(1/N)$, which can be explained in terms of a lost degree of freedom in comparison with the canonical ensemble (due to the conservation of the kinetic energy). Indeed, (Evans and Morriss) obtain a factor of $3N - 4$, which arises from writing the Hamiltonian in the form $\mathcal{H} = \sum_i (p_i - P)^2/m_i + \Phi(\mathbf{q})$, where $P = \sum_i p_i/N$.

implying that $\partial f_{K_O}/\partial t = 0$. Evans and Morriss go on to show that $\langle df_K/dt \rangle = \langle (3N - 1)\alpha \rangle = 0$ in the absence of an external field. In addition, the equilibrium time correlation functions are equal to the Newtonian time correlation functions in the thermodynamic limit, as is the case for Nose-Hoover dynamics. We note that the equations of motion for the Isokinetic thermostat are time-reversible. As with the Nose-Hoover thermostat, a further assumption of ergodicity implies that the time average along a single trajectory will be equal to the ensemble average.

In closing, we include two variations of the Isokinetic thermostat. The first is the form of the Isokinetic thermostat for the full SLLOD equations of motion. In this case, we determine the value for α by adopting the same form for the thermostat, and noting that (Evans and Morriss 1990)

$$0 = \dot{K} = \nabla K \cdot \mathbf{p} = \sum_i (\mathbf{F}_i - \mathbf{i}\gamma p_{y_i} - \alpha \mathbf{p}_i) \cdot \frac{\mathbf{p}_i}{m_i}$$

$$\Rightarrow \alpha = \frac{\sum_i \frac{\mathbf{F}_i \cdot \mathbf{p}_i - \gamma p_{x_i} p_{y_i}}{m_i}}{\sum_i \frac{\mathbf{p}_i \cdot \mathbf{p}_i}{m_i}}.$$

The second variation we consider is the form when we wish to maintain constant *energy*, rather than constant kinetic energy. For this form, called the Evans ergostat, the value for α is determined, using the same process as above, to be the value required to hold E constant (Evans 1983):

$$0 = \dot{\mathcal{H}} = \nabla K \cdot \dot{\mathbf{p}} + \nabla \Phi \cdot \dot{\mathbf{q}}$$

$$= \sum_i (\mathbf{F}_i - \mathbf{i}\gamma p_{y_i} - \alpha \mathbf{p}_i) \cdot \frac{\mathbf{p}_i}{m_i} - \sum_i \left(\frac{\mathbf{p}_i}{m_i} + \mathbf{i}\gamma y_i \right) \cdot \mathbf{F}_i$$

$$\Rightarrow \alpha = \gamma \frac{\sum_i F_{x_i} y_i - \frac{p_{x_i} p_{y_i}}{m_i}}{\sum_i \frac{\mathbf{p}_i \cdot \mathbf{p}_i}{m_i}}.$$

3.6 New Approaches to Thermostatting Systems

All of the thermostats discussed hitherto have one thing in common — they rely on altering the time-evolution of the momenta in the system so that the kinetic energy is controlled. They are either **hard**, as with the rescaling models of the isokinetic model, in that they fix the kinetic energy to remain constant (within marginal error), or conversely they are **soft**, such with the Nose-Hoover and Berendsen thermostats, in that they do not fix the instantaneous kinetic energy, but rather influence the long-time average behaviour.

One of our key interests will be the application of our thermostats in non-equilibrium systems. A major difficulty in thermostatting

non-equilibrium simulations, using current methods, is the need to thermostat the *peculiar* velocities. In an equilibrium system, it is clear that if we are not in the centre-of-mass frame of our system, the kinetic energy is no longer simply related to the temperature via the equipartition theorem. In a non-equilibrium system, this requirement becomes even more complicated. After all, the thermodynamic temperature — that property that we have been associating with various ensemble averages throughout this thesis — is an equilibrium property. The very notion, then, of temperature in a non-equilibrium environment requires careful definition. On the assumption of the existence of local equilibrium at each point in our system, we can assign a local temperature at each point (de Groot and Mazur 1962). The assumption of local equilibrium means, *inter alia*, that we expect the various temperature expressions derived in this thesis to hold^{||}. Consequently, the Equipartition theorem will hold, *as long as the momenta are peculiar to the local flow*. We can no longer remove the problems of peculiar kinetic energies by the consideration of the centre of mass of the whole system. The local temperature can only be determined using the locally peculiar velocities. Thermostatting a non-equilibrium system would therefore mean, in effect, setting the average of these local temperatures throughout the system to a constant value.

There are significant difficulties in determining these local flows, however. Let us consider the case of Couette flow. For very small values of shear rate, the assumption that the peculiar flow is the zero-wavevector profile ($\mathbf{u}(y) = \gamma y$) is a good one. However, as the shear rate increases, this approximation is less and less accurate (Evans and Morriss 1990). Thermostats that assume the nature of the local flow — so-called **profile-biased thermostats**, or PBTs — will in general produce systems at *lower* temperatures than the input temperature, as part of the constant kinetic energy will be local translational kinetic energy. A more significant problem arises at high shear rates, with the observation of strings (Erpenbeck 1984). These strings appear to be an artifact of the thermostat, as they are not observed when **profile-unbiased thermostats**, or PUTs are used (Evans and Morriss 1986). The principle of the PUT is to determine the velocity profile using information gained from the simulation, rather than assuming a profile *a priori*. The PUT is therefore a more computationally-intensive task than using a PBT — especially for simulations of rigid bodies, where bias can be removed from the rotational as well as translational degrees of freedom in the profile. However, PUTs have been found to generate more reliable results at high shear rates for rigid body systems (Travis,

^{||}assuming the locale of the local equilibrium is large enough for thermodynamic limit requirements to be satisfied

Daivis, and Evans 1995).

In view of these problems, we are interested in thermostats that alter the *coordinate* time-evolution, in order to control the temperature, rather than the momentum time-evolution. Our aim in this is to avoid the problems relating to local peculiar frames of reference altogether. We would like to be able to generalise both hard and soft thermostat approaches, in the context of the much broader set of temperature expressions that we have derived. We would like to develop expressions of the form

$$\dot{\Gamma} = \dot{\Gamma}_0 - \xi \mathbf{X}, \quad (3.18)$$

where $\dot{\Gamma}_0$ represents the usual Hamiltonian equations of motion, and \mathbf{X} represents a general vector field (hitherto, in §3.1-§3.5, the field $(0, \mathbf{p})$ or $\nabla K = (0, M^{-1}\mathbf{p})$). In the case of a soft thermostat, ξ would be a Nose-style variable representing a thermal bath, which would vary such that the probability distribution $f(\Gamma, \xi) \propto e^{-\beta\mathcal{H}}$. In the case of a hard thermostat, ξ would be a function that kept the temperature measure constant (akin to α in the isokinetic thermostat), and we would hope to thus generate a system with the probability distribution $f(\Gamma) \propto e^{-\beta\mathcal{H}}\delta(\mathcal{T}(\Gamma) - T)$ (where \mathcal{T} represents the expression whose average will yield the temperature T). Note that the inclusion of the thermostat within the equations of motion, without the use of a reference value (which is used in the Berendsen thermostat) will ensure time-reversibility.

We therefore begin with the more straightforward of the two — the Generalised Nose-Hoover thermostat (§3.6.1) — before moving on to consider how one might apply hard thermostats, in particular in the case of the configurational temperatures (§3.6.2).

3.6.1 Generalised Nose-Hoover

The Nose-Hoover approach, outlined in §3.2, can be extended beyond its usual form. Consider the following set of differential equations:

$$\begin{aligned} \dot{\mathbf{q}} &= \frac{\mathbf{p}}{m} - \xi \mathbf{X}_{\mathbf{q}}, \\ \dot{\mathbf{p}} &= \mathbf{F} - \xi \mathbf{X}_{\mathbf{p}}, \\ \dot{\xi} &= \dot{\xi}(\mathbf{p}, \mathbf{q}), \end{aligned}$$

where $\mathbf{X}_{\mathbf{q}}$ and $\mathbf{X}_{\mathbf{p}}$ represent the coordinate and momentum components of the vector field \mathbf{X} . The Liouville theorem tells us that, in the extended phase space $(\mathbf{q}, \mathbf{p}, \xi)$

$$\frac{df}{dt} = f\xi\nabla \cdot \mathbf{X}. \quad (3.19)$$

for the distribution function f . Under these equations of motion, we also see that

$$\frac{d}{dt} \left[-\beta\mathcal{H} - \beta\frac{Q\xi^2}{2} \right] = -\beta\dot{\mathcal{H}} - \beta Q\xi\dot{\xi} = \beta\xi \left[\nabla\mathcal{H} \cdot \mathbf{X} - Q\dot{\xi}(\mathbf{p}, \mathbf{q}) \right]. \quad (3.20)$$

If we set $\dot{\xi}(\mathbf{p}, \mathbf{q}) = \frac{1}{Q}[\nabla\mathcal{H} \cdot \mathbf{X} - \frac{1}{\beta}\nabla \cdot \mathbf{X}]$, then we obtain

$$\begin{aligned} \frac{d}{dt} \left[-\beta\mathcal{H} - \beta\frac{Q\xi^2}{2} \right] &= \beta\xi \left[\nabla\mathcal{H} \cdot \mathbf{X} + \frac{1}{\beta}\nabla \cdot \mathbf{X} - \nabla\mathcal{H} \cdot \mathbf{X} \right] \\ &= \xi\nabla \cdot \mathbf{X} \\ &= \frac{1}{f} \frac{df}{dt} \\ &= \frac{d}{dt} [\ln f], \end{aligned}$$

so that

$$\ln f + c = \left[-\beta\mathcal{H} - \beta\frac{Q\xi^2}{2} \right] \Rightarrow f \propto e^{-\beta[\mathcal{H} + \frac{Q\xi^2}{2}]}. \quad (3.21)$$

Thus the canonical distribution (over the real phase space coordinates) is preserved under the dynamics of these equations. Consequently the equations

$$\dot{\mathbf{q}} = \frac{\mathbf{p}}{m} - \xi\mathbf{X}_{\mathbf{q}}, \quad (3.22)$$

$$\dot{\mathbf{p}} = \mathbf{F} - \xi\mathbf{X}_{\mathbf{p}}, \quad (3.23)$$

$$\dot{\xi} = \frac{1}{Q} \left[\nabla\mathcal{H} \cdot \mathbf{X} - \frac{1}{\beta}\nabla \cdot \mathbf{X} \right], \quad (3.24)$$

form the **Generalised Nose-Hoover** (GNH) equations of motion. Substituting $\mathbf{X} = [0, \mathbf{p}]$ yields the Nose-Hoover equations of motion.

These equations of motion can clearly be used to control the temperature of a system. From the form of the distribution function given in Eqn.(3.21) we note that the ensemble average of ξ , and therefore the expected time average of ξ is zero. Consequently

$$\bar{\xi} = \frac{1}{Q} \left[\overline{\nabla\mathcal{H} \cdot \mathbf{X}} - \frac{1}{\beta}\overline{\nabla \cdot \mathbf{X}} \right] = 0,$$

from which we note that \mathbf{X} plays the role of \mathbf{B} in our general temperature expression Eqn.(2.16). For this reason, we describe these style of thermostats as the **B-Field Nose-Hoover** thermostats, of **B**-thermostats.

3.6.2 The Iso- \mathcal{T} Thermostats

The forms of the Nose-Hoover and Isokinetic equations of motion are strikingly similar. The equations of motion of the ‘real’ coordinates have the same form. However, while ξ is a variable in the Nose-Hoover system, whose value is determined by its own equation of motion, ξ is a function of \mathbf{q} and \mathbf{p} in the Isokinetic system. The ensemble explored by these two approaches is the same, apart from two important points — the Isokinetic ensemble is constrained to points of constant kinetic energy, and the temperatures of the systems differ by a term of $\mathcal{O}(1/N)$. We will therefore consider whether the Generalised Nose-Hoover system might have a similar hard-thermostatted equivalent, with the same relationship that exists between the standard Nose-Hoover thermostat and the Isokinetic thermostat. We shall call such a generalised thermostat an **Iso- \mathcal{T}** thermostat, and seek equations of motion such that $\dot{\mathcal{T}} = 0$, and such that the distribution $e^{-\beta\mathcal{H}}$ is preserved.

The case that will interest us most in Chapter 4 is when $\mathcal{T}(\mathbf{\Gamma}) = \mathcal{T}(\mathbf{q})$ is a configurational temperature. In this case, we recognise that the constraint $\mathcal{T} = T_0$ (along with $\dot{\mathcal{T}} = 0$) constitutes a holonomic constraint, and we can therefore apply Gauss’ principle to determine equations of motion that conserve \mathcal{T} . Such equations, however, will produce a *microcanonical* ensemble rather than a canonical one, as the energy will be conserved as well (§3.4.2). Thus, pursuing this approach will not lead to the system we seek.

Let us examine what happens to the distribution $f = e^{-\beta\mathcal{H}}$ under the influence of the equations of motion Eqn.(3.18). We have

$$\frac{1}{f} \frac{df}{dt} = -\beta\dot{\mathcal{H}} = -\beta \nabla\mathcal{H} \cdot \dot{\mathbf{\Gamma}} = \beta \nabla\mathcal{H} \cdot \xi\mathbf{X}, \quad (3.25)$$

and, if f is to be preserved, we require that

$$\begin{aligned} \frac{1}{f} \frac{df}{dt} &= -\nabla \cdot \dot{\mathbf{\Gamma}} = \nabla \cdot \xi\mathbf{X} = \beta \nabla\mathcal{H} \cdot \xi\mathbf{X}, \\ \Rightarrow \beta &= \frac{1}{kT} = \frac{\nabla \cdot \dot{\mathbf{\Gamma}}}{\nabla\mathcal{H} \cdot \dot{\mathbf{\Gamma}}} = \frac{\nabla \cdot \xi\mathbf{X}}{\nabla\mathcal{H} \cdot \xi\mathbf{X}}, \end{aligned} \quad (3.26)$$

where β is constant. Therefore, if our equations of motion can hold $\mathcal{T} = (\nabla\mathcal{H} \cdot \xi\mathbf{X})/(\nabla \cdot \xi\mathbf{X})$ constant, we will have an iso- \mathcal{T} thermostat. This can be achieved by setting

$$\begin{aligned} \dot{\mathcal{T}} = 0 &\Rightarrow \dot{\mathbf{\Gamma}} \cdot \nabla\mathcal{T} = 0 \\ &\Rightarrow \dot{\mathbf{\Gamma}}_0 \cdot \nabla\mathcal{T} = \xi\mathbf{X} \cdot \nabla\mathcal{T} \\ \Rightarrow \xi &= \frac{\dot{\mathbf{\Gamma}}_0 \cdot \nabla\mathcal{T}}{\mathbf{X} \cdot \nabla\mathcal{T}} = \frac{\dot{\mathbf{\Gamma}}_0 \cdot \nabla\left(\frac{\nabla\mathcal{H} \cdot \xi\mathbf{X}}{\nabla \cdot \xi\mathbf{X}}\right)}{\mathbf{X} \cdot \nabla\left(\frac{\nabla\mathcal{H} \cdot \xi\mathbf{X}}{\nabla \cdot \xi\mathbf{X}}\right)}. \end{aligned} \quad (3.27)$$

Eqn.(3.27) is a recursive relation. If, however, we can make the approximation $\nabla \cdot \xi \mathbf{X} \approx \xi \nabla \cdot \mathbf{X}$, then we can cancel ξ from the terms on the right hand side of Eqn.(3.27), removing the recursion to leading order. We note that ξ is $\mathcal{O}(1)$ or less if $\mathcal{O}(\dot{\Gamma}_0 \cdot \nabla T) \leq \mathcal{O}(\mathbf{X} \cdot \nabla T)$, which will be the case if $\mathcal{O}(N)$ of the elements of \mathbf{X} are themselves $\mathcal{O}(1)$ or greater. We note that this condition is met for the Isokinetic thermostat, which corresponds to the iso- \mathcal{T} when $\mathbf{X} = \nabla K$.

Furthermore, if $\mathcal{T}(\Gamma) = \mathcal{T}(\mathbf{q})$ is purely a function of the coordinates, then the constraint $\mathcal{T} = T$ is a holonomic constraint, on the presumption that $\nabla \cdot \xi \mathbf{X} \approx \xi \nabla \cdot \mathbf{X}$. The motion of the system obeys the constraints $\mathcal{T} = T$ and $\dot{\mathcal{T}} = 0$, so that we can derive expressions for the temperature using Eqn.(2.16) as long as \mathbf{B} is orthogonal to the hypersurface of constraint (§2.4.2). We note that a choice of $\mathbf{B} = \dot{\Gamma}/(\nabla \mathcal{H} \cdot \dot{\Gamma})$ obeys this condition, since the motion of the system must be in the hypersurface of constraint**. We note that the temperature expression determined from this choice of \mathbf{B} is consistent with Eqn.(3.26) to $\mathcal{O}(1/N)$. Interestingly, though, Eqn.(3.25), Eqn.(3.26) and Eqn.(3.27) do not require that \mathcal{T} be purely a function of positions.

In the following chapter, we shall consider applying the \mathbf{B} -thermostats and Iso- \mathcal{T} thermostats to develop thermostats that are independent of the momenta in our system.

**We cannot choose $\mathbf{B} = \dot{\Gamma}$, as we expect $\langle \nabla \mathcal{H} \cdot \dot{\Gamma} \rangle = \langle \dot{\mathcal{H}} \rangle = 0$.

Chapter 4

Simulation Applications

The purpose of this chapter is to report on applications of our theoretical developments to the computer simulation of molecular systems. Initially, we wish to ensure that the expressions that we have derived in Chapter 2 can indeed be used to determine the temperatures of simulated systems at equilibrium. In particular, given the capacity to measure the temperature of a system using only configurational information, we are interested in the practicability of using the configurational expressions to determine a system's temperature.

Beyond this, it is interesting to study the behaviour of these temperature expressions in non-equilibrium environments. Equilibrium was an essential ingredient in the theoretical work of the previous chapters — we do not expect the various temperature expressions to yield the same value in non-equilibrium simulations. We will therefore consider how these expressions behave in the context of Couette flow. At this point, we will examine the application of our temperature expressions to rigid-body systems as well as to atomic systems.

The focus of the final section of this chapter will be on the application of thermostats that involve changes to the coordinate equations of motion, rather than the momentum equations of motion. Such 'coordinate thermostats' have the advantage that they circumvent traditional difficulties in ensuring that momenta used to calculate the temperature are *peculiar* to the local flow. We will investigate two styles of thermostat. The first is a variant of the **B**-thermostat that was used in preliminary investigations. The second is the true **B**-thermostat of §3.6.1. For both techniques, we investigate their application to both equilibrium and non-equilibrium systems and compare these results with those of a 'traditional', momentum-based thermostat.

Each of the simulations reported on in this chapter was of a three-dimensional system. All results from simulated experiments

are quoted in reduced units.

4.1 Measurement of Equilibrium Properties

We recall that we have defined three ‘classes’ of temperature expression — the Rugh temperatures, of the form $1/\langle \nabla \cdot (\mathbf{B}/(\nabla \mathcal{H} \cdot \mathbf{B})) \rangle$, the fractional temperatures of the form $\langle \nabla \mathcal{H} \cdot \mathbf{B} \rangle / \langle \nabla \cdot \mathbf{B} \rangle$ and the $\mathcal{O}(1)$ temperatures of the form $1/\langle \nabla \cdot \mathbf{B} / \nabla \mathcal{H} \cdot \mathbf{B} \rangle$. For atomic systems, the configurational temperatures correspond to the choice of $\mathbf{B} = \nabla \Phi$, the normal temperatures correspond to the choice $\mathbf{B} = \nabla \mathcal{H}$, and the kinetic temperatures correspond to the choice $\mathbf{B} = \nabla K$. Finally, we recall that T_{KF} is the Equipartition temperature — the temperature determined from the Equipartition theorem. For rigid-body systems, the configurational temperature corresponds to the choice of $\mathbf{B} = \nabla_{\mathbf{r}} \Phi$, the quaternionic temperature corresponds to a choice of $\mathbf{B} = \nabla_{\mathbf{Q}} \Phi$, and the kinetic temperature corresponds to a choice of $\mathbf{B} = \nabla_{\mathbf{p}} K$.

In this section, we apply the various temperature expressions to simulations of equilibrium atomic systems. In §4.1.1 we consider the behaviour of the instantaneous normal, configurational, and kinetic temperature expressions defined in Chapter 2, and in §4.1.2 we consider their average values: the various ‘temperatures’ for the system.

4.1.1 Instantaneous Temperatures

In order to gain some insight into the expressions we will be using to determine the temperature, we examine the time evolution of the instantaneous values of the normal, configurational, and kinetic temperatures in three different types of simulations; a constant energy system, an Isokinetic system and a Nose-Hoover system.

Fig. 4.1 shows the instantaneous values of the six instantaneous temperature expressions $\mathcal{T}_{\text{N1}}, \mathcal{T}_{\text{NR}}, \mathcal{T}_{\text{C1}}, \mathcal{T}_{\text{CR}}, \mathcal{T}_{\text{K1}}$ and \mathcal{T}_{KR} during a constant-energy simulation of 864 WCA atoms near the Lennard-Jones triple-point ($\rho = 0.8442, T = 0.722$). For this system, $E/N \approx 1.85$. We recall that the instantaneous values for the fractional temperatures are identical to the instantaneous values of the $\mathcal{O}(1)$ temperatures, and that they differ only in the way in which these expressions are averaged. The data is reported for 1000 timesteps of $\delta t = 0.001$.

From Fig. 4.1 we note that the configurational and normal temperatures are hardly distinguishable on the scale of the graph. This is in part due to the fact that, in the normal temperature expres-

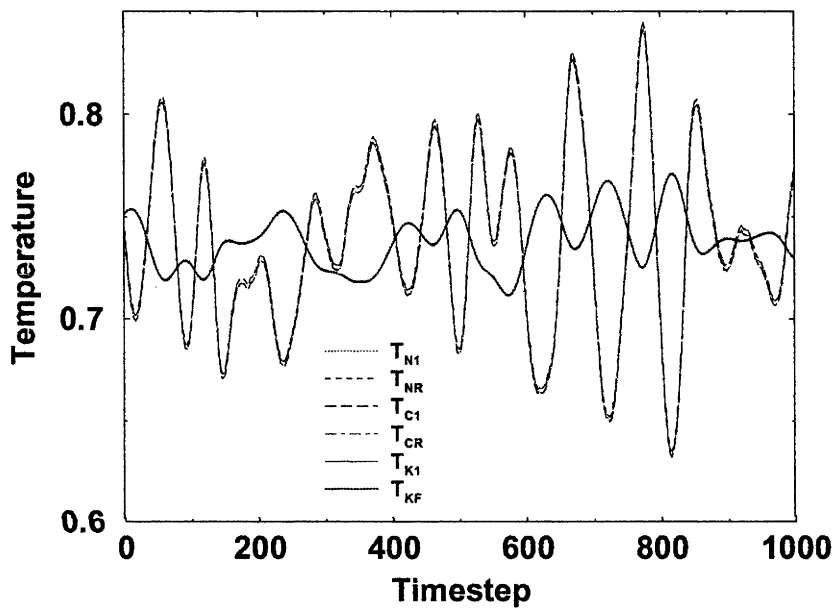


Figure 4.1: The instantaneous temperature expressions \mathcal{T}_{N1} , \mathcal{T}_{NR} , \mathcal{T}_{C1} , \mathcal{T}_{CR} , \mathcal{T}_{K1} and \mathcal{T}_{KR} , evaluated over 1000 timesteps of a constant-energy simulation of 864 WCA atoms at the LJ triple-point. The normal and configurational temperatures are almost indistinguishable of the scale of the graph, as are the kinetic temperatures.

sions, the configurational terms (terms involving functions of \mathbf{q} only) are three orders of magnitude larger than the kinetic terms (terms involving functions of \mathbf{p} only). As a result, the configurational and normal temperatures can be regarded as perturbations of one another. For our choice of (reduced) units, they are essentially equal.

They are also hardly distinguishable because, as we anticipated in Chapter 2, the difference between the Rugh and $\mathcal{O}(1)$ temperatures is indeed $\mathcal{O}(1/N)$ for the normal, configurational, and kinetic temperatures in this system. This relative behaviour is observed in the Isokinetic and Nose-Hoover simulations as well, and will be common to most of the systems studied in this chapter.

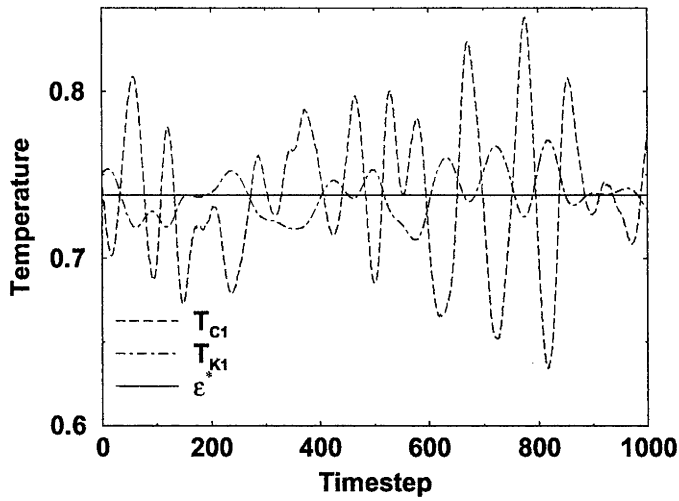
Given this relation between the normal, configurational and kinetic temperatures, our analysis of the instantaneous behaviour of the temperature expressions is simplified by considering only $\mathcal{T}_{C1}(= \mathcal{T}_{CF})$ and $\mathcal{T}_{K1}(= \mathcal{T}_{KF})$. In Fig. 4.2, we show the time evolution of these two temperatures for three different simulations of 864 WCA atoms at the Lennard-Jones triple point — Fig. 4.2a is taken from the constant-energy simulation described above, Fig. 4.2b is taken from a simulation of the same system, using an Isokinetic thermostat, and Fig. 4.2c is taken from a simulation of the same system, using a Nose-Hoover thermostat. Once again, the data is reported for 1000 timesteps of $\delta t = 0.001$.

As well as showing \mathcal{T}_{C1} and \mathcal{T}_{K1} on each graph of Fig. 4.2, we include a third quantity, that is related to the instantaneous total energy of the system at each timestep. Denoted \mathcal{E}^* , it is given by the formula

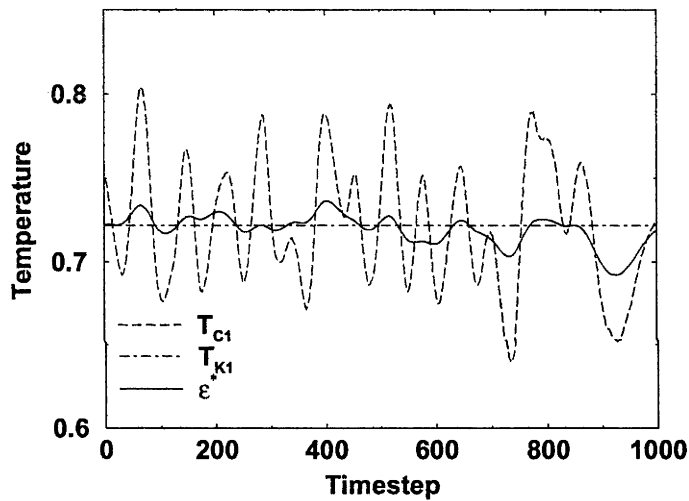
$$\mathcal{E}^* = \mathcal{E} \frac{kT}{E},$$

where \mathcal{E} represents the instantaneous value of the energy, and E and T represent the reported (or input) energy and temperature for the simulations, respectively. We note the following properties of \mathcal{E}^* . First, its average value over the course of the simulation is, by definition, T , so it is (*ex post facto*) a temperature-yielding function. It is therefore a quantity that can be compared with the other temperature-yielding functions \mathcal{T}_{C1} and \mathcal{T}_{K1} . Second, although its average over the simulation is necessarily the system temperature, it is also the value of the instantaneous temperature, multiplied by a constant rescaling factor. It can therefore also be thought of as a measurement of the instantaneous energy (using a different set of units).

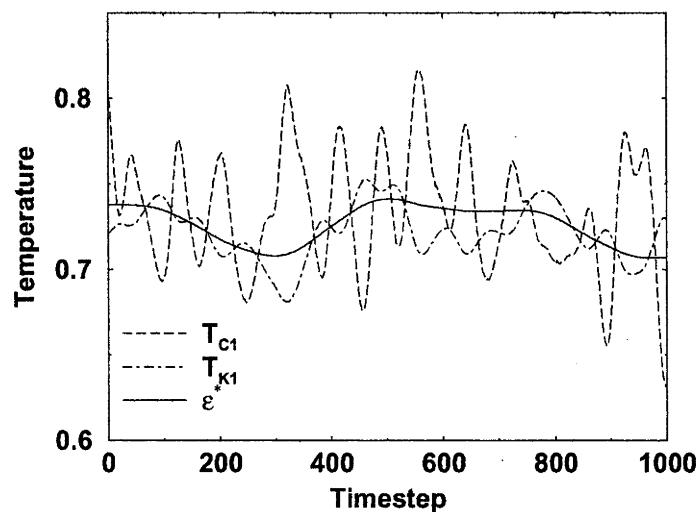
Given the coincidence of the values of the instantaneous configurational and normal temperatures apparent from Fig. 4.1, the conclusions that we draw from studying the instantaneous values of \mathcal{T}_{C1} in Fig. 4.2 will apply to the expressions \mathcal{T}_{CR} , \mathcal{T}_{N1} and \mathcal{T}_{NR} as well.



(a)



(b)



(c)

Figure 4.2: Instantaneous temperatures \mathcal{T}_{C1} and \mathcal{T}_{K1} , and the rescaled total energy \mathcal{E}^* , for 1000 timesteps of a (a) constant-energy, (b) Isokinetic, and (c) Nose-Hoover simulations of 864 WCA atoms at the LJ triple-point.

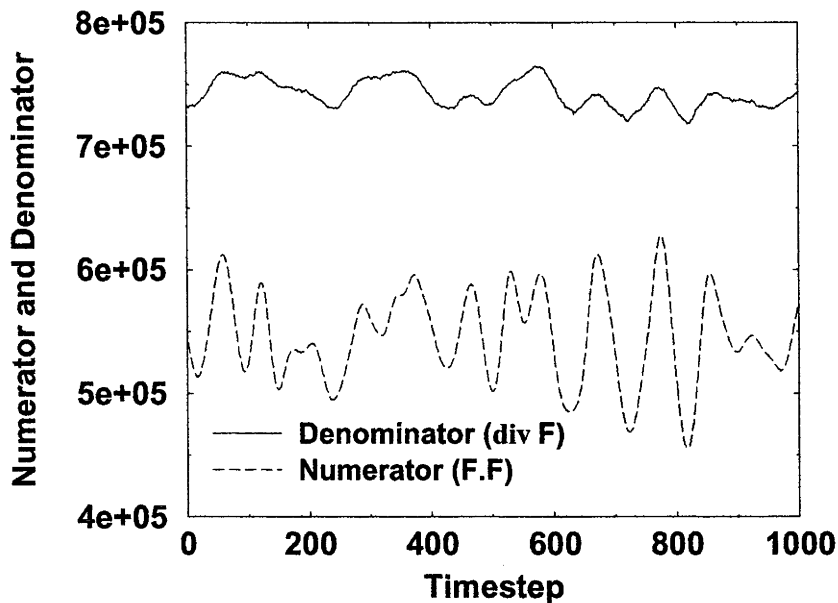


Figure 4.3: Instantaneous numerator and denominator terms of \mathcal{T}_{C1} for a constant energy simulation of 864 WCA atoms near the LJ triple point.

We note from Fig. 4.2 that \mathcal{T}_{C1} typically fluctuates with a larger amplitude than the kinetic temperatures. As a consequence, the statistical uncertainties in the thermodynamic temperature, as measured using \mathcal{T}_{C1} , will be greater than the statistical uncertainties when using the kinetic expressions.

We also note that the fluctuations of the kinetic and configurational temperatures appear to be 180° out of phase. Interestingly, the fluctuations of these two temperatures appear to be about a function that is well approximated by \mathcal{E}^* . This is a non-trivial, but not entirely surprising relationship, given that the total energy $E = K + \Phi$, and that the kinetic and configurational temperatures are explicitly functionals of ∇K and $\nabla \Phi$. It is also highly suggestive of the possibility of constructing a process by which these fluctuations can be ‘damped’, if not removed, for improved convergence. At this point, however, this possibility remains merely an interesting observation.

Although the above considerations give some indication of the expected behaviour of the instantaneous fractional temperatures, we must examine the numerator and denominator of these expressions separately in order to comment on the statistical uncertainties in the fractional temperatures themselves. The instantaneous values of the numerator and denominator of $\mathcal{T}_{CF} = (\mathbf{F} \cdot \mathbf{F})/(\nabla \cdot \mathbf{F})$ are shown in Fig. 4.3 for the same 1000 timesteps of the constant-energy simula-

tion described above. The comments we draw from that figure are analogous for the other two simulations. We note that the numerator fluctuates with much greater amplitude than the denominator. Furthermore, these fluctuations are correlated with the fluctuations in T_{CF} , as can be seen by comparing Fig. 4.3 with Fig. 4.2a. We also note that the fluctuations of the numerator and denominator are not independent, but are clearly correlated. This has the effect of reducing the resultant statistical uncertainty in T_{CF} , compared with T_{CR} and T_{C1} , as we shall observe in our later results.

Finally, in this subsection, we make a few remarks about the computation of the configurational temperatures. All the terms are straightforward to compute, except for the term $\sum_{ij} F_i F_j \frac{\partial F_j}{\partial r_i} = \sum_{ij} F_i F_j \frac{\partial^2 \Phi}{\partial r_i \partial r_j}$, which appears in the $\mathcal{O}(1/N)$ part of the Rugh configurational and normal temperatures (that is, in the term that is omitted from the corresponding $\mathcal{O}(1)$ temperatures). The complication that arises is due to the sparseness of the Hessian matrix of Φ , $[\frac{\partial^2 \Phi}{\partial r^2}]_{ij}$. The non-zero elements occur whenever r_i and r_j describe coordinates belonging to a pair of interacting particles, or to a single particle. For a simulation that incorporates cell code (§1.4.2), it is useful to be able to express $\sum_{ij} F_i F_j \frac{\partial F_j}{\partial r_i}$ as a sum of contributions from pairs of interacting particles. We now determine such an expression.

It is temporarily convenient to denumerate the set of coordinates using two indices — the first index represents the atom a coordinate belongs to, and the second index represents the coordinate axis (x , y or z). Thus we define $\partial_{i\alpha}\Phi$ as the derivative of the potential with respect to the α coordinate on the i -th particle (so that $\partial_{1x}\Phi$ is the x -component of the force on particle 1, which we write as the force F_{x1}). The term we are interested in is therefore

$$\begin{aligned} \sum_{i\alpha j\beta} F_{i\alpha} F_{j\beta} \partial_{i\alpha} \partial_{j\beta} \Phi \\ = \sum_{i\alpha\beta} F_{i\alpha} F_{i\beta} \partial_{i\alpha} \partial_{i\beta} \Phi + \sum_{\substack{i\alpha j\beta \\ i \neq j}} F_{i\alpha} F_{j\beta} \partial_{i\alpha} \partial_{j\beta} \Phi. \end{aligned} \quad (4.1)$$

We note that

$$\begin{aligned} \partial_{i\alpha} \partial_{j\beta} \Phi &= \partial_{i\alpha} \partial_{j\beta} \phi_{ij}, \quad (i \neq j), \text{ and} \\ \partial_{i\alpha} \partial_{i\beta} \Phi &= \sum_{\substack{j \\ i \neq j}} \partial_{i\alpha} \partial_{i\beta} \phi_{ij} = - \sum_{\substack{j \\ i \neq j}} \partial_{i\alpha} \partial_{j\beta} \phi_{ij}, \end{aligned}$$

so that Eqn.(4.1) becomes

$$\begin{aligned}
\sum_{i\alpha j\beta} F_{i\alpha} F_{j\beta} \partial_{i\alpha} \partial_{j\beta} \Phi &= \\
& - \sum_{i\alpha\beta} F_{i\alpha} F_{i\beta} \sum_{\substack{j \\ i \neq j}} \partial_{i\alpha} \partial_{j\beta} \phi_{ij} + \sum_{\substack{i\alpha j\beta \\ i \neq j}} F_{i\alpha} F_{j\beta} \partial_{i\alpha} \partial_{j\beta} \phi_{ij} \\
& = \sum_{\substack{i\alpha j\beta \\ i \neq j}} F_{i\alpha} (F_{j\beta} - F_{i\beta}) \partial_{i\alpha} \partial_{j\beta} \phi_{ij} \\
& = \sum_{\{ij\}} \sum_{\alpha\beta} (F_{i\alpha} - F_{j\alpha}) (F_{j\beta} - F_{i\beta}) \partial_{i\alpha} \partial_{j\beta} \phi_{ij},
\end{aligned}$$

where $\sum_{\{ij\}}$ denotes a sum over pairs of particles. In this form, the sum is explicitly over pairs of particles, as well as over the coordinates of each particle. Therefore, for each pair of particles, contributions to the various associated temperature terms can be calculated and summed. However, in order to determine these contributions, we must already know the various $F_{i\alpha}$. When using cell code (§1.4.2), we cannot rely on having already determined the force on a given particle when determining the contributions to $\sum_{ij} F_i F_j \frac{\partial^2 \Phi}{\partial r_i \partial r_j}$. We must therefore perform *two* force loops — the first to calculate the forces, and the second to calculate this term in the Rugh temperatures. When the force loop is written in a vector style, such that the inner-most loop cycles over the interaction of a single particle with every other, then only one loop is required. However, given that all this consideration must be paid to a term that we anticipate to be $\mathcal{O}(1/N)$, it would be convenient to save computer time by not calculating this term at all. This is a possibility we look to in the following results.

4.1.2 Temperature Variation with System Parameters

Having considered the behaviour of the instantaneous temperature expressions, we now turn to the averages of these expressions over the course of a simulation. Whilst we know from our work in Chapter 2 that all of the temperature expressions converge to the thermodynamic temperature in the thermodynamic limit, it is not clear *a priori* at what rates these expressions will converge. Furthermore, there are questions of efficacy that we should address. We have already seen how the Rugh and $\mathcal{O}(1)$ temperatures have extremely close instantaneous values for at least one state point of a WCA system, and that the normal and configurational temperatures are essentially equal in that system. It is important to know

under what circumstances these differences may not be negligible, and in such cases which temperature expression, if any, is to be preferred. Furthermore, we noted in the previous subsection that the $\mathcal{O}(1/N)$ term of the Rugh configurational temperature T_{CR} is computationally expensive, compared with T_{C1} and T_{CF} . We would therefore like to determine when calculating these $\mathcal{O}(1/N)$ terms can be avoided. In order to address these questions, we report on the results of simulations of a WCA fluid at a variety of different statepoints, and numbers of particles. All simulations were carried out over 2,000,000 timesteps of length $\delta t = 0.001$. The results of these simulations appear in (Jepps, Ayton, and Evans 2000).

The first temperature comparison was made between systems with the same density and size, but differing energies. The values of the temperatures $T_{\text{NF}}, T_{\text{NR}}, T_{\text{N1}}, T_{\text{CF}}, T_{\text{CR}}, T_{\text{C1}}, T_{\text{KF}}, T_{\text{KR}}$ and T_{K1} were calculated for a system of 500 WCA atoms with density $\rho = 0.8$, and energies per particle ranging from $E/N = 0.8$ to $E/N = 2.5$. The values of the three configurational temperatures and the three kinetic temperatures appear in Table 4.1. Errors were reported as the standard deviation in the ten ‘block’ averages, and the statistical inefficiency was determined to be $s \approx 25$, consistent with (Allen and Tildesley 1987) (see §1.4.5). The values of the normal temperatures do not appear in the table, as they agree with the corresponding configurational temperatures to within 0.01% — that is, to the number of digits shown. This can be explained by our observations in the previous section about the relative contributions of the configurational and kinetic terms in the normal temperatures.

We note that the temperatures are all in good agreement. The fractional and Rugh temperatures agree to within $\approx 0.3\%$, which is consistent with a discrepancy of $\mathcal{O}(1/N)$ for a system of size $N = 500$. Furthermore, the discrepancy between T_{CF} and T_{CR} is $\approx 0.1\%$, as is the discrepancy between T_{KF} and T_{KR} . The $\mathcal{O}(1)$ temperatures are a good approximation to the Rugh temperatures, for this system. In terms of the relative fluctuations of the temperatures, we note that the reported errors are generally larger for the configurational temperatures, by as much as five times. This is consistent with our observations in §4.1.1.

It is interesting to note that, from the theory, we expect the Rugh temperatures to agree to within statistical error, as the pseudo-entropy S_{B} is the actual entropy S for the Rugh temperatures. The deviation between these temperatures is approximately 0.2% of T_{KR} , which corresponds to a discrepancy of exactly $1/N$. Such a discrepancy could be explained in terms of the degrees of freedom of the system — momentum conservation implies that there are only $3N - 3$ degrees of freedom in our system, rather than $3N$. If we defined $1/T_{\text{KR}} = (3N - 5)/K$ (rather than $1/T_{\text{KR}} = (3N - 2)/K$) in

Table 4.1: A comparison of values of the configurational and kinetic temperatures for constant-energy simulations of 500 WCA atoms at density $\rho = 0.8$, for various energies per particle. For each temperature, two values are reported. The first is the temperature as determined from the simulation, and the second is the deviation of that temperature from the equipartition temperature T_{KF} , given as a percentage of T_{KF} . The numbers in brackets indicate the error in the last decimal place.

E/N	T_{CF}		T_{CR}		T_{C1}	
	value	dev (%)	value	dev (%)	value	dev (%)
0.8	0.5090 (1)	0.19	0.5097 (2)	0.31	0.5065 (2)	-0.31
1.0	0.6381 (2)	0.11	0.6389 (3)	0.24	0.6348 (3)	-0.41
1.2	0.7694 (1)	0.20	0.7705 (2)	0.34	0.7652 (2)	-0.35
1.5	0.9687 (2)	0.24	0.9701 (3)	0.38	0.9631 (3)	-0.34
1.8	1.1694 (2)	0.20	1.1709 (4)	0.32	1.1621 (3)	-0.43
2.0	1.3042 (2)	0.14	1.3060 (3)	0.28	1.2958 (3)	-0.51
2.2	1.4403 (4)	0.12	1.4424 (5)	0.26	1.4307 (5)	-0.55
2.5	1.6473 (4)	0.14	1.6497 (4)	0.28	1.6359 (4)	-0.55

E/N	T_{KF}		T_{KR}		T_{K1}	
	value	dev (%)	value	dev (%)	value	dev (%)
0.8	0.5081 (1)	0.00	0.5086 (1)	0.10	0.5079 (1)	-0.04
1.0	0.6374 (1)	0.00	0.6380 (1)	0.09	0.6371 (1)	-0.05
1.2	0.7679 (1)	0.00	0.7686 (1)	0.09	0.7676 (1)	-0.04
1.5	0.9664 (1)	0.00	0.9673 (1)	0.09	0.9660 (1)	-0.04
1.8	1.1671 (1)	0.00	1.1682 (1)	0.09	1.1666 (1)	-0.04
2.0	1.3024 (1)	0.00	1.3036 (1)	0.09	1.3018 (1)	-0.05
2.2	1.4386 (1)	0.00	1.4399 (1)	0.09	1.4380 (1)	-0.04
2.5	1.6450 (1)	0.00	1.6465 (1)	0.09	1.6443 (1)	-0.04

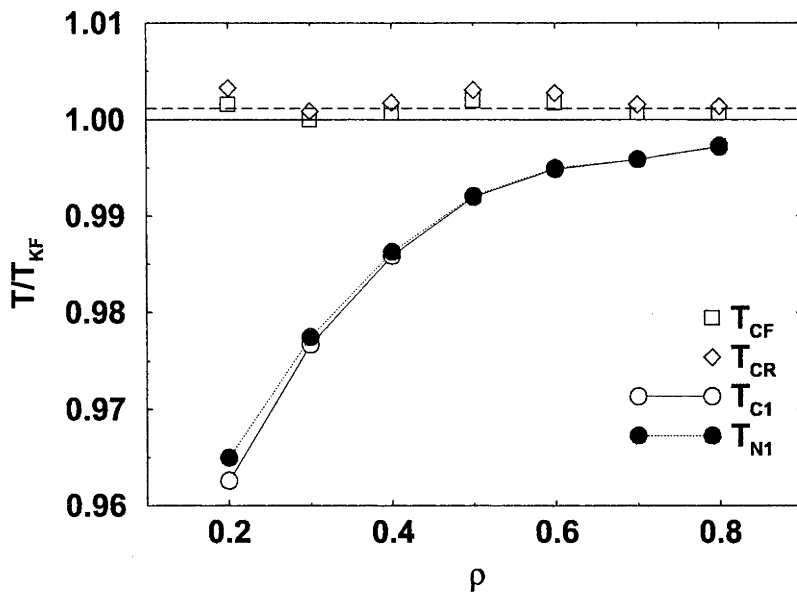


Figure 4.4: Effect of density variation on T_{CF} , T_{CR} , T_{C1} and T_{N1} , for constant-energy simulations of 864 WCA atoms, $E/N = 1.5$. Temperatures are reported as a fraction of the equipartition temperature — the solid line corresponds to $T = T_{KR}$, and the dashed line corresponds to $T = (1 + 1/N)T_{KF}$, indicating the order of $1/N$ deviations for this system.

light of this argument, the two temperatures would agree to within statistical uncertainty. Indeed, $1/T_{KR} = (3N - 5)/K$ is the correct form for the kinetic Rugh temperature if one replaces the momenta \mathbf{p}_i in the Hamiltonian with the *peculiar* momenta ($\mathbf{p}_i - \sum_j \mathbf{p}_j/N$). It is not clear *a priori* why one should prefer this formula to the usual Hamiltonian, when $\sum_i \mathbf{p}_i = 0$. Certainly, either form will yield the correct temperature in the thermodynamic limit.

In the normal temperature expressions at high densities, the size of the configurational terms is much greater than the size of the momentum terms at liquid temperatures. Indeed, given this dependence on the physical structure of the system rather than on its momentum distribution, it is interesting to note that the normal and configurational temperature expressions yield the correct temperature across the solid-liquid phase transition, despite the difference in the microscopic arrangements of atoms on either side of the transition temperature. At lower densities, however, when the number of interactions between particles is fewer, the configurational terms do not dominate the normal temperature expressions, and the normal temperatures are a more balanced combination of kinetic and configurational contributions. To confirm this, we compare a series of systems with fixed energy per particle ($E/N = 1.5$) and system size

($N = 864$), but with densities varying from $\rho = 0.2$ – 0.8 . Fig. 4.4 shows the effect of a change in density on the configurational and normal temperatures. Interestingly, the configurational and normal temperatures are only distinguishable on the scale of the graph in Fig. 4.4 for the low density $\mathcal{O}(1)$ temperature. Therefore, we show all three configurational temperatures, but only the $\mathcal{O}(1)$ normal temperature appears in Fig. 4.4.

We expect the Rugh temperatures to agree, independent of density, because the pseudo-entropy $S_{\mathbf{B}}$ is the actual entropy S for both T_{CR} and T_{NR} . In the case of the fractional and $\mathcal{O}(1)$ temperatures, the kinetic terms in the normal temperatures act to ‘correct’* the configurational temperatures towards the equipartition value. The effect is much larger in the $\mathcal{O}(1)$ temperatures, however, as the discrepancy with the equipartition temperatures is much greater. Indeed, the fractional and Rugh temperatures lie within about 0.1% of the kinetic temperature, again consistent with an error of $\mathcal{O}(1/N)$.

It is clear from Fig. 4.4 that T_{C1} and T_{N1} are inefficient measures of the thermodynamic temperature at low densities. This is due to the fact that the omitted $\mathcal{O}(1/N)$ term becomes more important as the density drops[†]. We note that in the thermodynamic limit, we still expect these temperatures to converge to the thermodynamic temperature. This result indicates that, while T_{N1} and T_{NR} must converge towards the thermodynamic temperature, irrespective of the density, larger system sizes are required for the same degree of convergence of T_{N1} as the density drops.

Finally, we consider the system-size dependence of our temperature expressions. It is important to know which temperatures will converge the most quickly. We have already seen how, at low densities, T_{C1} converges more slowly than the other temperatures in the thermodynamic limit. To further examine the system size dependence of our temperatures, we consider a single state point ($\rho = 0.8$, $E/N = 1.5$), and compare the variation of the configurational temperatures with system size. Fig. 4.5 shows the effects of system size, for values of N ranging from $N = 108$ to $N = 2048$. At this density, the difference between the normal temperatures and the corresponding configurational temperatures is not distinguishable on the scale of the graph for all but the 108 particle system (where the discrepancy is 0.02%). We observe, within the uncertainty of our calculations, the convergence of all four temperatures towards a common value. We would interpret this value as the thermodynamic temperature of a system at that state point, in the thermodynamic limit.

*In the case of the $\mathcal{O}(1)$ temperatures, T_{KF} is clearly a more reliable value.

[†]or, perhaps more accurately, the configurational contributions decrease at a lesser rate in the $\mathcal{O}(1/N)$ term than in the $\mathcal{O}(1)$ term

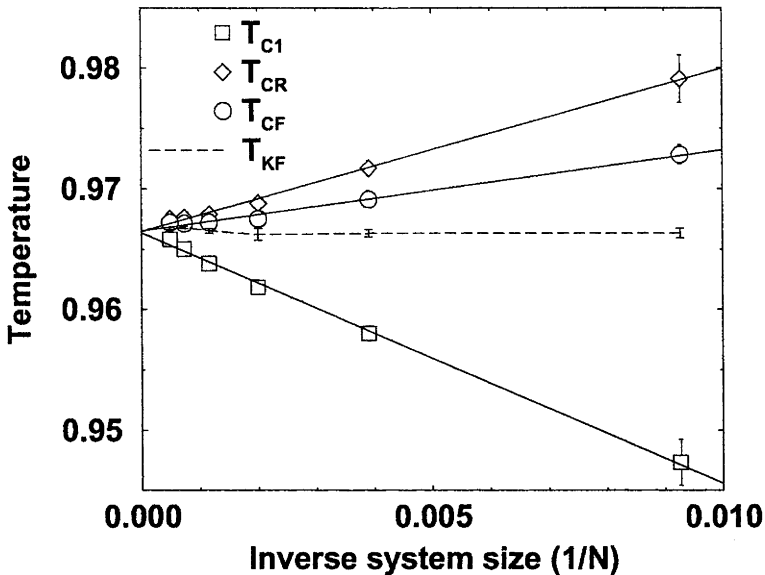


Figure 4.5: Effects of system size variation on the configurational temperatures for constant energy simulations of WCA atoms at the state point $\rho = 0.8$, $E/N = 1.5$.

Perhaps not surprisingly from the results hitherto observed, we infer from Fig. 4.5 that T_{CF} is the most efficient choice of configurational temperature, for these systems. Its convergence in the thermodynamic limit appears to be faster than the other configurational temperatures. It is also reliable at various densities, as is T_{CR} . The statistical uncertainties in its reported values are typically smaller than the other configurational temperatures. However, the absence of complicated, computationally-costly higher-derivative terms is a real advantage in terms of real-time calculation. In terms of efficiency and effectiveness, T_{CF} appears to be the best choice among the three configurational temperatures, for choosing the temperature of a system.

4.1.3 Heat Capacity Calculations

In §2.2.2, we derived a general expression for the (isochoric) heat capacity, and in §2.5.1 we developed two expressions for the heat capacity, of the form

$$\frac{1}{C_{V\eta}} = 1 - \frac{T_\eta^2 + (\boldsymbol{\eta} \cdot \nabla) T_\eta}{T_\eta^2}, \quad (4.2)$$

for a Rugh temperature $T_\eta = \langle \nabla \cdot \boldsymbol{\eta} \rangle$ (where $\boldsymbol{\eta} = (\mathbf{B}/(\mathbf{B} \cdot \nabla \mathcal{H}))$ for some field \mathbf{B}). It is interesting to compare this result with existing methods for calculating the heat capacity of constant-energy

systems, to determine whether this is a useful additional tool for practitioners of molecular simulations.

In order to make such a test, we calculate the **specific heat capacity** — the heat capacity per particle — of a system using four different methods. In addition to calculating the kinetic heat capacity C_{VK} (Eqn.(2.40)) and configurational heat capacity C_{VC} (Eqn.(2.41)), we calculate the specific heat capacity by the following two methods. First, we use the formula of Lebowitz et al. for the specific heat capacity c_{LPV} of a constant-energy system (Lebowitz et al. 1967, Eq.(3.9))

$$\frac{1}{c_{LPV}} = \frac{2}{3} \left(1 - \frac{2\beta^2}{3N} (\overline{\Phi^2} - \overline{\Phi}^2) \right).$$

Second, we note that the heat capacity $C_V = \partial E / \partial T \approx \Delta E / \Delta T$, if ΔE represents the difference in energy between two systems whose temperatures differ by $\Delta T (\ll T)$. Thus, if we simulate a second system whose energy is 1% higher than the first, we can make a further estimate of the specific heat capacity $c_\Delta = \Delta E / N \Delta T$.

The system we have chosen to simulate is a 2048-particle WCA fluid near the LJ triple point, ie $E/N \approx 1.78$, $\rho = 0.8442$. Table 4.2 contains the data from which c_{LPV} and c_Δ were calculated. The first row of data contains the RMS error in the potential energy, used to calculate c_{LPV} . The subsequent rows contain data from two simulations — the system described above, and another with energy about 1% higher than the first system — that is used to determine c_Δ .

Table 4.3 shows the data that was collected in order to calculate the new heat capacity expressions C_{VK} and C_{VC} . The first column contains the expression calculated (in the form in which it appears in Eqn.(4.2)). The second and third columns contain the evaluations of these expressions for C_{VK} and C_{VC} . The values in brackets in the bottom row indicate the range of possible values of the C_V , ignoring the unphysical negative results also contained within the range of error. We note that the values reported in Table 4.3 are calculated using the full 16-digit machine accuracy. A comparison of the four specific heat capacities appears in Table 4.4.

We calculate c_{LPV} and c_Δ from the data in Table 4.2. Estimating $\beta = (0.7115 \pm 0.0002)^{-1}$, $\overline{\Phi^2} - \overline{\Phi}^2 = (24.3 \pm 0.2)^2$ and $N = 2048$ yields a final value for $c_{LPV} = 2.42 \pm 0.02$ (assuming a 1% error in the RMS fluctuations in the potential energy). We further estimate $\Delta E = 36.5 \pm 0.4$ and $\Delta T = 0.0071 \pm 0.0001$ (based on the agreement among all the temperatures with this range), leading to a value of $c_\Delta = 36.50 / 14.54 = 2.51 \pm 0.05$.

From Table 4.2, there are clearly significant errors involved in the determination of the heat capacity using expressions of the form

Table 4.2: Data used to determine the specific heat capacity estimates c_{LPV} and c_{Δ} — the RMS error in the potential energy, the total energy, and various temperatures — from two systems of 2048 WCA atoms near the LJ triple point — $\rho = 0.8442$, $E_1/N \approx 1.85$, $E_2/N \approx 1.87$. The fourth column contains the differences between the energy and temperature values. Figures in brackets indicate the error in the last decimal place.

	Simulation 1	Simulation 2	Δ
RMS(Φ)	24.3 (2)		
E	3650.4 (2)	3686.9 (2)	36.5 (4)
T_{CF}	0.7113 (2)	0.7184 (6)	0.0071 (8)
T_{CR}	0.7115 (6)	0.7186 (9)	0.0071 (15)
T_{C1}	0.7105 (6)	0.7175 (9)	0.0070 (15)
T_{KF}	0.7114 (2)	0.7185 (2)	0.0071 (4)
T_{KR}	0.7115 (2)	0.7187 (2)	0.0072 (4)
T_{K1}	0.7113 (2)	0.7185 (2)	0.0072 (4)

Table 4.3: Data used to determine the kinetic and configurational heat capacities (Eqn.(2.40) and Eqn.(2.41)) from a system of 2048 WCA atoms near the LJ triple point — $E/N \approx 1.85$, $\rho = 0.8442$. Figures in brackets indicate the error in the last decimal place, except in the bottom row, where they indicate the range of possible values from these calculations.

	C_{VK}	C_{VC}
$\langle T^2 + (\boldsymbol{\eta} \cdot \nabla)T \rangle_E$	1.9760 (13)	1.9803 (33)
T	0.7115 (2)	0.7115 (6)
T^2	0.5062 (3)	0.5062 (9)
$\frac{T^2 + (\boldsymbol{\eta} \cdot \nabla)T}{T^2}$	1.000202 ± 0.0012	1.000389 ± 0.003
C_V	4960 (700– ∞)	2570 (300– ∞)

Table 4.4: Four estimates of the heat capacity for a system of 2048 WCA atoms near the LJ triple point — $E/N \approx 1.85$, $\rho = 0.8442$. Figures in brackets indicate the error in the last decimal place, or the range of possible values.

Specific heat capacity	Estimate
c_{VK}	2.42 (0.34– ∞)
c_{VC}	1.25 (0.15– ∞)
c_{LPV}	2.42 (2)
c_{Δ}	2.51 (5)

Eqn.(4.2), where the heat capacity is the reciprocal of a very small number — a very small number that is the difference between two much larger numbers. Consequently, a very small error in the determination of either the numerator or denominator will result in large errors in our estimate for c_V . The kinetic expression, with its smaller fluctuations, provides a more reasonable approximation of the heat capacity than the configurational expression. It is possible that errors in equating the simulation time average and ensemble average of the new heat capacity expressions would be improved by reducing the timestep of the simulation. However, given the dissatisfactory errors inherent in this approach, and the existence of more effective ways of determining the heat capacity, such an investigation was not pursued.

4.1.4 Other Equilibrium Results

In §4.1.2, we evaluated the temperature expressions of §2.5 in a constant-energy environment. Similar results can be obtained for these temperatures under conditions of constant temperature. T_{C1} has been tested in a constant-temperature environment, using the Monte Carlo technique (Butler, Ayton, Jepps, and Evans 1998). Applying this technique is particularly interesting, as the Monte Carlo simulation contains only configurational information. The absence of kinetic information provides an excellent test of our theory, as well as a useful additional test to ensure that the simulated temperature is indeed the desired temperature.

Butler et al. performed three experiments. The first was to examine the system-size dependence of T_{C1} , by calculating T_{C1} for a two-dimensional Lennard-Jones fluid ($R_{\text{cutoff}} = 6\sigma$) at $\rho = 0.35$, $T = 1$, with system sizes ranging from 50-100,000 (see Fig. 4.6). The convergence of the temperature is consistent with that observed in the constant-energy simulations.

The second experiment was to perform a quench on the system, in order to determine the relaxation rate of T_{C1} , compared with other system properties. The results from this experiment (Fig. 4.7) indicate that T_{C1} relaxes much more quickly than do other macroscopic quantities, such as pressure and temperature.

The third experiment was to include an error in the simulation that violated microscopic reversibility, and whose effect was imperceptible in terms of its influence on traditionally-calculated system properties, such as pressure and energy. The value of T_{C1} was then determined, to see if it could be used to discriminate between the correct and incorrect simulations. T_{C1} was indeed more sensitive to this error than the other system properties, with an error of 3% being observed for a system of size $N = 50,000$.

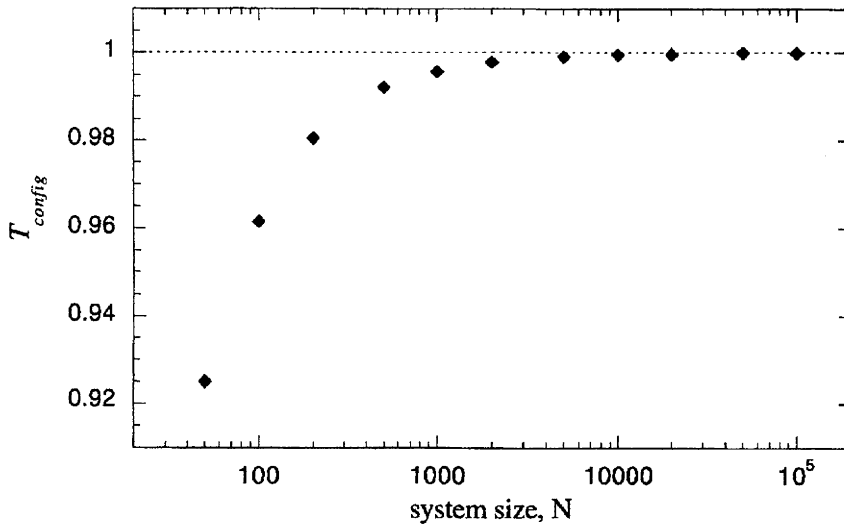


Figure 4.6: System-size dependence of T_{C1} for a Monte Carlo simulation with input temperature $T = 1$ (Butler, Ayton, Jepps, and Evans 1998)

This final observation may be explained by the dependence of the temperature on the potential. The energy and pressure depend on the zeroth and first derivatives respectively, whereas T_{C1} depends on the second derivatives. Given the ‘sharp’ nature of these derivatives, from the form of the WCA and LJ potentials, it is possible that small errors are amplified through the differentiation process, leaving the configurational temperature expressions more sensitive to errors in the positions of particles than the other quantities. With the possibility of creating temperature expressions that depend on higher-than-second-order derivatives of the potential comes the possibility of determining expressions with even greater sensitivity to errors in the simulation.

Ennis and Evans have looked at the application of the configurational temperatures to Brownian Dynamics simulations, which can also be implemented with only configurational information about the system being simulated (Allen and Tildesley 1987). They also find that T_{CF} is a more consistently accurate measure of the temperature (particularly in relation to convergence in the thermodynamic limit) than T_{C1} , for their Brownian Dynamics simulation of a 3D LJ fluid ($r_{\text{cutoff}} = 4\sigma$, $\eta = 200$). Ennis and Evans also look at the normalised auto-correlation function $C_{T_{\text{C1}}}(\delta t) = \overline{T(t)T(t+\delta t)}/\overline{T(t)}\overline{T(t)}$ for the configurational temperatures in four systems with different potentials — the LJ potential, r^{-12} potential, r^{-6} potential, and r^{-4} potential. The auto-correlation function is indicative of the relaxation rate of T_{C1} in the fluid. They find that, as the potential

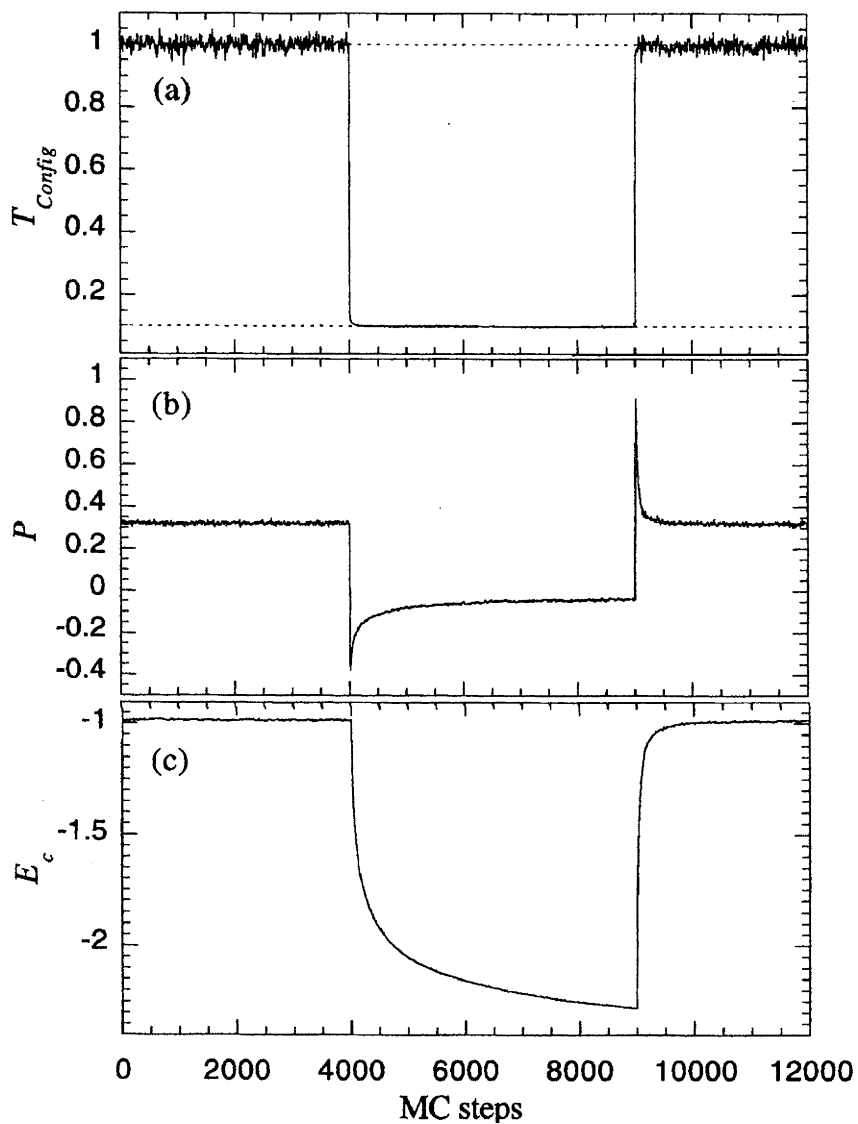


Figure 4.7: Relaxation of T_{C1} , pressure P and potential energy E_C during a Monte Carlo quench and reheating simulation (Butler, Aytton, Jepps, and Evans 1998).

becomes more short-ranged, T_{C1} relaxes more quickly. In particular, the LJ potential exhibits the fastest relaxation, which they explain by cancellation effects on the relaxation process, due to the attractive and repulsive parts of the LJ potential. These results are consistent with, and indeed provide valuable insight into those of Butler et al. They also imply that, for longer range potentials, the relaxation of T_{C1} may not be as fast, relative to other macroscopic observables.

Baranyai has also considered the derivation of configurational temperatures for open systems and dilute gases, using the radial distribution $g(r)$. He has also performed calculations to determine the effects due to truncation of the LJ potential, which for a cutoff of 2.5σ he evaluates to less than 1% (Baranyai 2000).

4.2 Measurement of Non-Equilibrium Temperatures

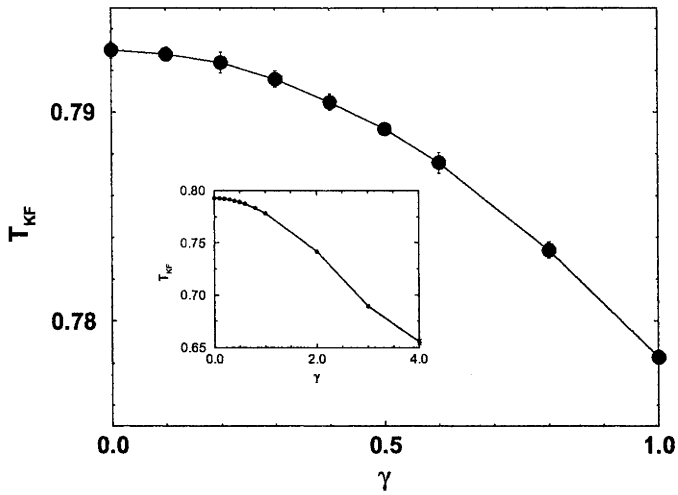
While we expect the various temperature expressions to be equal for equilibrium systems, we can have no such expectation for non-equilibrium systems. We will therefore investigate the behaviour of our temperature expressions in both atomic (§4.2.1) and rigid-body (§4.2.2) systems undergoing Couette flow, examining the shear-rate dependence of the temperatures and their differences.

4.2.1 Atomic Non-Equilibrium Systems

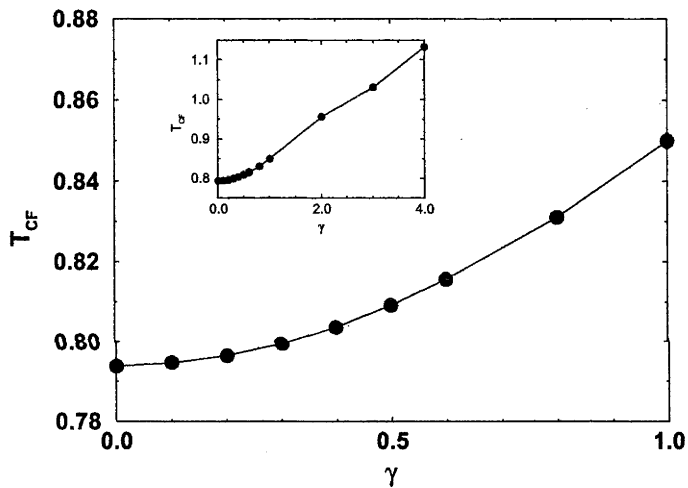
Because Couette flow is a dissipative process, it is necessary to introduce some means of maintaining the system at a non-equilibrium steady state. To achieve this, we use the Evans ergostat (§3.5) to maintain the system at a constant energy. The results in this subsection are reported from simulations of a system of 864 WCA atoms, with energy per particle $E/N = 1.0$ and density $\rho = 0.6$. The SLLOD equations of motion were used to simulate Couette flow, with Lees-Edwards boundary conditions, for shear rates up to $\gamma = 4.0$.

Table 4.5 shows the values of the various temperature expressions, as well as the pressures, obtained for three different shear rates — $\gamma = 0.0, 0.5$ and 1.0 . We note that the configurational and normal temperatures lie within 1% of one another — in particular, the Rugh and fractional temperatures $T_{NR}, T_{CR}, T_{NF}, T_{CF}$ lie within 0.1% of one another. The kinetic temperatures also agree to within 0.1%. Consequently, we consider only the configurational and kinetic fractional temperatures T_{CF} and T_{KF} for the detailed discussion of temperature variation with shear rate.

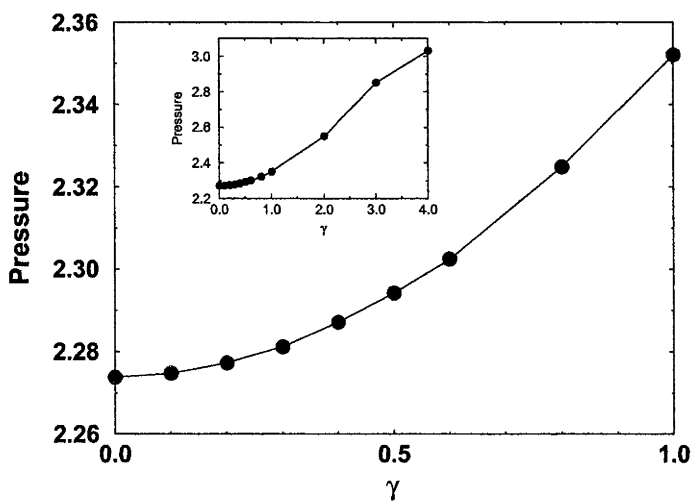
Fig. 4.8 shows shear-rate variation of T_{CF} and T_{KF} . We note



(a)



(b)



(c)

Figure 4.8: Behaviour of (a) T_{KF} (b) T_{CF} and (c) the pressure P for a system of 864 WCA atoms ($E/N = 1.0$ and $\rho = 0.6$) undergoing Couette flow at constant energy.

Table 4.5: Reported values of various temperature expressions for a system of 864 WCA atoms ($E/N = 1.0$ and $\rho = 0.6$) undergoing Couette flow at constant energy. Data is present for three shear rates — $\gamma = 0.0, 0.5$, and 1.0 .

γ	0.0	0.5	1.0
$T_{N1}(\gamma)$	0.7889 (3)	0.8038 (2)	0.8436 (3)
$T_{NR}(\gamma)$	0.7946 (3)	0.8097 (2)	0.8499 (3)
$T_{NF}(\gamma)$	0.7938 (3)	0.8090 (2)	0.8494 (3)
$T_{K1}(\gamma)$	0.7929 (1)	0.7890 (1)	0.7782 (1)
$T_{KR}(\gamma)$	0.7935 (1)	0.7897 (1)	0.7788 (1)
$T_{KF}(\gamma)$	0.7930 (1)	0.7892 (1)	0.7783 (1)
$T_{C1}(\gamma)$	0.7888 (3)	0.8039 (2)	0.8440 (3)
$T_{CR}(\gamma)$	0.7946 (3)	0.8099 (2)	0.8505 (3)
$T_{CF}(\gamma)$	0.7938 (3)	0.8092 (2)	0.8500 (3)
$P(\gamma)$	2.2738 (5)	2.2943 (3)	2.3522 (3)

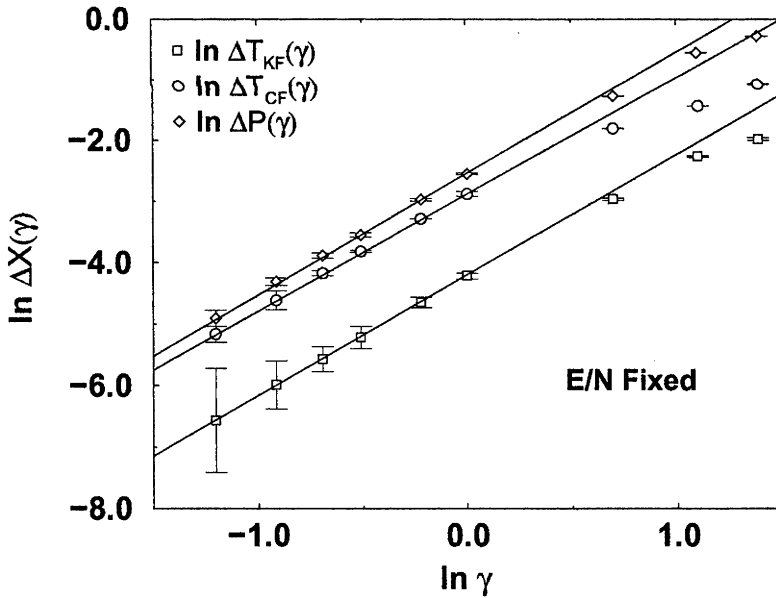


Figure 4.9: Deviation of T_{KF} , T_{CF} and pressure from their equilibrium values with increasing shear rate, for the same system studied in Fig. 4.8. The slope of the lines of best fit are: T_{KF} — 1.97 ; T_{CF} — 1.92 ; P — 2.00.

that while the kinetic temperature (Fig. 4.8a) decreases with increasing shear rate, the configurational temperature (Fig. 4.8b) increases with increasing shear rate. Furthermore, we note that the qualitative behaviour of these two temperatures is similar to that of the pressure (Fig. 4.8c). Mode-coupling theory predicts that the shear-rate dependence of the pressure in Couette flow is of the form $P(\gamma) - P(0) \propto \gamma^{3/2}$ (Kawasaki and Gunton 1973). This prediction has been observed in various computer simulations[†], including the simulation of constant energy Couette flow (Evans 1983). In order to determine the γ -dependence of T_{CF} and T_{KF} , we compare their shear-dependent behaviour with that of the pressure. We plot $\ln(\Delta T(\gamma)) = \ln(T(\gamma) - T(0))$ against $\ln \gamma$ for both temperatures, and compare these results with the behaviour of $\ln(\Delta P(\gamma))$ in Fig. 4.9.

We see from Fig. 4.9 that T_{CF} , T_{KF} , and P all show a consistent shear-rate dependence in our system. We have omitted the results with the lowest shear rates, as the uncertainties in the values of $\ln \Delta X (X = T_{\text{CF}}, T_{\text{KF}}, P)$ are too large to provide meaningful data. We note that the slope of the lines of best fit indicate a γ -dependence of γ^2 for our system. While the error bars for T_{KF} data admits a slope of $3/2$, this is not the case for T_{CF} or for the pressure. Furthermore, we note that the consistency observed in the nature of this power-law relation between the kinetic and configurational temperatures implies that the *divergence* of these temperatures is *also* described by the same power-law relation[§].

We conclude from these results that the configurational and kinetic temperatures can indeed diverge in non-equilibrium settings. While the exponent of the power-law relation between the pressure and γ , T_{CF} and γ , and T_{KF} and γ is not in accordance with the Kawasaki power-law relation, the shear-rate dependences of T_{CF} , T_{KF} , and P are self-consistent, for this system. Our results are qualitatively consistent with the observation of (Butler, Ayton, Jepps, and Evans 1998), where an introduced error provided a source of off-equilibrium behaviour. Furthermore, the divergence of the configurational and kinetic temperatures in Couette flow appears to be characterised by the same power-law relation that governs their individual shear-rate dependence.

4.2.2 Rigid-Body Non-Equilibrium Systems

The simulation of rigid bodies introduces a new range of coordinate-based temperatures that we can apply to our computer simulation. In §2.5 we derived the quaternionic temperature expressions T_{QF}

[†]recently reviewed in (Travis, Searles, and Evans 1998)

[§]on the assumption that the zero-shear values are equal, which is true in the thermodynamic limit

and T_{Q1} . In this subsection, we examine the behaviour of both the quaternionic temperatures and configurational temperatures in the simulation of a rigid-body system.

We report on results from simulating a system of 864 P2[¶] rigid-bodies at a temperature $T = 1.2$, density $\rho = 0.6$ and an anisotropy factor in the potential of $\lambda = 0.15$. We set the diagonal elements of the principle moment of inertia tensor to be $I_{xx} = I_{yy} = 0.04$ (in reduced units). A cutoff radius of 4.5σ was chosen for our system. The selection of this state point was to ensure that the equilibrium results could be compared with existing data (Luckhurst and Romano 1980). The system was held at constant temperature using the isokinetic equations of motion. The introduction of Couette flow was achieved by the usual SLLOD equations of motion in the translation degrees of freedom — no adjustment was made to the orientational equations of motion. An advantage of simulating a P2 system is the simple orientation dependence of the potential energy. We note that, despite this simple dependence, the temperature expressions are still extremely complicated. The calculations were performed over 500,000 timesteps of $\delta t = 0.002$ ^{||}.

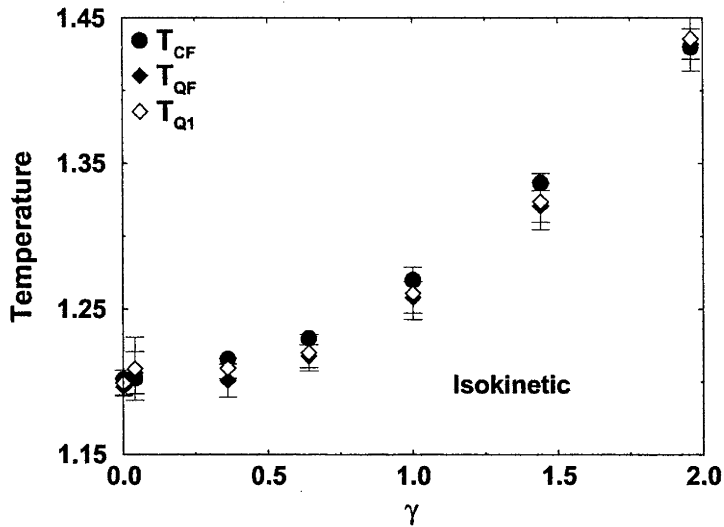
The shear-dependent behaviour of temperature expressions T_{CF} , T_{C1} , T_{QF} , T_{Q1} and $T_{\omega F}$ for this system are shown in Fig. 4.10. $T_{\omega F}$ represents the rotational equipartition temperature^{**}. For clarity, we have divided the data into two groups, with T_{CF} acting as a common reference set of data for both groups. In Fig. 4.10a we compare T_{CF} and the two quaternionic temperatures T_{QF} and T_{Q1} . In Fig. 4.10b we compare T_{CF} , T_{C1} and $T_{\omega F}$. We note that, once again, the normal temperature is dominated by configurational contributions which are two orders of magnitude larger than the quaternionic and kinetic contributions.

We observe from Fig. 4.10 that the values of all five temperatures converge in the zero-shear limit. T_{CF} appears to exhibit a similar shear-rate dependence to that observed in the atomic Couette flow system. To confirm this, we compare its shear-rate dependence with that of the pressure, by comparing both $\Delta T_{CF}(\gamma)$ and $\Delta P(\gamma)$ for various shear rates in Fig. 4.11. We observe a (γ^2) power-law relation similar to that determined in §4.2.1. In Fig. 4.12, we show similar data for the configurational and quaternionic temperatures, with the hope of identifying similar power-law relations. We note, however, that while such behaviour is clearly seen for the configurational temperatures (T_{C1} and T_{CF} are coincident in Fig. 4.12b), the

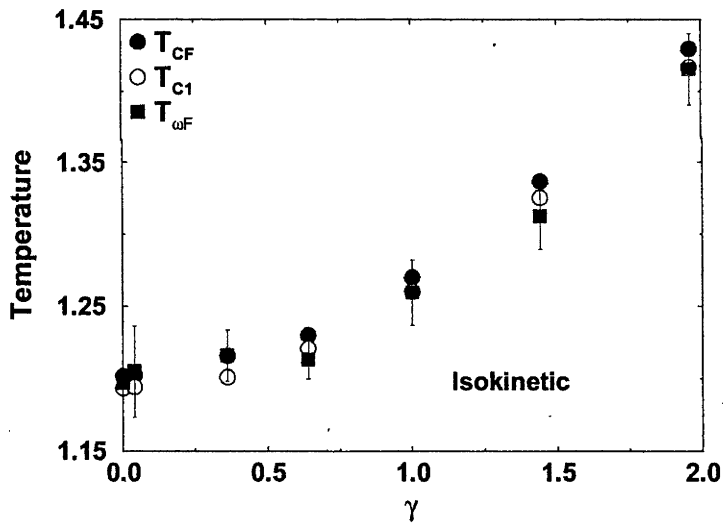
[¶]see Eqn.(1.9)

^{||}and took approximately two CPU-months on the ANU's Fujitsu VPP300 supercomputer

^{**}that is, the rotational energy per degree of rotational freedom (of which there are $2N$) in our system



(a)



(b)

Figure 4.10: Behaviour of (a) T_{CF} , T_{QF} , and T_{Q1} , and (b) T_{CF} , T_{C1} , $T_{\omega F}$ for a system of 864 P2 rigid bodies ($T = 1.2$, $\rho = 0.6$) undergoing Couette flow. The temperature is constrained using the Isokinetic thermostat.

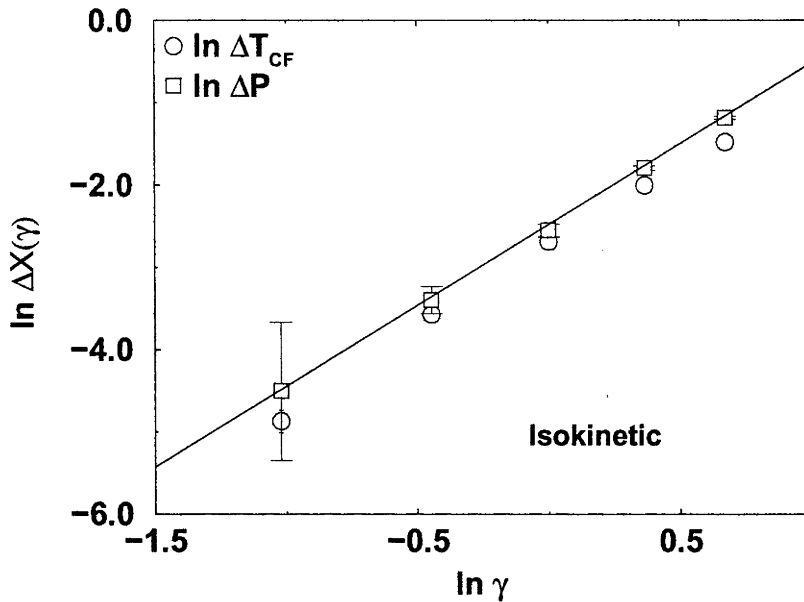
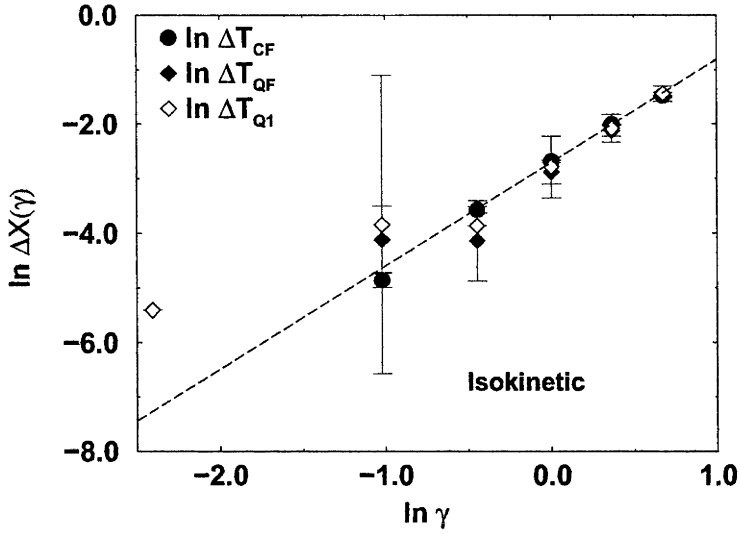


Figure 4.11: Deviation of T_{CF} and pressure from their equilibrium values with increasing shear rate, for a system of 864 P2 rigid bodies ($T = 1.2, \rho = 0.6$) undergoing Isokinetic Couette flow. The line of best fit for T_{CF} has slope 1.96

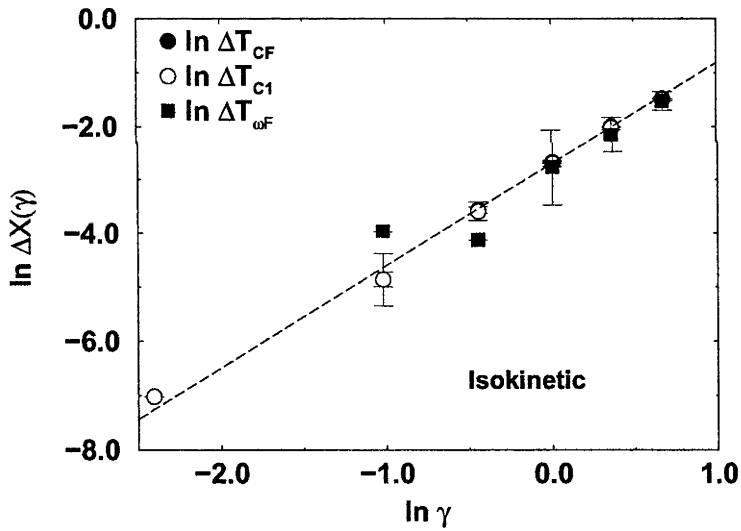
other temperatures do not exhibit the same consistent power-law behaviour. While there is a definite, consistent qualitative trend towards such behaviour, there are unsystematic deviations from this trend. Also unexpected are the large errors associated with $T_{\omega F}$. The kinetic temperatures to this point have exhibited smaller fluctuations than the configurational temperatures. In this situation, the fluctuations in $T_{\omega F}$ are *greater* than those of T_{QF} .

A possible cause of these unsystematic deviations could be that the system has not reached a non-equilibrium steady state. In considering this possibility, the cumulative averages of T_{CF}, T_{QF} and $T_{\omega F}$ for the system with a shear rate of $\gamma = 0.36$ are displayed in Fig. 4.13. We note from Fig. 4.13 that the fluctuations in the cumulative average of T_{QF} and $T_{\omega F}$ are much greater than the fluctuations of T_{CF} . It is not clear whether the values obtained after 500,000 timesteps are indeed the correct steady-state values in the non-equilibrium case. While the values of T_{CF} appear to have properly converged, this does not appear to be the case for the other temperature expressions presented.

Despite this uncertainty, the qualitative trends in the data appear to be consistent with our results for atomic non-equilibrium systems. Furthermore, the agreement among the temperatures in the zero-shear limit with the thermostatted temperature $T_{KF} = 1.2$



(a)



(b)

Figure 4.12: Deviation of (a) T_{CF} , T_{QF} , and T_{Q1} , and (b) T_{CF} , T_{C1} , $T_{\omega F}$, from their equilibrium values with increasing shear rate, for a system of 864 P2 rigid bodies ($T = 1.2, \rho = 0.6$) undergoing Isokinetic Couette flow. The line of best fit for T_{CF} has slope 1.89.

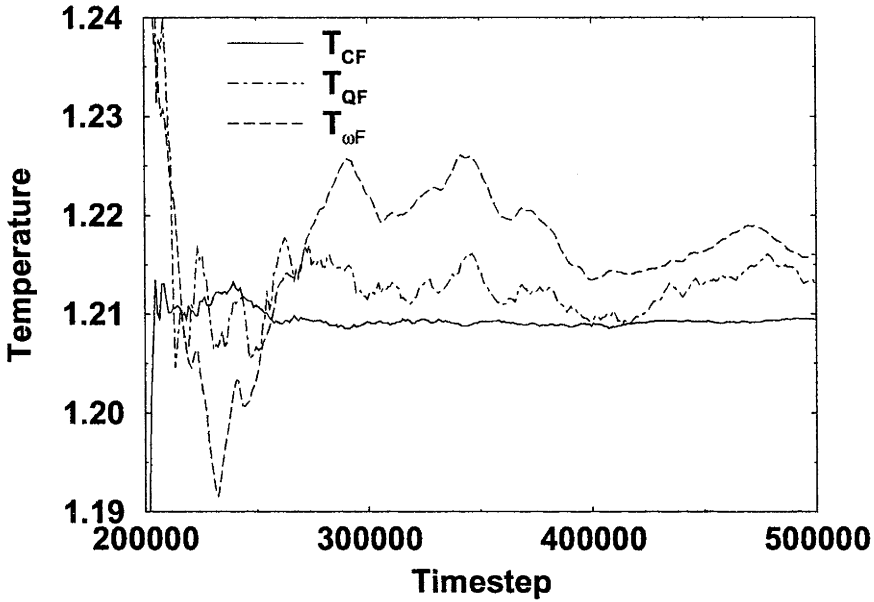


Figure 4.13: Cumulative averages of T_{CF} , T_{QF} and $T_{\omega F}$, reported for a system of 864 P2 rigid bodies ($T = 1.2$, $\rho = 0.6$) at a shear rate of $\gamma = 0.36$. The accumulation begins at $t = 200,000$.

indicates that the quaternionic temperatures provide useful additional measures of a temperature of an equilibrium system.

4.2.3 Other Non-Equilibrium Results

The configurational and normal temperatures have been exploited in various other non-equilibrium systems. For some time, practitioners of Non-equilibrium Molecular Dynamics have observed that heat can flow in systems with spatially-varying strain rates without the existence of a temperature gradient (Baranyai, Evans, and Daivis 1992). This is not predicted by Fourier's law. Such heat flow has been theoretically associated with the gradient of the square of the local strain rate, $\nabla\gamma^2(\mathbf{r})$ (Baranyai, Evans, and Daivis 1992; Risso and Cordero 1998; Nettleton 1999), leading to the so-called **strain rate coupling** constitutive relation for heat flow:

$$\mathbf{J}_Q = -\lambda\nabla T - \zeta\nabla[\nabla\mathbf{u} : [\nabla\mathbf{u}]^T], \quad (4.3)$$

where \mathbf{J} represents the heat flow, λ is the thermal conductivity, T is the local temperature, ζ is the strain rate coupling transport coefficient, \mathbf{u} is the velocity field and $:$ is the dyadic tensor operator. Difficulties in calculating ζ led to concerns that the local kinetic temperature was not a suitable definition of the local temperature in Eqn.(4.3). Other recent work, involving the calculation of 'op-

erational temperatures'^{††} in systems far from equilibrium, supports such concerns (Baranyai 2000). Rugh's normal temperature was therefore applied as an alternative definition for the local temperature (Ayton, Jepps, and Evans 1999). As such, it accounted for heat fluxes in non-equilibrium molecular dynamics simulations of two-dimensional sinusoidal transverse field (STF) and three-dimensional Poiseuille flow more correctly than kinetic temperature.

Lue and Delhommelle have separately considered the application of the configurational temperature to various atomic and molecular non-equilibrium systems. Such applications require that bond-length constraints be taken into account when calculating the temperature. This led to the first study of the conditions required under which Eqn.(2.16) can be applied to systems with constrained degrees of freedom (Lue and Evans 2000). In developing these conditions, Lue successfully measured the temperature of freely-jointed chain polymers undergoing Couette flow. Subsequently, Delhommelle has measured the temperatures T_{C1} and T_{CF} for atomic and molecular systems undergoing Poiseuille flow, noting that the fractional temperature is more reliable, and less dependent on the system size, than the $\mathcal{O}(1)$ expression (Delhommelle and Evans 2001a; Delhommelle and Evans 2001b).

4.3 Constant Temperature Simulations

The final section of this chapter focusses on the implementation of **coordinate thermostats**. These thermostats maintain a system at constant temperature by changing the coordinate equations of motion, rather than the momentum equations of motion. In (§4.3.1) we introduce the three coordinate thermostats that we will examine in §4.3.2 and §4.3.3. The first is the **Configurational Gradient-Field Nose-Hoover Thermostat**, or **C ∇ -thermostat**, which was used initially to control the configurational temperature T_{C1} of a system. The implementation of this thermostat predates the theoretical developments of Chapter 3. Consequently, we will compare the theoretical justification of the **C ∇ -thermostat** with the theory of the GNH thermostats (§3.6.1). We will then introduce the **Configurational B-Field Nose-Hoover Thermostat**, or **CB-thermostat**. This thermostat was used to control T_{CF} , and corresponds to a choice of $\mathbf{X} = \mathbf{B} = \nabla\Phi$ in the GNH theory. As well as these two configurational thermostats, we consider a quaternionic thermostat — a **B-thermostat** applied to a rigid-body system. Finally, we will consider the **Quaternionic B-Field Nose-Hoover Thermostat**, or

^{††}temperatures assigned on the basis that they would reflect the heat flow predicted by Fourier's law

QB-thermostat, which can be used to control the quaternionic temperature T_{QF} .

In §4.3.2 we will apply the CV-thermostat, CB-thermostat, and the Isokinetic thermostat to control the temperature of an atomic system at equilibrium. We will apply the QB-thermostat and the Isokinetic thermostat to a P2 system at equilibrium. In §4.3.3, we will introduce Couette flow to the atomic system, and examine the behaviour of the system away from equilibrium, for each thermostat.

In the following subsections, we only consider the soft GNH-style thermostats, and not the hard iso- \mathcal{T} thermostats. There are several reasons why we have preferred the use of the soft thermostats. One of the most compelling, from a practical point of view, is the ability to choose the value of the system temperature using the GNH thermostats. The nature of the GNH thermostats makes the system temperature an input variable. Consequently, the system temperature can be controlled. This allows for the possibility of controlling the temperature during a simulation, such as in the simulation of quenches. For the hard thermostats, this is not generally possible. An exception is the isokinetic thermostat, where the thermostatted temperature is the kinetic equipartition temperature T_{KF} . Rescaling the momenta therefore rescales the temperature (without breaking conditions of momentum conservation). However, for the configurational temperatures, no such simple rescaling is known. Consequently, in order to control the value of the system temperature, one must introduce some form of (Berendsen-like) thermostat, or trimmer, that directs the system towards the desired temperature. The production of such a trimmer is a possible direction for future work. However, we have not explored this to date.

A further practical reason for preferring the GNH thermostats relates to the timestep required for the simulation. The iso- \mathcal{T} thermostats require a timestep such that the actual change in the temperature is exactly corrected by the change estimated from differential calculus. If a simulation is to be maintained at a constant temperature, the gradient vector of the instantaneous temperature expression must vary slowly on the scale of the timestep sizes. For a complicated temperature expression, such as T_{C1} , we require time steps typically of the order of 10–50 times smaller than when the same system is thermostatted isokinetically. Thus, simulations must be run 10–50 times longer, in order to cover the same real-time period. Conversely, if the simulation is run at longer timesteps, then the configurational temperature tends to fluctuate unpredictably about an average value that is not *a priori* known.

4.3.1 The Coordinate Thermostats

The $\mathbf{C}\nabla$ -thermostat is based on the natural choice to control the value of $T_{\mathbf{C1}}$ by correcting the unthermostatted Newtonian equations of motion in the direction of $\nabla\mathcal{T}_{\mathbf{C1}}$. This method was inspired by the relationship between the isokinetic and Nose-Hoover thermostats, both of which correct the Newtonian equations of motion by a term $-\alpha\nabla\mathcal{T}_{\text{KF}}$ (where α is a phase function in the isokinetic case, and a variable in the Nose-Hoover case). The resultant equations of motion for the $\mathbf{C}\nabla$ -thermostat are

$$\begin{aligned}\dot{\mathbf{\Gamma}} &= \dot{\mathbf{\Gamma}}_0 - \xi\nabla\mathcal{T}_{\mathbf{C1}}, \\ \dot{\xi} &= \frac{1}{Q} \left[1 - \frac{T_0}{T_{\mathbf{C1}}} \right],\end{aligned}$$

where the equation of motion for $\dot{\xi}$ derives from our anticipation that

$$0 = \langle \dot{\xi} \rangle = \frac{1}{Q} \left\langle 1 - \frac{T_0}{T_{\mathbf{C1}}} \right\rangle \Rightarrow \frac{1}{T_0} = \left\langle \frac{1}{T_{\mathbf{C1}}} \right\rangle.$$

We note that, for the $\mathbf{C}\nabla$ -thermostat, the system temperature is given by $T_{\mathbf{C1}}$.

The fact that $\langle 1/T_{\mathbf{C1}} \rangle = 1/T$ does not ensure that the ensemble average of other quantities will match the canonical ensemble average to $\mathcal{O}(1/N)$. The Liouville theorem can be used at this point to suggest some sort of ‘on average’ justification. The ultimate test, however, will be in comparing the equilibrium values of macroscopic observables obtained using the $\mathbf{C}\nabla$ -thermostat, with those obtained using traditional thermostats.

By substituting $\mathbf{X} = \mathbf{B} = \nabla_{\mathbf{r}}\Phi$ into the GNH equations of motion (§3.6.1), we obtain the \mathbf{CB} -thermostat equations of motion

$$\begin{aligned}\dot{\mathbf{\Gamma}} &= \dot{\mathbf{\Gamma}}_0 - \xi\nabla_{\mathbf{r}}\Phi, \\ \dot{\xi} &= \frac{1}{Q} \left[\nabla_{\mathbf{r}}\Phi \cdot \nabla_{\mathbf{r}}\Phi - \frac{1}{\beta} \nabla_{\mathbf{r}} \cdot \nabla_{\mathbf{r}}\Phi \right].\end{aligned}$$

From the equations of motion, we obtain $T = \beta^{-1} = T_{\text{CF}}$. In the following subsections, we will compare results obtained from applying the $\mathbf{C}\nabla$ -thermostat, \mathbf{CB} -thermostat, and Isokinetic thermostat to simulations of an atomic system. We examine the momentum distribution and various macroscopic variables at equilibrium (§4.3.2), as well as the variation of macroscopic observables P , E , and η and the various temperature expressions with shear rate (§4.3.3), for a system of 864 WCA atoms at the LJ triple point at equilibrium, and undergoing Couette flow.

Before examining these simulation results, we make some remarks about the calculation of $\nabla\mathcal{T}_{\mathbf{C1}}$ for the $\mathbf{C}\nabla$ -thermostat. Cal-

culating $\nabla\mathcal{T}_{C1}$ is a complicated and computationally-expensive procedure. We must calculate derivatives of the numerator and denominator of \mathcal{T}_{C1} . In terms of the notation introduced in §4.1.2, these are $\partial_{i\alpha} \sum_{j\beta} \partial_{j\beta} \partial_{j\beta} V$ and $\partial_{i\alpha} \sum_{j\beta} \partial_{j\beta} V \partial_{j\beta} V$. Once again, through rearrangement these can be performed during the force loop. By noting that

$$\begin{aligned}
 \sum_{j\beta} \partial_{i\alpha} \partial_{j\beta} \partial_{j\beta} V &= \sum_{\substack{j\beta \\ j \neq i}} \partial_{i\alpha} \partial_{j\beta} \partial_{j\beta} V + \sum_{\beta} \partial_{i\alpha} \partial_{i\beta} \partial_{i\beta} V \\
 &= \sum_{\substack{j\beta \\ j \neq i}} \partial_{i\alpha} \partial_{j\beta} \partial_{j\beta} \phi_{ij} + \sum_{j\beta, j \neq i} \partial_{i\alpha} \partial_{i\beta} \partial_{i\beta} \phi_{ij} \\
 &= \sum_{\substack{j\beta \\ j \neq i}} \partial_{i\alpha} \partial_{j\beta} \partial_{j\beta} \phi_{ij} + \partial_{i\alpha} \partial_{j\beta} \partial_{j\beta} \phi_{ij} \\
 &= \sum_{\substack{j\beta \\ j \neq i}} 2\partial_{i\alpha} \partial_{j\beta} \partial_{j\beta} \phi_{ij},
 \end{aligned}$$

and that

$$\begin{aligned}
 \sum_{j\beta} \partial_{i\alpha} \partial_{j\beta} V \partial_{j\beta} V &= \sum_{\substack{j\beta \\ j \neq i}} 2\partial_{j\beta} V \partial_{i\alpha} \partial_{j\beta} V + \sum_{\beta} 2\partial_{i\beta} V \partial_{i\alpha} \partial_{i\beta} V \\
 &= \sum_{\substack{j\beta \\ j \neq i}} 2\partial_{j\beta} V \partial_{i\alpha} \partial_{j\beta} \phi_{ij} + \sum_{\substack{j\beta \\ j \neq i}} 2\partial_{i\beta} V \partial_{i\alpha} \partial_{i\beta} \phi_{ij} \\
 &= \sum_{\substack{j\beta \\ j \neq i}} 2\partial_{j\beta} V \partial_{i\alpha} \partial_{j\beta} \phi_{ij} - 2\partial_{i\beta} V \partial_{i\alpha} \partial_{j\beta} \phi_{ij} \\
 &= \sum_{\substack{j\beta \\ j \neq i}} 2(\partial_{j\beta} V - \partial_{i\beta} V) \partial_{i\alpha} \partial_{j\beta} \phi_{ij},
 \end{aligned}$$

these derivatives appear as explicit sums over the pair potentials, facilitating their calculation during the force loop.

In contrast, the CB-thermostat does not require the calculation of $\nabla\mathcal{T}_{C1}$. Only the values of \mathbf{F} , $\nabla \cdot \mathbf{F}$, and $\mathbf{F} \cdot \mathbf{F}$ are required. These values, however, are already calculated during the simulation, either to determine the configurational temperatures, or to solve the equations of motion. Because the CB-thermostat does not require additional quantities to be calculated, it is a more efficient thermo-

stat, running in excess of twice as fast as the CV -thermostat^{††} for the same system.

The final new thermostating method that we propose is the Quaternionic \mathbf{B} -field Nose-Hoover thermostat, or QB -thermostat, which is implemented through the equations of motion

$$\begin{aligned}\dot{\Gamma} &= \dot{\Gamma}_0 - \xi \nabla_{\mathbf{Q}} \Phi, \\ \dot{\xi} &= \frac{1}{Q} \left[\nabla_{\mathbf{Q}} \Phi \cdot \nabla_{\mathbf{Q}} \Phi - \frac{1}{\beta} \nabla_{\mathbf{Q}} \cdot \nabla_{\mathbf{Q}} \Phi \right].\end{aligned}$$

This corresponds to a choice of $\mathbf{X} = \mathbf{B} = \nabla_{\mathbf{Q}} \Phi$ in the Generalised Nose-Hoover equations of motion. We note that $\nabla_{\mathbf{Q}} \Phi$ is related to the torque applied to the rigid bodies. Although $\nabla_{\mathbf{Q}} \Phi$ appears in the quaternionic temperature expression, the numerator and denominator of T_{QF} can be calculated during the simulation without determining the individual elements of the vector $\nabla_{\mathbf{Q}} \Phi$. Consequently, the QB -thermostat *does* involve the calculation of additional terms. However, these additional calculations are quite straightforward, requiring little additional computation. Using the notation of §2.5, we recall that (§2.5)

$$\partial_{i\alpha} \Phi_{\text{rot}} = 2\kappa \sum_j r_{ij}^{-6} (\hat{\mathbf{n}}_i \cdot \hat{\mathbf{n}}_j) (\partial_{i\alpha} \hat{\mathbf{n}}_i \cdot \hat{\mathbf{n}}_j).$$

Contributions to $\nabla_{\mathbf{Q}} \Phi$ can therefore be calculated for each pair of particles, and summed appropriately. We further note that the terms required to calculate an analogy to the CV -thermostat for the quaternionic temperatures (a ‘ QV -thermostat’) would require considerable addition calculation.

4.3.2 Thermostating Equilibrium Systems

The first set of data which we present was obtained from applying an Isokinetic thermostat, a CB -thermostat and a CV -thermostat to a system of 864 WCA atoms at the LJ triple point ($T = 0.722$, $\rho = 0.8442$). Each simulation was run at a timestep of $\delta t = 0.001$. Values of Q — the feedback parameter in the CB -thermostat and CV -thermostat equations of motion — were determined by trial and error: the final value used in each case was the lowest value of Q for which the equations of motion could still be solved by the integrator. These values were $Q = 1.87 \times 10^9$ for the CB -thermostat, and $Q = 18.7$ for the CV -thermostat. We note that there is a large difference between these quantities due to the different terms in the $\dot{\xi}$ equations for either thermostat. The quantity Q divides terms of $\mathcal{O}(1)$ in the CV -thermostat, whereas it divides terms of $\mathcal{O}(N)$ in

Table 4.6: Reported values of various system properties for a system of 864 WCA atoms at the LJ triple point ($T = 0.722$ and $\rho = 0.8442$) for three different thermostats.

	Isokinetic	CB-thermostat	C ∇ -thermostat
K	935.7120	935 (2)	940 (1)
Φ	628 (1)	626 (1)	629 (1)
\mathcal{H}	1563 (1)	1561 (3)	1568 (2)
P	6.397 (9)	6.38 (1)	6.407 (10)
T_{N1}	0.7211 (11)	0.7195 (1)	0.7220 (1)
T_{NR}	0.7219 (11)	0.7220 (1)	0.7244 (1)
T_{NF}	0.7226 (5)	0.7220 (0)	0.7242 (1)
T_{K1}	0.7220 (1)	0.7206 (14)	0.7231 (11)
T_{KR}	0.7222 (1)	0.7211 (14)	0.7236 (11)
T_{KF}	0.7220 (1)	0.7211 (14)	0.7235 (11)
T_{C1}	0.7211 (11)	0.7195 (1)	0.7220 (1)
T_{CR}	0.7220 (11)	0.7220 (1)	0.7243 (1)
T_{CF}	0.7226 (5)	0.7220 (0)	0.7242 (1)

the CB-thermostat (where the coefficient of N is quite large).

In order to compare the equilibrium properties of the three systems, we report the values for various system properties determined using each of the three styles of thermostat. Averages were taken over 200,000 timesteps for each simulation. This data appears in Table 4.6.

We note that the values of the kinetic, configurational and total energy, as well as the pressure of the system, are equal within statistical uncertainty. Once again, we note that the configurational and normal temperatures are almost indistinguishable (equal to within $\approx 0.01\%$, in this case). Each thermostat successfully yields the input temperature for (at least) one of the temperature expressions. We note that while there is general agreement (within uncertainty) among all of the temperature expressions in the Isokinetic simulation, the values of the $\mathcal{O}(1)$ temperatures are consistently lower than the values of the Rugh and fractional temperatures.

For the configurationally-thermostatted systems, the low statistical uncertainties of *each* of the configurational (and normal) temperatures, leads us to conclude that the differences $T_{CR} - T_{C1}$ and $T_{CF} - T_{C1}$ are *essentially constant* during the simulation. While the statistical uncertainty in configurational temperatures during constant-energy or Isokinetic simulations is typically larger than this separation, this is not the case for the configurationally-thermostatted

^{††}when cell code is used. It is potentially faster for vector based code, where the order of redundant calculations would be $\mathcal{O}(N^2)$ rather than $\mathcal{O}(N)$.

Table 4.7: Reported values of various system properties for a system of 864 P2 rigid bodies ($T = 1.2$ and $\rho = 0.6$) for the **QB**-thermostat and Isokinetic thermostat.

	Isokinetic	QB -thermostat
Translational K	1555.2 (1)	1548 (23)
Rotational K	1034 (8)	1031 (11)
K	2589 (8)	2579 (26)
Φ_{rot}	-57.0 (5)	-56.6 (3)
Φ	-3570 (1)	-3574 (10)
E	-981 (7)	-996 (35)
P	0.156 (3)	0.14 (4)
T_{KF}	1.198 (3)	1.19 (1)
T_{N1}	1.193 (2)	1.18 (2)
T_{NF}	1.2018 (5)	1.19 (1)
T_{CF}	1.2019 (5)	1.19 (1)
T_{QF}	1.196 (6)	1.2000 (1)
T_{K1}	1.196 (7)	1.19 (1)
T_{C1}	1.193 (1)	1.19 (2)
T_{Q1}	1.199 (9)	1.2023 (5)

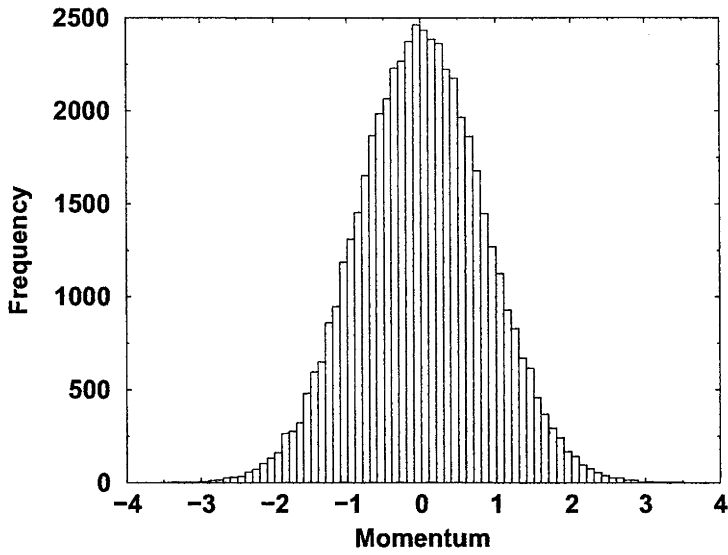
systems.

A second test of the equilibrium properties of the system was performed by recording p_x , p_y and p_z of each particle in the system at regular intervals (every 5000 timesteps) in the latter stages of the simulations. The distribution of these momenta for each of the configurationally-thermostatted systems is shown in Fig. 4.14. We note the bell-shape of the distributions, as would be expected if the simulations were correctly sampling the canonical-ensemble distribution. Furthermore, the value of the temperature can be estimated by the width of the bell. The momenta values which occur half as frequently as the peak (zero) value are approximately $p = \pm(1.0 \pm 0.1)$ in both distributions. This implies that

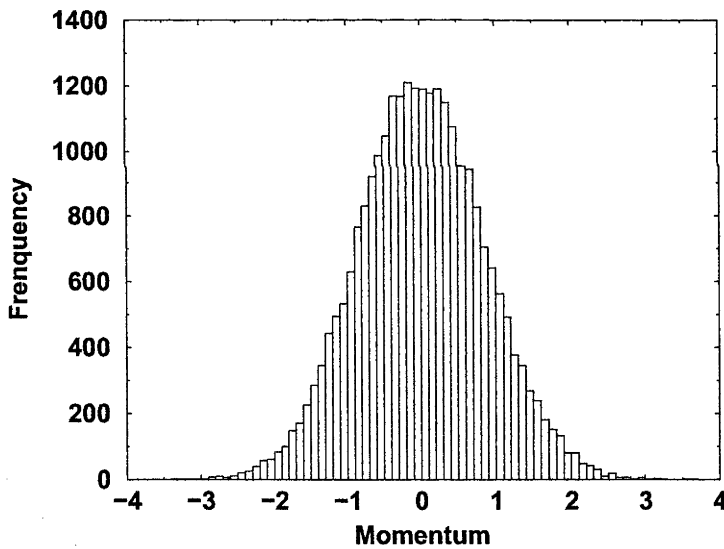
$$e^{-\frac{\beta p^2}{2m}} = 0.5 \Rightarrow T = \frac{1}{\beta} = \frac{1 \pm 0.2}{2 \ln 2} = 0.72 \pm 0.14,$$

agreeing with the input temperature of $T = 0.722$ for the simulation.

The third set of data that we present was obtained from two constant-temperature simulations of a system of 864 P2 rigid bodies at the same state point and conditions as in §4.2.2 ($T = 1.2$, $\rho = 0.6$, $\lambda = 0.15$). The first was thermostatted using the **QB**-thermostat, and the second was thermostatted using the Isokinetic thermostat. A value of $Q = 7.7 \times 10^6$ was chosen for the **QB**-thermostat simulation: while Q divides terms of $\mathcal{O}(N)$, these terms are not as



(a)



(b)

Figure 4.14: Comparison of the equilibrium momentum distribution of a system of 864 WCA atoms, at the LJ triple point ($T = 0.722, \rho = 0.8442$), thermostatted by the (a) CB-thermostat and (b) CV-thermostat. The widths of the distributions are consistent with the system temperature.

large as for the **CB**-thermostat. Each simulation was run for 500000 timesteps of timestep $\delta t = 0.002$.

In order to compare the equilibrium properties of the two systems, we report the values for various system properties determined using both the **QB**-thermostat and Isokinetic thermostat. This data appears in Table 4.7.

We note immediately that the uncertainty in the value of quantities is much larger for the constant-quaternionic temperature system than for the Isokinetic system. This would appear to be consistent with our results in §4.2.2, where it was noted that much longer times were required for the convergence of quantities related to the orientation of bodies in the system. Again, we observe that the difference $T_{\text{QF}} - T_{\text{Q1}}$ is much less than the statistical error in these two quantities, implying that this difference is relatively constant during the simulation.

Despite the higher uncertainties in the quaternionically-thermostatted system, we note that there is general agreement between the values reported for both simulations.

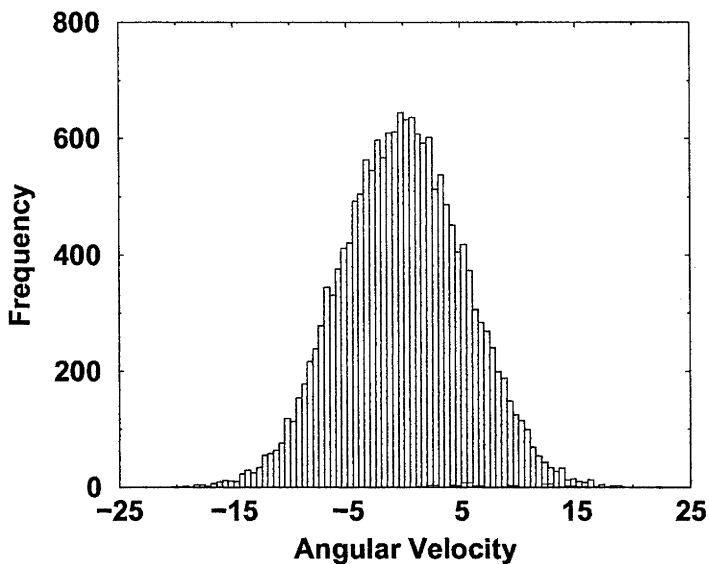
A second test of the equilibrium properties of the P2 system was performed by recording the momenta p_x , p_y and p_z and the angular velocities ω'_x and ω'_y for each rigid body in the system, at 5000-timestep intervals. The distribution of velocities and momenta obtained from using the **QB**-thermostat is shown in Fig. 4.15. We again note the bell-shape of the distributions, as expected if the canonical ensemble is correctly sampled. The distribution for the angular velocities Fig. 4.15a appears to be closer to the ideal distribution than that of the linear momenta Fig. 4.15b. We estimate the value of the temperature from the width of the bell. For the linear momenta, the values which occur half as frequently as the peak (zero) value are approximately $p = \pm 1.3 \pm 0.1$ in both distributions. This implies that

$$e^{-\frac{\beta p^2}{2m}} = 0.5 \Rightarrow T = \frac{1}{\beta} = \frac{1.69 \pm 0.26}{2 \ln 2} = 1.2 \pm 0.2,$$

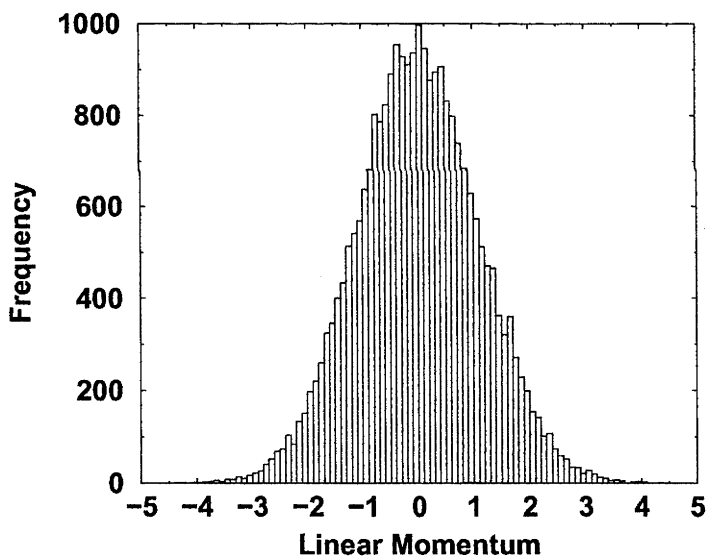
agreeing with the input temperature of $T = 1.2$. For the angular velocities, the values which occur half as frequently as the peak (zero) value are approximately $p = \pm 6.5 \pm 0.5$ in both distributions. Therefore (since $I_{xx} = I_{yy}$)

$$e^{-\frac{\beta I_{xx} \omega^2}{2}} = 0.5 \Rightarrow T = \frac{1}{\beta} = \frac{0.04(42 \pm 6.5)}{2 \ln 2} = 1.2 \pm 0.2,$$

which is again consistent with the input temperature.



(a)



(b)

Figure 4.15: Comparison of the equilibrium momentum distribution for the (a) angular velocities and (b) linear momenta of a system of 864 P2 rigid bodies ($T = 1.2$, $\rho = 0.6$), thermostatted by the QB-thermostat. The widths of the distributions are consistent with the system temperature.

4.3.3 Thermostatting Non-Equilibrium Systems

The CB-thermostat and CV-thermostat were also compared with the Isokinetic thermostat for the simulation of the same 864 WCA atom system undergoing Couette flow. To make such a comparison, the values of the pressure, total energy and shear viscosity at various shear rates were determined for simulations using the three different thermostats. We note that, for the highest shear rates examined, the CV-thermostat method required smaller timesteps, and a consequent variation in the value of Q . It is for this reason that an additional data point — evaluated at $\gamma = 1.69$ — appears for simulations using this thermostat. The other methods require no such variation.

The values of the pressure, total energy and shear viscosity appear in Fig. 4.16. We note from this figure that the values obtained using the configurational thermostats agree with one another more closely than they do with the results from the Isokinetic system. This is particularly true in the case of the viscosity, where the values obtained using the configurational temperatures only diverge noticeably beyond $\gamma = 1.0^*$. As noted from the data reported in Table 4.6 (§4.3.2), all three thermostats give consistent values for the pressure, total energy and viscosity in the limit of zero shear.

As a final comparison, we examine the behaviour of the temperature expressions. As we have noted previously, the configurational and normal temperatures are essentially identical. In the following, we report on the shear-dependent behaviour of T_{CF}, T_{C1}, T_{KF} and T_{K1} , representing the four distinguishable temperatures in our system. In Fig. 4.17 we show the shear-rate dependence of these temperatures, observed for simulations using the three different thermostats. For clarity, we do not include in Fig. 4.17b the configurational temperatures measured during the configurationally-thermostatted simulations, as they do not exhibit any unexpected behaviour.

The shear-dependent behaviour of both of the shown sets of temperatures is somewhat unexpected. We recall from Fig. 4.9 that when the energy of the system was held constant, the configurational temperatures increased with increasing shear rate, while the kinetic temperatures decreased with increasing shear rate. The results of Fig. 4.17a would seem to be inconsistent with these results — while the kinetic temperature is unsurprisingly constant during the Isokinetic simulation, it increases with increasing shear rate in the configurationally-thermostatted systems. We note, however, the following interesting property of the configurational thermostats — they appear to maintain a constant (with 2-3%) kinetic-

*Uncertainty in the low-shear rate viscosity restricts us from drawing conclusions about the relative behaviour of the viscosities measured in this region.

Table 4.8: Kinetic-to-potential energy ratios observed during configurationally-thermostatted simulations of 864 WCA atoms undergoing Couette flow, for two different state points.

γ	LJ triple point, $T = 0.722, \rho = 0.8442$		$T = 1.0, \rho = 0.6$
	C ∇ -thermostat	CB-thermostat	CB-thermostat
0.00	0.669 (2)	0.670 (3)	0.261 (2)
0.04	0.671 (2)	0.671 (3)	-
0.09	0.672 (2)	0.672 (3)	0.261 (2)
0.36	0.684 (2)	0.684 (2)	0.261 (2)
0.64	0.694 (2)	0.695 (2)	0.261 (2)
1.00	0.698 (2)	0.700 (2)	0.260 (2)
1.44	0.689 (3)	0.698 (3)	0.256 (2)
1.69	0.681 (4)	-	-
1.96	0.67 (4)	0.686 (3)	0.250 (2)

energy-to-potential-energy ratio as the shear rate is increased (see Table 4.8). It is not obvious why the kinetic-energy-to-potential-energy ratio should be conserved using the configurational thermostats. This ratio is clearly not preserved for the constant-energy Couette flow experiments of §4.2.1, where the kinetic temperature (and hence the kinetic energy) drops with increasing shear-rate. In the configurationally-thermostatted systems, the increase in energy includes a proportional increase in kinetic energy, and hence an increase in T_{KF} .

The results from Fig. 4.17b are also unexpected — the configurational temperatures do not demonstrate a monotonic divergence from the kinetic temperatures in the Isokinetically thermostatted system. This is in direct contrast to the behaviour of the configurational temperatures in the constant-energy Couette flow simulation of §4.2.1, where a shear-rate dependence of γ^2 was observed. In order to further investigate this phenomenon[†], a different state point was chosen, and the above non-equilibrium experiments repeated with the Isokinetic thermostat and CB-thermostat.

Fig. 4.18 shows the shear-dependent behaviour of the total energy, viscosity and pressure of a system of 864 WCA atoms at the state point ($T = 1.0, \rho = 0.6$). We recognise the same qualitative behaviour in these results as was observed in Fig. 4.16 for the simulations at the LJ triple point. However, the qualitative behaviour of the configurational and kinetic temperatures at the new

[†]and after having ensured that the data obtained from our Isokinetic simulation concurs with existing data for Isokinetic Couette flow of WCA particles at the LJ triple point (Travis, Searles, and Evans 1998), where such comparison is possible.

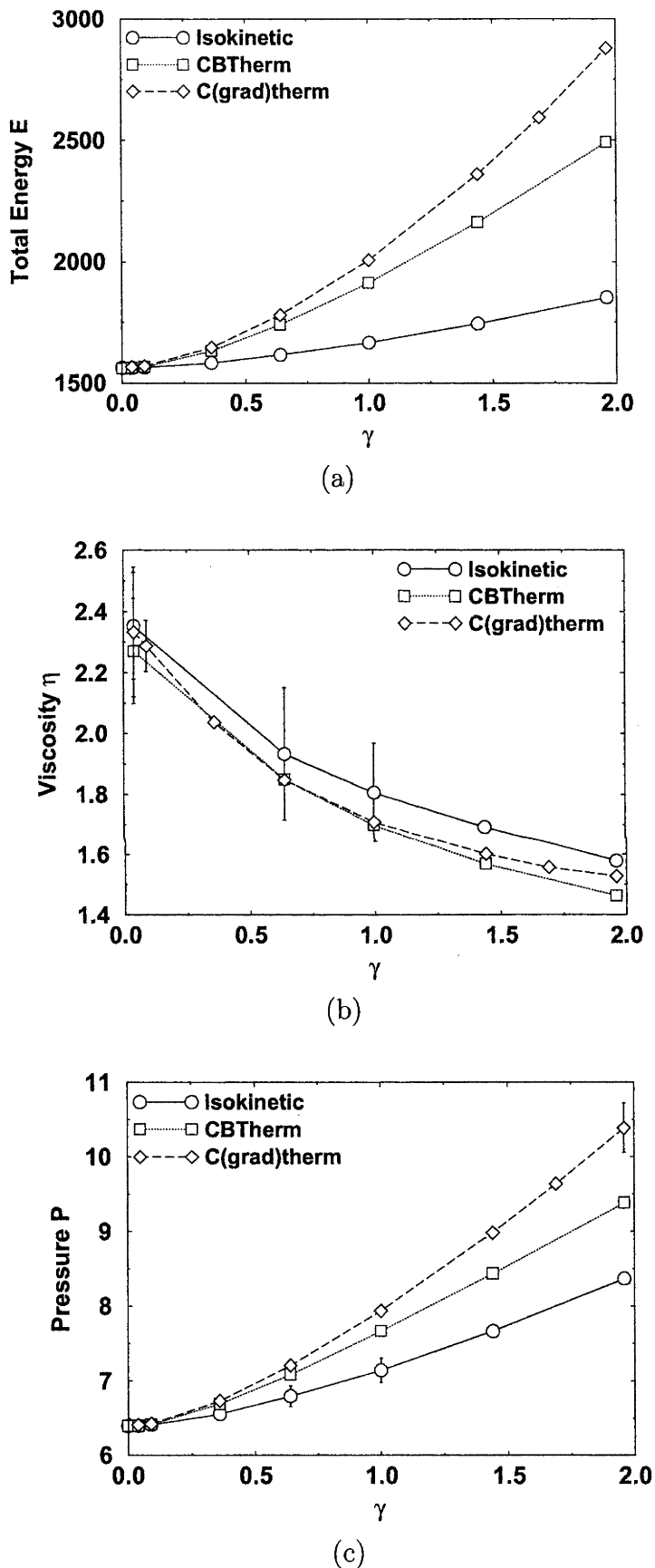
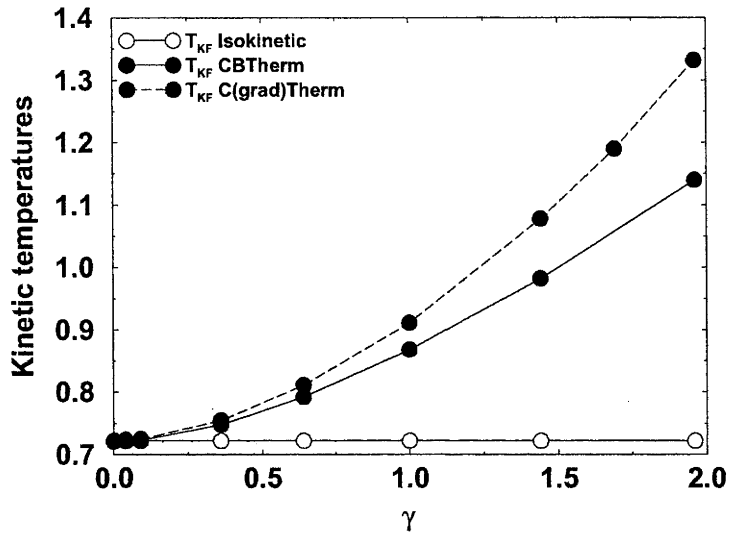
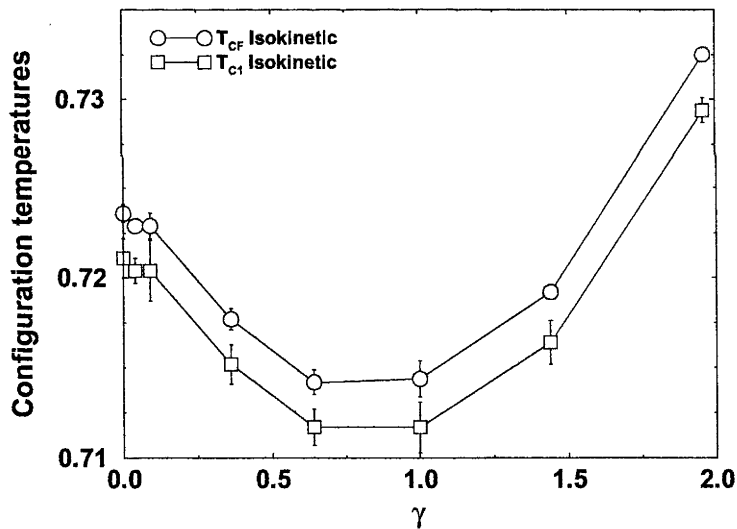


Figure 4.16: Comparison of the shear-rate dependence of the (a) total energy, (b) viscosity and (c) pressure for a system of 864 WCA atoms at the LJ triple point undergoing Couette flow.



(a)



(b)

Figure 4.17: Comparison of shear-rate dependence of (a) the kinetic temperatures for all three thermostatting methods, and (b) the configuration temperatures for the Isokinetic simulation, of 864 WCA atoms at the LJ triple point undergoing Couette flow.

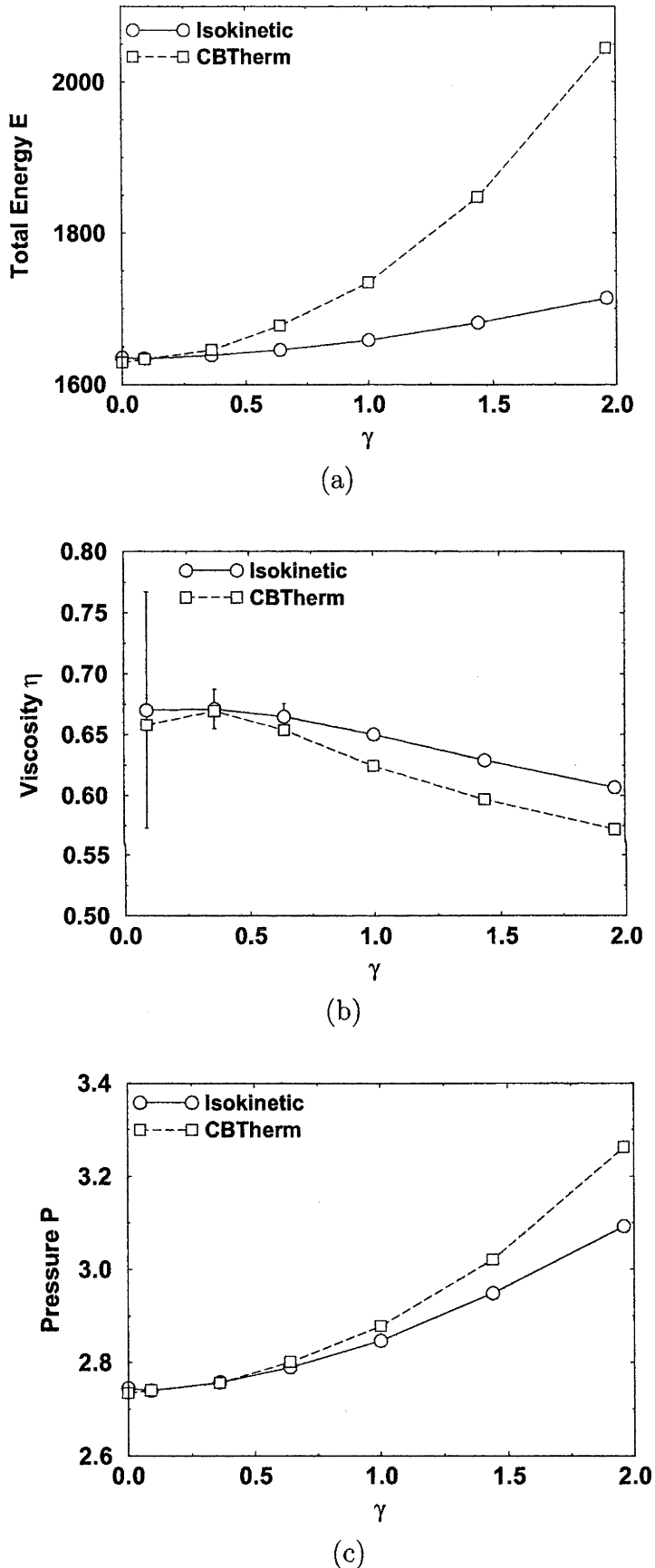
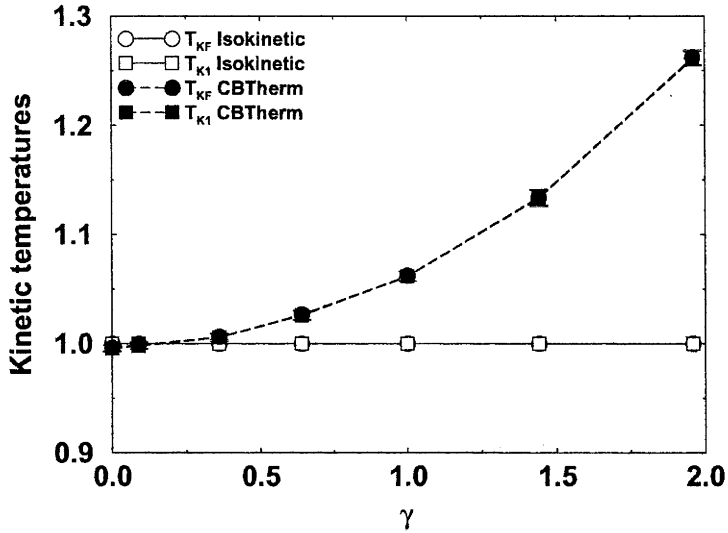
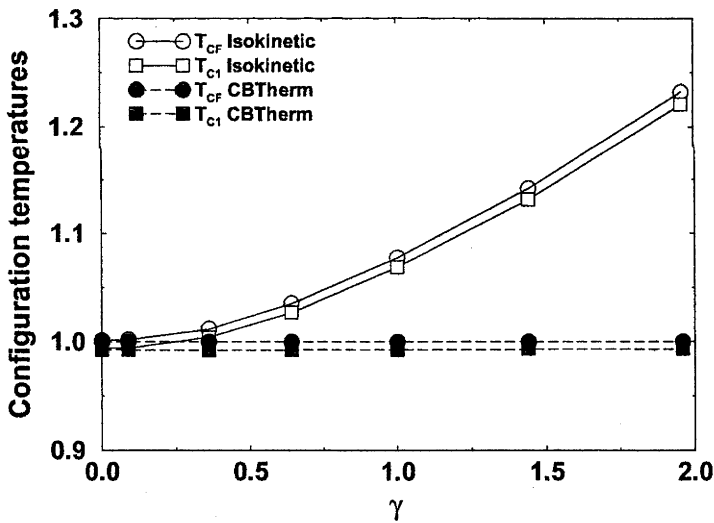


Figure 4.18: Comparison of the shear-rate dependence of the (a) total energy, (b) viscosity and (c) pressure for a system of 864 WCA atoms ($T = 1.0, \rho = 0.6$) undergoing Couette flow.



(a)



(b)

Figure 4.19: Comparison of shear-rate dependence of the (a) kinetic and (b) configuration temperatures for the CB-thermostat and Isokinetic simulations of 864 WCA atoms ($T = 1.0, \rho = 0.6$) undergoing Couette flow.

state point (Fig. 4.19) is consistent with the constant-energy Couette flow results of §4.2.1. We note that, for both simulations, the ‘un-thermostatted’ temperature is greater than the thermostatted temperature. For the CB-thermostatted system, the ratio of kinetic to potential energy also appears to be preserved, to within a few percent (Table 4.8). Consequently, the increase in total energy is again matched by an increase in kinetic energy, and hence kinetic temperature. For the Isokinetic simulation, the increase in total energy implies an increase in potential energy. However, it does not immediately follow that the configurational temperatures, as functions of the potential energy, should also increase[‡]. While it is possible that the results observed at the triple point are peculiar to that particular state point, we are not aware of any reason that explains the behaviour of the configurational temperatures for the WCA fluid undergoing Isokinetic Couette flow at the LJ triple point.

[‡]especially in light of our earlier results for the Isokinetic Couette flow simulations at LJ triple point

Chapter 5

Conclusion

The investigations of this thesis have been motivated by the realisation that there are many different expressions for the thermodynamic temperature in statistical mechanics. As we have seen in Chapter 2, this is not a new idea: various expressions for the temperature of a system have been previously derived. Indeed, we have used one of them extensively in our work — our configurational temperature T_{CF} , whose derivation can be found in (Gray and Gubbins 1984).

However, as it stands, Eqn.(2.16) provides a useful tool for generating temperature expressions. To our knowledge, it is the most general means of generating such expressions. It is important to realise, however, that Eqn.(2.16) is a somewhat idealised result. It requires that we have a representation of a real system using canonical coordinates. While these conditions may not seem *prima facie* to be particularly idealised, it is important to consider in what contexts Eqn.(2.16) might be applied. In our own area of application — the computer simulation of molecular systems — coordinate systems that do not meet these conditions are commonly chosen. If one restricts oneself to issues of mechanical properties, then such a choice is of little consequence. If one is interested in thermodynamic properties, however, this becomes a substantive issue, as our definition of temperature is based on geometric properties of phase space that no longer hold for arbitrary coordinate systems.

Apart from breaking the requirement that we use canonical coordinate systems, one can also break the requirement that the simulated systems are ‘real’ — it is in this category that the application of periodic boundary conditions lies. If one were to try to identify a reason why interest in configurational temperature expressions have been subordinated by kinetic temperatures, the complications introduced by periodic boundary systems would be an excellent place to begin. The simple expressions that hold for real systems with walls, such as Clausius’ virial theorem, no longer hold when those walls

are removed. Consequently, such expressions are of no use to practitioners of molecular simulations in determining the temperature.

In §2.4 we have derived the necessary extensions to Eqn.(2.16) so that this result can be applied in these more general situations. These extensions provide a significant bridge between theory and practice, allowing us both to understand how Eqn.(2.16) can fail if the appropriate conditions are not enforced, and to apply Eqn.(2.16) to real simulations of molecular systems.

Having developed general expressions for the thermodynamic temperature that can be used in simulations, we turn our attention to practical applications for such general expressions. In particular, we focus on the possibility of running simulations of systems at constant temperature. The common feature of all existing simulation techniques is that they control the temperature of the system by controlling the behaviour of the momenta. The Berendsen thermostat is the most sophisticated of a group of thermostats which simply rescale* the kinetic energy of the system, so that the average kinetic energy per degree of freedom will correspond to the input temperature value. These approaches are justified, *inter alia*, through the Equipartition theorem — indeed, the distinction between temperature and kinetic energy per degree of freedom is not always made.

The Isokinetic and Nose-Hoover thermostats differ from these, by showing a correspondance between the invariant distribution function of the equations of motion, and the canonical distribution required of a constant-temperature system. In both cases, however, the equations of motion are the usual Hamiltonian ones, with an extra term in the momenta equations. As we have seen in Chapter 3, these approaches can be generalised. Interestingly, the Generalised Nose-Hoover equations of motion are derived independent of the results of Chapter 2. It is interesting to note, however, that $\xi = 0$ if (and only if) Eqn.(2.16) holds for the vector field used to thermostat the system. From our theory we anticipate that this result will indeed hold, and our simulation results (which we shall consider shortly) are consistent with this result. The iso- \mathcal{T} thermostat, on the other hand, is a generalisation of the isokinetic approach, where we fix the value of a temperature-yielding quantity (determined through Eqn.(2.16)), and then seek to justify this approach by considering the invariant distribution function of the resultant equations of motion. Such a justification proves less straightforward for the iso- \mathcal{T} thermostat than for the Generalised Nose-Hoover thermostat — we must impose conditions on the thermostating vector field, so that the thermostatted trajectory visits phase space with the correct dis-

*The Berendsen thermostat can be considered as a rescaling at the differential level.

tribution, to leading order in N . It is encouraging, however, that such a justification can be made at all, and we anticipate these approximations to be small for the temperature expressions we shall consider.

At this point our interest turns from theory to application. At the beginning of Chapter 4, we began by examining the behaviour of a selection of temperature expressions. These expressions can be grouped in various ways, but of primary interest were the behaviour of the untested configurational temperatures. As it turns out, these temperatures, and the normal temperatures, are equal in almost every application that we choose. This is certainly an artifact of the units that we use to describe our system, as was made evident when the density of the system studied in §4.1.2 was reduced. At this point, the configurational and kinetic contributions to the normal temperature become more comparable — an effect that is highlighted when the temperatures T_{C1} and T_{N1} diverge from T_{K1} at low density. Since the positions and momenta in our system can be rescaled independently, the notion of a ‘natural’ temperature that could in some sense be preferred[†] is somewhat ill-defined, unless we can identify *a priori* some naturally preferable system of units.

Nevertheless, the results of §4.1 indicate that the configurational temperatures are indeed an accurate means of identifying the temperature of a system. In terms of efficiency, they are inferior to the kinetic expressions in the systems we have chosen to study. This is largely because the expression for the kinetic energy of our system is much less complicated than the expression for the potential energy. Furthermore, due to the high-inverse-power-law nature of the interaction potentials, these instantaneous configurational temperatures tend to fluctuate much further from their average value than the kinetic expressions. Consequently, we conclude that the kinetic temperature expressions provide a more effective means of determining the temperature of a system, compared to the configurational alternatives, in these systems. However, it is possible that there are real, thermodynamic systems where the fluctuations of the configurational temperature expressions are not as great as those examined in this thesis. In systems with harmonic potentials, for example, the quadratic form of both the kinetic and potential energies would lead us to expect similar fluctuations in both the configurational and kinetic temperatures. Thus the nature of the interaction potential plays a vital role in determining the most efficacious temperature expressions, in terms of computational intensity and instantaneous fluctuations.

In terms of the configurational expressions themselves, it seems

[†]as we suggested in (Ayton, Jepps, and Evans 1999), after noting that T_{NF} was a more reliable indicator of heat flow than T_{KF}

that the fractional form T_{CF} is the best choice. Perhaps not surprisingly, T_{C1} is the slowest of the three temperatures to converge in the thermodynamic limit, and seems more sensitive to the system density than the other temperatures. While we would expect T_{CR} to be the most accurate, since the pseudo-entropy S_B is the real entropy for the Rugh temperatures, it is also the least efficient computationally, requiring complicated higher-order derivatives than the other two. Given these two factors, T_{CF} would appear the best choice for a configurational temperature expression.

In the non-equilibrium, we observe the divergence of the kinetic and configurational temperatures. There are potentially interesting applications of this seemingly inconsequential result, however. By no means the least of these is the capacity to use the configurational temperatures as a simulation check in Monte Carlo simulations, as was mooted in (Butler, Ayton, Jepps, and Evans 1998). An intriguing alternative application is to a long-standing problem in the study of binary glass systems. Determining the glass transition temperature — the temperature at which the behaviour of the system becomes ‘glassy’[†] — is notoriously difficult. The transition is one from equilibrium to non-equilibrium, yet the system is non-dissipative — energy is still conserved. It is possible that the configurational temperature may be able to identify the point at which non-equilibrium behaviour begins, by the divergence of different temperature expressions. Practical issues related to such an experiment include the need to use temperatures whose fluctuations are not too great, in order that a clear separation can be observed. The configurational temperatures, as they stand, are therefore not ideal candidates. Furthermore, the very feature that allows us to associate the behaviours of WCA and LJ systems proves a disadvantage for this application — the configurational temperatures are generally insensitive to the long-range correlations in the system, which provide one of the distinctive features of the glassy transition. It is likely that the configurational temperature, being sensitive to the short range particle-particle interactions, would not be affected by the larger-range changes in the system. At this stage, therefore, such an application remains an interesting proposal for future work.

One of the important consequences of these results for practitioners of non-equilibrium MD simulations is that the Equipartition temperature is only one of an infinity of functions by which the equilibrium thermodynamic temperature can be measured, and therefore through which a system can be thermostatted. As was demonstrated in §4.3, systems can be quite successfully thermostatted with no explicit reference to their kinetic energy. In particular,

[†]marked by order-of-magnitude changes in transport coefficients, as well as by spatial heterogeneities in local properties such as local relaxation times

the **B**-thermostats provide an excellent alternative to the traditional thermostatting methods.

They could also provide the solution to an existing problem in the thermostatting of non-equilibrium systems using kinetic thermostats. Kinetic thermostats require that the velocities *peculiar to the local flow* be thermostatted: otherwise, the quantity thermostatted is an over-estimate of the true peculiar kinetic energy per degree of freedom. Determining such true peculiar velocities is a challenging problem. This challenge can be circumvented by the implementation of coordinate thermostats. In periodic boundary systems where particles interact through pair potentials, configurational temperatures depend only on relative particle positions, and are therefore independent of local streaming velocities. It is interesting to note, from our results in §4.3, that when a non-equilibrium system is held at a particular temperature using different thermostats, the other macroscopic properties of the system will not necessarily be equal. The full implications of this result are a source of future research.

There is good reason to prefer the Equipartition temperature expression when determining the temperature of a molecular simulation. It is also enlightening to realise that this relationship is not definitive — it is only one of a host of equally valid expressions that identify the thermodynamic temperature within the framework of statistical mechanics. It is possible that some outstanding difficulties in the contemporary research of molecular systems may benefit from the consequences of this realisation.

Bibliography

- Alder, B. J. and T. E. Wainwright (1957). *J. Chem. Phys.* 27, 1208.
- Allen, M. P. and D. J. Tildesley (1987). *Computer Simulation of Liquids*. Oxford: Clarendon Press.
- Andersen, H. C. (1980). *J. Chem. Phys.* 73, 2384–2393.
- Ayton, G., O. G. Jepps, and D. J. Evans (1999). *Mol. Phys.* 96(6), 915–920.
- Balescu, R. (1975). *Equilibrium and Non-equilibrium Statistical Mechanics*. John Wiley & Sons.
- Baranyai, A. (2000). *J. Chem. Phys.* 112(9), 3964–6.
- Baranyai, A., D. J. Evans, and P. J. Daivis (1992). *Phys. Rev. A* 46(12), 7592–7600.
- Barojas, J., D. Levesque, and B. Quentrec (1973). *Phys. Rev. A* 7, 1092.
- Beck, C. and F. Schlögl (1995). *Thermodynamics of Chaotic Systems: An Introduction*. Number 4 in Cambridge Nonlinear Science Series. Cambridge Nonlinear Science Series.
- Bell, E. T. (1965). *Men of Mathematics 2*. Pelican.
- Berendsen, H. J. C. and W. F. van Gunsteren (1985). Practical algorithms for dynamic simulations. In *Molecular dynamics simulation of statistical mechanical systems*, pp. 43–65. Soc. Italiana di Fisica, Bologna. Enrico Fermi Summer School, Varenna.
- Butler, B. D., G. Ayton, O. G. Jepps, and D. J. Evans (1998). *J. Chem. Phys.* 109, 6519.
- de Groot, S. R. and P. Mazur (1962). *Non-equilibrium Thermodynamics*. North-Holland Publications.
- Delhommelle, J. and D. J. Evans (2001a). *J. Chem. Phys.*, accepted for publication.
- Delhommelle, J. and D. J. Evans (2001b). *J. Chem. Phys.*, accepted for publication.

- Ennis, J. and D. J. Evans (2000). *Mol. Sim.*, accepted for publication.
- Erpenbeck, J. J. (1984). *Phys. Rev. Lett.* 52, 1333.
- Erpenbeck, J. J. and W. W. Wood (1977). *Statistical Mechanics Part B: Time-Dependent Processes*. Plenum Press.
- Euler, L. (1776). *Novi Comment. Petrop.* xx, 208.
- Evans, D. J. (1975). *The Statistical Mechanics of Polyatomic Molecules with Particular Reference to Benzene*. Ph.D. thesis, Australian National University.
- Evans, D. J. (1977). *Mol. Phys.* 34(2), 317–320.
- Evans, D. J. (1983). Couette flow. *J. Chem. Phys.* 78(6), 3297–3302.
- Evans, D. J. and B. L. Holian (1985). *J. Chem. Phys.* 83(8), 4069–4074.
- Evans, D. J. and G. P. Morriss (1983a). *Phys. Rev. Lett.* 51, 1776.
- Evans, D. J. and G. P. Morriss (1983b). *Chem. Phys.* 77, 63.
- Evans, D. J. and G. P. Morriss (1986). *Phys. Rev. Lett.* 56(20), 2172–2175.
- Evans, D. J. and G. P. Morriss (1990). *Statistical Mechanics of Nonequilibrium Liquids*. London: Academic Press.
- Evans, D. J. and S. Murad (1977). *Mol. Phys.* 34(2), 327–331.
- Frenkel, D. and B. Smit (1996). *Understanding Molecular Simulation*. Academic Press.
- Gear, W. C. (1971). *Numerical initial value problems in ordinary differential equations*. Prentice-Hall.
- Goldstein (1980). *Classical Mechanics*. Addison-Wesley.
- Gray, C. G. and K. E. Gubbins (1984). *Theory of Molecular Fluids*, Volume 1. Oxford: Oxford University Press.
- Green, H. S. (1969). *The Molecular Theory of Fluids*. Dover Publications Ltd.
- Hamilton (1969). *Quaternions*. Chelsea Publishing.
- Hoover, W. (1985). *Phys. Rev. A* 31(3), 1695.
- Huang, K. (1963). *Statistical Mechanics*. John Wiley & Sons.
- Jepps, O. G., G. Ayton, and D. J. Evans (2000). *Phys. Rev. E* 62(4), 4757–4763.
- Kawasaki, K. and J. D. Gunton (1973). *Phys. Rev. A* 8, 2048.

- Ladd, A. J. C. (1990). Molecular dynamics. In C. R. A. Catlow, S. C. Parker, and M. P. Allen (Eds.), *Computer Modelling of Fluids, Polymers and Solids*, NATO ASI C, pp. 55–82. Dordrecht, Holland: Kluwer Academic Press.
- Lebowitz, J. L., J. K. Percus, and L. Verlet (1967). *Phys. Rev.* *153*(1), 250–4.
- Lees, A. W. and S. F. Edwards (1972). *J. Phys., Ser. C* *5*, 1921.
- Luckhurst, G. R. and S. Romano (1980). *Proc. R. Soc. London A* *373*, 111–130.
- Lue, L. and D. J. Evans (2000). *Phys. Rev. E* *62*(4), 4764–4768.
- MacQuarrie, D. A. (1976). *Statistical Mechanics*. Harper & Row.
- Maitland, G. C. e. a. (1981). *Intermolecular forces*. Oxford: Clarendon Press.
- Metropolis, N., A. W. Rosenbluth, M. N. Rosenbluth, A. Teller, and H. Teller (1953). *J. Chem. Phys* *21*, 1087.
- Morriss, G. P. and D. J. Evans (1984). *Phys. Rev. A* *30*, 1528.
- Morriss, G. P. and L. Rondoni (1999). *Phys. Rev. E* *59*, R5.
- Münster, A. (1969). *Statistical Thermodynamics, Volume I*. Heidelberg: Springer-Verlag.
- Nettleton, R. E. (1999). *Eur. Phys. J. B* *11*, 287–292.
- Nose, S. (1984). *Mol. Phys.* *52*(2), 255–68.
- Petersen, K. (1983). *Ergodic Theory*. Cambridge University Press.
- Rickayzen, G. and J. G. Powles (2001). *J. Chem. Phys.* *114*(9), 4333–4.
- Risso, D. and P. Cordero (1998). *Phys. Rev. E* *58*, 546–553.
- Rudin, W. (1987). *Real and Complex Analysis*. Singapore: McGraw-Hill Book Company.
- Ruelle, D. (1969). *Statistical mechanics: rigorous results*. W. A. Benjamin.
- Rugh, H. H. (1997, February). *Phys. Rev. Lett.* *78*(5), 772–774.
- Rugh, H. H. (1998). *J. Phys A-Math. and Gen.* *31*, 7761.
- Sinai, I. (1970). *Russian Math. Surv.* *25*, 137.
- Sklar, L. (1995). *Physics and Chance: Philosophical Issues in the Foundations of Statistical Mechanics*. Cambridge University Press.
- Tolman, R. C. (1918). *Phys. Rev.* *11*, 261.
- Tolman, R. C. (1979). *The Principles of Statistical Mechanics*. New York: Dover Publications, Inc.

- Torretti, R. (1999). *Philosophy of Physics*. Cambridge University Press.
- Travis, K., P. J. Davis, and D. J. Evans (1995). *J. Chem. Phys.* 103(24), 10638–10651.
- Travis, K., D. J. Searles, and D. J. Evans (1998). *Mol. Phys.* 95(2), 195–202.
- Val, P. D. (1964). *Homographies, Quaternions and Rotations*. Oxford Mathematical Monographs. Oxford: Clarendon Press.
- Watts, R. O. and I. J. McGee (1976). *Liquid state chemical physics*. New York: Wiley.
- Weeks, J. W., D. Chandler, and H. C. Andersen (1971). *J. Chem. Phys.* 54(12), 5237–47.
- Whittaker, E. T. (1952). *A Treatise on the Analytical Dynamics of Particles and Rigid Bodies with an introduction to the problem of three bodies*. Cambridge University Press.
- Woodcock, L. V. (1971). *Chem. Phys. Lett.* 10(3), 257–261.